DESIGN AND IMPLEMENTATION OF LINEAR-PHASE AND/OR PAIRWISE-SYMMETRIC PERFECT-RECONSTRUCTION FIR MULTIRATE FILTER BANKS

Thesis by

Truong Quang Nguyen

In Partial Fulfillment of the Requirements

for the Degree of

Doctor of Philosophy

California Institute of Technology

Pasadena, California

1989

(Submitted April 14, 1989)

ACKNOWLEDGEMENTS

It is my pleasure to acknowledge and thank people by whom I have been influenced throughout the course of this research. I am most grateful to Professor P. P. Vaidyanathan, for investing so much of his time and effort in me during my studies at Caltech. I appreciate especially his intuition, creativity and optimism. His technical insights have proven to be fruitful and invaluable during the course of my research, and the constant encouragement and friendship that he has extended to me have made my stay at Caltech an enjoyable experience.

I would like to thank my colleagues in our research group, Zinnur Doganata, Quan Phuong Hoang, David Koilpillai, Vincent Liu and Vinay Sathe, for many helpful discussions and encouragement. Especially, I would like to thank Zinnur Doganata, who has made a valuable contribution to my work. Special thanks are extended to Dr. Tapio Saramaki of Tampere University, Finland, for the stimulating talks we had.

I would like to thank all members of my thesis committee: Prof. Vaidyanathan, Prof. J. Franklin, Prof. R. J. McEliece, Prof. Y. S. Abu-Mostafa and Dr. L. Swanson.

I gratefully acknowledge that the second year of my graduate studies was supported in part by a fellowship grant from the Program in Advanced Technologies at Caltech, sponsored by Aerojet General, General Motors, GTE and TRW. I would also like to acknowledge the financial support from the National Science Foundation grants, ECS 84-04245, DCI 8552579 and MIP 8604456. I would like to thank all my friends at Caltech for their encouragement and for our good times together. I

also like to thanks Ms. Nelle Baird for proofreading the final version of the thesis.

Constant love and encouragement have come from my family and my uncle. Words fail to describe the endless support and love that they have given me, and it is to them that I dedicate this thesis.

ABSTRACT

This thesis studies the structures, design procedures and implementations of FIR perfect-reconstruction digital filter banks. The first part of the thesis deals with the structures and the design procedures of the perfect-reconstruction filter banks where the polyphase transfer matrices are lossless. These structures are parameterized by a set of rotation angles [37]. The usual procedure is to *blindly* optimize these angles to minimize an objective function where the objective function consists of all the stopband energies of the filters which we would like to design. This procedure is very time-consuming because of the nonlinear objective function and the large number of parameters to be optimized. The pairwise-symmetry property is imposed on these perfect reconstruction systems as a means of decreasing the number of parameters (rotation angles). The pairwise-symmetric property together with a method to *initialize* these rotation angles gives a very efficient design procedure. Design examples and complexity of the pairwise-symmetric, perfect-reconstruction FIR filter banks have compared well with the approximate perfect-reconstruction systems.

The second part of the thesis studies the structures and the design procedures of perfect-reconstruction filter banks which yield linear-phase filters. By confining the problem to a class, we are able to count exactly the number of linear-phase, perfect-reconstruction filter banks in this class. For the two-channel filter banks, we have obtained structures and design procedures for all nontrivial systems. Comparison with the approximated perfect-reconstruction systems in terms of complexity and performance is made. In our subclass of linear-phase, perfect-reconstruction, there are three structures for the case of three-channel filter banks. By limiting the problem to one of these systems, we obtain structures which yield linear-phase,

perfect-reconstruction filters. The implementation complexity is studied. Design examples for all new methods presented here are included, along with tabulation of lattice and filter coefficients.

TABLE OF CONTENTS

List of figures

List of Tables

To my family and my uncle

CHAPTER I
INTRODUCTION

The last decades have seen a rapid growth of high-speed integrated circuits, along with which digital signal processing has expanded greatly in both theoretical and implementational aspects. Systems that could not be implemented in the past due to the lack of high speed circuits can now be built in research laboratories and companies around the world. The digital-signal processor and its development systems, which have recently emerged for commercial uses, have helped in bridging the gap between theory and practice in digital-signal processing. Digital-signal processors are thus used in many applications such as speech synthesis and recognition, image processing and spectrum estimation, to name a few. Improvements in VLSI technology have led to increasing speeds of operation of the digital-signal processors, yet there is a need for algorithms which can be executed in real time. The search for faster algorithms has led to the advent of a new avenue, viz, Multirate Signal Processing.

Unlike a single rate system where the sample spacing is constant, sample spacing in a multirate system can vary from point to point. This often results in a more efficient processing of signals, because the sampling rates at various internal points can be kept as small as possible. One example of a multirate system is a block filtering system, which converts a signal into M parallel subsignals via a switch as shown in Fig. 1.1. If the sampling rate of the input signal $x(n)$ is B Hertz, then the sampling rate of each subsignal $u_i(n)$ is B/M Hertz. The advantage of the above system is that the $u_i(n)$ can now be processed in parallel at a much smaller rate.

Encouraged by the efficiency of implementation of multirate systems, many re-

searchers have recently used them in communications, speech and image processing, radar systems and antenna systems. An excellent tutorial article on the application of multirate systems appears in [34,38]. In particular, [34] points out the applications in digital-audio systems, in subband coding techniques (used in speech and image compression) and in analog voice privacy systems (for standard telephone communications). Further applications include new techniques for efficient coding of impulse response sequences of narrow band filters, design of FIR filters with adjustable multilevel responses, adaptive filtering in subbands and derivation of new sampling theorems for efficient compression of signals [34].

One of the topics which has recently received a lot of attention is digital filter banks, since it finds many applications in image processing, speech analysis, bandwidth compression, voice privacy, radar and sonar signal processing and spectrum parameterization of signals. Nearly all of these systems have, as their basis, some form of filter bank decomposition and/or reconstruction of signal in which the filter bank components occur in decimated form. The spectrum of any physical signals have different energy concentrations depending on the nature of the signals. For example, most of the energy of a speech signal usually concentrates at the low-frequency end of its spectrum. In order to encode or transmit these signals efficiently, it is judicious to assign more bits per sample to the low-frequency bands and less bits per sample to the high-frequency bands, provided that we have a method to separate these frequency bands. We will propose a filter bank system which enables us to accomplish the above goals.

Fig. 1.2(a) illustrates the basic framework of an M-channel filter bank. The filter bank analyzer splits the input signal $x(n)$ into M subband signals, which in turn are decimated by M and encoded prior to transmission. At the receiving end,

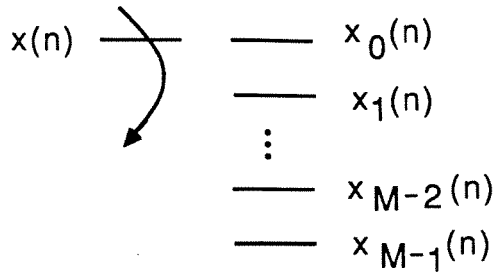

Fig. 1.1 A simple example of a multirate system.

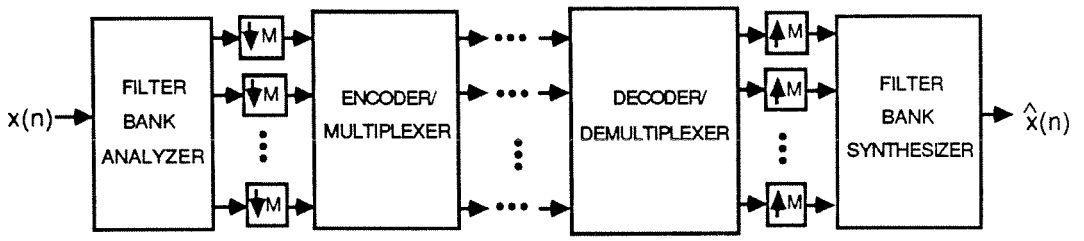

Fig. 1.2 (a) Filter bank system.

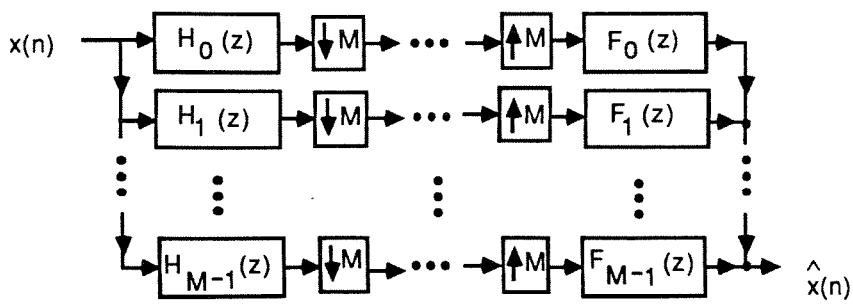

Fig 1.2 (b). Filter bank system where the filter bank analyzer and synthesizer are sets of filters in parallel.

the M subband signals are decoded (possibly after demultiplexing), interpolated and recombined using the filter bank synthesizer. The decimator, which decreases the sampling rate of the signal, and the interpolator, which increases the sampling rate of the signal, are denoted respectively by the down-arrowed and up-arrowed boxes in the figure. We will elaborate on their functions in Chapter 2. In addition to separating the spectrum of a signal, the above filter bank is also useful in transmitting a high-bandwidth signal over a narrow-band channel. Physically, the channel can take many forms such as telephone lines and fiber optic lines, or it can even be the atmosphere. Of course, if the channel is the atmosphere, one should time-multiplex the M-subband signals before transmission.

The filter bank analyzer and synthesizer are sets of filters as shown in Fig. 1.2(b). $H_k(z)$ and $F_k(z)$ are called the analysis and synthesis filters, respectively. The filter banks in which $H_k(z)$ and $F_k(z)$ reside are called the analysis bank and the synthesis bank, respectively. Normally, we will design $H_0(z)$ and $F_0(z)$ to be lowpass filters; $H_1(z)$ and $F_1(z)$ to be bandpass filters, etc. The last filters $H_{M-1}(z)$ and $F_{M-1}(z)$ are highpass filters. The frequency responses of these filters are shown in Fig. 1.2(c). From now on, we will work only with the filter bank shown in Fig. 1.2(b), where the filters have frequency responses as shown in Fig. 1.2(c).

Ignoring the nonideal channel characteristics and the nonlinear encoding/decoding error, the signal $\hat{x}(n)$ suffers from three errors, namely, aliasing because of change in the sampling rate, amplitude and phase distortions. These are due to the nonideal nature of the analysis and synthesis filters. The objective is to design both filter banks in such a way that all three distortions are eliminated; that is, $\hat{x}(n)$ is a delayed version of $x(n)$. The system where all three errors are eliminated is called a "perfect reconstruction" system, in short, a PR system. Moreover, such a system

should also be designed and implemented at a finite cost.

To illustrate the use of the above digital filter bank in speech compression, let us consider the system for transmission of a speech signal in Fig. 1.3. To transmit this signal, we need to encode it with 8 bits/sample. Since the sampling rate is 8 KHz, the total number of bits needed here is 64 Kbits per second. However, as is evident from Fig. 1.3, the energy in the low-frequency band is generally much more than that of the high-frequency band. Thus, it is judicious to allocate less bits per sample in the frequency band which has little or no energy, viz, the high-frequency band. As an example, let us split the spectrum of the above signal into 4 subbands and allocate the following bits for the subbands: 8 bits/sample, 4 bits/sample, 3 bits/sample and 2 bits/sample for the first, second, third and last subbands, respectively. Since the sampling rate in each subband is one-fourth of the original sampling rate, the total bits needed for this technique are 34Kbits per second. Thus, we are able to compress the speech signal from 64 Kbits per second to 34 Kbits per second, which gives us a compression ratio of 1.82.

Many approximate solutions to the above problem of eliminating the three types of error in multirate filter banks have appeared recently in the literature. Most of these systems cancel aliasing introduced by the change in the sampling rate. Depending on the filters used in these systems, they either cancel amplitude distortion while minimizing phase distortion, or vice versa. For instance, by taking the synthesis and analysis filters to be linear phase FIR (finite impulse response), the design in [32] is able to eliminate phase distortion. Then they focus on designing these filters such that the amplitude distortion is minimized. In the other design [83], the amplitude distortion is eliminated by choosing the filters to be allpass. The phase distortion is then minimized by carefully designing these allpass filters. For a while

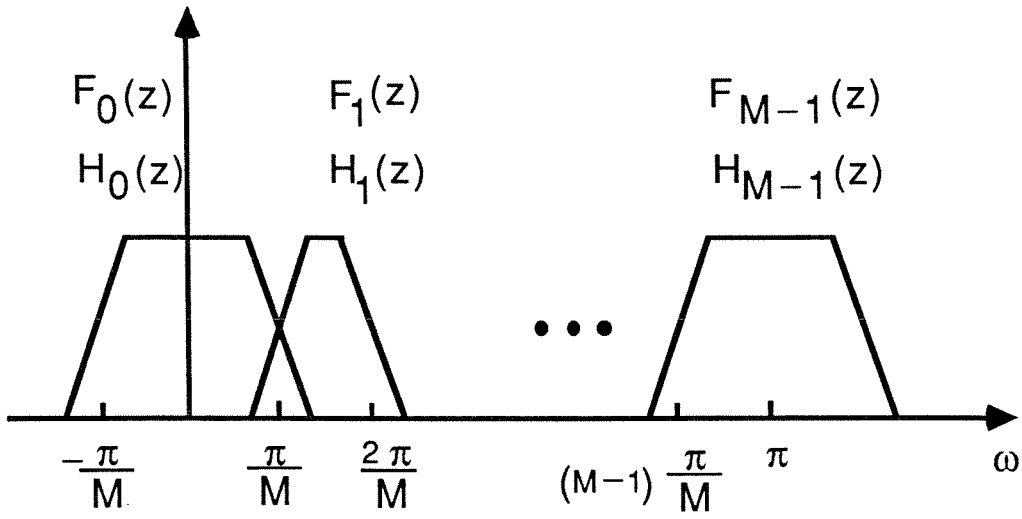

Fig. 1.2(c) Desired frequency responses of both analysis and synthesis filters.

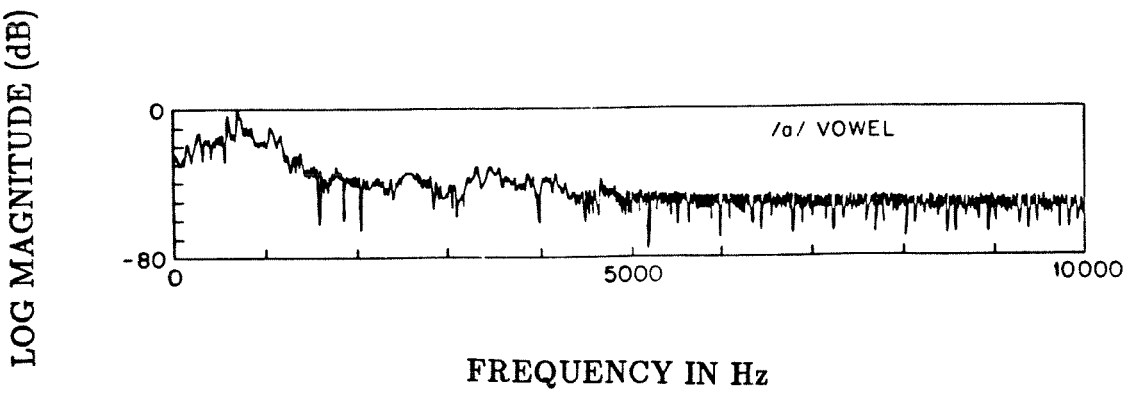

Fig. 1.3. Spectrum of vowel "a" for a 20KHz sampling rate. (p. 173 of [98]).

it seems that the PR system is impossible to design.

When doubts were cast on the existence of a PR system, new light in the case of two channels shone in [5]. This discovery led to a frenzy of researchers trying to find PR systems with an arbitrary number of channels -M. By using a tree-structured architecture, the problem can be solved if $M = 2^k$. However, tree-structured systems are known to have unnecessarily large group delays and thus can have a big effect on applications where small group delays are crucial. Two independent theories in [7,11] have shown that a PR system indeed exists for systems with an arbitrary number of channels. They also have a design procedure for a PR system.

The system in [7] involves orthogonal matrix functions and lattice structure theory. The difficulty, however, lies in the design method of producing these filters efficiently. In other words, it can take a long time (days) to design a set of filter banks for a particular set of specifications. Moreover, filters with high attenuation and sharp cut-off band edges are difficult (if not impossible) to design. Basically in these PR systems, the filter banks are realized in the form of a cascade of lattice sections. The difficulty is partly due to the optimization of a large number of parameters in these lattice sections. Typically, one optimizes these parameters in the lattice sections to yield good filters $H_k(z)$ and $F_k(z)$ in Fig. 1.2(b). Apart from the intrinsic relations imposed on both filter banks (so as to yield PR property), the analysis filters $H_k(z)$ and the synthesis filters $F_k(z)$ are not related among themselves. If we impose additional constraint such as the pairwise symmetric condition (to be explained) on each filter bank, then the number of parameters to be optimized is cut by a factor of 2. As a result, we would be able to design these systems faster. To illustrate the idea, let us consider the filter bank for three

channels. Here, incorporating the mirror-image constraint together with applying the initialization procedure (to be elaborated), we are able to design the analysis filter bank as shown in Fig. 1.4 very fast compared to the design in [7]. The three-channel PR FIR analysis filter bank in Fig. 1.4 satisfies the pairwise-symmetric condition; i.e., $H_2(z) = H_0(-z)$ and $H_1(z) = \alpha_1(z^2)$, where $\alpha_1(z)$ is an arbitrary polynomial.

It is important in image coding to preserve phase imformation. The filters of the PR system in [7], however, do not have linear-phase responses. They instead satisfy the power-complementary property, namely,

$$\sum_{k=0}^{M-1} |H_k(e^{j\omega})|^2 = 1. \tag{1.1}$$

Furthermore, it is shown in [31] for the case of two channels that only trivial filters exist if both linear phase and power-complementary properties are imposed on the structure. It turns out that power-complementary property is not necessary for PR systems. Thus, by sacrificing the power-complementary property for the case of two channels, we are able to obtain PR system with linear-phase responses. For the arbitrary number of channels, however, we will show that there are PR systems that have both power-complementary and linear-phase properties in their filters.

Thesis outline: In Chapter 2, basic tools such as decimators, interpolators and digital filter banks are reviewed, along with the interconnection properties of these building blocks. Some of the important results about the decomposition of the PR system into a cascade of lattice sections as well as the initialization of these lattice sections are also described in Chapter 2. Chapter 3 introduces the concept of mirror-image filter banks and their structures. Design examples are given to illustrate the theory. Comparisons between the new PR filter bank and the approximated

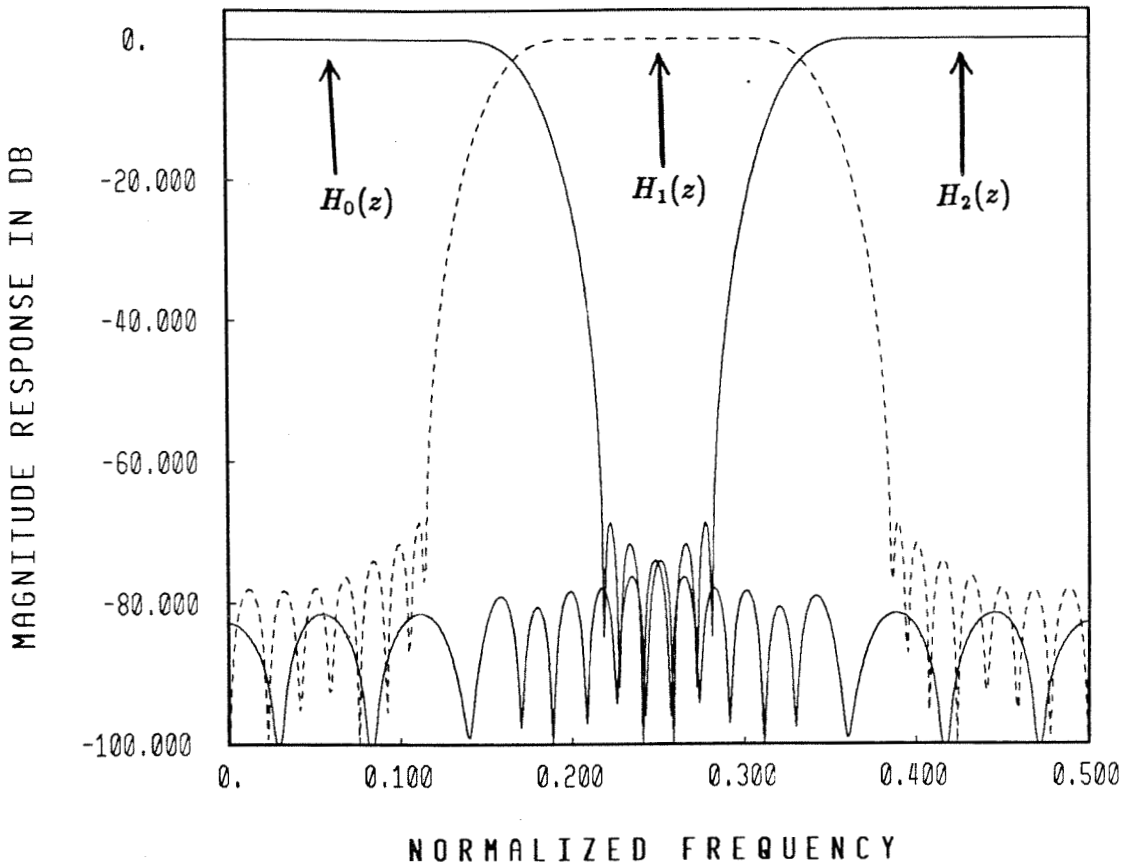

Fig. 1.4. Frequency response plots of the optimized analysis filters where mirror-image conditions are imposed.

conventional filter banks are also studied. A table of the analysis filter coefficients for several sets of specifications are given at the end of the chapter for future use. The linear-phase PR systems are addressed in Chapter 4. Here, we will show that for a particular M (number of channels), there are many feasible classes of linear-phase PR systems. We study extensively one of these classes for the case of two and three channels. Consequently, explicit lattice structures for these linear-phase PR filter banks are derived. Design examples and comparisons with approximate PR systems are also studied.

In the initialization of the lattice sections in a PR system, we use the concept of an eigenfilter. Appendix A elaborates on the design and applications of eigenfilters in both normal and multirate digital-signal processing. Basically, eigenfilters are linear-phase FIR filters with minimum stopband and passband errors in energies (to be elaborated). An eigenfilter's coefficients come from the eigenvector corresponding to the minimum eigenvalue of a particular, real, symmetric, and positive definite matrix. In terms of optimality and design time, eigenfilters perform no worse than filters designed using the equiripple method [62,92]. Appendix B concentrates on a new method to design half-band filters, which find application in multirate signal processing in the form of decimation and interpolation filters. A comparison with the conventional approach is also made.

Notations used in the thesis: The variable ω is used as frequency variable, whereas the term "normalized frequency" is used to denote $f = \omega/2\pi$. The frequency response of a transfer function $H(z)$ is expressed as $H(e^{j\omega}) = |H(e^{j\omega})|e^{j\phi(\omega)}$, where $|H(e^{j\omega})|$ is the magnitude response and $\phi(\omega)$ the phase response. The quantity $\tau(\omega) = -d\phi(\omega)/d\omega$ is the group delay of $H(z)$. If $|H(e^{j\omega})|$ is constant for all ω, $H(z)$ is allpass. If $\phi(\omega)$ has the form $k_0 - k_1\omega$, then $H(z)$ is said to have lin-

ear phase and the group delay is a constant k_1; physically, if the input to such a filter $H(z)$ has energy only in the passband of $H(z)$, then the output is a delayed version of the input, by k_1 samples. Unless mentioned otherwise, a lowpass filter has real coefficients so that $|H(e^{j\omega})|$ is symmetric and $\phi(\omega)$ is antisymmetric with respect to $\omega = 0$. Usually $|H(e^{j\omega})|$ is plotted for $0 \leq f \leq 0.5$ (i.e., for $0 \leq \omega \leq \pi$), since $|H(e^{j\omega})| = |H(e^{j(2\pi-\omega)})|$ for $\pi \leq \omega \leq 2\pi$. $H(z)$ is a spectral factor of $G(z)$ if $G(z) = H(z)H(z^{-1})$. FIR and IIR are abbreviations for *finite impulse response* and *infinite impuse response*, respectively.

We say "$H(z)$ is symmetric" if the impulse response $h(n)$ of $H(z)$ is symmetric, and so on. The center of a linear phase FIR transfer function is defined to be the center of symmetry or antisymmetry of $h(n)$. Clearly, the center of $H(z)$ could be either an integer or an odd multiple of $(1/2)$. The mirror image of $H(z)$, denoted by $\hat{H}(z)$, is defined as $\hat{H}(z) \triangleq z^{-(N-1)}H(z^{-1})$. Here, $h(N-1)$ is the highest nonzero coefficient of $H(z)$, and $N-1$ is called the degree of $H(z)$.

Bold-faced quantities denote matrices and vectors, as in $\mathbf{A}$, $\mathbf{H}(z)$, etc. The symbol $\mathbf{I}_k$ denotes the $k \times k$ identity matrix (with subscript often omitted). The quantities $\mathbf{A}^T$, $\mathbf{A}^\dagger$ and $\mathbf{A}^*$ denote the transpose, transpose-conjugate, and conjugate of $\mathbf{A}$, respectively. For functions $\mathbf{H}(z)$, the notation $\mathbf{H}_*(z)$ denotes conjugation of the coefficients without conjugating z. For example, if $H(z) = a + bz^{-1}$, then $H_*(z) = a^* + b^*z^{-1}$. Thus, $\mathbf{H}^*(z) = \mathbf{H}_*(z^*)$. The notation $\widetilde{\mathbf{H}}(z)$ stands for $\mathbf{H}_*^T(z^{-1})$. In other words, conjugate the coefficients, take transpose (if matrix) and replace z with z^{-1}. When $z = e^{j\omega}$ (i.e., on the unit circle), we have $\widetilde{\mathbf{H}}(z) = \mathbf{H}^\dagger(z)$. A $p \times r$ matrix $\mathbf{A}$ is said to be unitary (orthogonal if it is real), if $\mathbf{A}^\dagger\mathbf{A} = c\mathbf{I}_r$, $c \neq 0$. The degree of a $p \times M$ system (also called McMillian degree [57]) $\mathbf{H}(z)$ is equal to the number of scalar delays (i.e., z^{-1} building blocks) required to implement it. The

symbol W_M stands for $e^{-j2\pi/M}$. The subscript M is usually deleted because its value is often clear from the context. This quantity appears in the definition of a discrete Fourier Transform (DFT) [95],[96]. Thus, an M-point sequence $[x_0, x_1, \ldots, x_{M-1}]$ has the M-point DFT sequence

$$X_k = \sum_{k=0}^{M-1} x_n W^{kn}, \quad 0 \leq k \leq M-1. \tag{1.2}$$

The inverse DFT (IDFT) is given by

$$x_n = \frac{1}{M} \sum_{k=0}^{M-1} X_k W^{-nk}. \tag{1.3}$$

The most crucial property of W, which finds repeated use in multirate signal processing, is the following:

$$\sum_{k=0}^{M-1} W^{kn} = \begin{cases} M, & k = \text{multiple of } M \\ 0, & \text{otherwise.} \end{cases} \tag{1.4}$$

For any pair of integers k, n we have $W^k = W^n$ if and only if $k - n$ is an integer multiple of M. In particular, therefore, $W^k \neq W^n$ for $0 \leq k < n \leq M-1$.

CHAPTER II
BASIC BUILDING BLOCKS AND VARIOUS RESULTS ON DIGITAL FILTER BANKS

In this section, we introduce the decimator and interpolator along with their frequency-domain characteristics, and interconnection behavior. Furthermore, the polyphase decomposition, a tool for analyzing digital filter banks, is also studied. This representation yields the polyphase transfer matrices associated with both analysis and synthesis filter banks. Consequently, the necessary and sufficient condition for which the filter bank in Fig. 1.2(b) is a PR system can be derived [7]. For FIR structures, a necessary and sufficient condition for them to be PR is that the determinants of their polyphase transfer matrices are delays. Structures in which their polyphase transfer matrices are lossless [7], [97] are special cases. These lossless filter banks are parameterized by a set of rotation angles [37]. Thus, by constraining the structure to be lossless, we can search for a set of rotation angles, which yields filters with good responses as in Fig. 1.2(c). This procedure is as complicated as finding a way down the Himalayas blind-folded, with a stick. This Himalayan task will be easier if one can start near the ground and search for the way down. Therefore, given any filter $H_k(z)$, if we can somehow initialize the lattice coefficients, then only a few iterations are needed to obtain the optimal result. We will elaborate on this procedure in this chapter. This initialization procedure is the backbone for the fast design of PR systems.

2.1. Decimator and interpolator

Fig. 2.1 shows block diagrams of these building blocks. The decimator is char-

acterized by the following input-output relation

$$y_D(n) = x(Mn), \tag{2.1}$$

which says that the output at time n is equal to the input at time Mn. As a consequence, only the input samples with a sample number equal to a multiple of M are retained. This sampling rate reduction by a factor of M is demonstrated in Fig. 2.2(b) for the case of $M = 3$. Since decimation corresponds to compression in the time domain, one might expect a stretching effect in the frequency domain. To be more precise, the z-transform of $y_D(n)$ is given by [2]

$$Y_D(z) = \frac{1}{M} \sum_{k=0}^{M-1} X(z^{1/M} W^k). \tag{2.2}$$

On the unit circle, (i.e., $z = e^{j\omega}$), $Y_D(e^{j\omega})$ is such that $MY_D(e^{j\omega}) = \sum_{k=0}^{M-1} X(e^{j(\omega - 2k\pi)/M})$. The term with $k = 0$ is indeed the M-fold stretched version of $X(e^{j\omega})$. The remaining $(M-1)$ terms with $k > 0$ are uniformly shifted versions of this stretched version. Fig. 2.3(b) demonstrates this effect for $M = 3$. The $(M-1)$ terms with $k > 0$ are called the aliasing terms, since they involve the shifted version of $X(e^{j\omega})$. As long as $x(n)$ is bandlimited to $|\omega| < \pi/M$, there is no overlap of these terms with the $k = 0$ term.

On the other hand, the L-fold interpolator is characterized by the input-output relation

$$y_I(n) = \begin{cases} x(\frac{n}{L}) & ; \text{if } n \text{ is a multiple of } L \\ 0 & ; \text{otherwise.} \end{cases} \tag{2.3}$$

The output $y_I(n)$ is obtained by inserting $(L-1)$ zero-valued samples between adjacent samples of $x(n)$, as demonstrated in Fig. 2.2(c). The z-transform of the interpolator ouput $y_I(n)$ is given by [2]

$$Y_I(z) = X(z^L). \tag{2.4}$$

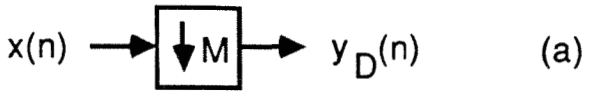

The M-fold decimator.

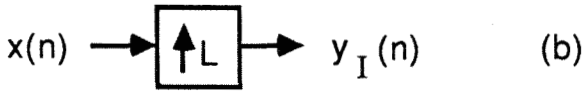

The L-fold interpolator.

Fig. 2.1 The decimator and interpolator building blocks.

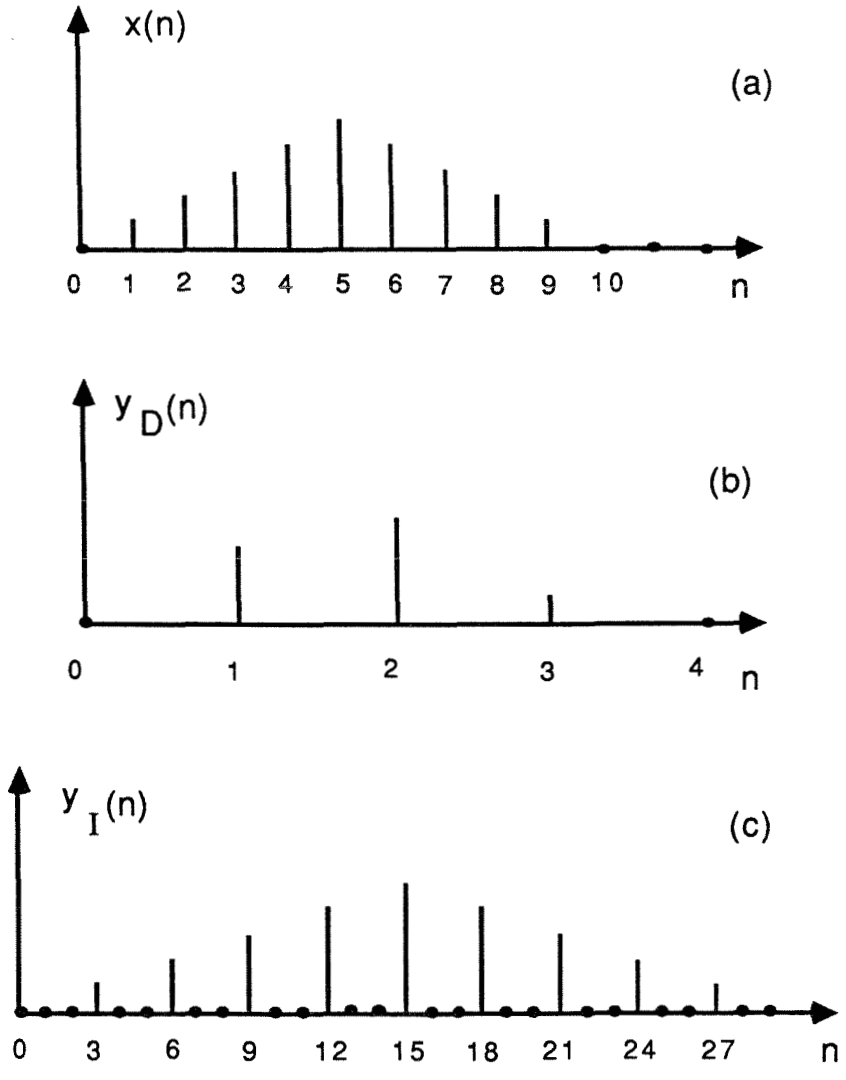

Fig. 2.2 Demonstration of decimation for M=3 and interpolation for L=3.

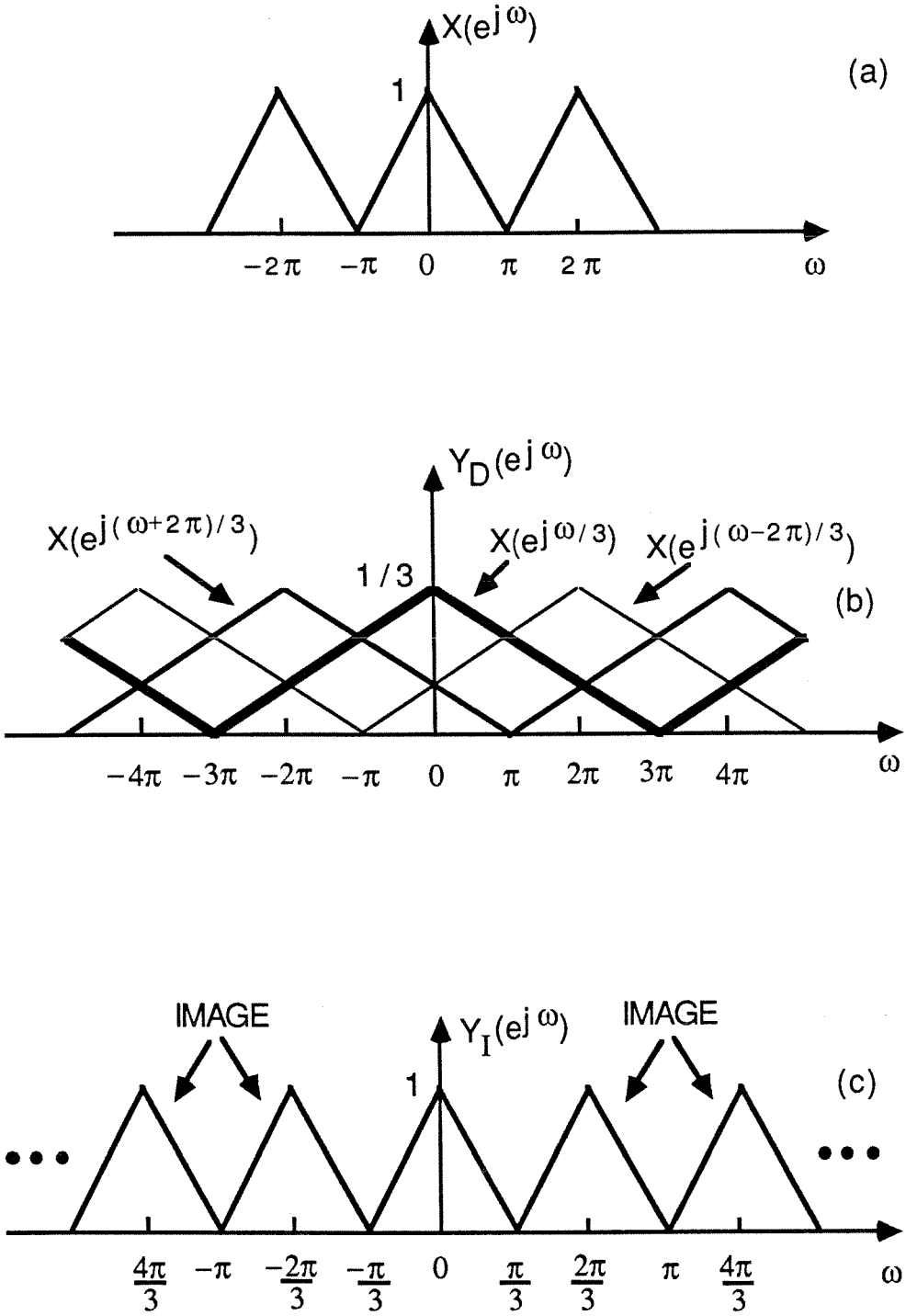

Fig. 2.3 Transform-domain effects of decimation and interpolation.

On the unit circle, $Y_I(e^{j\omega}) = X(e^{j\omega L})$, which implies that $Y_I(e^{j\omega})$ is an L-fold compressed version of $X(e^{j\omega})$ as demonstrated in Fig. 2.3(c). The multiple copies of the basic spectrum in Fig. 2.3(c) are images created by the interpolator.

Interpolator and decimation are linear systems, but are time-variant [2]. Cascades of decimators and interpolators, as in Fig. 2.4 are often encountered in filter-bank systems. We can verify that

$$y(n) = \begin{cases} x(n); & n \text{ multiple of } M \\ 0; & \text{otherwise,} \end{cases} \tag{2.5}$$

and the transform domain relation is (by using both (2.2) and (2.4)):

$$Y(z) = \frac{1}{M} \sum_{k=0}^{M-1} X(zW^k), \tag{2.6}$$

which in turn means that $MY(e^{j\omega})$ is the sum of $X(e^{j\omega})$ with the $(M-1)$ uniformly shifted versions $X(e^{j(\omega - 2k\pi/M)})$.

Let us now study cascades of a decimator or an interpolator and a transfer function as shown in Fig. 2.5, since these forms of cascades are used in the filter bank (see Fig. 1.2(b)). The identity in Fig. 2.5(a) can be proved based on (2.2), provided that $G(z)$ is a rational transfer function (i.e., a ratio of polynomials in z^{-1}). In a similar manner, the two cascades in Fig. 2.5(b) are equivalent (provided that $G(z)$ is rational) as can be proved from (2.4). These identities are very valuable in many applications for efficient implementation of filters and filter banks.

2.2. Polyphase decomposition (representation)

We shall now represent the filters in "polyphase form" [2], [17] for convenience. Suppose each of the analysis filters $H_k(z)$ is represented as

$$H_k(z) = \sum_{\ell=0}^{M-1} z^{-\ell} E_{k,\ell}(z^M). \tag{2.7}$$

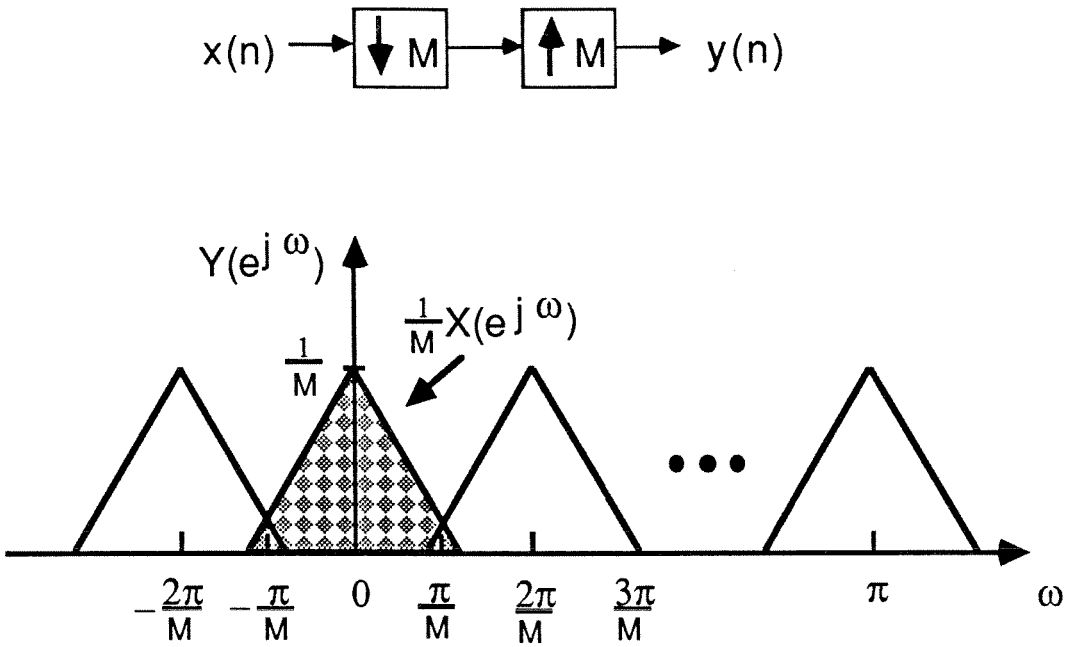

Fig. 2.4 The effect of decimation followed by interpolation.

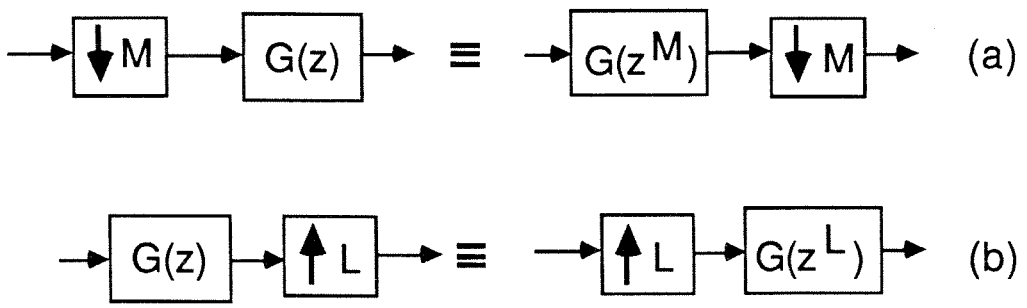

Fig. 2.5. Identities for multirate systems.

Similarly, let each synthesis filter $F_k(z)$ be represented as

$$F_k(z) = \sum_{\ell=0}^{M-1} z^{-(M-1-\ell)} R_{\ell,k}(z^M). \tag{2.8}$$

Note that given $H_k(z)$ and $F_k(z)$, the above representations are always possible. We can collect the two equations for all $H_k(z)$ and $F_k(z)$ in a matrix form as follows:

$$\begin{pmatrix} H_0(z) \\ \vdots \\ H_{M-1}(z) \end{pmatrix} = \begin{pmatrix} E_{0,0}(z^M) & \dots & E_{0,M-1}(z^M) \\ \vdots & \ddots & \vdots \\ E_{M-1,0}(z^M) & \dots & E_{M-1,M-1}(z^M) \end{pmatrix} \begin{pmatrix} 1 \\ \vdots \\ z^{-(M-1)} \end{pmatrix} \tag{2.9}$$

and

$$\begin{pmatrix} F_0(z) & \dots & F_{M-1}(z) \end{pmatrix} = \begin{pmatrix} z^{-(M-1)} & \dots & 1 \end{pmatrix} \begin{pmatrix} R_{0,0}(z^M) & \dots & R_{0,M-1}(z^M) \\ \vdots & \ddots & \vdots \\ R_{M-1,0}(z^M) & \dots & R_{M-1,M-1}(z^M) \end{pmatrix} \tag{2.10}$$

With this representation, we can always redraw [7] Fig. 1.2(b) in the form of Fig. 2.6, where $\mathbf{E}(z) = [E_{k,\ell}(z)]; 0 \le k, \ell \le M-1$ and $\mathbf{R}(z) = [R_{\ell,k}(z)], 0 \le k, \ell \le M-1$. Fig. 2.6 is precisely the polyphase representation of the filter bank in Fig. 1.2(b). We can employ the identities in Fig. 2.5(a) and (b) to move the decimator and interpolator, resulting in Fig. 2.7(a). It is clear that if the filters $H_k(z)$ and $F_k(z)$ are such that

$$\mathbf{R}(z)\mathbf{E}(z) = z^{-K}\mathbf{I}, \tag{2.11}$$

then the system in Fig. 2.7(a) becomes Fig. 2.7(b), which is a PR system. The sets of filters $H_k(z)$ and $F_k(z)$, which satisfy (2.11), are called sets of PR filters. Given an FIR polyphase transfer matrix $\mathbf{E}(z)$, the obvious choice of $\mathbf{R}(z)$ which satisfies (2.11) is

$$\mathbf{R}(z) = z^{-K}\mathbf{E}^{-1}(z). \tag{2.12}$$

The above choice of $\mathbf{R}(z)$, in general, yields IIR synthesis filters. Furthermore, the resulting synthesis bank might not be stable for any choice of $\mathbf{E}(z)$. In order to ensure stability for the synthesis filter bank, $\mathbf{E}(z)$ is such that its determinant is

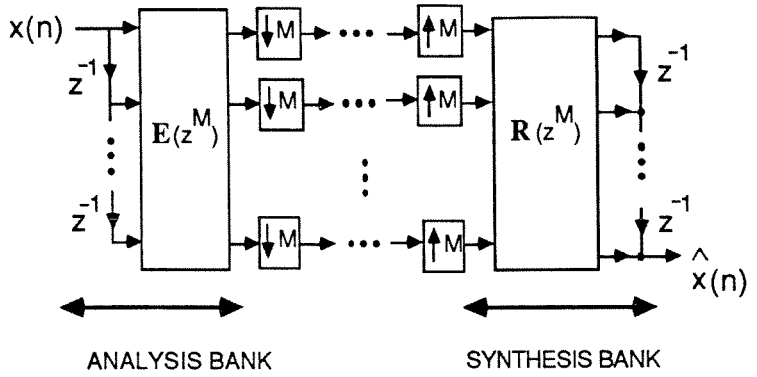

Fig. 2.6. The polyphase representation of the filter bank in Fig. 1.2(b).

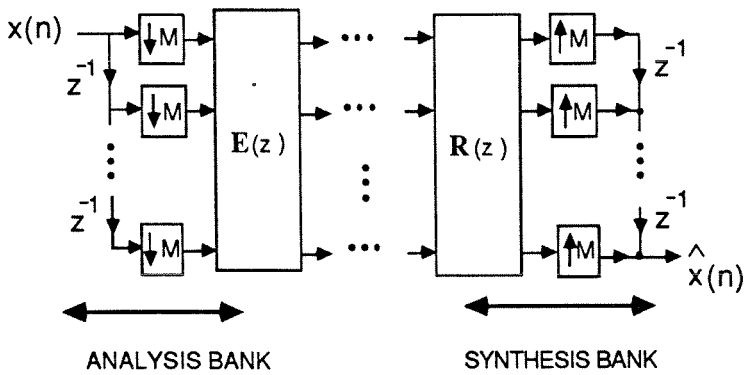

Fig. 2.7(a). Equivalent filter bank for Fig. 2.6.

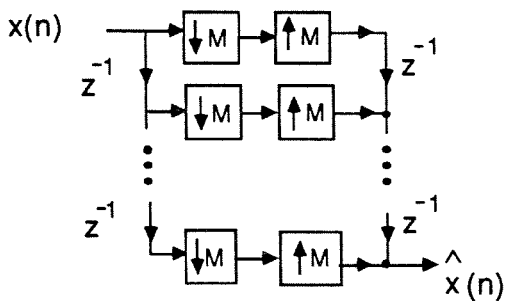

Fig. 2.7(b). Equivalent structure of Fig. 2.7(a) where $\mathbf{R}(z)\mathbf{E}(z) = \mathbf{I}$.

a minimum-phase polynomial (all zeros are inside the unit circle). On the other hand, if *only* FIR filter banks are permitted, then for a PR system, the determinant of $\mathbf{E}(z)$ has to be a delay (within a scale factor). A subclass of FIR matrices for which the determinant of $\mathbf{E}(z)$ is a delay is the family of lossless matrices [7], [99]. In order to design FIR PR QMF banks systematically, we now turn attention to this family.

2.3. Discrete-time lossless systems:

A transfer function $\mathbf{H}(z)$ is said to be lossless [16], [99] if for all z

$$\widetilde{\mathbf{H}}(z)\mathbf{H}(z) = c\mathbf{I}, \tag{2.13}$$

where $c \neq 0$. On the unit circle ($z = e^{j\omega}$), $\mathbf{H}(z)$ is unitary; i.e., $\mathbf{H}^{\dagger}(e^{j\omega})\mathbf{H}(e^{j\omega}) = c\mathbf{I}$. Thus, a constant unitary matrix is a trivial example of a lossless system. A causal stable allpass function $\mathbf{H}(z)$ is also another example of a lossless system since by definition, $|H(e^{j\omega})| =$ constant. Lossless examples with $p = r = 2$ are the 2×2 orthogonal matrix $\begin{pmatrix} 1 & -\alpha \\ \alpha & 1 \end{pmatrix}$ and the matrix $\begin{pmatrix} 1 & 0 \\ 0 & z^{-1} \end{pmatrix}$.

To explain the concept of the lossless system physically, let us consider a $p \times r$ system with transfer function $\mathbf{H}(z)$. This system has r-inputs and p-outputs, denoted by the vectors $\mathbf{u}(n)$ and $\mathbf{y}(n)$, respectively. The input and output energies are defined respectively as $E_{\mathbf{u}} = \sum_{n=-\infty}^{\infty} \mathbf{u}^{\dagger}(n)\mathbf{u}(n)$ and $E_{\mathbf{y}} = \sum_{n=-\infty}^{\infty} \mathbf{y}^{\dagger}(n)\mathbf{y}(n)$. A lossless system has the property that $E_{\mathbf{y}} = cE_{\mathbf{u}}$ where $c \neq 0$. Note that if $c = 1$, then $E_{\mathbf{y}} = E_{\mathbf{u}}$, or in other words, the output energy is the same as the input energy. Thus, the system does not dissipate any energy, thereby justifying the name "lossless system."

When $p = r$, the inverse of a FIR transfer matrix is obtained from (2.13),

$$\mathbf{H}^{-1}(z) = \frac{\widetilde{\mathbf{H}}(z)}{c}. \tag{2.14}$$

Therefore, $\mathbf{H}(z)$ satisfies the property that $\det \mathbf{H}(z) = dz^{-K}$, where K is an integer and d is a constant [37], [97]. In other words, the inverse is not only guaranteed to exist, but can be found from $\mathbf{H}(z)$ simply by writing $\widetilde{\mathbf{H}}(z)$. For example, let

$$\mathbf{H}(z) = \begin{pmatrix} 1 & 1 \\ 1 & -1 \end{pmatrix} \begin{pmatrix} 1 & 0 \\ 0 & z^{-1} \end{pmatrix} \begin{pmatrix} 1 & 1 \\ 1 & -1 \end{pmatrix} = \begin{pmatrix} 1+z^{-1} & 1-z^{-1} \\ 1-z^{-1} & 1+z^{-1} \end{pmatrix}. \tag{2.15}$$

$\mathbf{H}(z)$ is therefore lossless since it is a cascade of lossless systems. The inverse is given by

$$\mathbf{H}^{-1}(z) = \widetilde{\mathbf{H}}(z) = \frac{1}{2} \begin{pmatrix} 1 & 1 \\ 1 & -1 \end{pmatrix} \begin{pmatrix} 1 & 0 \\ 0 & z \end{pmatrix} \frac{1}{2} \begin{pmatrix} 1 & 1 \\ 1 & -1 \end{pmatrix} = \frac{1}{4} \begin{pmatrix} 1+z & 1-z \\ 1-z & 1+z \end{pmatrix}. \tag{2.16}$$

It is clear from (2.14) that $\mathbf{H}^{-1}(z)$ is lossless if and only if $\mathbf{H}(z)$ is lossless. In order to physically realize the above transfer matrix $\mathbf{H}^{-1}(z)$, we will need to make it causal by multiplying $\mathbf{H}^{-1}(z)$ to a delay; i.e.,

$$z^{-1}\mathbf{H}^{-1}(z) = \frac{1}{4} \begin{pmatrix} 1+z^{-1} & -1+z^{-1} \\ -1+z^{-1} & 1+z^{-1} \end{pmatrix}. \tag{2.17}$$

2.4. Use of lossless system in digital filter bank design.

Returning to the filter bank in Fig. 2.7(a), let us restrict $\mathbf{E}(z)$ to be real-coefficient, FIR and lossless and choose $\mathbf{R}(z)$ as

$$\mathbf{R}(z) = z^{-K}\widetilde{\mathbf{E}}(z) = cz^{-K}\mathbf{E}^{-1}(z), \tag{2.18}$$

so that PR is guaranteed. The delay z^{-K} ensures causality of the synthesis bank. For example, if $\mathbf{E}(z)$ is as in (2.15), then $\mathbf{R}(z)$ should be as in (2.17). With the above choice of $\mathbf{E}(z)$ and $\mathbf{R}(z)$ as in (2.15) and (2.17), the analysis filters $H_k(z)$ and the synthesis filters $F_k(z)$ obtained from (2.9) and (2.10) are:

$$H_0(z) = 1 + z^{-1} + z^{-2} - z^{-3}, \quad H_1(z) = 1 + z^{-1} - z^{-2} + z^{-3}, \tag{2.19}$$

and

$$F_0(z) = -1 + z^{-1} + z^{-2} + z^{-3}, \quad F_1(z) = 1 - z^{-1} + z^{-2} + z^{-3}. \tag{2.20}$$

Thus, a simple choice of lossless $\mathbf{E}(z)$ results in a FIR PR filter bank.

Any arbitrary choice of lossless $\mathbf{E}(z)$ does not necessarily yield good filters as evidenced from (2.19) and (2.20). These filters are only third-order filters. Therefore, one needs a systematic procedure to design good filters $H_k(z)$ and $F_k(z)$ and at the same time guarantee that $\mathbf{E}(z)$ is lossless. Naturally, the better the filter performance, the higher the order of the required filter. Thus, given any order $\mathbf{E}(z)$, if we can come up with a structure that spans all lossless $\mathbf{E}(z)$ with that order, then by optimizing the parameters of this structure, we might be able to obtain good filters.

A structural representation for lossless $\mathbf{E}(z)$, developed in [15], [37] is shown in Fig. 2.8. This is a cascade of N (real) orthogonal matrices $\mathbf{K}_k; 0 \leq k \leq N-1$, separated by diagonal matrices of the form

$$\Lambda(z) = \begin{pmatrix} 1 & 0 & \dots & 0 & 0 \\ 0 & 1 & \dots & 0 & 0 \\ \vdots & \vdots & \ddots & \vdots & \vdots \\ 0 & 0 & \dots & 1 & 0 \\ 0 & 0 & \dots & 0 & z^{-1} \end{pmatrix}. \tag{2.21}$$

Recall that an arbitrary $M \times M$ real orthogonal matrix requires $\binom{M}{2}$ parameters (rotation angles) for complete characterization. The $N-1$ matrices $\mathbf{K}_k, 0 \leq k \leq N-2$ are special types of orthogonal matrices with $M-1$ planar rotation operators of the form $\begin{pmatrix} \cos\theta & \sin\theta \\ \sin\theta & -\cos\theta \end{pmatrix}$. The rightmost matrix $\mathbf{K}_{N-1}$, on the other hand, is a general orthogonal matrix characterized by $\binom{M}{2}$ planar rotations as in Fig. 2.9(b). It is shown in [37] that every real-coefficient FIR lossless system $\mathbf{E}(z)$ of degree $N-1$ can be represented as in Fig. 2.8(b) with matrices as in Fig. 2.9. Conversely,

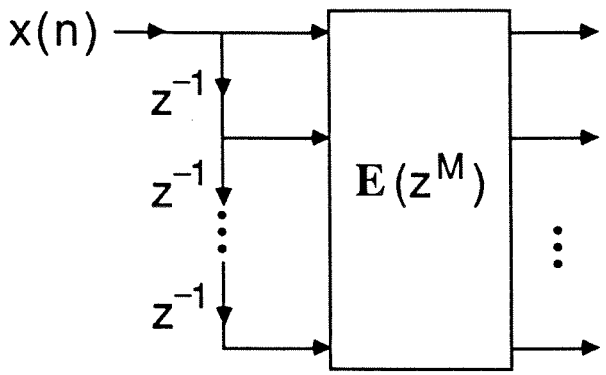

(a)

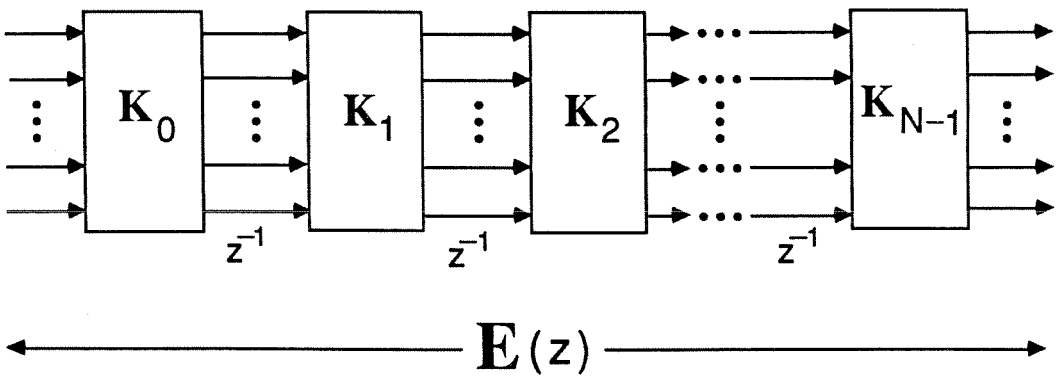

(b)

Fig. 2.8. Implementation of FIR lossless $\mathbf{E}(z)$ as a cascade of unitary matrices seperated by delays.

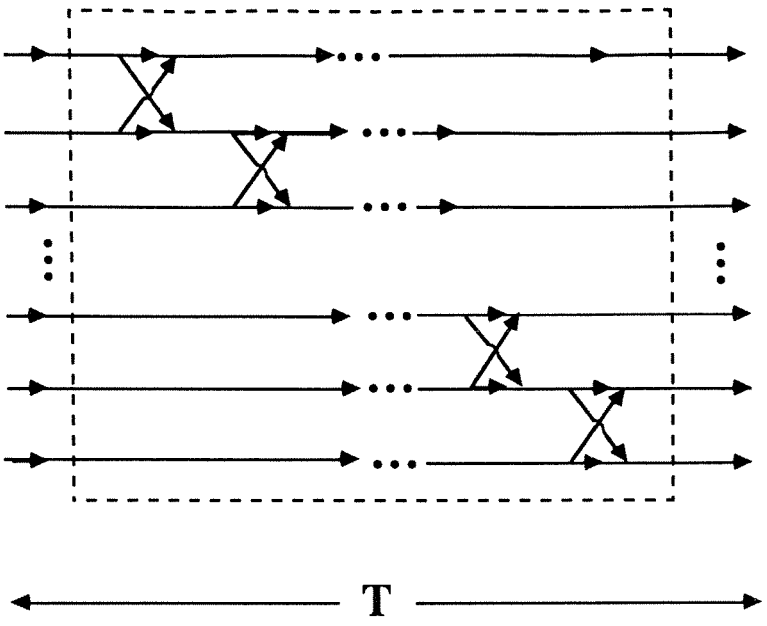

Stages 0 to N-2

(a)

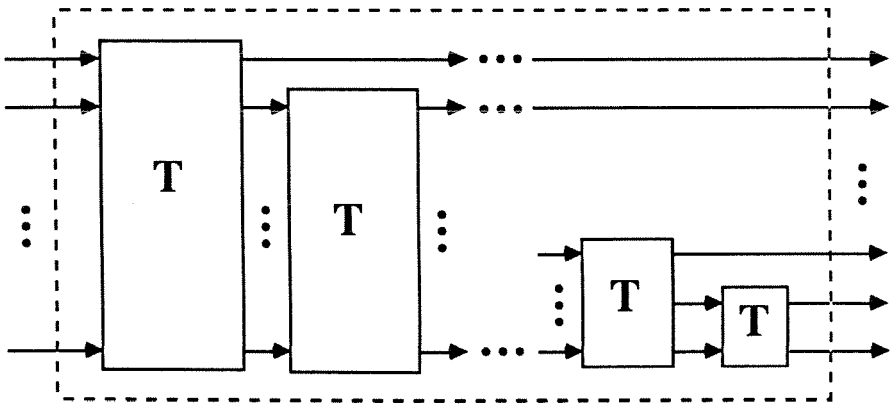

Stage N-1

(b)

Fig. 2.9. Details of the building blocks in Fig. 2.8(b).

the structure in Fig. 2.8(b) with matrices as in Fig. 2.9 necessarily represents a real-coefficient FIR lossless system. Thus, the angles in Fig. 2.9 form a complete set for characterizing real-coeficient FIR lossless $\mathbf{E}(z)$. Moreover, the representation in Fig. 2.8(b) is canonic (i.e., minimal) in number of delays, and in number of planar rotation parameters.

The total number of planar rotations in Fig. 2.8(b) is

$$N_p = (M-1)(N-1) + \binom{M}{2}, \tag{2.22}$$

and the maximum length of an analysis filter with this setup is

$$L = M(N-1) + M - 1. \tag{2.23}$$

The number of parameters N_p clearly grows linearly with respect to L and quadratically with respect to M. For example, with $M = 3$ and analysis filters of length 56, we have $N_p = 39$. Let us define an objective function related to the error in the analysis filter bank as

$$\phi = \sum_{k=0}^{M-1} \int_{k^{th}\,stopband} |H_k(e^{j\omega})|^2 d\omega. \tag{2.24}$$

For lossless $\mathbf{E}(z)$, the analysis filters $H_k(z)$ satisfy the power-complementary property as in (1.1) [7]. Thus, it is sufficient to include in ϕ only the stopbands of $H_k(z)$. Notice that in terms of the rotation angles in Fig. 2.8(b), the objective function in (2.24) is highly nonlinear. We thus have a formidable task in optimizing these rotation angles to yield analysis filters $H_k(z)$, which minimize the above objective function.

It is shown in [36] that if we can make an initial guess of any analysis filters of length L, say $H_0(z)$, then all of N_p parameters except

$$N_f = \binom{M}{2} - (M-1) \tag{2.25}$$

parameters can be initialized based on $H_0(z)$. Thus, once $H_0(z)$ is known, only N_p parameters are still underdetermined in Fig. 2.8(b). Eq. (2.25) therefore measures the number of degrees of freedom available for the design of $H_k(z), 1 \leq k \leq M-1$, once $H_0(z)$ has been fixed. In other words, losslessness in $\mathbf{E}(z)$ puts a constraint on $H_k(z), k \neq 0$ once $H_0(z)$ is fixed.

For instance, with $M = 2$, we have $N_f = 0$, which shows that we have no freedom of choice of $H_1(z)$, once $H_0(z)$ is fixed. This is consistent with the earlier observations [5], [7], [19] that for the $M = 2$ case, losslessness of $\mathbf{E}(z)$ completely constrains $H_1(z)$ to be $H_1(z) = z^{-(L-1)}H_0(-z^{-1})$. For the $M = 3$ case, $N_f = 1$, so that, once $H_0(z)$ is fixed, only one degree of freedom can be exercised in choosing $H_1(z)$ and $H_2(z)$. It is important to realize that N_f is independent of the filter length L. Consequently, if $H_0(z)$ is known, we have to optimize only the remaining N_f parameters, regardless of filter length, to obtain $H_k(z), 1 \leq k \leq M-1$. In practice, however, we have the option of reoptimizing all the parameters after initializing of a subset of parameters based on the initial choice of $H_0(z)$.

In order to exploit this to our advantage, it is first necessary to find an appropriate initialization for $H_0(z)$, which is the purpose of this section. We can mathematically express $H_0(z)$ as

$$H_0(z) = [1 \;\; z^{-1} \;\; \ldots \;\; z^{-(M-1)}]\mathbf{e}_0(z^M), \tag{2.26}$$

where $\mathbf{e}_0^T(z)$ is the 0^{th} row of $\mathbf{E}(z)$. By replacing z with zW^{-k} for $0 \leq k \leq M-1$, we can arrive at M equations like (2.26). Stacking these filters together, we obtain

$$\begin{pmatrix} H_0(z) \\ H_0(zW^{-1}) \\ \vdots \\ H_0(zW^{-(M-1)}) \end{pmatrix} = \mathbf{W}\mathbf{\Lambda}(z)\mathbf{e}_0^T(z^M), \tag{2.27}$$

where $\mathbf{W}$ is the $M \times M$ DFT matrix and $\Lambda(z)$ is the diagonal matrix of delays

$$\Lambda(z) = \begin{pmatrix} 1 & 0 & \dots & 0 \\ 0 & z^{-1} & \dots & 0 \\ \vdots & \vdots & \ddots & 0 \\ 0 & 0 & \dots & z^{-(M-1)} \end{pmatrix}. \tag{2.28}$$

Since $\mathbf{E}(z)$ is lossless, the vector $\mathbf{e}_0(z)$ is lossless. The matrices $\mathbf{W}$ and $\Lambda(z)$ are clearly lossless; therefore, the product in (2.27) is lossless; i.e.,

$$\sum_{k=0}^{M-1} \widetilde{H}_0(zW^{-k}) H_0(zW^{-k}) = c, \tag{2.29}$$

where $c \neq 0$. This proves that $G_0(z) = \widetilde{H}_0(z)H_0(z)$ is an M^{th}-band filter. Recall that an M^{th}-band filter $G_0(z)$ satisfies the condition $\sum_{k=0}^{M-1} G_0(zW^{-k}) = c$. In other words, $H_0(z)$ is a spectral factor of an M^{th}-band filter. It can then be verified that $\mathbf{e}_0(z)$ is lossless [36]. Let $N-1$ denote the degree of $\mathbf{e_0}$; then $\mathbf{e}_0(z)$ can be represented as [36]

$$\mathbf{e}_0(z) = \mathbf{U}(z)\mathbf{P}_0, \tag{2.30}$$

where $\mathbf{U}(z) = \mathbf{U}_{N-1}(z)\mathbf{U}_{N-2}(z)\dots\mathbf{U}_2(z)\mathbf{U}_1(z)$ and $\mathbf{P}_0$ is a $M \times 1$ unit-norm vector. If we construct an unitary matrix

$$\mathbf{H}_0 = [\mathbf{P}_0\mathbf{P}_1\dots\mathbf{P}_{M-1}] \tag{2.31}$$

by using the Gram-Shmidt procedure, starting with the 0^{th} column to be $\mathbf{P}_0$, then the $M \times M$ FIR system

$$\mathbf{S}(z) = \mathbf{U}(z)\mathbf{H}_0 \tag{2.32}$$

is clearly lossless of degree $N-1$. By defining $\mathbf{E}(z) \triangleq \mathbf{S}^T(z)$, we obtain the FIR analysis filters $H_k(z)$ according to Fig. 2.8(a). This shows that once a spectral factor $H_0(z)$ of an M^{th}-band filter $G_0(z)$ is obtained, it is easy to find a set of $M-1$ analysis filters $H_k(z)$, $1 \leq k \leq M-1$ of the perfect-reconstruction system. The number of freedoms in the above construction of $H_k(z)$ is exactly the number of

freedoms available in constructing an $M \times M$ orthogonal matrix when a column is fixed. This number is

$$N_f = \binom{M}{2} - (M-1). \tag{2.33}$$

As shown in [36], this technique covers every possible set of causal FIR filter $H_k(z)$, $0 \leq k \leq M-1$, provided that the degree of $H_0(z)$ is $(M(N-1)+M-1)$. In other words, $H_0(z)$ is assumed to have the maximal possible degree in the structure of Fig. 2.8(a). Since this is a reasonable assumption in practice, we will assume it unless mentioned otherwise.

The design procedure based on the above results would typically run as follows [36]: First design a linear-phase FIR M^{th}-band filter $G_0(z)$ with nonnegative amplitude response. Then identify a spectral factor of $G_0(z)$ and label it as one of the analysis filters, say $H_0(z)$. These two steps can be designed using the eigenfilter method described in Appendix A. The choice of the length of $G_0(z)$, of course, depends on the attenuation requirement of $H_0(z)$. Next, figure out the polyphase-component vector $\mathbf{e}_0(z)$, using (2.26). This is guaranteed to be LBR. Synthesize it in the form (2.30), and using the Gram-Schmidt procedure to construct an orthogonal matrix $\mathbf{H}_0$ as described in (2.31). The polyphase transfer matrix $\mathbf{E}(z)$ is chosen such that $\mathbf{E}(z) = \mathbf{S}^T(z)$, where $\mathbf{S}(z)$ is as in (2.32). This process initializes all except N_f parameters in $\mathbf{H}_0$. Optimize the remaining N_f rotation angles θ_k to minimize the stopband energies of $H_k(z), 1 \leq k \leq M-1$.

The response of $H_0(z)$ is usually very good. The responses of the other filters, after optimization, however, are usually much worse than that of $H_0(z)$. Therefore, it is judicious to optimize not only the remaining N_f rotation angles, but all N_p of them so that all filters (including $H_0(z)$) tend to come out equally good. This, of course, takes a longer computation time, but is still much faster than the "random

initialization" used in [7].

In Chapter 3, we study the PR structure, which yields pairwise-mirror image filters $H_k(z)$ and $F_k(z)$. Since this structure can also be chosen to be lossless, we will apply the above initialization approach to design the filter bank. For $M = 3$, the filter $H_1(z)$ (rather than $H_0(z)$) was obtained as a spectral factor of a 3^{rd}-band linear-phase filter. All N_p parameters are then optimized to minimize the objective function in (2.24). Compared to the earlier method [7], [19], the new method converges very fast and always leads to much improved attenuation characteristics for a given filter length. The analysis filters $H_k(z)$ in Fig. 1.4 are designed using this method.

CHAPTER III
MAXIMALLY DECIMATED PR FIR FILTER BANKS WITH PAIRWISE MIRROR IMAGE ANALYSIS (AND SYNTHESIS) FREQUENCY RESPONSES

As discussed in the previous chapters, any perfect reconstruction structure with lossless $\mathbf{E}(z)$ can be realized as a cascade of lossless systems; i.e.,

$$\mathbf{E}(z) = \mathbf{K}_{N'-1}\Lambda_{N'-2}(z)\ldots\Lambda_0(z)\mathbf{K}_0, \tag{3.1}$$

where $\mathbf{K}_i$ are constant unitary matrices, i.e., $\mathbf{K}_i^{\dagger}\mathbf{K}_i = \mathbf{I}, 0 \leq i \leq N'-1$, and

$$\Lambda_i(z) = \begin{pmatrix} 1 & 0 & \ldots & 0 & 0 \\ 0 & 1 & \ldots & 0 & 0 \\ \vdots & \vdots & \ddots & \vdots & \vdots \\ 0 & 0 & \ldots & 1 & 0 \\ 0 & 0 & \ldots & 0 & z^{-1} \end{pmatrix}.$$

Since we consider only real coefficient QMF banks, thus $\mathbf{K}_i$ are real orthogonal matrices, that can be realized by a sequence of $\binom{M}{2}$ planar rotations [7,9]. The filters $H_k(z)$ of the analysis bank in Fig. 3.1(a) are automatically guaranteed [7] to satisfy the condition

$$\sum_{k=0}^{M-1} |H_k(e^{j\omega})|^2 = 1 \tag{3.2}$$

by the lossless property of $\mathbf{E}(z)$. An objective function which represents the stopband energies of the analysis filters is

$$\Phi_1 = \sum_{k=0}^{M-1} \int_{k^{th}\,stopband} |H_k(e^{j\omega})|^2 d\omega. \tag{3.3}$$

Since the constraint (3.2) is structurally enforced, the passbands of $H_k(z)$ are also "good" if their stopbands are good. The optimization of the parameters of $\mathbf{K}_i$ is time-consuming since the objective function Φ_1 is a nonlinear function of many parameters (the parameters being the planar rotation angles mentioned above).

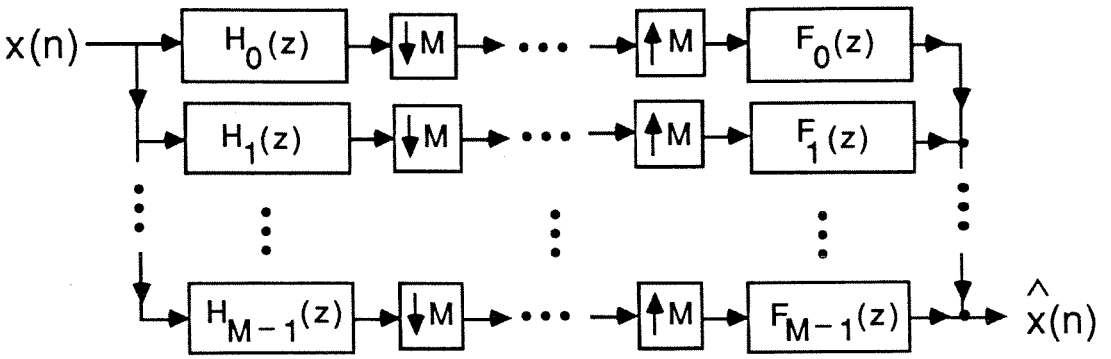

Fig. 3.1(a). The M-channel maximally decimated parallel QMF bank.

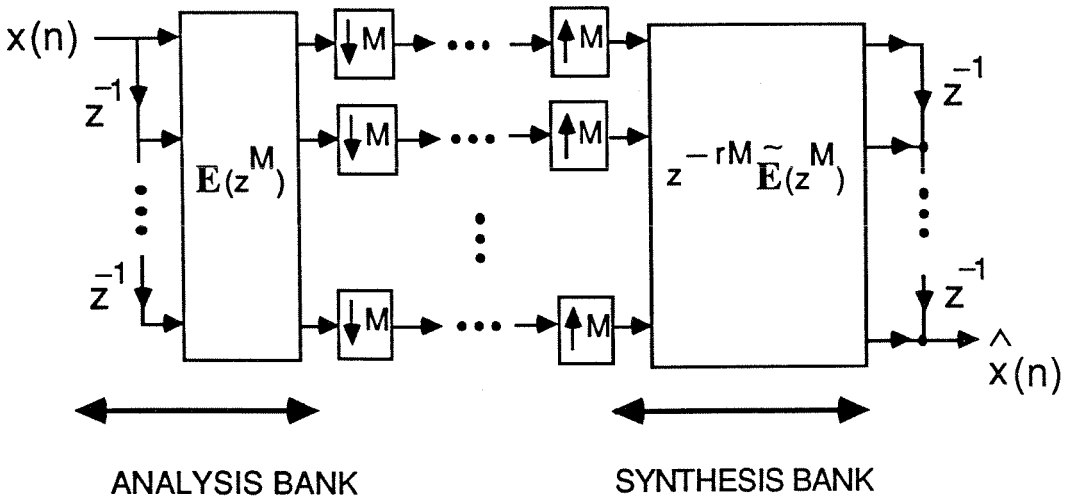

Fig. 3.1(b). Polyphase implementation of Fig. 3.1(a).

In an earlier design of perfect-reconstruction structure with lossless $\mathbf{E}(z)$ [7], the magnitude responses of $H_{M-1-k}(z)$ and $H_k(z)$ are mirror images with respect to $\pi/2$, even though this condition is not imposed on the system. In other words, the resulting set of analyis filters $H_k(z)$ tends to converge to a solution where $|H_{M-1-k}(e^{j\omega})| = |H_k(e^{j(\omega+\pi)})|$, $0 \leq k \leq M-1$. It is judicious, therefore, to *a priori* impose this pairwise mirror image property on the filter bank before optimizing the parameters. The advantage here is that the number of parameters associated with the pairwise mirror image structure is about half of that of the original PR structure in [37]. Furthermore, the new objective function consists of only the stopbands of $H_k(z)$, $0 \leq k \leq M/2$ (assuming that M is even). Consequently, the design time for this new pairwise mirror image structure is substantially reduced.

There are many ways in the time domain to impose pairwise mirror-image property on the system to yield filters where $|H_{M-1-k}(e^{j\omega})| = |H_k(e^{j(\omega+\pi)})|$, $0 \leq k \leq M-1$. The two easiest possibilities are

$$H_{M-1-k}(z) = H_k(-z) \tag{3.4a}$$

and

$$H_{M-1-k}(z) = z^{-r} H_k(-z^{-1}) \tag{3.4b}$$

for $0 \leq k \leq M-1$. Here, r is a positive integer large enough to ensure the causality of $H_{M-1-k}(z)$. The other choices of time-domain relations are more difficult to write. We therefore will consider only the pairwise mirror image structures which obey either (3.4a) or (3.4b). An analysis bank satisfying (3.4) will be called a "pairwise-symmetric analysis bank" in this chapter. We will use both "pairwise symmetry" and "pairwise mirror-image" interchangeably in this chapter. For instance, if $M = 3$, then

$$H_2(z) = H_0(-z), H_1(z) = \alpha_1(z^2) \tag{3.5}$$

for some $\alpha_1(z)$. Moreover, it is sufficient to optimize

$$\Phi_2 = \int_{(\pi/3)+\epsilon}^{\pi} |H_0(e^{j\omega})|^2 d\omega + \int_0^{(\pi/3)-\epsilon} |H_1(e^{j\omega})|^2 d\omega, \tag{3.6}$$

where ϵ depends on the desired stopband edges. In the next two sections, we modify the structure of Fig. 3.1(b) such that the properties described in (3.4) are structurally enforced. The number of parameters in the resulting structure is approximately half those in our earlier structure [7]; thus, the design time for this new structure is substantially reduced.

For reasons that will become clear as we progress, it is convenient to consider two separate cases, viz., odd M and even M. Using the PR properties in Chapter 2 with appropriate constraints (3.4), we derive new PR structures in Sections 3.1 and 3.2, for odd and even M, respectively. In each section, we demonstrate theoretical results by design examples. For $M = 4$, we compare the filter lengths, the complexity of the analysis bank, and the overall group delay caused by the QMF bank, to the comparable tree-structure-based design [18,19].

3.1. Odd M.

Recall that *any* set of M transfer functions $H_k(z)$, $0 \leq k \leq M-1$ can always be represented as in Fig. 3.1(b), where $\mathbf{E}(z)$ is an $M \times M$ matrix. If we impose the condition

$$H_{M-1-k}(z) = H_k(-z), \qquad 0 \leq k \leq M-1, \tag{3.7}$$

then we can write

$$\begin{pmatrix} H_k(z) \\ \\ H_{M-1-k}(z) \end{pmatrix} = \frac{1}{\sqrt{2}} \begin{pmatrix} 1 & 1 \\ \\ 1 & -1 \end{pmatrix} \begin{pmatrix} \alpha_k(z^2) \\ \\ z^{-l_k}\alpha_{M-1-k}(z^2) \end{pmatrix}, \tag{3.8}$$

where l_k is some odd integer (with $l_k = 1$, this representation is *always* possible). Accordingly, the analysis bank can be redrawn as in Fig. 3.2, where $L = (M-1)/2$

(M being odd). In this figure, the $M \times M$ matrix $\mathbf{R}$ has the form

$$\mathbf{R} = \frac{1}{\sqrt{2}} \begin{pmatrix} 1 & 0 & \dots & \dots & \dots & 0 & 1 \\ 0 & 1 & \dots & \dots & \dots & 1 & 0 \\ \vdots & \vdots & \ddots & \vdots & \iddots & \vdots & \vdots \\ 0 & 0 & \dots & \sqrt{2} & \dots & 0 & 0 \\ \vdots & \vdots & \iddots & \vdots & \ddots & \vdots & \vdots \\ 0 & 1 & \dots & \dots & \dots & -1 & 0 \\ 1 & 0 & \dots & \dots & \dots & 0 & -1 \end{pmatrix} \tag{3.9}$$

and is orthogonal. By writing $\alpha_k(z)$ in the form

$$\alpha_k(z) = \sum_{l=0}^{M-1} z^{-l} E'_{kl}(z^M), \quad 0 \le k \le M-1, \tag{3.10}$$

we can redraw Fig. 3.2 as in Fig. 3.3, where $\Gamma'(z)$ is an $M \times M$ diagonal matrix of the form,

$$\Gamma'(z) = \begin{pmatrix} \mathbf{I}_{L+1} & \mathbf{0} \\ \\ \mathbf{0} & \mathbf{J}_L(z) \end{pmatrix}. \tag{3.11}$$

Here, $\mathbf{J}_L(z)$ is a diagonal matrix with the diagonal elements z^{-l_k}. With $l_k = 1$ for all k (so that $\mathbf{J}_L(z) = z^{-1}\mathbf{I}_L$), any set of M transfer functions $H_k(z)$ with the constraint (3.7) can be realized as in Fig. 3.3. If we restrict $l_k = n_k M$ (i.e., integer multiples of M so that $\Gamma'(z) = \Gamma(z^M)$), we can realize a restricted class of such transfer functions. If l_k are so restricted, and if $\mathbf{E}'(z)$ is lossless, then the complete QMF bank (shown in Fig. 3.4) is a perfect reconstruction system. This can be seen by drawing it as in Fig. 3.5 and recognizing that $\tilde{\mathbf{E}}'(z^2)\tilde{\Gamma}(z)\mathbf{R}^T\mathbf{R}\Gamma(z)\mathbf{E}'(z^2) = \mathbf{I}$ so that Fig. 3.4 reduces to Fig. 2.7(b) except that z^{-1} is replaced by z^{-2}. It can be shown that with the diagonal elements z^{-l_k} in $\Gamma'(z)$ restricted to be of the form $z^{-n_k M}$, where n_k are arbitrary integers, losslessness of $\mathbf{E}'(z)$ in Fig. 3.3 is equivalent to that of $\mathbf{E}(z)$ in Fig. 3.1(b). [1] Furthermore, the synthesis filters $F_k(z)$ in Fig. 3.4 satisfy $F_k(z) = z^{-(SM+2M-2)}\tilde{H}_k(z)$, and the synthesis bank in Fig. 3.4 is equivalent to that of Fig. 3.1(b) [7]. Consequently, the synthesis filters are pairwise mirror-image with respect to $\pi/2$ if the analysis filters are.

[1] See Appendix 3.A for further clarification of this perfect-reconstruction property.

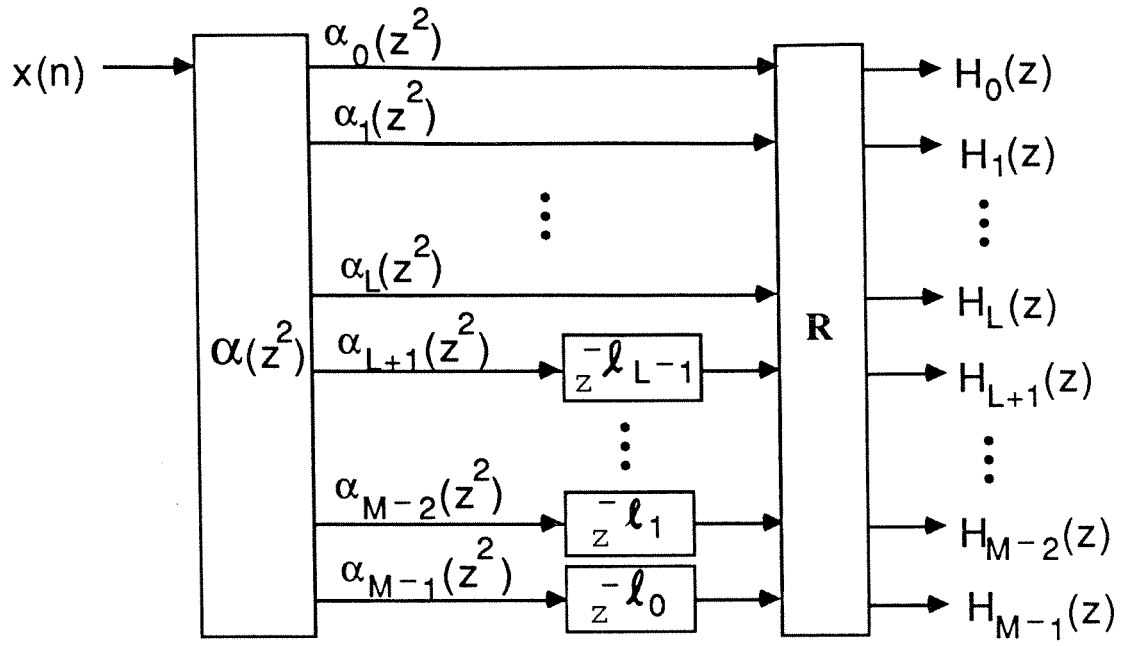

Fig. 3.2. The analysis bank for odd M.

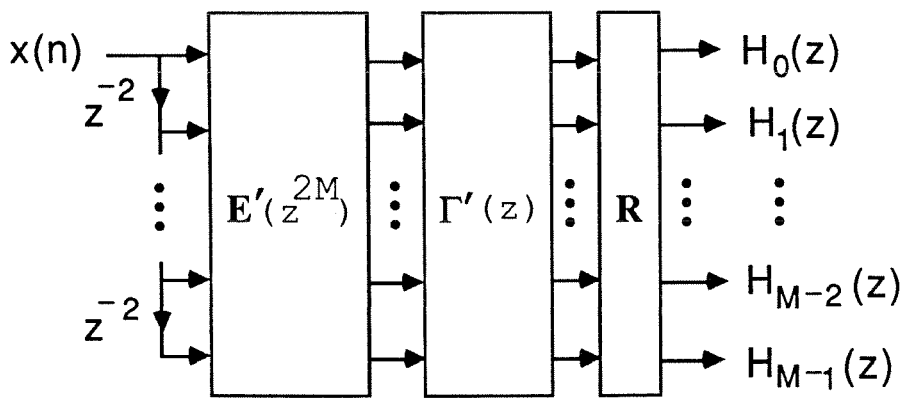

Fig. 3.3. The M-channel analysis bank in which the filter's frequency responses are pairwise mirror image about $\pi/2$. (M is odd).

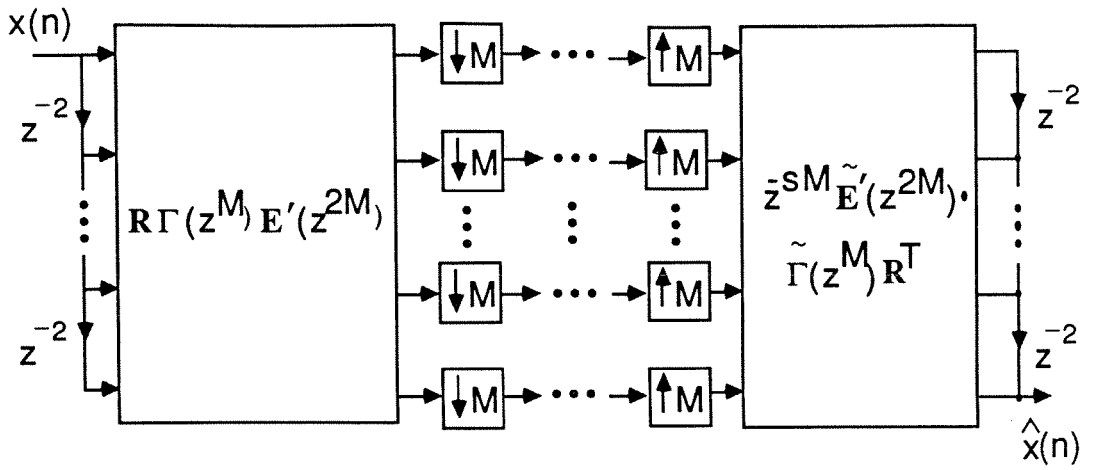

Fig. 3.4. A QMF bank in which the analysis bank (in Fig. 3.3) satisfies $\Gamma'(z) = \Gamma(z^M)$.

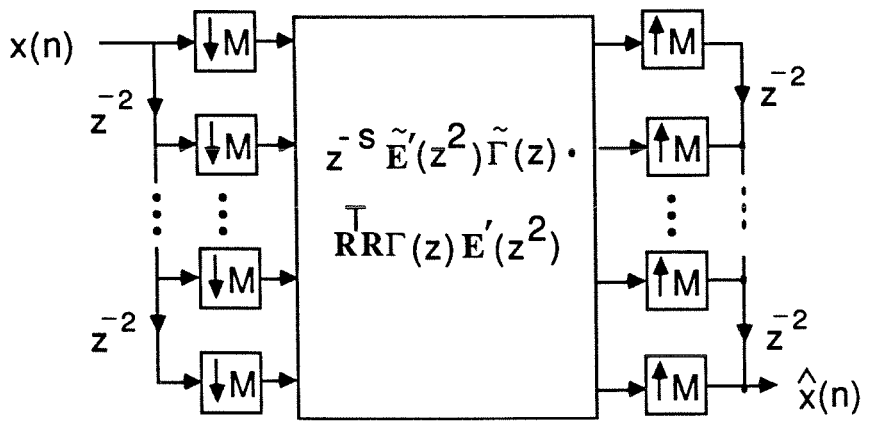

Fig. 3.5. An equivalent structure for Fig. 3.4.

Even though the condition $l_k = n_k M$ makes it easier to see how to build a perfect reconstruction system (satisying (3.7)), this condition is not necessary. As an example, consider an analysis bank as in Fig. 3.1(b) with $M = 5$ and

$$\mathbf{E}(z) = \begin{pmatrix} 1 & 1 & 0 & 1 & 1 \\ 1 & 1 & 0 & -1 & -1 \\ 0 & 0 & 2 & 0 & 0 \\ 1 & -1 & 0 & 1 & -1 \\ 1 & -1 & 0 & -1 & 1 \end{pmatrix}. \tag{3.12}$$

$\mathbf{E}(z)$ is orthogonal (and hence lossless) and moreover, (3.7) is satisfied. If we now draw the analysis bank as in Fig. 3.3, we can verify that

$$\mathbf{E}'(z) = \begin{pmatrix} 1 & 0 & 1 & 0 & 0 \\ 1 & 0 & -1 & 0 & 0 \\ 0 & 2 & 0 & 0 & 0 \\ 1 & -1 & 0 & 0 & 0 \\ 1 & 1 & 0 & 0 & 0 \end{pmatrix}, \quad \Gamma'(z) = \begin{pmatrix} 1 & 0 & 0 & 0 & 0 \\ 0 & 1 & 0 & 0 & 0 \\ 0 & 0 & 1 & 0 & 0 \\ 0 & 0 & 0 & z^{-1} & 0 \\ 0 & 0 & 0 & 0 & z^{-1} \end{pmatrix}, \tag{3.13}$$

so that $\mathbf{E}'(z)$ is not lossless and $\Gamma'(z)$ is not of the form $\Gamma(z^5)$ (i.e., l_k not multiples of M). Yet, it is a perfect reconstruction system, satifying (3.7)!

In summary, even though Fig. 3.3 with lossless $\mathbf{E}'(z)$, orthogonal $\mathbf{R}$ and with $\Gamma'(z) = \Gamma(z^M)$ (diagonal matrix of delays) leads to a perfect reconstruction system satisfying (3.7), it does not cover all such systems. We can obtain a *relatively* more general system by not restricting $\mathbf{R}$ to be as in (3.9). We now proceed to this issue:

Lemma 3.1: Consider the analysis-bank structure of Fig. 3.3, where $\Gamma'(z)$ is of the form

$$\Gamma'(z) \equiv \Gamma(z^M) = \begin{pmatrix} \mathbf{I}_{M-M_1} & \mathbf{0} \\ \mathbf{0} & z^{-M}\mathbf{I}_{M_1} \end{pmatrix} \tag{3.14}$$

with M odd and where M_1 is an integer with $0 \leq M_1 \leq M-1$. The relation (3.7) holds if and only if $\mathbf{R}$ is of the form

$$\mathbf{R} = \begin{pmatrix} \mathbf{A} & \mathbf{B} \\ \mathbf{C} & \mathbf{0} \\ \mathbf{P}_1\mathbf{A} & -\mathbf{P}_1\mathbf{B} \end{pmatrix}, \tag{3.15}$$

where $\mathbf{A}$ is $L \times (M - M_1)$, $\mathbf{B}$ is $L \times M_1$, $\mathbf{C}$ is $1 \times (M - M_1)$, and $\mathbf{P}_1$ is the $L \times L$ permutation matrix given by

$$\mathbf{P}_1 = \begin{pmatrix} 0 & & 1 \\ & \cdots & \\ 1 & & 0 \end{pmatrix}. \tag{3.16}$$

Here, M_1 is the number of connecting lines between $\mathbf{E}'(z^{2M})$ and $\mathbf{R}$ with delay z^{-M}, and $M = 2L + 1$. A proof of the above lemma can be found in Appendix 3.B. Notice that M_1 does not have to be equal to L (which is $(M-1)/2$), even though this was the natural choice when we derived the structures of Fig. 3.2 and Fig. 3.3.

Next, by forcing $\mathbf{E}'(z)$ to be lossless and $\mathbf{R}$ to be orthogonal, we can obtain perfect reconstruction. Orthogonality of $\mathbf{R}$ implies

$$\mathbf{R}\mathbf{R}^T = \begin{pmatrix} \mathbf{A}. & \mathbf{B} \\ \mathbf{C} & \mathbf{0} \\ \mathbf{P}_1\mathbf{A} & -\mathbf{P}_1\mathbf{B} \end{pmatrix} \begin{pmatrix} \mathbf{A}^T & \mathbf{C}^T & \mathbf{A}^T\mathbf{P}_1 \\ \mathbf{B}^T & 0^T & -\mathbf{B}^T\mathbf{P}_1 \end{pmatrix} = \mathbf{I}, \tag{3.17}$$

which is equivalent to the three following conditions

$$\begin{cases} \mathbf{C}\mathbf{C}^T = 1, \\ \mathbf{A}\mathbf{A}^T = \mathbf{B}\mathbf{B}^T = \frac{1}{2}\mathbf{I}_L, \\ \mathbf{A}\mathbf{C}^T = \mathbf{0}. \end{cases} \tag{3.18}$$

Since $\mathbf{R}$ is a square matrix, (3.17) also implies $\mathbf{R}^T\mathbf{R} = \mathbf{I}$, which is equivalent to the following conditions

$$\begin{cases} 2\mathbf{A}^T\mathbf{A} + \mathbf{C}^T\mathbf{C} = \mathbf{I}_{M-M_1}, \\ \mathbf{B}^T\mathbf{B} = \frac{1}{2}\mathbf{I}_{M_1}, \end{cases} \tag{3.19}$$

in terms of the submatrices $\mathbf{A}$, $\mathbf{B}$, and $\mathbf{C}$.

The condition $\mathbf{B}\mathbf{B}^T = \frac{1}{2}\mathbf{I}_L$ in (3.18) implies that $M_1 \geq L$, whereas $\mathbf{B}^T\mathbf{B} = \frac{1}{2}\mathbf{I}_{M_1}$ in (3.19) implies that $L \geq M_1$. In other words, the only choice of M_1 that is

permitted by an orthogonal $\mathbf{R}$ of the form (3.15) is $M_1 = L$. With this, $\Gamma'(z)$ and $\mathbf{R}$ in (3.14) and (3.15), respectively, take simpler forms; i.e.,

$$\Gamma'(z) = \begin{pmatrix} \mathbf{I}_{L+1} & \mathbf{0} \\ \mathbf{0} & z^{-M}\mathbf{I}_L \end{pmatrix}, \qquad \text{and} \qquad \mathbf{R} = \begin{pmatrix} \mathbf{A} & \mathbf{B} \\ \mathbf{C} & \mathbf{0} \\ \mathbf{P}_1\mathbf{A} & -\mathbf{P}_1\mathbf{B} \end{pmatrix}, \tag{3.20}$$

where $\mathbf{A}$ is $L \times (L+1)$, $\mathbf{B}$ is $L \times L$ and $\mathbf{C}$ is $1 \times (L+1)$. The pairwise symmetric structure of Fig. 3.3, with $\Gamma'(z)$ and $\mathbf{R}$ as in (3.20), is redrawn as Fig. 3.6. We can simplify the structure in Fig. 3.6 further by observing that $\mathbf{R}$ can be written as

$$\mathbf{R} = \begin{pmatrix} \mathbf{I}_L & 0 & \mathbf{0} \\ \mathbf{0} & 1 & \mathbf{0} \\ \mathbf{0} & 0 & \mathbf{P}_1 \end{pmatrix} \begin{pmatrix} \mathbf{I}_L & 0 & \mathbf{I}_L \\ \mathbf{0} & 1 & \mathbf{0} \\ \mathbf{I}_L & 0 & -\mathbf{I}_L \end{pmatrix} \begin{pmatrix} \mathbf{A} & \mathbf{0} \\ \mathbf{C} & \mathbf{0} \\ \mathbf{0} & \mathbf{B} \end{pmatrix}. \tag{3.21}$$

Form a square matrix $\mathbf{D}$ as follows:

$$\mathbf{D} = \begin{pmatrix} \mathbf{A} \\ \mathbf{C} \end{pmatrix}_{(L+1)\times(L+1)}. \tag{3.22}$$

The orthogonal requirements for $\mathbf{A}$ and $\mathbf{C}$ in (3.18) reflect into the following condition on $\mathbf{D}$:

$$\mathbf{D}\mathbf{D}^T = \begin{pmatrix} \frac{1}{2}\mathbf{I}_L & \mathbf{0} \\ \mathbf{0} & 1 \end{pmatrix}. \tag{3.23}$$

Such $\mathbf{D}$ is easy to construct. For instance, denote the rows of an $(L+1) \times (L+1)$ orthogonal matrix $\mathbf{D}'$ by $\mathbf{d}_0^T, \mathbf{d}_1^T, \ldots, \mathbf{d}_L^T$; then the matrix

$$\mathbf{D} = \begin{bmatrix} \frac{\mathbf{d}_0}{\sqrt{2}} & \frac{\mathbf{d}_1}{\sqrt{2}} & \cdots & \frac{\mathbf{d}_{L-1}}{\sqrt{2}} & \mathbf{d}_L \end{bmatrix}^T \tag{3.24}$$

satisfies (3.23). Using the above orthogonal matrix $\mathbf{D}'$, $\mathbf{R}$ in (3.21) is equivalent to

$$\mathbf{R} = \begin{pmatrix} \mathbf{I}_L & 0 & \mathbf{0} \\ \mathbf{0} & 1 & \mathbf{0} \\ \mathbf{0} & 0 & \mathbf{P}_1 \end{pmatrix} \begin{pmatrix} \frac{1}{\sqrt{2}}\mathbf{I}_L & 0 & \frac{1}{\sqrt{2}}\mathbf{I}_L \\ \mathbf{0} & 1 & \mathbf{0} \\ \frac{1}{\sqrt{2}}\mathbf{I}_L & 0 & -\frac{1}{\sqrt{2}}\mathbf{I}_L \end{pmatrix} \begin{pmatrix} \mathbf{D}' & \mathbf{0} \\ \mathbf{0} & \sqrt{2}\mathbf{B} \end{pmatrix}. \tag{3.25}$$

We observe from Fig. 3.6 that $\mathbf{D}'$ in $\mathbf{R}$ can be moved to the left of the delays and can be combined into the general lossless matrix $\mathbf{E}'(z)$, since the delay lines affect only the last L lines of the structure. Furthermore, as evident from (3.18),

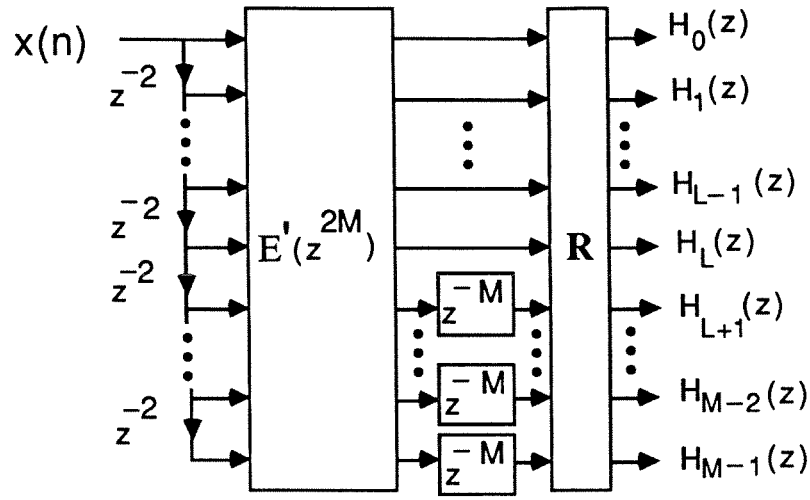

Fig. 3.6. An equivalent structure for Fig. 3.3.

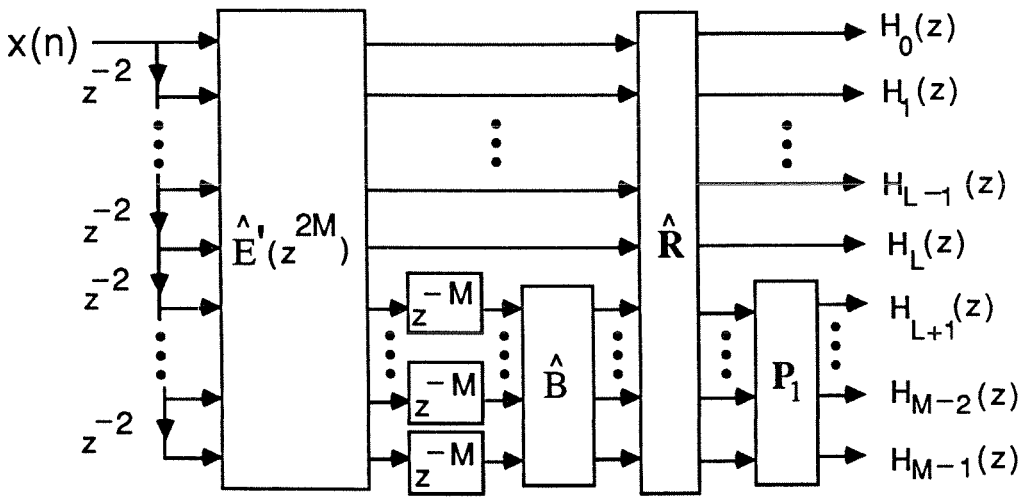

Fig. 3.7. An equivalent and simplified structure for Fig. 3.6.

$\hat{\mathbf{B}} = \sqrt{2}\mathbf{B}$ is an $L \times L$ orthogonal matrix of unit norm. Fig. 3.6, consequently, can be redrawn as Fig. 3.7, where $\hat{\mathbf{E}}'(z)$ is a general $M \times M$ lossless transfer function matrix and $\hat{\mathbf{R}}$ is

$$\hat{\mathbf{R}} = \begin{pmatrix} \frac{1}{\sqrt{2}}\mathbf{I}_L & 0 & \frac{1}{\sqrt{2}}\mathbf{I}_L \\ \mathbf{0} & 1 & \mathbf{0} \\ \frac{1}{\sqrt{2}}\mathbf{I}_L & 0 & -\frac{1}{\sqrt{2}}\mathbf{I}_L \end{pmatrix}. \tag{3.26}$$

In summary, having chosen $\hat{\mathbf{B}}$ to be any $L \times L$ orthogonal matrix of unit norm, the analysis bank in Fig. 3.7, with $\hat{\mathbf{R}}$ defined as in (3.26), is the analysis bank of a perfect reconstruction structure in which the filters satisfy the pairwise image property. Here, $\hat{\mathbf{E}}'(z)$, as shown in Chapter 2, is realized as in Fig. 2.9 and 2.10, respectively.

Example 3.1: Let $M = 3$, so that the symmetric requirement (3.7) on the analysis filters becomes $H_2(z) = H_0(-z), H_1(z) = \alpha_1(z^2)$. We also have $L = 1$ here, and thus $\hat{\mathbf{B}} = 1$ and $\mathbf{P}_1 = 1$. $\hat{\mathbf{R}}$ has the form

$$\hat{\mathbf{R}} = \frac{1}{\sqrt{2}} \begin{pmatrix} 1 & 0 & 1 \\ 0 & \sqrt{2} & 0 \\ 1 & 0 & -1 \end{pmatrix}. \tag{3.27}$$

The structure in Fig. 3.7 is reduced to Fig. 3.8, where $\hat{\mathbf{E}}'(z)$ is explicitly shown as a cascade of orthogonal building blocks interlaced by delays. The synthesis bank, shown in Fig. 3.9, is obtained by transposing each building block in Fig. 3.8. Note that a delay $z^{-(6N+1)}$ is multiplied to the synthesis bank in order to obtain a causal system. Using (2.22) to count the number N_p of rotation angles $\theta_{i,j}$, we have (counted in the analysis bank only)

$$N_p = 2N + 1. \tag{3.28}$$

These N_p rotation angles in the lattice structure for $\hat{\mathbf{E}}'(z)$ are optimized to minimize (3.6). As mentiond in Chapter 2, minimizing (3.6) by "random initializing" of $\theta_{i,j}$ is very time consuming. Often, the solution converges to a local minimum. If we

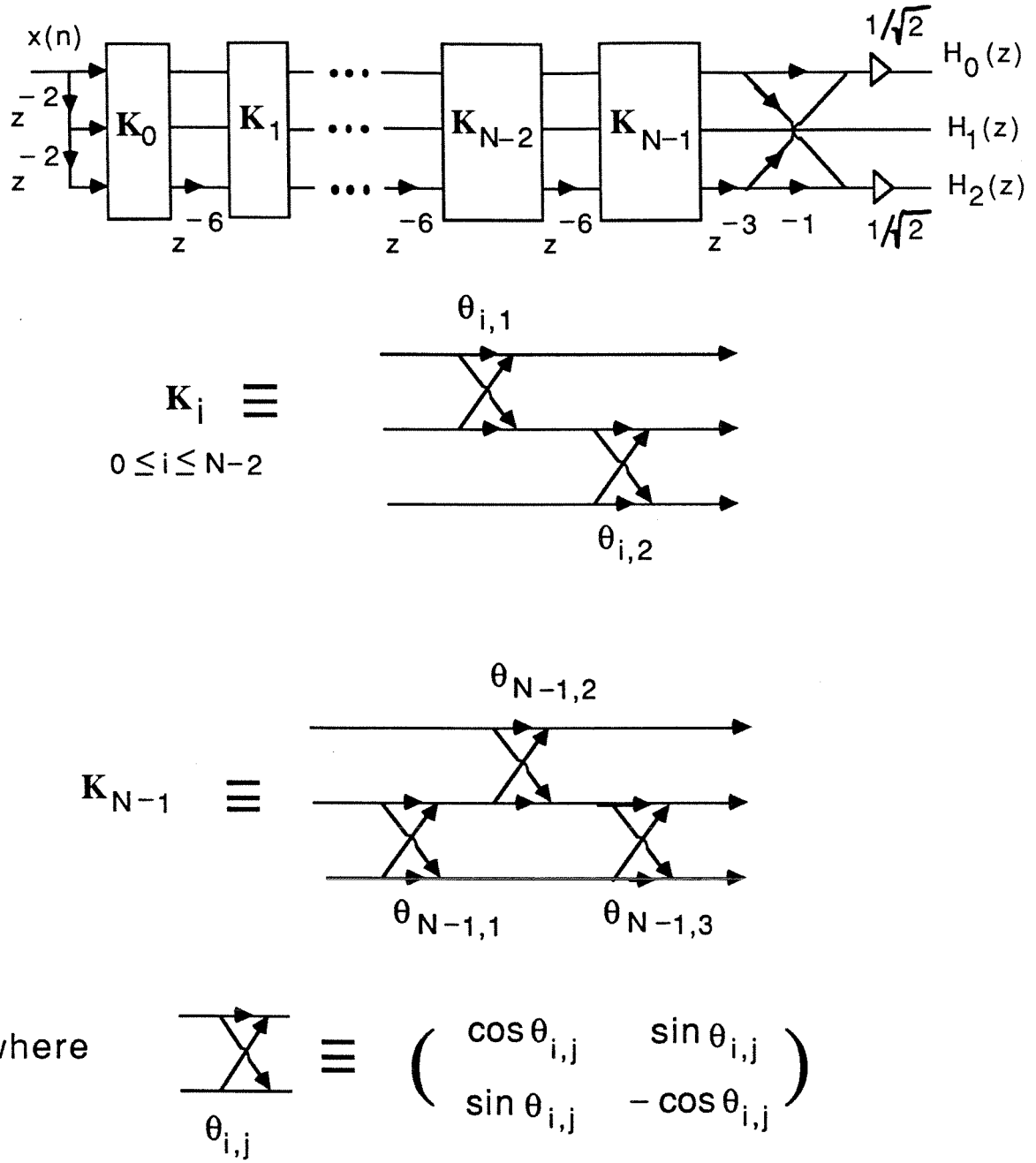

Fig. 3.8. The analysis bank of a perfect-reconstruction FIR QMF bank which yields pairwise-mirror analysis filters.

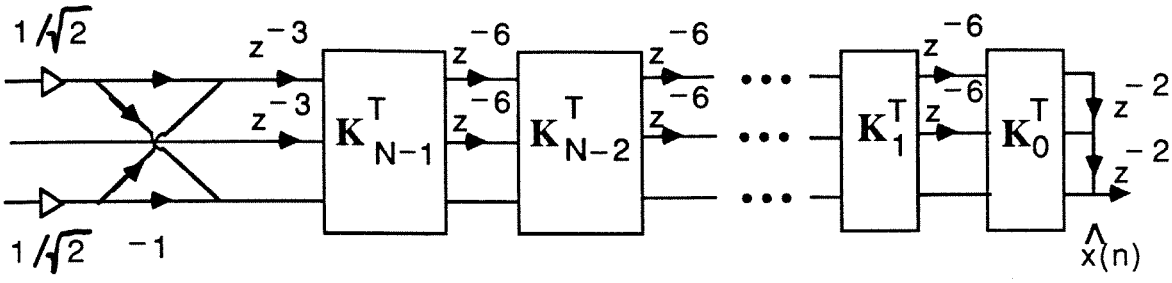

$$\mathbf{K}_i^T \equiv \qquad 0 \le i \le N-2$$

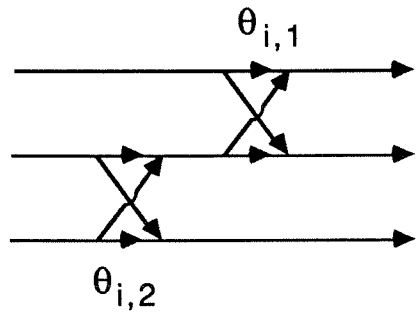

$$\mathbf{K}_{N-1}^T \equiv$$

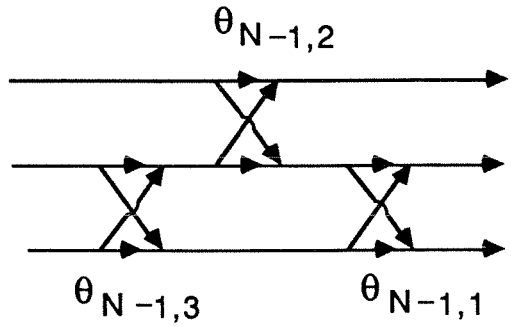

where 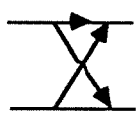 $\equiv \begin{pmatrix} \cos\theta_{i,j} & \sin\theta_{i,j} \\ \sin\theta_{i,j} & -\cos\theta_{i,j} \end{pmatrix}$

$\theta_{i,j}$

Fig. 3.9. The synthesis bank of the analysis bank in Fig. 3.8.

can initialize these rotation angles somehow, then the minimization process would be much faster and it would also yield much better results.

This is indeed possible. As outlined in Chapter 2, we know that each analysis filter $H_k(z)$ is a spectral factor of a 3^{rd}-band filter. Furthermore, given any $H_k(z)$, say $H_1(z)$, we also outlined a procedure to initialize these rotation angles. As a design example, let the number of orthogonal matrices $\mathbf{K}_m$ be $N = 10$. Then the lengths of $H_0(z)$ and $H_2(z)$ are 62 each, whereas the length of $H_1(z)$ is 59. Since we would like to use $H_1(z)$ to initialize the lattice structure, we can first design a 3^{rd}-band filter $G_1(z)$ of length 117 by using the eigenfilter method. The minimum-phase spectral factor of $G_1(z)$ is obtained and the rotation angles $\theta_{i,j}$ are initialized (20 angles). These initialized 20 rotation angles together with the $N_f = 1$ rotation angle in the lattice structure for $\hat{\mathbf{E}}'(z)$ were optimized using IMSL subroutines [10] on a computer so as to minimize (3.6). The resulting frequency response magnitudes for $\epsilon = 0.0625\pi$ are shown in Fig. 3.10. The lattice coefficients $\theta_{i,j}$ and the impulse response coefficients $h_m(n)$ are shown in Tables 3.1 and 3.2, respectively.

Example 3.2: Using the initialization technique outlined in the design of the three-channel FIR PR QMF bank in example 3.1, we design a set of filters with different specifications. We tabulate the properties of these filter banks as well as the lattice coefficients and the filter coefficients in three tables in Appendix 3.F. The filter length, transition bandwidth, stopband attenuation, etc; are shown in Table 3.F.1. Tables 3.F.2 and 3.F.3 give the lattice coefficients and the filter coefficients of these filter banks, respectively. Since the filter coefficients of $H_0(z)$ and $H_2(z)$ are related as $h_2(n) = (-1)^n h_0(n)$, we show only $h_0(n)$ and $h_1(n)$ in Table 3.F.3.

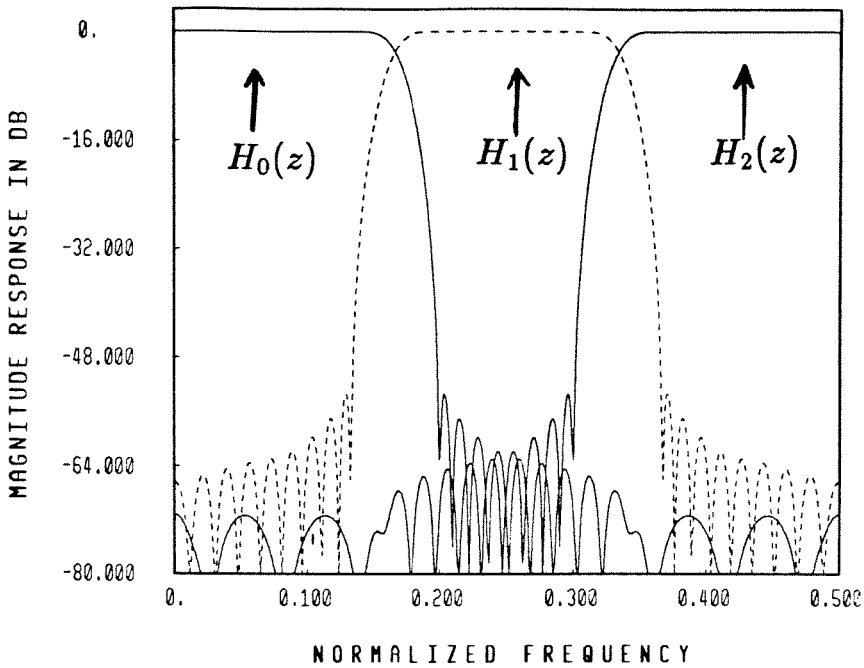

Fig. 3.10. Ex. 3.1. Magnitude response plots for the optimized analysis filters.

Table 3.1 Lattice coefficients $\theta_{m,i}$ (in radians) of the optimized analysis filters in Ex. 3.1.

m	$\theta_{m,1}$	$\theta_{m,2}$	$\theta_{m,3}$
0	1.259059×10^{0}	-1.526818×10^{0}	
1	2.368147×10^{0}	-1.963775×10^{0}	
2	-3.146314×10^{-1}	7.844229×10^{-1}	
3	1.171648×10^{-1}	-2.639372×10^{0}	
4	3.362273×10^{-2}	-5.973011×10^{0}	
5	8.665927×10^{-3}	-2.963820×10^{0}	
6	3.794835×10^{-2}	8.909689×10^{-2}	
7	-7.217059×10^{-2}	3.556300×10^{-2}	
8	-1.055272×10^{0}	-9.922895×10^{-3}	1.572479×10^{0}

Table 3.2 Impulse responses of the optimized analysis filters in Ex. 3.1.

n	$h_0(n)$	$h_1(n)$
0	2.543807×10^{-3}	5.776660×10^{-4}
1	0.	0.
2	-3.118806×10^{-2}	1.610769×10^{-3}
3	-1.204284×10^{-1}	0.
4	-2.723899×10^{-1}	-1.267537×10^{-3}
5	-4.387807×10^{-1}	0.
6	-5.262056×10^{-1}	-3.568539×10^{-3}
7	-4.534693×10^{-1}	0.
8	-2.237543×10^{-1}	5.855130×10^{-3}
9	5.345022×10^{-2}	0.
10	2.252414×10^{-1}	2.619256×10^{-3}
11	2.054070×10^{-1}	0.
12	4.180549×10^{-2}	-1.487865×10^{-2}
13	-1.200825×10^{-1}	0.
14	-1.553794×10^{-1}	1.017898×10^{-2}
15	-5.698214×10^{-2}	0.
16	7.189854×10^{-2}	1.706194×10^{-2}
17	1.159408×10^{-1}	0.
18	5.107901×10^{-2}	-3.646554×10^{-2}
19	-4.816175×10^{-2}	0.
20	-8.698478×10^{-2}	1.049357×10^{-2}
21	-4.009365×10^{-2}	0.
22	3.552927×10^{-2}	4.850350×10^{-2}
23	6.499536×10^{-2}	0.
24	2.888206×10^{-2}	-7.050226×10^{-2}
25	-2.777611×10^{-2}	0.
26	-4.789591×10^{-2}	4.084510×10^{-3}
27	-1.907818×10^{-2}	0.
28	2.228407×10^{-2}	1.019727×10^{-1}
29	3.425984×10^{-2}	0.
30	1.124890×10^{-2}	-1.243129×10^{-1}
31	-1.769298×10^{-2}	0.
32	-2.350616×10^{-2}	-1.122346×10^{-3}
33	-5.539725×10^{-3}	0.
34	1.368588×10^{-2}	1.816790×10^{-1}
35	1.515546×10^{-2}	0.
36	1.698867×10^{-3}	-2.313869×10^{-1}
37	-9.973167×10^{-3}	0.
38	-8.990222×10^{-3}	5.041226×10^{-2}
39	4.167714×10^{-4}	0.
40	6.867099×10^{-3}	2.693288×10^{-1}
41	4.678399×10^{-3}	0.
42	-1.438907×10^{-3}	-5.199865×10^{-1}
43	-4.160525×10^{-3}	0.
44	-1.932038×10^{-3}	5.599947×10^{-1}
45	1.433994×10^{-3}	0.
46	2.303490×10^{-3}	-4.122640×10^{-1}
47	4.285001×10^{-4}	0.
48	-1.286605×10^{-3}	2.107532×10^{-1}
49	-8.147421×10^{-4}	0.
50	4.146013×10^{-4}	-6.791403×10^{-2}
51	4.782894×10^{-4}	0.
52	-5.948637×10^{-5}	9.744202×10^{-3}
53	-1.541260×10^{-4}	0.
54	0.	0.
55	2.211377×10^{-5}	0.

3.1.1. *Comment on generality:*

The main difference of the design technique here as compared to [7] is that we have structurally imposed the symmetry conditions, so as to cut down the number of planar rotation angles in the optimization. Using this initialization method together with the above pairwise-symmetric structures, we have been able to obtain designs with much better stopband attenuation than before. This method has led to faster optimization programs according to our experiences. We, however, can not claim that our methods to enforce the symmetry are completely general, as evidenced by the counter example of Equations (3.12), (3.13).

3.2. Even M.

Suppose that we use the pairwise symmetric structure in Fig. 3.7 for even M where $L = M/2$ here. For even M, all delays in this structure are even orders; therefore, the resulting analyis filters $H_k(z)$ are functions of z^2. Thus, this system is very limited. Instead of (3.4a), let us impose a different kind of pairwise symmetry on the analysis filters as follows:

$$H_{M-1-k}(z) = z^{-r} H_k(-z^{-1}); \qquad 0 \leq k \leq M-1, \tag{3.29}$$

where r is a positive integer large enough to ensure the causality of $H_{M-1-k}(z)$. For the case of $M = 2$, $H_1(z) = z^{-r} H_0(-z^{-1})$. One recognizes that this is the condition that Smith and Barnwell [18] and Mintzer [6] imposed on their analysis filters for the 2 channel QMF bank. We shall generate this symmetry property by employing the structure of Fig. 3.11. We shall constrain $\mathbf{E}(z)$ to be lossless by constraining $\mathbf{K}_i$ to be orthogonal matrices. $\mathbf{K}_i$ and $\mathbf{K}_{i+1}$ are separated by a transfer matrices of the form $\begin{pmatrix} \mathbf{I}_L & \mathbf{0} \\ \mathbf{0} & z^{-M}\mathbf{I}_L \end{pmatrix}$, where $L = M/2$. It can be verified that a cascade of orthogonal matrices and the above transfer matrices $\begin{pmatrix} \mathbf{I}_L & \mathbf{0} \\ \mathbf{0} & z^{-M}\mathbf{I}_L \end{pmatrix}$ yields lossless $\mathbf{E}(z)$.

It is clear that any arbitrary choices of $\mathbf{K}_i$ do not yield pairwise symmetric analysis filters. Thus, what form does $\mathbf{K}_i$ take so that $H_k(z)$ satisfy (3.4b). In other words, let $H_{m,k}(z)$ denote the transfer function from the input $x(n)$ to the k^{th} output terminal of $\mathbf{K}_m$ (Fig. 3.11 denotes several examples of $H_{m,k}(z)$). Suppose that $H_{m,k}(z)$ have the two following properties: (Fig. 3.12)

1. They form a set of PR filters.

2. They obey the pairwise symmetry property; i.e.,

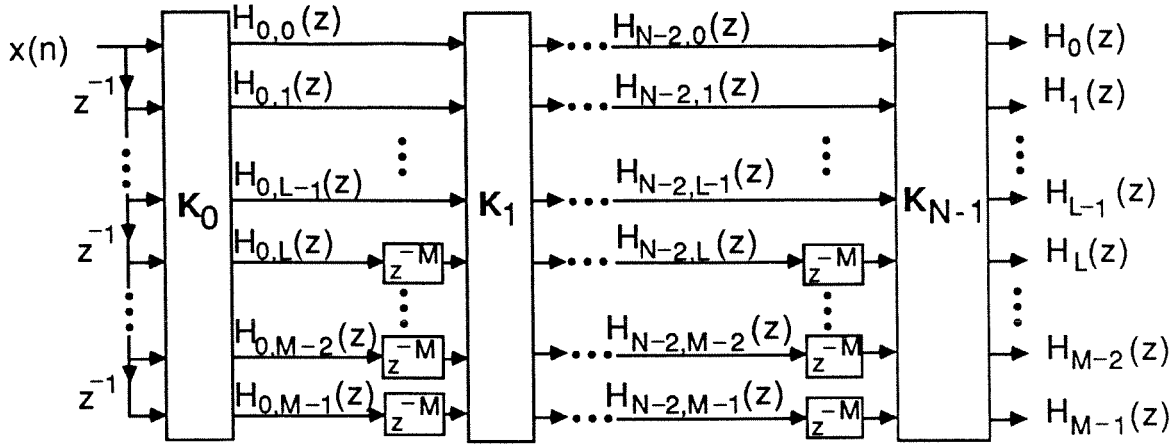

Fig. 3.11. The M-channel analysis bank in which the filter's frequency responses are pairwise mirror-image about π /2. (M is even).

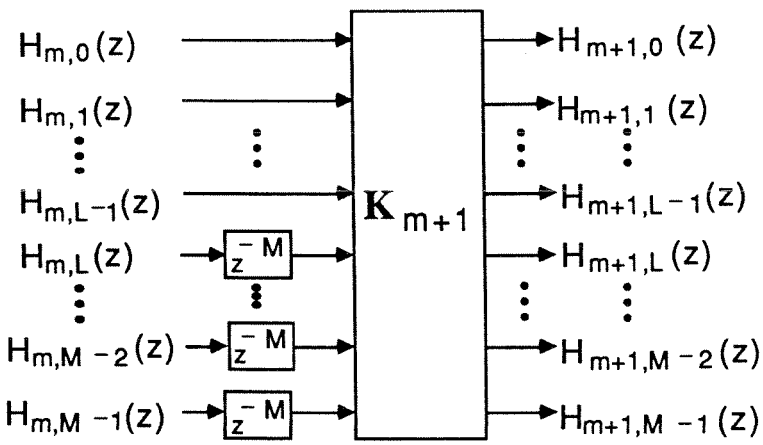

Fig. 3.12. One stage of the analysis bank in Fig. 3.11.

$$H_{m,M-1-k}(z) = z^{-((m+1)M-1)} H_{m,k}(-z^{-1}). \tag{3.30}$$

The filters $H_{m,k}(z)$ in consideration here, are assumed to have the maximum order possible; namely, $((m+1)M-1)$. The idea is to find $\mathbf{K}_{m+1}$ such that the same above two properties are propagated to the $(m+1)^{th}$ stage; i.e., $H_{m+1,k}(z)$ form a set of PR filters and

$$H_{m+1,M-1-k}(z) = z^{-((m+2)M-1)} H_{m+1,k}(-z^{-1}). \tag{3.31}$$

By considering only orthogonal matrices $\mathbf{K}_i$, the first condition above is automatically satisfied. To propagate the pairwise symmetric property, the only matrix $\mathbf{K}_{m+1}$ for which (3.31) holds for any set of $H_{m,k}(z)$ satisfying (3.30) is (see Appendix 3.C for a proof)

$$\mathbf{K}_{m+1} = \begin{pmatrix} \mathbf{J}_{m+1,1} & \mathbf{J}_{m+1,2} \\ \\ -\mathbf{P}_1\mathbf{J}_{m+1,2}\mathbf{P}_1 & \mathbf{P}_1\mathbf{J}_{m+1,1}\mathbf{P}_1 \end{pmatrix}, \tag{3.32}$$

where $\mathbf{P}_1$ is defined in (3.16). Here $\mathbf{J}_{m+1,1}$ and $\mathbf{J}_{m+1,2}$ are arbitrary $L \times L$ matrices. We observe that using (3.32) for $\mathbf{K}_0$ does not yield a set of transfer functions $H_{0,k}(z)$ that satisfy the pairwise-symmmetry property, since the delay chain $(1\ z^{-1} \ldots z^{-(M-1)})^T$ does not satisfy (3.29). Hence, we need to initiate the induction process by looking for an orthogonal matrix $\mathbf{K}_0$ such that $H_{0,k}(z)$ satisfy (3.29), for $0 \leq k \leq M-1$. Notice that

$$\begin{pmatrix} H_{0,0}(z) \\ H_{0,1}(z) \\ \vdots \\ H_{0,M-1}(z) \end{pmatrix} = \mathbf{K}_0 \begin{pmatrix} 1 \\ z^{-1} \\ \vdots \\ z^{-(M-1)} \end{pmatrix}. \tag{3.33}$$

The only $\mathbf{K}_0$ in (3.33) for which $H_{0,k}(z)$ satisfy (3.29) has the form (see Appendix 3.D for a proof)

$$\mathbf{K}_0 = \begin{pmatrix} \mathbf{J}_{0,1} & \mathbf{J}_{0,2} \\ \\ \mathbf{P}_1\mathbf{J}_{0,2}\mathbf{P}_3 & \mathbf{P}_1\mathbf{J}_{0,1}\mathbf{P}_2 \end{pmatrix}, \tag{3.34}$$

where $\mathbf{J}_{0,1}$, $\mathbf{J}_{0,2}$ are arbitrary $L \times L$ matrices, $\mathbf{P}_1$ is as in (3.16) and

$$\mathbf{P}_2 = \begin{pmatrix} \mathbf{0} & & & 1 \\ & & -1 & \\ & 1 & & \\ \cdot^{\cdot} & & & \mathbf{0} \end{pmatrix}_{L\times L} \quad ; \quad \mathbf{P}_3 = \begin{pmatrix} \mathbf{0} & & & \cdot^{\cdot} \\ & & -1 & \\ & 1 & & \\ -1 & & & \mathbf{0} \end{pmatrix}_{L\times L} . \tag{3.35}$$

$\mathbf{K}_{m+1}$ and $\mathbf{K}_0$ in (3.32) and (3.34) can be rewritten as

$$\mathbf{K}_{m+1} = \begin{pmatrix} \mathbf{I}_L & \mathbf{0} \\ \mathbf{0} & \mathbf{P}_1 \end{pmatrix} \cdot \mathbf{T}_{m+1} \cdot \begin{pmatrix} \mathbf{I}_L & \mathbf{0} \\ \mathbf{0} & \mathbf{P}_1 \end{pmatrix}, \tag{3.36}$$

$$\mathbf{K}_0 = \begin{pmatrix} \mathbf{I}_L & \mathbf{0} \\ \mathbf{0} & \mathbf{P}_1 \end{pmatrix} \cdot \mathbf{T}_0 \cdot \begin{pmatrix} \mathbf{I}_L & \mathbf{0} \\ \mathbf{0} & \mathbf{P}_2 \end{pmatrix} \tag{3.37}$$

where

$$\mathbf{T}_{m+1} = \begin{pmatrix} \mathbf{J}_{m+1,1} & \mathbf{J}_{m+1,2}\mathbf{P}_1 \\ -\mathbf{J}_{m+1,2}\mathbf{P}_1 & \mathbf{J}_{m+1,1} \end{pmatrix}, \tag{3.38}$$

$$\mathbf{T}_0 = \begin{pmatrix} \mathbf{J}_{0,1} & -\mathbf{J}_{0,2}\mathbf{P}_3 \\ \mathbf{J}_{0,2}\mathbf{P}_3 & \mathbf{J}_{0,1} \end{pmatrix}. \tag{3.39}$$

Making use of the identities (3.36) and (3.37) in Fig. 3.11, it can be redrawn as in Fig. 3.13, where $\mathbf{P}_1$, $\mathbf{P}_2$ are defined as in (3.16), (3.35), respectively. Fig. 3.13 is the analysis bank of a perfect reconstruction structure in which the analysis filters $H_k(z)$ and $H_{M-1-k}(z)$ have the pairwise symmetry property if $\mathbf{T}_{m+1}$ and $\mathbf{T}_0$ are orthogonal, i.e., if

$$\mathbf{T}_{m+1}^T \mathbf{T}_{m+1} = \mathbf{I} \qquad \text{and} \qquad \mathbf{T}_0^T \mathbf{T}_0 = \mathbf{I}. \tag{3.40}$$

Using the identities

$$\mathbf{P}_1^T = \mathbf{P}_1, \quad \mathbf{P}_1^2 = \mathbf{I}, \quad \text{and} \quad \mathbf{P}_3\mathbf{P}_2 = -\mathbf{I}, \tag{3.41}$$

(3.40) is equivalent to

$$\begin{cases} \mathbf{J}_{m+1,1}^T\mathbf{J}_{m+1,1} + \mathbf{P}_1\mathbf{J}_{m+1,2}^T\mathbf{J}_{m+1,2}\mathbf{P}_1 = \mathbf{I} \\ \mathbf{P}_1\mathbf{J}_{m+1,1}^T\mathbf{J}_{m+1,2} = (\mathbf{P}_1\mathbf{J}_{m+1,1}^T\mathbf{J}_{m+1,2})^T. \end{cases}, \quad \text{and} \quad \begin{cases} \mathbf{J}_{0,1}^T\mathbf{J}_{0,1} + \mathbf{P}_3^T\mathbf{J}_{0,2}^T\mathbf{J}_{0,2}\mathbf{P}_3 = \mathbf{I}. \\ \mathbf{P}_2^T\mathbf{J}_{0,1}^T\mathbf{J}_{0,2} = (\mathbf{P}_2^T\mathbf{J}_{0,1}^T\mathbf{J}_{0,2})^T. \end{cases} \tag{3.42}$$

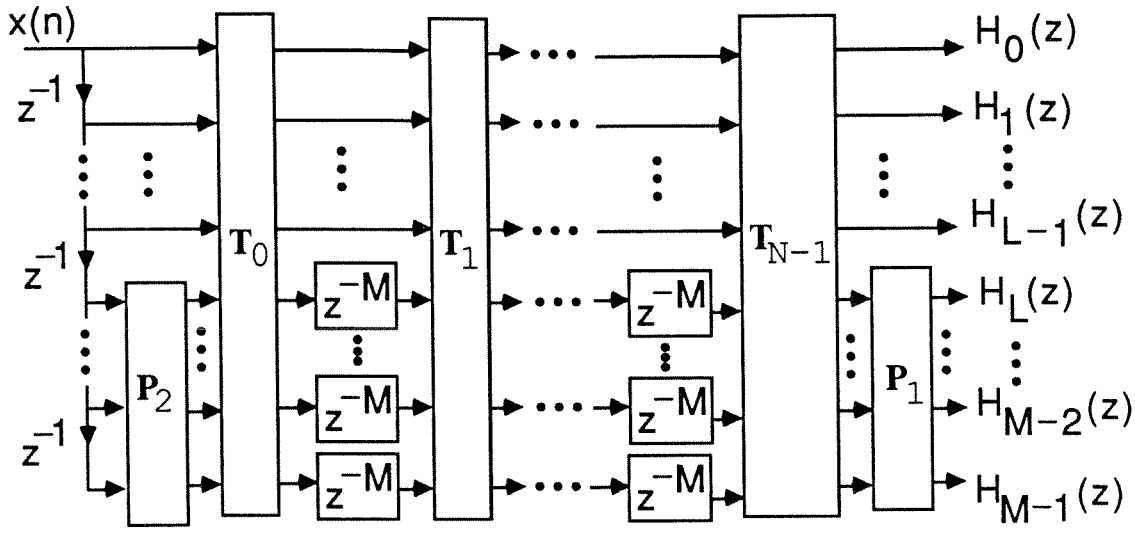

Fig. 3.13. An equivalent structure of Fig. 3.11.

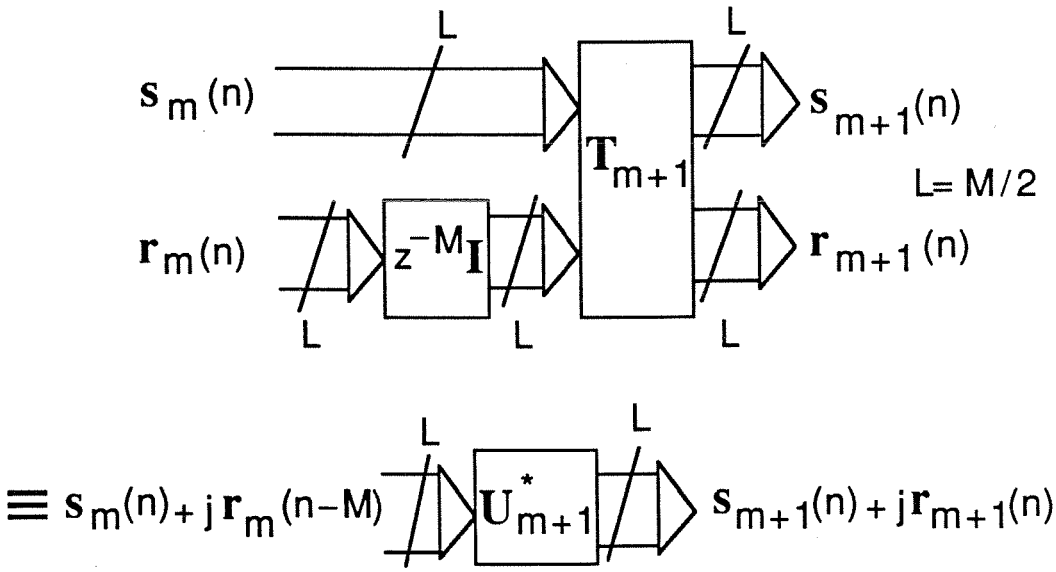

Fig. 3.14. The "complex domain" interpretation of each stage in Fig. 3.13.

If we define

$$\mathbf{U}_{m+1} = \mathbf{J}_{m+1,1} + j\mathbf{J}_{m+1,2}\mathbf{P}_1 \qquad \text{and} \qquad \mathbf{U}_0 = \mathbf{J}_{0,1} + j\mathbf{J}_{0,2}\mathbf{P}_3, \tag{3.43}$$

then it is clear that the unitariness of $\mathbf{U}_{m+1}$ and $\mathbf{U}_0$ implies the orthogonality of $\mathbf{T}_{m+1}$ and $\mathbf{T}_0$, respectively, and vice versa. Consequently, to form orthogonal $M \times M$ matrices $\mathbf{T}_{m+1}$ and $\mathbf{T}_0$ of the specific form (3.38), (3.39), we first construct arbitrary $L \times L$ unitary matrices $\mathbf{U}_{m+1}$ and $\mathbf{U}_0$. A general procedure to generate an arbitrary $L \times L$ unitary matrix is described in [9] and requires L^2 angles. Having formed $\mathbf{U}_{m+1}$ and $\mathbf{U}_0$, $\mathbf{T}_{m+1}$ and $\mathbf{T}_0$ are constructed as follows:

$$\mathbf{T}_{m+1} = \begin{pmatrix} Re(\mathbf{U}_{m+1}) & Im(\mathbf{U}_{m+1}) \\ -Im(\mathbf{U}_{m+1}) & Re(\mathbf{U}_{m+1}) \end{pmatrix}, \quad \text{and} \quad \mathbf{T}_0 = \begin{pmatrix} Re(\mathbf{U}_0) & -Im(\mathbf{U}_0) \\ Im(\mathbf{U}_0) & Re(\mathbf{U}_0) \end{pmatrix}. \tag{3.44}$$

This procedure guarantees that $\mathbf{T}_{m+1}$ and $\mathbf{T}_0$ are orthogonal, and hence Fig. 3.12 is the analysis bank of a perfect reconstruction structure with pairwise-symmetric response analysis filters. Compared to the earlier method [7], which requires $\binom{2L}{2}$ rotational angles, the symmetric structure described above requires at most L^2 angles [9]. Thus, the above structure yields faster optimization algorithms. The relation between $\mathbf{T}_{m+1}$ and $\mathbf{U}_{m+1}$ leads us to the equivalence shown in Fig. 3.14. Thus, the analysis bank is essentially a cascade of $L \times L$ complex unitary building blocks, with delays inserted into the imaginary paths of the signals. Appropriate adjustments are done at the left and right ends in order to obtain the correct initializations and the correct outputs. The initialization is done by setting

$$\begin{pmatrix} \mathbf{s}_0(n) \\ \\ \mathbf{r}_0(n) \end{pmatrix} = \mathbf{T}_0 \begin{pmatrix} \mathbf{s}_{-1}(n) \\ \\ \mathbf{P}_2\mathbf{r}_{-1}(n) \end{pmatrix},$$

where $\mathbf{s}_{-1}(n) = [x(n)\ x(n-1)\ \ldots\ x(n-L+1)]^T$ and $\mathbf{r}_{-1}(n) = [x(n-L)\ \ x(n-L-1)\ \ \ldots\ x(n-2L+1)]^T$ (recall $L = M/2$). The analysis transfer functions are

obtained as $\mathbf{H}_0(z) = \mathbf{s}_{N-1}(z)/X(z)$ and $\mathbf{H}_1(z) = \mathbf{P}_1\mathbf{r}_{N-1}(z)/X(z)$, where $\mathbf{H}_0(z) = [H_0(z)\ H_1(z)\ \ldots\ H_{L-1}(z)]^T$ and $\mathbf{H}_1(z) = [H_L(z)\ H_{L+1}(z)\ \ldots\ H_{M-1}(z)]^T$.

3.2.1. *Comment on the generality*

The structure in Fig. 3.13 yields PR pairwise symmetric analysis filters. In other words, for any choices of $\mathbf{T}_i$ satisfying (3.38) and (3.39), this structure is a PR structure, which yields pairwise symmetric filters. However, it *does not* cover all sets of PR pairwise symmetric filters.

Example 3.3: For $M = 4$, the analysis filters of a perfect reconstruction structure satisfy the pairwise frequency response image property,

$$\begin{cases} H_3(z) = z^{-(NM-1)}H_0(-z^{-1}), \\ \\ H_2(z) = z^{-(NM-1)}H_1(-z^{-1}), \end{cases} \tag{3.45}$$

where N is the number of sections in the structure. Let the unitary matrices $\mathbf{U}_0$ and $\mathbf{U}_m$ be

$$\mathbf{U}_0 = \frac{1}{\sqrt{2}} \begin{pmatrix} c_{0,1} - js_{0,1} & c_{0,2} + js_{0,2} \\ \\ -j(c_{0,1} - js_{0,1}) & j(c_{0,2} + js_{0,2}) \end{pmatrix}, \tag{3.46}$$

and

$$\mathbf{U}_m = \frac{1}{\sqrt{2}} \begin{pmatrix} c_{m,1} + js_{m,1} & c_{m,2} + js_{m,2} \\ \\ j(c_{m,1} + js_{m,1}) & -j(c_{m,2} + js_{m,2}) \end{pmatrix}, \tag{3.47}$$

then

$$\mathbf{T}_0 = \frac{1}{\sqrt{2}} \begin{pmatrix} c_{0,1} & c_{0,2} & s_{0,1} & -s_{0,2} \\ -s_{0,1} & -s_{0,2} & c_{0,1} & -c_{0,2} \\ -s_{0,1} & s_{0,2} & c_{0,1} & c_{0,2} \\ -c_{0,1} & c_{0,2} & -s_{0,1} & -s_{0,2} \end{pmatrix} \tag{3.48}$$

and

$$\mathbf{T}_m = \frac{1}{\sqrt{2}} \begin{pmatrix} c_{m,1} & c_{m,2} & s_{m,1} & s_{m,2} \\ -s_{m,1} & s_{m,2} & c_{m,1} & -c_{m,2} \\ -s_{m,1} & -s_{m,2} & c_{m,1} & c_{m,2} \\ -c_{m,1} & c_{m,2} & -s_{m,1} & s_{m,2} \end{pmatrix}, \tag{3.49}$$

where $c_{m,i} = \cos(\theta_{m,i})$, $s_{m,i} = \sin(\theta_{m,i})$ and $\theta_{m,i}$ are the planar rotation angles at the m^{th} stage. It can be easily verified that the above $\mathbf{T}_0$ and $\mathbf{T}_m$ are orthogonal.

The above forms for $\mathbf{U}_0$ and $\mathbf{U}_m$ do not represent the most general 2×2 unitary matrices (which actually require 4 angles to be completely characterized). These forms are meant only to be examples. We choose $N = 15$ in this example, so that the length of each (FIR) analysis filter is 60. There are 30 angles $\theta_{m,i}$ $0 \leq m \leq 14$, $0 \leq i \leq 1$ in the lattice structure of Fig. 3.13, and these are optimized using the IMSL subroutine to minimize the following objective function

$$\phi = \int_{\frac{\pi}{4}+\epsilon}^{\pi} |H_0(e^{j\omega})|^2 d\omega + \int_0^{\frac{\pi}{4}-\epsilon} |H_1(e^{j\omega})|^2 d\omega + \int_{\frac{\pi}{2}+\epsilon}^{\pi} |H_1(e^{j\omega})|^2 d\omega \qquad (3.50)$$

for $\epsilon = 0.05\pi$. Note that we do not include the stopband energies of $H_2(e^{j\omega})$ and $H_3(e^{j\omega})$ in ϕ, since they will be small if the stopband energies of their images, $H_0(e^{j\omega})$ and $H_1(e^{j\omega})$, are small because of the pairwise-symmetry property. Moreover, because of the structural form of Fig. 3.13, the constraint $\sum_{k=0}^{M-1} |H_k(e^{j\omega})|^2 = 1$ automatically holds, hence the passband errors automatically come out to be small. The magnitude responses of the resulting analysis filters are shown in Fig. 3.15. The impulse response coefficients of $H_0(z)$ and $H_1(z)$ are displayed in Table 3.4, whereas the 30 rotation angles $\theta_{m,i}$ are shown in Table 3.3, respectively. Based on the relation $H_{M-1-k}(z) = z^{-r} H_k(-z^{-1})$, the impulse response coefficients of $H_2(z)$ and $H_3(z)$ can be readily obtained from Table 3.4.

3.2.2. *Complexity of the analysis bank*

Let us calculate the complexity of the analysis bank using both the direct-form structure and the lattice structure. If we implement $H_k(z)$ of length $\hat{S}$ in direct form and if we share the multipliers of $H_k(z)$ and $H_{M-1-k}(z)$, a total of $\hat{S} = 2 \times 60 = 120$ multiplications are involved per computed output sample (see Fig. 30 of [52]). Having shared the multipliers of the pairwise symmetric analysis filters, we cannot, however, take advantage of the decimation factor of 4. A more efficient direct-form

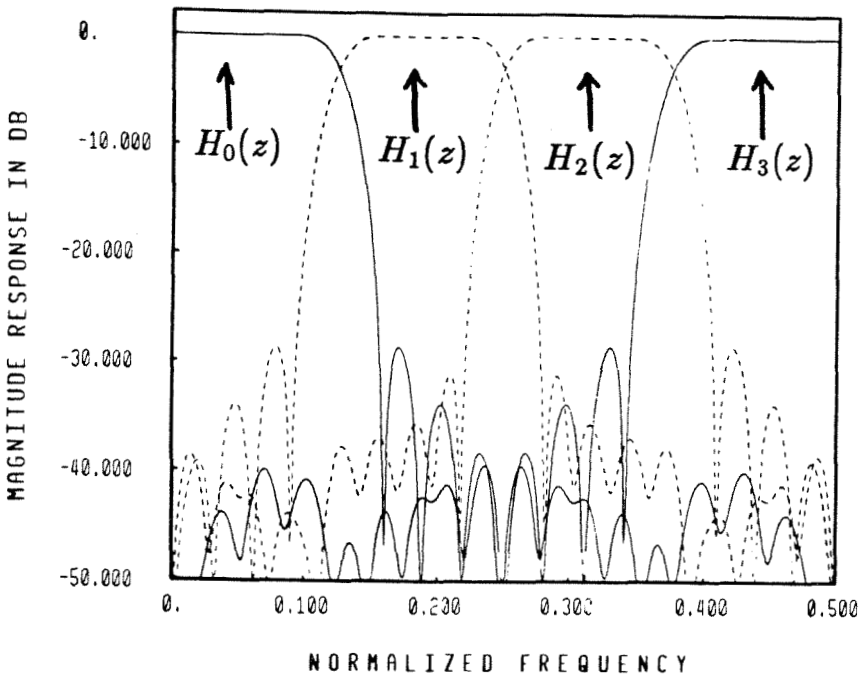

Fig. 3.15. Ex. 3.3. Magnitude response plots for the optimized analysis filters.

Table 3.3 Lattice coefficients $c_{m,i}$ of the optimized analysis filters in Ex. 3.3.

m	$c_{m,1}$ (radians)	$c_{m,2}$ (radians)
0	$7.41084775035 \times 10^{-1}$	$2.138794011844 \times 10^{0}$
1	$1.573215834853 \times 10^{0}$	$3.68082394900 \times 10^{-2}$
2	$-2.611144973198 \times 10^{0}$	$-9.40422532957 \times 10^{-1}$
3	$6.42547910295 \times 10^{-1}$	$1.839316933945 \times 10^{0}$
4	$2.30923183185 \times 10^{-1}$	$-6.24448685365 \times 10^{-1}$
5	$9.61854454362 \times 10^{-1}$	$-1.610307594321 \times 10^{0}$
6	$1.344451892866 \times 10^{0}$	$-1.106309251254 \times 10^{0}$
7	$-4.35627660700 \times 10^{-1}$	$-1.270607254565 \times 10^{0}$
8	$1.986567539096 \times 10^{0}$	$-6.18479910740 \times 10^{-2}$
9	$-7.14097642235 \times 10^{-1}$	$-1.713180166432 \times 10^{0}$
10	$4.48694392230 \times 10^{-2}$	$3.68294469924 \times 10^{-1}$
11	$-2.235042579105 \times 10^{0}$	$2.969970589153 \times 10^{0}$
12	$-2.296783189526 \times 10^{0}$	$2.305628909293 \times 10^{0}$
13	$7.60167304861 \times 10^{-1}$	$-1.152288299267 \times 10^{0}$
14	$-1.209970845496 \times 10^{0}$	$-2.649477562481 \times 10^{0}$

Table 3.4 Impulse responses of the optimized analysis filters in Ex. 3.3. $h_{2,n}$ and $h_{3,n}$ can be computed by $h_{2,n} = (-1)^n h_{1,(59-n)}$ and $h_{3,n} = (-1)^n h_{0,(59-n)}$.

m	Coefficients $h_{0,m}$	Coefficients $h_{1,m}$
0	-4.112909×10^{-7}	-1.036139×10^{-5}
1	3.132275×10^{-5}	7.856715×10^{-5}
2	-5.893893×10^{-6}	-2.425497×10^{-5}
3	-3.186979×10^{-5}	-8.157047×10^{-5}
4	-1.105067×10^{-4}	2.188679×10^{-4}
5	3.307961×10^{-4}	-1.633159×10^{-4}
6	-2.371339×10^{-4}	7.728539×10^{-5}
7	3.715518×10^{-4}	1.795792×10^{-4}
8	1.576836×10^{-3}	-2.973126×10^{-3}
9	1.496360×10^{-3}	5.881045×10^{-3}
10	5.629141×10^{-4}	-3.572236×10^{-3}
11	-1.136803×10^{-3}	-6.725697×10^{-3}
12	-4.113295×10^{-3}	2.115079×10^{-2}
13	-8.030231×10^{-3}	3.692664×10^{-2}
14	-4.718402×10^{-3}	5.707743×10^{-4}
15	2.775006×10^{-3}	-3.065480×10^{-2}
16	6.557429×10^{-3}	-2.204044×10^{-2}
17	1.559687×10^{-2}	-2.946152×10^{-2}
18	1.385026×10^{-2}	-8.008066×10^{-2}
19	5.375807×10^{-3}	-4.002172×10^{-2}
20	-1.627377×10^{-2}	1.032986×10^{-1}
21	-3.569490×10^{-2}	1.714444×10^{-1}
22	-2.318588×10^{-2}	7.857019×10^{-2}
23	1.570406×10^{-2}	-3.284753×10^{-2}
24	5.158685×10^{-2}	-1.239302×10^{-1}
25	5.101791×10^{-2}	-2.658401×10^{-1}
26	5.751899×10^{-3}	-2.618550×10^{-1}
27	-6.403119×10^{-2}	1.608913×10^{-1}
28	-1.033400×10^{-1}	6.293975×10^{-1}
29	-5.718426×10^{-2}	3.947782×10^{-1}
30	9.967532×10^{-2}	-4.133726×10^{-1}
31	3.394553×10^{-1}	-7.269581×10^{-1}
32	5.816531×10^{-1}	-1.198777×10^{-1}
33	7.294070×10^{-1}	5.004390×10^{-1}
34	7.171285×10^{-1}	3.264686×10^{-1}
35	5.430961×10^{-1}	-1.651893×10^{-1}
36	2.735978×10^{-1}	-1.857216×10^{-1}
37	1.288885×10^{-2}	9.795945×10^{-2}
38	-1.532637×10^{-1}	1.029023×10^{-1}
39	-1.888961×10^{-1}	-1.243248×10^{-1}
40	-1.148823×10^{-1}	-1.461468×10^{-1}
41	-8.670705×10^{-3}	5.699251×10^{-2}
42	7.366400×10^{-2}	1.086455×10^{-1}
43	9.577717×10^{-2}	-1.099477×10^{-2}
44	4.897745×10^{-2}	-3.296077×10^{-2}
45	-1.455038×10^{-3}	2.179891×10^{-2}
46	-4.316611×10^{-2}	2.694672×10^{-2}
47	-4.025652×10^{-2}	-1.983401×10^{-2}
48	-2.236369×10^{-2}	-1.728839×10^{-2}
49	7.961925×10^{-3}	3.941657×10^{-3}
50	2.070427×10^{-2}	1.732675×10^{-2}
51	3.895899×10^{-3}	1.367387×10^{-3}
52	-2.326464×10^{-4}	2.488686×10^{-4}
53	-6.643766×10^{-5}	6.785641×10^{-5}
54	2.626722×10^{-4}	-2.771207×10^{-4}
55	-2.793461×10^{-4}	1.765755×10^{-4}
56	-8.010599×10^{-5}	2.913810×10^{-5}
57	2.863498×10^{-5}	-1.406389×10^{-5}
58	7.631467×10^{-5}	-2.712121×10^{-5}
59	1.506388×10^{-5}	-9.182824×10^{-6}

implementation is to take advantage of the decimation ratio without sharing the multiplers. This requires a total of $4\hat{S}/4 = 240/4 = 60 = \hat{S}$ MPU for the complete analysis bank.

On the other hand, if we implement the lattice structure of Fig. 3.13 directly, we can take further advantage of the orthogonal form of $\mathbf{T}_m$. At the output of each stage, we would have to compute

$$\begin{pmatrix} y_0 \\ y_1 \\ y_2 \\ y_3 \end{pmatrix} = \begin{pmatrix} c_{m,1} & c_{m,2} & s_{m,1} & s_{m,2} \\ -s_{m,1} & s_{m,2} & c_{m,1} & -c_{m,2} \\ -s_{m,1} & -s_{m,2} & c_{m,1} & c_{m,2} \\ -c_{m,1} & c_{m,2} & -s_{m,1} & s_{m,2} \end{pmatrix} \begin{pmatrix} u_0 \\ u_1 \\ u_2 \\ u_3 \end{pmatrix}, \tag{3.51}$$

where u_i and y_i are the inputs and outputs of each block $\mathbf{T}_m$. Rewrite the above equation as

$$\begin{pmatrix} y_0 \\ y_1 \end{pmatrix} = \begin{pmatrix} c_{m,1} & s_{m,1} \\ -s_{m,1} & c_{m,1} \end{pmatrix} \begin{pmatrix} u_0 \\ u_2 \end{pmatrix} + \begin{pmatrix} c_{m,2} & s_{m,2} \\ s_{m,2} & -c_{m,2} \end{pmatrix} \begin{pmatrix} u_1 \\ u_3 \end{pmatrix} = \begin{pmatrix} a_0 \\ a_1 \end{pmatrix} + \begin{pmatrix} b_0 \\ b_1 \end{pmatrix}, \tag{3.52}$$

$$\begin{pmatrix} y_2 \\ y_3 \end{pmatrix} = \begin{pmatrix} -s_{m,1} & c_{m,1} \\ -c_{m,1} & -s_{m,1} \end{pmatrix} \begin{pmatrix} u_0 \\ u_2 \end{pmatrix} + \begin{pmatrix} -s_{m,2} & c_{m,2} \\ c_{m,2} & s_{m,2} \end{pmatrix} \begin{pmatrix} u_1 \\ u_3 \end{pmatrix}. \tag{3.53}$$

Having computed $(a_0 \;\; a_1)^T$ and $(b_0 \;\; b_1)^T$, we have

$$\begin{pmatrix} y_2 \\ y_3 \end{pmatrix} = \begin{pmatrix} a_1 - b_1 \\ -a_0 + b_0 \end{pmatrix}.$$

Since each 2×2 block in (3.52) is an orthogonal block, we can compute it using 3 multiplications and 3 additions [60]. Thus, (3.51) requires 6 multiplications and 10 additions. The complexity of the normalized lattice structure is, therefore, $6\times$ number of stages $= 6N = 6/4 \times \hat{S} = 90$ MPU, where $\hat{S}$ is the length of $H_k(z)$. Since the decimators can be moved all the way to the left of the building block $\mathbf{T}_0$ in Fig. 3.13, the actual number of MPU's is only $3\hat{S}/8 \approx 23$. Notice that the 4×4 matrix (3.51) is orthogonal; hence, the lattice structure is automatically L_2 scaled. It is possible to obtain a more efficient (but denormalized) lattice structure by noting

that if we divide each element on $\mathbf{T}_m$ by a constant, say $c_{m,1}$, the responses of $H_k(z)$ are unchanged (except for a scale factor.) Thus, (3.52) and (3.53) are written as

$$\begin{pmatrix} y'_0 \\ y'_1 \end{pmatrix} = \begin{pmatrix} 1 & s'_{m,1} \\ -s'_{m,1} & 1 \end{pmatrix} \begin{pmatrix} u_0 \\ u_2 \end{pmatrix} + \begin{pmatrix} c'_{m,2} & s'_{m,2} \\ s'_{m,2} & -c'_{m,2} \end{pmatrix} \begin{pmatrix} u_1 \\ u_3 \end{pmatrix} = \begin{pmatrix} a'_0 \\ a'_1 \end{pmatrix} + \begin{pmatrix} b'_0 \\ b'_1 \end{pmatrix}, \quad (3.54)$$

$$\begin{pmatrix} y'_2 \\ y'_3 \end{pmatrix} = \begin{pmatrix} -s'_{m,1} & 1 \\ -1 & -s'_{m,1} \end{pmatrix} \begin{pmatrix} u_0 \\ u_2 \end{pmatrix} + \begin{pmatrix} -s'_{m,2} & c'_{m,2} \\ c'_{m,2} & s'_{m,2} \end{pmatrix} \begin{pmatrix} u_1 \\ u_3 \end{pmatrix}. \quad (3.55)$$

By noting that $(a'_0 \;\; a'_1)^T$ can be computed by 2 multiplications, each denormalized orthogonal block $\mathbf{T}_m$ requires only 5 multiplications. Hence, the total complexity for the analysis bank is $5\hat{S}/16 \approx 19$ MPU.

3.2.3. *Comparison between tree-structured design and the proposed lattice structure*

The conventional procedure to design a four-channel perfect-reconstruction system would be to use the tree structure [18] of the form in Fig. 3.16. Here, $[H_{00}(z), H_{01}(z)]$ is a two-channel perfect-reconstruction pair, and so is $[H'_{00}(z), H'_{01}(z)]$. (Appendix 3.E reviews the design procedure of the two-channel PR system in [5], and [18]. Also, its relation to lattice structure [19] is briefly discussed.) These pairs are designed by spectral factorization of appropriate half-band filters [18]. The overall analysis filters are $H_0(z) = H_{00}(z)H'_{00}(z^2)$, $H_1(z) = H_{00}(z)H'_{01}(z^2)$, and so on. In order to obtain the same transition bandwidth Δf as in Fig. 3.15, we should take the transition bandwidth of $H_{00}(z)$ to be Δf and that of $H'_{00}(z)$ to be $2\Delta f$. The stopband attenuation seen in Fig. 3.15 can be obtained with the tree structure if $H_{00}(z)$ and $H'_{00}(z)$, designed as in [18], are of lengths 30 and 16, respectively. Thus, each analysis filter has length $= (29 + 2 \times 15 + 1) = 60$. The responses are shown in Fig. 3.17. It seems to be an interesting coincidence that the analysis filters $H_k(z)$ corresponding to Fig. 3.15 and Fig. 3.17 have the same length ($= 60$). It is not clear to us at this time as to whether this is a general property of the two methods

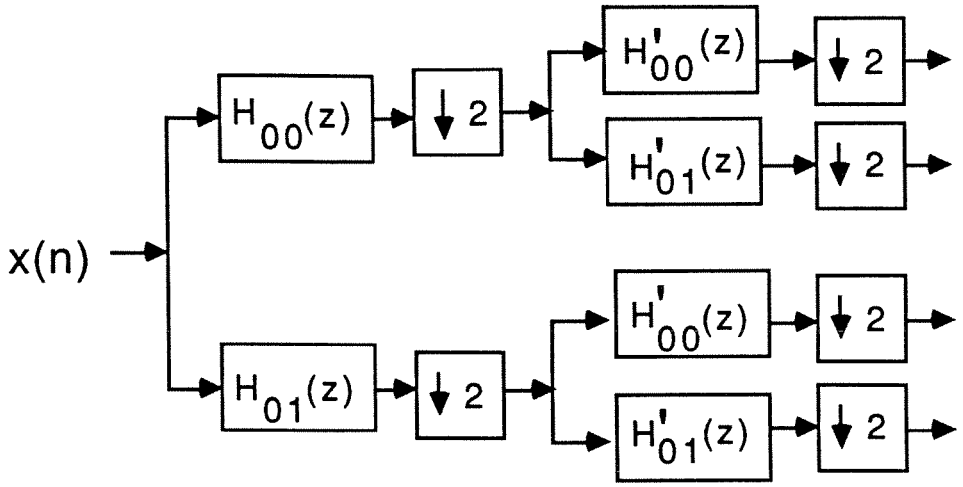

Fig. 3.16. The 4x4 tree-structured QMF analysis bank.

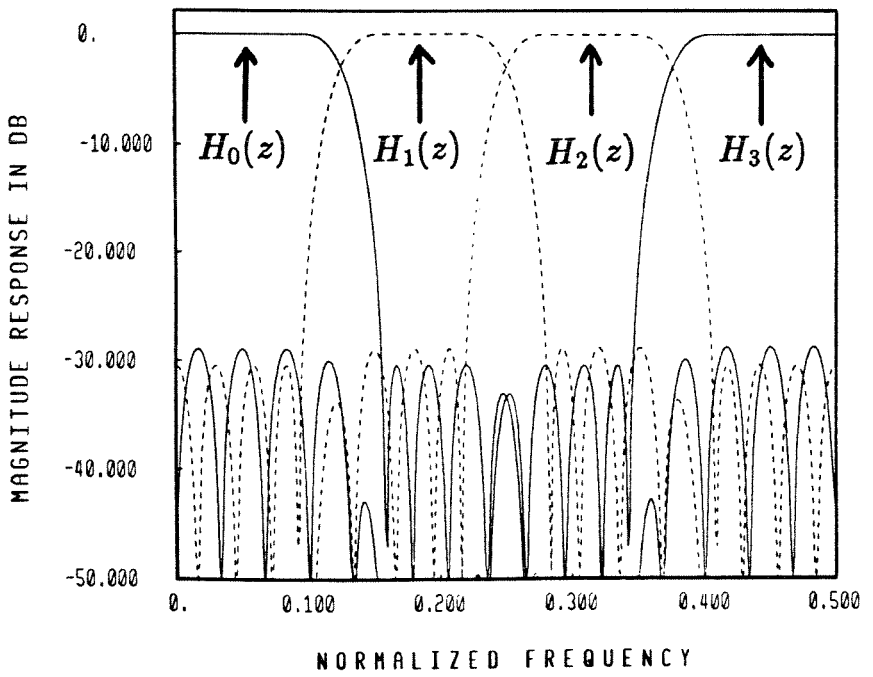

Fig. 3.17. Ex. 3.3. Magnitude response plots for the analysis filters designed based on the tree structure.

for power-of-two M. The overall group delay of the QMF system is equal to 59 samples, for both methods.

It is interesting to compare the complexity (in terms of both MPU and APU) for the two designs. For the tree-structured design, we can implement each two-channel branch in Fig. 3.16 by either direct-form [18] or lattice structure [19]. In our implementation, two factors which can potentially contribute to savings in the number of multiplication are: a). the relation $H_{01}(z) = z^{-29}H_{00}(-z^{-1})$, and b). decimation by a factor of two. In a direct-form structure we cannot *simultaneously* exploit both of these factors because the order is necessarily odd (29 in our example.) Based on either one of these factors, it is easy to implement the pair $[H_{00}(z), H_{01}(z)]$ using only (29+1) MPU. Galand and Nussbaumer have proposed a modified direct-form scheme [61] whereby both the above contributing factors can be *partially* exploited to obtain an implementation with only $3/4 \times (29 + 1)$ MPU. Thus, the pair $[H_{00}(z), H_{01}(z)]$ requires $3/4 \times 30$ multiplications per computed output sample [61]. Similarly, because of the decimation factor, each $[H'_{00}(z), H'_{01}(z)]$ pair requires $1/2 \times 3/4 \times (16) = 6$ MPU. Hence, in a modified direct-form implementation, the analysis bank designed based on the tree structure requires $3/4 \times (30) + 3/4 \times (16) \approx$ 35 MPU.

The lattice structure implementation is based on the lossless property of the polyphase filter matrix $\mathbf{E}(z)$ [19]. The denormalized two-channel lattice requires $S/2$ MPU (see [19]), where S is the length of each analysis filter. The normalized lattice structure, on the other hand, has automatic internal L_2 scaling property, as the internal building blocks are planar rotation operators. Each such operator is mathematically identical to a single complex multiplication, and can be implemented [60] using 3 real multiplications (and 3 real additions). As a result, the

entire normalized analysis bank requires only $3S/4$ MPU, which is exactly the same as the best known [61]. The complexity of the pair $[H_{00}(z), H_{01}(z)]$, hence, is 23 and 15 MPU for the normalized and denormalized implementations, respectively. Similarly, because of the decimation factor, each $[H'_{00}(z), H'_{01}(z)]$ pair requires 6 and 4 MPU for the normalized and denormalized structures, respectively. Implemented by lattice structure, the total complexity of the analysis bank designed based on tree structure is $23 + 2 \times 6 = 35$ MPU and $15 + 2 \times 4 = 23$ for the normalized and denormalized structures, respectively.

Table 3.5 summarizes the comparison between the new design and the tree-structured design. As is evident from it, the complexity of the new pairwise symmetric lattice structure implementations is less than that of the tree-structured implementation. In fact, with a denormalized lattice, the MPU count is the smallest ($= 19$). Besides the complexity advantage, the pairwise symmetric lattice structure can be used for designing filters with arbitrary M, which is not necessarily a power of 2.

Table 3.5 Comparison of the number of multiplications per unit time in the analysis bank for various four-channel QMF bank implementations. Here "unit time" is the sampling period corresponding to the input $x(n)$ in Fig. 3.1(a). The normalized two-channel lattice is assumed to be implemented with 3 multiplications per section.

	Tree-structure based design				Non-tree lattice-based design		
	Direct Form		Lattice [19]		Direct Form	New Lattice	
	Regular	Galand [61]	Denorm	Norm		Norm	Denorm
General expression for MPU	$N_0 + N_1$	$\frac{3}{4}(N_0 + N_1)$	$\frac{1}{2}(N_0 + N_1)$	$\frac{3}{4}(N_0 + N_1)$	$\hat{S}$	$\frac{3}{8}\hat{S}$	$\frac{5}{16}\hat{S}$
No. of MPU with $N_0 = 30$ $N_1 = 16$ $\hat{S} = 60$	46	35	23	35	60	23	19
Order of $H_k(z) =$ Group delay	59	59	59	59	59	59	59

- N_0 = length of the analysis filters in stage 1 (Tree structure).
- N_1 = length of the analysis filters in stage 2 (Tree structure).
- $\hat{S}$= length of analysis filters in the new lattice.

Appendix 3.A

We shall state and prove two lemmas here.

Lemma 3.A.1: If the analysis filters can be written in two ways:

$$\begin{pmatrix} H_0(z) \\ H_1(z) \\ \vdots \\ H_{M-1}(z) \end{pmatrix} = \mathbf{E}(z^M) \begin{pmatrix} 1 \\ z^{-1} \\ \vdots \\ z^{-(M-1)} \end{pmatrix} = \mathbf{G}(z^M) \begin{pmatrix} 1 \\ z^{-i} \\ \vdots \\ z^{-i(M-1)} \end{pmatrix}, \qquad (3.A.1)$$

where [2] $(i, M) = 1$, then

$$\tilde{\mathbf{E}}\mathbf{E} = \mathbf{I} \qquad \text{if and only if} \qquad \tilde{\mathbf{G}}\mathbf{G} = \mathbf{I}. \qquad (3.A.2)$$

Lemma 3.A.2: Consider the structure in Fig. 3.18. If $(i, M) = 1$, then this is a perfect-reconstruction system.

When $i = 2$ and M is odd, the above two lemmas can be applied to Fig. 3.3 to conclude two features:

1). If $\mathbf{E}'(z^{2M})$ is lossless and $\mathbf{R}$ is orthogonal, then $\mathbf{R}\boldsymbol{\Gamma}(z^M)\mathbf{E}'(z^{2M}) = \mathbf{G}(z^M)$ is lossless; hence, the complete structure in Fig. 3.4 has perfect-reconstruction property by Lemma 3.A.2.

2). Imposing losslessness on $\mathbf{E}'(z)$ is equivalent to imposing losslessness on $\mathbf{E}(z)$.

Proof: (Lemma 3.A.1) First consider the $M \times M$ DFT matrix. This is unitary because $\mathbf{W}^\dagger\mathbf{W} = M\mathbf{I}$; i.e.,

$$\sum_{k=0}^{M-1} W^{-\ell' k} W^{\ell k} = \begin{cases} 0, & \text{if } \ell = \ell'; \\ M, & \text{if } \ell = \ell', \end{cases}$$

[2] Here (i, M) denotes the greatest common divisor of i and M.

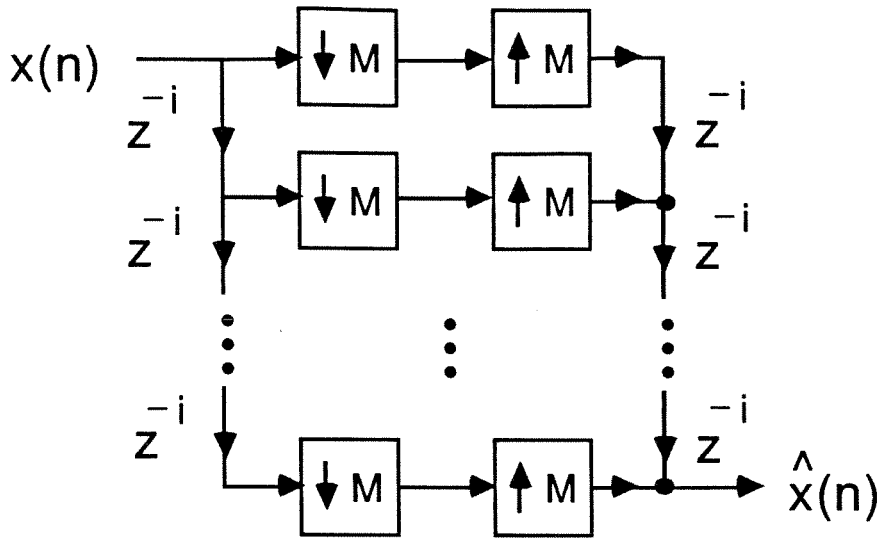

Fig. 3.18. Pertaining to Appendix 3.A.

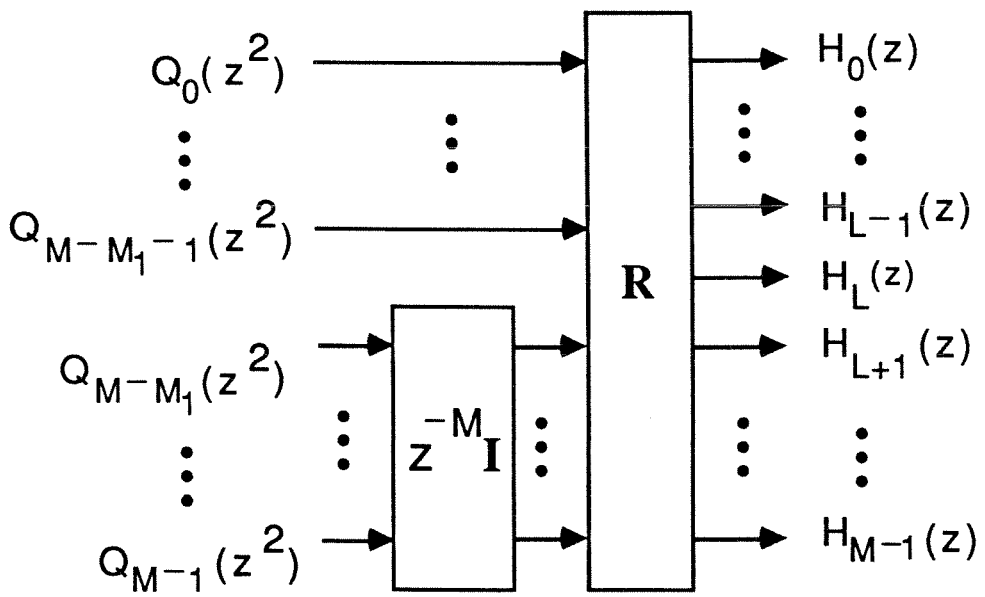

Fig. 3.19. Pertaining to Appendix 3.B.

where $0 \le \ell, \ell' \le M-1$. Suppose we replace W with W^S, where $(S,M)=1$, then

$$\sum_{k=0}^{M-1} W^{-\ell' ks} W^{\ell ks} = \sum_{k=0}^{M-1} W^{ks(\ell-\ell')} = \begin{cases} 0, & \text{if } s(\ell-\ell') \neq \text{multiple of } M; \\ M, & \text{otherwise.} \end{cases} \qquad (3.A.3)$$

Since $|\ell-\ell'| \le M$, we see that $s(\ell-\ell')$ is a multiple of M only if s contains a factor of M. This cannot happen if $(s,M)=1$. Hence,

$$\sum_{k=0}^{M-1} W^{ks(\ell-\ell')} = \begin{cases} 0, & \text{if } \ell \neq \ell'; \\ M, & \ell = \ell'. \end{cases} \qquad (3.A.4)$$

The modified DFT matrix, denoted $\mathbf{W}^{(s)}$, is therefore also unitary. Now (3.A.1) implies

$$\mathbf{E}(z^M) \begin{pmatrix} 1 & & & \mathbf{0} \\ & z^{-1} & & \\ & & \ddots & \\ \mathbf{0} & & & z^{-(M-1)} \end{pmatrix} \begin{pmatrix} 1 \\ W^k \\ \vdots \\ W^{(M-1)k} \end{pmatrix} =$$

$$\mathbf{G}(z^M) \begin{pmatrix} 1 & & & \mathbf{0} \\ & z^{-i} & & \\ & & \ddots & \\ \mathbf{0} & & & z^{-i(M-1)} \end{pmatrix} \begin{pmatrix} 1 \\ W^{ki} \\ \vdots \\ W^{(M-1)ki} \end{pmatrix}$$

for any k. This implies

$$\mathbf{E}(z^M)\lambda(z)\mathbf{W} = \mathbf{G}(z^M)\Lambda(z^i)\mathbf{W}^{(i)}, \qquad (3.A.5)$$

where $\Lambda(z) = \text{diag}\,[z^{-k}]$. Since $\Lambda(z)$, $\mathbf{W}$, $\Lambda(z^i)$ and $\mathbf{W}^i$are lossless, we conclude that (3.A.2) is true as long as $(i,M)=1$.

Proof (Lemma 3.A.2):

$$\hat{X}(z) = \frac{1}{M} \sum_{k=0}^{M-1} \sum_{\ell=0}^{M-1} F_k(z) H_k(zW^\ell) X(zW^\ell). \qquad (3.A.6)$$

In Fig. 3.18, $H_k(z) = z^{-ki}$ and $F_k(z) = z^{-(M-1-k)i}$, so (3.A.6) becomes

$$\hat{X}(z) = \frac{1}{M} \sum_{k=0}^{M-1} \sum_{\ell=0}^{M-1} z^{-(M-1-k)i} (zW^\ell)^{-ki} X(zW^i)$$

$$= \frac{1}{M} \sum_{\ell=0}^{M-1} X(zW^{\ell}) \sum_{k=0}^{M-1} z^{-(M-1-k)i} z^{-ki} W^{-k\ell i}$$

$$= \frac{1}{M} \sum_{\ell=0}^{M-1} X(zW^{\ell}) z^{-(M-1)i} \sum_{k=0}^{M-1} W^{-k\ell i}. \qquad (3.A.7)$$

Note that $\sum_{k=0}^{M-1} W^{-k\ell i} = 0$, unless ℓi is a multiple of M. Since $0 \leq \ell \leq M-1$ and $(i, M) = 1$, ℓ has to be 0. Thus, (3.A.7) simplifies to

$$\hat{X}(z) = \frac{1}{M} X(z) z^{-(M-1)i} M = z^{-(M-1)i} X(z).$$

The structure in Fig. 3.18 is, therefore, a perfect-reconstruction structure. We will now find the relation between the analysis and synthesis filters of Fig. 3.4. With $\mathbf{G}(z^M) \triangleq \mathbf{R}\Lambda(z^M)\mathbf{E}'(z^{2M})$, the synthesis filters $F_k(z)$ in Fig. 3.4 are given by

$$[F_0(z) \;\; F_1(z) \;\; \ldots \;\; F_{M-1}(z)] = [z^{-(M-1)i} \;\; z^{-(M-2)i} \;\; \ldots \;\; z^{-i} \;\; 1]\tilde{\mathbf{G}}(z^M) z^{-sM} \qquad (3.A.8)$$

with $i = 2$. However,

$$[\tilde{H}_0(z) \;\; \tilde{H}_1(z) \;\; \ldots \;\; \tilde{H}_{M-1}(z)] = [1 \;\; z^{i} \;\; \ldots \;\; z^{i(M-1)}]\tilde{\mathbf{G}}(z^M)$$

$$= z^{i(M-1)}[z^{-(M-1)i} \;\; z^{-(M-2)i} \;\; \ldots \;\; 1]\tilde{\mathbf{G}}(z^M)$$

$$= z^{i(M-1)}[F_0(z) \;\; F_1(z) \;\; \ldots \;\; F_{M-1}(z)]z^{sM}.$$

Thus,

$$F_k(z) = z^{-(sM+iM-i)} \tilde{H}_k(z). \qquad (3.A.9)$$

If the analysis banks of Fig. 3.3 and Fig. 3.1(b) are related as in (3.A.1), are the synthesis banks of Fig. 3.3 and Fig. 3.1(b) identical? From (3.A.1), we have

$$[1 \;\; z \;\; \ldots \;\; z^{(M-1)}]\tilde{\mathbf{E}}(z^M) = [1 \;\; z^{i} \;\; \ldots \;\; z^{i(M-1)}]\tilde{\mathbf{G}}(z^M),$$

which implies

$$z^{(M-1)}[z^{-(M-1)} \;\; \ldots \;\; z^{-1} \;\; 1]\tilde{\mathbf{E}}(z^M) = z^{i(M-1)}[z^{-i(M-1)} \;\; \ldots \;\; z^{-i} \;\; 1]\tilde{\mathbf{G}}(z^M). \qquad (3.A.10)$$

Hence, the synthesis banks in Fig. 3.3 and Fig. 3.1(b) are identical, except for a possible overall delay.

Appendix 3.B

Fig. 3.19 shows the terminal blocks of the analysis bank for odd M, where $M = 2L+1$, and the number of connecting lines with delays z^{-M} are $M_1 \leq M$. We will derive the necessary and sufficient conditions for $\mathbf{R}$ so that $H_k(z)$ satisfy the pairwise symmetry property (3.7). Let

$$\mathbf{h}^1(z) = \begin{pmatrix} H_0(z) \\ \vdots \\ H_{L-1}(z) \end{pmatrix}, \quad \mathbf{h}^2(z) = \begin{pmatrix} H_{L+1}(z) \\ \vdots \\ H_{M-1}(z) \end{pmatrix},$$

$$\mathbf{q}^1(z) = \begin{pmatrix} Q_0(z^2) \\ \vdots \\ Q_{M-M_1-1}(z^2) \end{pmatrix}, \quad \mathbf{q}^2 = \begin{pmatrix} Q_{M-M_1}(z^2) \\ \vdots \\ Q_{M-1}(z^2) \end{pmatrix}.$$

Thus the pairwise symmetry property on $H_k(z)$ yields

$$\mathbf{P}_1 \mathbf{h}^2(z) = \mathbf{h}^1(-z), \tag{3.A.11}$$

where $\mathbf{P}_1$ is defined as in (3.16). Let $\mathbf{R}$ be partitioned into

$$\mathbf{R} = \begin{pmatrix} \mathbf{A} & \mathbf{B} \\ \mathbf{C} & \mathbf{D} \\ \mathbf{E} & \mathbf{F} \end{pmatrix}_{M \times M}, \tag{3.A.12}$$

where $\mathbf{A}$ is $L \times (M - M_1)$, $\mathbf{B}$ is $L \times M_1$, $\mathbf{C}$ is $1 \times (M - M_1)$, $\mathbf{D}$ is $1 \times M_1$, $\mathbf{E}$ is $L \times (M - M_1)$ and $\mathbf{F}$ is $L \times M_1$. Thus,

$$\begin{pmatrix} \mathbf{h}^1(z) \\ H_L(z) \\ \mathbf{h}^2(z) \end{pmatrix} = \mathbf{R}\Gamma(z^M) \begin{pmatrix} \mathbf{q}^1(z^2) \\ \\ \mathbf{q}^2(z^2) \end{pmatrix} = \begin{pmatrix} \mathbf{A}\mathbf{q}^1(z^2) + z^{-M}\mathbf{B}\mathbf{q}^2(z^2) \\ \\ \mathbf{C}\mathbf{q}^1(z^2) + z^{-M}\mathbf{D}\mathbf{q}^2(z^2) \\ \\ \mathbf{E}\mathbf{q}^1(z^2) + z^{-M}\mathbf{F}\mathbf{q}^2(z^2) \end{pmatrix}. \tag{3.A.13}$$

Our aim is to find a structural form for $\mathbf{R}$ such that for *any* set of polynomials $\mathbf{q}^1(z)$ and $\mathbf{q}^2(z)$, the vectors $\mathbf{h}^1(z)$ and $\mathbf{h}^2(z)$ are related by (3.A.11). By the pairwise-symmetry property, $H_L(z) = H_L(-z) =$ a function of z^2. Since M is odd, it is clear

from (3.*A*.13) that $\mathbf{D} = \mathbf{0}$. Substituting (3.*A*.13) into (3.*A*.11) and simplifying, we have

$$(\mathbf{A} - \mathbf{P}_1\mathbf{E})\mathbf{q}^1(z^2) = z^{-M}(\mathbf{P}_1\mathbf{F} + \mathbf{B})\mathbf{q}^2(z^2). \tag{3.A.14}$$

Since M is odd, the RHS of (3.*A*.14) has only odd powers of z^{-1}, whereas the LHS has only even powers. With arbitrary $\mathbf{q}^1(z)$ and $\mathbf{q}^2(z)$, this is possible if and only if $\mathbf{A} - \mathbf{P}_1\mathbf{E} = \mathbf{0}$, and $\mathbf{P}_1\mathbf{F} + \mathbf{B} = \mathbf{0}$. Thus, $\mathbf{E} = \mathbf{P}_1^{-1}\mathbf{A} = \mathbf{P}_1\mathbf{A}$ and $\mathbf{F} = -\mathbf{P}_1^{-1}\mathbf{B} = -\mathbf{P}_1\mathbf{B}$ as in (3.15).

Appendix 3.C

Let

$$\mathbf{h}_m^1(z) = \begin{pmatrix} H_{m,0}(z) \\ \vdots \\ H_{m,L-1}(z) \end{pmatrix}, \ \mathbf{h}_m^2(z) = \begin{pmatrix} H_{m,L}(z) \\ \vdots \\ H_{m,M-1}(z) \end{pmatrix}, \ \mathbf{K}_{m+1} = \begin{pmatrix} \mathbf{A} & \mathbf{C} \\ \mathbf{B} & \mathbf{D} \end{pmatrix},$$

where $\mathbf{A}, \mathbf{B}, \mathbf{C}$ and $\mathbf{D}$ have dimensions $L \times L$. We will derive the necessary and sufficient condition on $\mathbf{K}_{m+1}$ such that (3.31) holds if (3.30) holds. In terms of $\mathbf{h}_m^1(z)$ and $\mathbf{h}_m^2(z)$, (3.30) and (3.31) are equivalent to

$$\mathbf{P}_1\mathbf{h}_m^2(z) = z^{-((m+1)M-1)}\mathbf{h}_m^1(-z^{-1}), \tag{3.A.15}$$

$$\mathbf{P}_1\mathbf{h}_{m+1}^2(z) = z^{-((m+2)M-1)}\mathbf{h}_{m+1}^1(-z^{-1}), \tag{3.A.16}$$

where $\mathbf{P}_1$ is as in (3.16). We would like to find the structural form of $\mathbf{K}_{m+1}$ such that (3.*A*.16) holds for any set of $\mathbf{h}_m^1(z)$ and $\mathbf{h}_m^2(z)$ satisfying (3.*A*.15). From Fig. 3.15,

$$\begin{pmatrix} \mathbf{h}_{m+1}^1(z) \\ \\ \mathbf{h}_{m+1}^2(z) \end{pmatrix} = \begin{pmatrix} \mathbf{A} & \mathbf{C} \\ \\ \mathbf{B} & \mathbf{D} \end{pmatrix} \begin{pmatrix} \mathbf{I}_L & \mathbf{0} \\ \\ \mathbf{0} & z^{-M}\mathbf{I}_L \end{pmatrix} \begin{pmatrix} \mathbf{h}_m^1(z) \\ \\ \mathbf{h}_m^2(z) \end{pmatrix} = \begin{pmatrix} \mathbf{A}\mathbf{h}_m^1(z) + z^{-M}\mathbf{C}\mathbf{h}_m^2(z) \\ \\ \mathbf{B}\mathbf{h}_m^1(z) + z^{-M}\mathbf{D}\mathbf{h}_m^2(z) \end{pmatrix}. \tag{3.A.17}$$

Substituting (3.*A*.15) into (3.*A*.17), we have

$$\mathbf{P}_1\mathbf{h}_{m+1}^2(z) = -\mathbf{P}_1\mathbf{B}\mathbf{P}_1\mathbf{h}_m^2(-z^{-1})z^{-((m+1)M-1)} + \mathbf{P}_1\mathbf{D}\mathbf{h}_m^2(z)z^{-M}. \tag{3.A.18}$$

$$z^{-((m+2)M-1)}\mathbf{h}^1_{m+1}(-z^{-1}) = \mathbf{A}\mathbf{P}_1\mathbf{h}^2_m(z)z^{-M} + \mathbf{C}\mathbf{h}^2_m(-z^{-1})z^{-((m+1)M-1)}. \quad (3.A.19)$$

If (3.A.16) has to hold, then the right-hand sides of (3.A.18) and (3.A.19) should be the same, so that

$$(\mathbf{P}_1\mathbf{B}\mathbf{P}_1 + \mathbf{C})\mathbf{h}^2_m(-z^{-1})z^{-((m+1)M-1)} = z^{-M}(\mathbf{P}_1\mathbf{D} - \mathbf{A}\mathbf{P}_1)\mathbf{h}^2_m(z). \quad (3.A.20)$$

For arbitrary causal FIR $\mathbf{h}^2_m(z)$, the function $\mathbf{h}^2_m(-z^{-1})z^{-((m+1)M-1)}$ is also causal and FIR, and in general has the form $h_0 + z^{-1}h_1 + \ldots$. Since the RHS of (3.A.20) has a power of z^{-1} starting from z^{-M}, (3.A.20) holds for *arbitrary* $\mathbf{h}^2_m(z)$ if and only if $\mathbf{P}_1\mathbf{B}\mathbf{P}_1 + \mathbf{C} = \mathbf{0}$, which in turn implies $\mathbf{A}\mathbf{P}_1 - \mathbf{P}_1\mathbf{D} = \mathbf{0}$. Simplying these relations, we obtain $\mathbf{B} = -\mathbf{P}_1\mathbf{C}\mathbf{P}_1$ and $\mathbf{D} = \mathbf{P}_1\mathbf{A}\mathbf{P}_1$ resulting in the form (3.32) for $\mathbf{K}_{m+1}$.

Appendix 3.D

Consider the even M case. Let $\mathbf{h}^1_{-1}(z) = (1 \;\; z^{-1} \ldots z^{-(L-1)})^T$ and $\mathbf{h}^2_{-1} = (z^{-L} \ldots z^{-(M-1)})^T$, where $L = M/2$. Using the notations in Appendix B with $\mathbf{K}_0 = \begin{pmatrix} \mathbf{A} & \mathbf{C} \\ \mathbf{B} & \mathbf{D} \end{pmatrix}$, we will derive the necessary and sufficient conditions on $\mathbf{K}_0$ such that

$$\begin{pmatrix} \mathbf{h}^1_0(z) \\ \\ \mathbf{h}^2_0(z) \end{pmatrix} = \begin{pmatrix} \mathbf{A} & \mathbf{C} \\ \\ \mathbf{B} & \mathbf{D} \end{pmatrix} \begin{pmatrix} \mathbf{h}^1_{-1}(z) \\ \\ \mathbf{h}^2_{-1}(z) \end{pmatrix} = \begin{pmatrix} \mathbf{A}\mathbf{h}^1_{-1}(z) + \mathbf{C}\mathbf{h}^2_{-1}(z) \\ \\ \mathbf{B}\mathbf{h}^1_{-1}(z) + \mathbf{D}\mathbf{h}^2_{-1}(z) \end{pmatrix} \quad (3.A.21)$$

satisfies the pairwise-symmetry property; i.e., $\mathbf{P}_1\mathbf{h}^2_0(z) = z^{-(M-1)}\mathbf{h}^1_0(-z^{-1})$. Accordingly, (3.A.21) is simplified to

$$\mathbf{P}_1\mathbf{B}\mathbf{h}^1_{-1}(z) + \mathbf{P}_1\mathbf{D}\mathbf{h}^2_{-1}(z) = z^{-(M-1)}\{\mathbf{A}\mathbf{h}^1_{-1}(-z^{-1}) + \mathbf{C}\mathbf{h}^2_{-1}(-z^{-1})\}. \quad (3.A.22)$$

However, $\mathbf{h}^1_{-1}(-z^{-1})z^{-(M-1)} = \mathbf{P}_2\mathbf{h}^2_{-1}(z)$, and $\mathbf{h}^2_{-1}(-z^{-1})z^{-(M-1)} = \mathbf{P}_3\mathbf{h}^1_{-1}(z)$, where $\mathbf{P}_2$ and $\mathbf{P}_3$ are as in (3.35). Hence, (3.A.22) simplifies to

$$(\mathbf{P}_1\mathbf{B} - \mathbf{C}\mathbf{P}_3)\mathbf{h}^1_{-1}(z) = z^{-L}(\mathbf{A}\mathbf{P}_2 - \mathbf{P}_1\mathbf{D})\mathbf{h}^1_{-1}(z). \quad (3.A.23)$$

The matrices $(\mathbf{P}_1\mathbf{B}-\mathbf{C}\mathbf{P}_3)$ and $(\mathbf{A}\mathbf{P}_2-\mathbf{P}_1\mathbf{D})$ are $L\times L$. The left-hand side has the powers $z^{-k}, 0\leq k\leq L-1$ and the right-hand side contains $z^{-k}, L\leq k\leq M-1$. It can therefore be easily verified that we must have $\mathbf{P}_1\mathbf{B}-\mathbf{C}\mathbf{P}_3=\mathbf{0}$, $\mathbf{A}\mathbf{P}_2-\mathbf{P}_1\mathbf{D}=\mathbf{0}$. This can be rewritten, yielding $\mathbf{B}=\mathbf{P}_1\mathbf{C}\mathbf{P}_3$, $\mathbf{D}=\mathbf{P}_1\mathbf{A}\mathbf{P}_2$ and thus $\mathbf{K}_0$ in (3.34) is the only form which forces $H_{0,k}(z)$ to have the pairwise symmetry property.

Appendix 3.E

We review the design process in the two-channel perfect-reconstruction FIR QMF banks [5], [18] in this appendix. Its relation with the lattice structure reported in [19] is also discussed. Consider the two-channel QMF bank, where $H_0(z)$ and $H_1(z)$ are analysis filters, whereas $F_0(z)$ and $F_1(z)$ are synthesis filters. Here, $H_0(z)$ and $F_0(z)$ are lowpass transfer functions and $H_1(z)$ and $F_1(z)$ are highpass transfer functions, respectively. Using the standard identities in multirate signal processing [2], the reconstructed signal $\hat{X}(z)$ is

$$\hat{X}(z)=\frac{1}{2}[H_0(z)F_0(z)+H_1(z)F_1(z)]X(z)+\frac{1}{2}[H_0(-z)F_0(z)+H_1(-z)F_1(z)]X(-z). \tag{3.A.24}$$

The term $X(-z)$ is precisely the aliasing term, and thus it is required to be made equal to zero, since the objective is to choose $H_k(z)$ and $F_k(z)$ such that $\hat{X}(z)=\frac{1}{2}X(-z)$. Eq (3.A.24) yields

$$\begin{pmatrix} H_0(z) & H_1(z) \\ H_0(-z) & H_1(-z) \end{pmatrix}\begin{pmatrix} F_0(z) \\ F_1(z) \end{pmatrix}=\begin{pmatrix} 1 \\ 0 \end{pmatrix}, \text{ for all } z. \tag{3.A.25}$$

In the scheme of Smith and Barnwell [5], [18], the following relations between the transfer functions are enforced:

$$\begin{cases} H_1(z)=z^{-(N-1)}H_0(-z^{-1}) \\ F_0(z)=z^{-(N-1)}H_0(z^{-1}) \\ F_1(z)=z^{-(N-1)}H_1(z^{-1}), \end{cases} \tag{3.A.26}$$

where $N-1$ is the order of $H_0(z)$ (and it is odd). With the above choices in (3.A.26), (3.A.25) simplified to

$$H_0(z^{-1})H_0(z) + H_1(z^{-1})H_1(z) = 1 \quad \text{for all } z. \tag{3.A.27}$$

Note that the above choices (3.A.26) cancel the aliasing term in (3.A.24). To ensure the PR property, the design procedure proposed in [5] based on the spectral factorization of a linear-phase FIR halfband filter with positive amplitude response.

Substituting $H_1(z) = z^{-(N-1)}H_0(-z^{-1})$ into (3.A.27), we have

$$H_0(z^{-1})H_0(z) + H_0(-z)H_0(-z^{-1}) = 1 \text{ for all } z. \tag{3.A.28}$$

If we define $G_0(z) \triangleq H_0(z)H_0(z^{-1})$, then it follows from (3.A.28) that $G_0(z)$ is a halfband filter. In other words,

$$G_0(z) + G_0(-z) = 1. \tag{3.A.29}$$

The design procedure is thus as follows: First, design a linear-phase FIR halfband filter $G_0(z)$ with positive amplitude response. Obtain a spectral factor $H_0(z)$ of $G_0(z)$. Once $H_0(z)$ is designed, the remaining set of filters are chosen as according in (3.A.26).

Given the pair of odd-order PR filters $H_0(z)$ and $H_1(z)$, which satisfies $H_1(z) = z^{-(N-1)}H_0(-z^{-1})$. It is shown in [19] that there is a lattice structure associated with this pair. These lattice structures consist of a cascade of orthogonal building blocks and the transfer matrix $\begin{pmatrix} 1 & 0 \\ 0 & z^{-2} \end{pmatrix}$. In other words, this lattice structure spans all two-channel PR FIR QMF filter banks with lossless $\mathbf{E}(z)$.

Appendix 3.F

This appendix tabulates the properties, lattice coefficient and filter-coefficient values for a set of PR pairwise symmetric QMF designs based on the material in Section 3.1. Although this design procedure is capable of designing filters for any QMF bank which has odd number of channels, we consider only the case of three channels here. Table 3.F.1 summarizes the properties of the PR QMF structures. The first column lists the code number of the filters, whereas the second and third columns give the number of sections (number of blocks $\mathbf{K}_i$ in Fig. 3.8) and the lengths of the filters, respectively. The width of the transition band (normalized to 2π) is shown in column 4. The cut-off frequencies of the analysis filters are shown explicitly in Fig. 3.20. The last column tabulates the stopband attenuation (in dB) of the filters. Table 3.F.2 displays the lattice coefficients rotation angles in radians) of the PR system in Figs. 3.8 and 3.9. Similarly, table 3.F.3 displays the impulse responses $h_0(n)$ and $h_1(n)$. $h_2(n)$ can be computed from $h_0(n)$ by $h_2(n) = (-1)^n h_0(n)$.

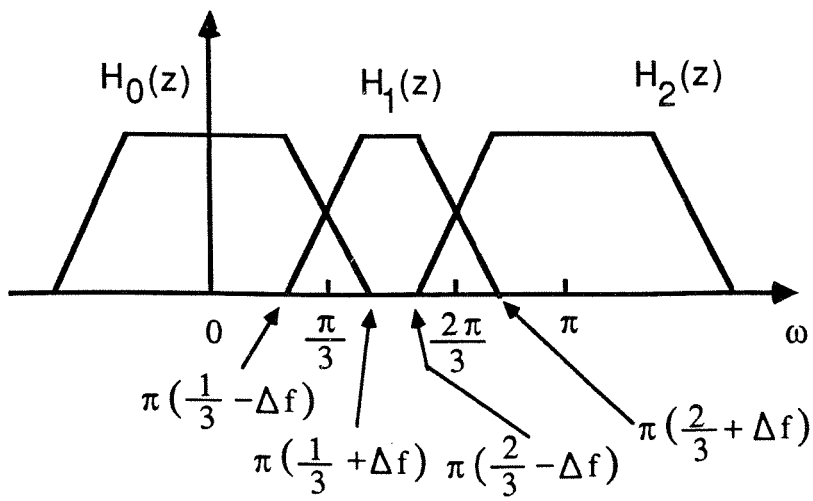

Fig. 3.20. The cutoff frequencies of the analysis filters. (M=3).

Table 3.F.1. Properties of the PR pairwise mirror-image QMF structures

Filter Number	Number of sections N	Length of filters L	Δf	Stopband Attenuation (dB)
$14A$	2	14	0.17	30.5
$20A$	3	20	0.15	38.5
$26A$	4	26	0.15	48.6
$32A$	5	32	0.14	58.8
$38A$	6	38	0.14	63.5
$14B$	2	14	0.14	26.2
$20B$	3	20	0.12	31.1
$26B$	4	26	0.11	37.8
$32B$	5	32	0.11	44.6
$38B$	6	38	0.10	52.6
$44B$	7	44	0.10	59.2
$50B$	8	50	0.10	67.8
$20C$	3	20	0.09	24.2
$26C$	4	26	0.08	27.4
$32C$	5	32	0.07	31.2
$38C$	6	38	0.07	35.4
$44C$	7	44	0.07	40.0
$50C$	8	50	0.067	44.3
$56C$	9	56	0.066	48.7
$62C$	10	62	0.0625	53.3
$68C$	11	68	0.0625	58.5
$26D$	4	26	0.072	22.8
$32D$	5	32	0.07	25.2
$38D$	6	38	0.052	27.7
$44D$	7	44	0.046	30.3
$50D$	8	50	0.043	33.2
$56D$	9	56	0.043	36.0
$62D$	10	62	0.043	39.4
$68D$	11	68	0.043	42.7
$74D$	12	74	0.043	45.4

Table 3.F.2 Lattice coefficients of the PR pairwise mirror-image QMF structures as in Fig. 3.8 (in radians).

m	$\theta_{m,1}$	$\theta_{m,2}$	$\theta_{m,3}$
0	7.889362×10^{-1}	-1.290822×10^{0}	
1	-1.393950×10^{0}	2.741418×10^{-1}	1.561524×10^{0}

$\neg 14A$

m	$\theta_{m,1}$	$\theta_{m,2}$	$\theta_{m,3}$
0	1.015547×10^{0}	-1.436481×10^{0}	
1	-3.288864×10^{-1}	-3.770520×10^{0}	
2	-1.979185×10^{0}	3.258931×10^{0}	-1.541848×10^{0}

$20A$

m	$\theta_{m,1}$	$\theta_{m,2}$	$\theta_{m,3}$
0	1.152554×10^{0}	-1.495570×10^{0}	
1	-5.270068×10^{-1}	-4.045233×10^{0}	
2	-3.133296×10^{0}	-2.828454×10^{0}	
3	-1.991644×10^{0}	-3.190360×10^{0}	4.699373×10^{0}

$26A$

m	$\theta_{m,1}$	$\theta_{m,2}$	$\theta_{m,3}$
0	1.256508×10^{0}	-1.529259×10^{0}	
1	-7.018357×10^{-1}	-4.264039×10^{0}	
2	-1.563627×10^{-1}	-5.583935×10^{-1}	
3	-9.737239×10^{-2}	-1.708695×10^{-1}	
4	-1.975414×10^{0}	3.164616×10^{0}	-1.565013×10^{0}

$32A$

m	$\theta_{m,1}$	$\theta_{m,2}$	$\theta_{m,3}$
0	1.285258×10^{0}	-1.536589×10^{0}	
1	-7.594440×10^{-1}	-4.325963×10^{0}	
2	-3.355990×10^{0}	-2.493288×10^{0}	
3	6.088302×10^{-2}	2.324549×10^{-1}	
4	-2.393026×10^{-1}	3.900940×10^{-2}	
5	-1.779651×10^{0}	-3.140755×10^{0}	4.711517×10^{0}

$38A$

Table 3.F.2. continued ...

m	$\theta_{m,1}$	$\theta_{m,2}$	$\theta_{m,3}$
0	7.821646×10^{-1}	-1.256961×10^{0}	
1	-1.391219×10^{0}	2.992991×10^{-1}	1.585338×10^{0}

$14B$

m	$\theta_{m,1}$	$\theta_{m,2}$	$\theta_{m,3}$
0	9.619833×10^{-1}	-1.395508×10^{0}	
1	-3.468966×10^{-1}	-3.733590×10^{0}	
2	-2.014923×10^{0}	3.293236×10^{0}	-1.542973×10^{0}

$20B$

m	$\theta_{m,1}$	$\theta_{m,2}$	$\theta_{m,3}$
0	1.083212×10^{0}	-1.461476×10^{0}	
1	-4.899440×10^{-1}	-3.954979×10^{0}	
2	-3.168664×10^{0}	-2.826728×10^{0}	
3	-2.052735×10^{0}	-3.218707×10^{0}	4.695468×10^{0}

$26B$

m	$\theta_{m,1}$	$\theta_{m,2}$	$\theta_{m,3}$
0	-1.969248×10^{0}	-1.642414×10^{0}	
1	6.100624×10^{-1}	-2.154381×10^{0}	
2	1.308800×10^{-1}	4.877309×10^{-1}	
3	5.753037×10^{-2}	-2.961514×10^{0}	
4	-1.093589×10^{0}	-4.017559×10^{-2}	1.579736×10^{0}

$32B$

m	$\theta_{m,1}$	$\theta_{m,2}$	$\theta_{m,3}$
0	1.244511×10^{0}	-1.523928×10^{0}	
1	-7.213549×10^{-1}	-4.270358×10^{0}	
2	-3.371184×10^{0}	-2.487036×10^{0}	
3	-1.641178×10^{-2}	3.107217×10^{-1}	
4	-8.777516×10^{-2}	1.080026×10^{-1}	
5	-2.033658×10^{0}	-3.163403×10^{0}	4.707651×10^{0}

$38B$

Table 3.F.2. continued ...

m	$\theta_{m,1}$	$\theta_{m,2}$	$\theta_{m,3}$
0	-1.843580×10^{0}	-1.602942×10^{0}	
1	8.171906×10^{-1}	-1.909064×10^{0}	
2	3.235922×10^{-1}	7.992793×10^{-1}	
3	-3.221718×10^{0}	-3.584532×10^{0}	
4	3.109705×10^{-2}	-3.342445×10^{0}	
5	1.013878×10^{-1}	-3.206451×10^{0}	
6	-2.015603×10^{0}	-3.129827×10^{0}	4.714877×10^{0}

$44B$

m	$\theta_{m,1}$	$\theta_{m,2}$	$\theta_{m,3}$
0	1.314091×10^{0}	-1.542106×10^{0}	
1	-8.553542×10^{-1}	-4.409263×10^{0}	
2	-3.511535×10^{0}	-2.274937×10^{0}	
3	-1.188242×10^{-1}	5.218099×10^{-1}	
4	3.151793×10^{-3}	2.720721×10^{-1}	
5	5.830462×10^{-2}	1.132076×10^{-1}	
6	-1.085227×10^{-1}	3.252496×10^{-2}	
7	-1.988790×10^{0}	-3.146652×10^{0}	4.711361×10^{0}

$50B$

m	$\theta_{m,1}$	$\theta_{m,2}$	$\theta_{m,3}$
0	8.945377×10^{-1}	-1.333874×10^{0}	
1	2.785525×10^{0}	-2.608744×10^{0}	
2	-1.094877×10^{0}	-1.764123×10^{-1}	1.591191×10^{0}

$20C$

m	$\theta_{m,1}$	$\theta_{m,2}$	$\theta_{m,3}$
0	9.894995×10^{-1}	-1.401938×10^{0}	
1	-4.423849×10^{-1}	-3.831530×10^{0}	
2	-5.525427×10^{-2}	-3.436775×10^{0}	
3	-1.034047×10^{0}	1.052406×10^{-1}	1.554306×10^{0}

$26C$

m	$\theta_{m,1}$	$\theta_{m,2}$	$\theta_{m,3}$
0	1.063557×10^{0}	-1.445086×10^{0}	
1	2.624068×10^{0}	-2.322231×10^{0}	
2	-1.105770×10^{-1}	4.065872×10^{-1}	
3	-1.779356×10^{-2}	1.817825×10^{-1}	
4	-1.021430×10^{0}	-6.392832×10^{-2}	1.581442×10^{0}

$32C$

Table 3.F.2. continued ...

m	$\theta_{m,1}$	$\theta_{m,2}$	$\theta_{m,3}$
0	1.124431×10^{0}	-1.475312×10^{0}	
1	-5.866328×10^{-1}	-4.071116×10^{0}	
2	-3.302413×10^{0}	-2.631016×10^{0}	
3	-3.163378×10^{0}	-3.405785×10^{0}	
4	-3.095913×10^{0}	-3.024040×10^{0}	
5	-1.024235×10^{0}	-3.948337×10^{-2}	1.577458×10^{0}

$38C$

m	$\theta_{m,1}$	$\theta_{m,2}$	$\theta_{m,3}$
0	1.176900×10^{0}	-1.497973×10^{0}	
1	2.488870×10^{0}	-2.115603×10^{0}	
2	-2.114394×10^{-1}	6.089280×10^{-1}	
3	5.437487×10^{-2}	-2.795370×10^{0}	
4	-1.219718×10^{-2}	-6.102737×10^{0}	
5	5.927725×10^{-2}	-3.063457×10^{0}	
6	-1.032645×10^{0}	-2.477249×10^{-2}	1.574979×10^{0}

$44C$

m	$\theta_{m,1}$	$\theta_{m,2}$	$\theta_{m,3}$
0	1.222008×10^{0}	-1.514865×10^{0}	
1	-7.157628×10^{-1}	-4.250893×10^{0}	
2	-3.404906×10^{0}	-2.440528×10^{0}	
3	-3.227385×10^{0}	-3.567924×10^{0}	
4	-3.153726×10^{0}	-2.895972×10^{0}	
5	2.864640×10^{-2}	1.262810×10^{-1}	
6	-6.708751×10^{-2}	5.265698×10^{-2}	
7	-1.043370×10^{0}	-1.568459×10^{-2}	1.573445×10^{0}

$50C$

m	$\theta_{m,1}$	$\theta_{m,2}$	$\theta_{m,3}$
0	1.259059×10^{0}	-1.526818×10^{0}	
1	2.368147×10^{0}	-1.963775×10^{0}	
2	-3.146314×10^{-1}	7.844229×10^{-1}	
3	1.171648×10^{-1}	-2.639372×10^{0}	
4	3.362273×10^{-2}	-5.973011×10^{0}	
5	8.665927×10^{-3}	-2.963820×10^{0}	
6	3.794835×10^{-2}	8.909689×10^{-2}	
7	-7.217059×10^{-2}	3.556300×10^{-2}	
8	-1.055272×10^{0}	-9.922895×10^{-3}	1.572479×10^{0}

$56C$

Table 3.F.2. continued ...

m	$\theta_{m,1}$	$\theta_{m,2}$	$\theta_{m,3}$
0	1.285825×10^{0}	-1.534282×10^{0}	
1	-8.202775×10^{-1}	-4.369512×10^{0}	
2	-3.501571×10^{0}	-2.288635×10^{0}	
3	-3.288091×10^{0}	-3.710320×10^{0}	
4	-3.194762×10^{0}	-2.772133×10^{0}	
5	-7.057860×10^{-3}	2.279622×10^{-1}	
6	-2.079377×10^{-2}	1.281631×10^{-1}	
7	4.413916×10^{-2}	6.195599×10^{-2}	
8	-7.862157×10^{-2}	2.345415×10^{-2}	
9	-1.071565×10^{0}	-6.046309×10^{-3}	1.571831×10^{0}

$62C$

m	$\theta_{m,1}$	$\theta_{m,2}$	$\theta_{m,3}$
0	1.301740×10^{0}	-1.538209×10^{0}	
1	2.289791×10^{0}	-1.882854×10^{0}	
2	-3.936397×10^{-1}	9.014223×10^{-1}	
3	1.705478×10^{-1}	-2.521113×10^{0}	
4	6.997561×10^{-2}	-5.864222×10^{0}	
5	-2.023129×10^{-2}	-2.868788×10^{0}	
6	8.204649×10^{-3}	1.661274×10^{-1}	
7	-2.832165×10^{-2}	9.084692×10^{-2}	
8	4.823233×10^{-2}	4.216924×10^{-2}	
9	-7.951581×10^{-2}	1.514166×10^{-2}	
10	-1.083366×10^{0}	-3.640705×10^{-3}	1.571426×10^{0}

$68C$

m	$\theta_{m,1}$	$\theta_{m,2}$	$\theta_{m,3}$
0	9.365405×10^{-1}	-1.360060×10^{0}	
1	2.720531×10^{0}	-2.519339×10^{0}	
2	-3.214592×10^{0}	-3.424655×10^{0}	
3	-1.004843×10^{0}	1.221843×10^{-1}	1.556140×10^{0}

$26D$

m	$\theta_{m,1}$	$\theta_{m,2}$	$\theta_{m,3}$
0	9.978047×10^{-1}	-1.402604×10^{0}	
1	2.668163×10^{0}	-2.418660×10^{0}	
2	-1.058754×10^{-1}	-2.778163×10^{0}	
3	-6.288918×10^{-3}	-2.959249×10^{0}	
4	-9.806912×10^{-1}	-8.186542×10^{-2}	1.581302×10^{0}

$32D$

Table 3.F.2. continued ...

m	$\theta_{m,1}$	$\theta_{m,2}$	$\theta_{m,3}$
0	1.049386×10^{0}	-1.433984×10^{0}	
1	2.619487×10^{0}	-2.330947×10^{0}	
2	-3.278107×10^{0}	-3.579362×10^{0}	
3	-3.170675×10^{0}	-2.900512×10^{0}	
4	1.921471×10^{-2}	-3.016729×10^{0}	
5	-9.740291×10^{-1}	-5.585902×10^{-2}	1.578006×10^{0}

$38D$

m	$\theta_{m,1}$	$\theta_{m,2}$	$\theta_{m,3}$
0	1.094398×10^{0}	-1.458513×10^{0}	
1	2.573059×10^{0}	-2.252415×10^{0}	
2	-1.670062×10^{-1}	-2.633753×10^{0}	
3	-4.818136×10^{-2}	-2.843818×10^{0}	
4	-3.420471×10^{-4}	1.703268×10^{-1}	
5	-3.200752×10^{-2}	8.833464×10^{-2}	
6	-9.748608×10^{-1}	-3.861705×10^{-2}	1.575740×10^{0}

$44D$

m	$\theta_{m,1}$	$\theta_{m,2}$	$\theta_{m,3}$
0	1.134709×10^{0}	-1.478364×10^{0}	
1	2.527932×10^{0}	-2.180879×10^{0}	
2	-1.983834×10^{-1}	-2.566778×10^{0}	
3	-6.633776×10^{-2}	-2.788713×10^{0}	
4	-1.485067×10^{-2}	-2.926058×10^{0}	
5	-3.128086×10^{0}	-3.266123×10^{0}	
6	-3.101974×10^{0}	-3.077865×10^{0}	
7	2.162344×10^{0}	-2.697203×10^{-2}	1.567372×10^{0}

$50D$

m	$\theta_{m,1}$	$\theta_{m,2}$	$\theta_{m,3}$
0	1.171009×10^{0}	-1.494483×10^{0}	
1	2.483912×10^{0}	-2.115791×10^{0}	
2	-2.308970×10^{-1}	-2.502610×10^{0}	
3	-8.464936×10^{-2}	-2.735055×10^{0}	
4	-2.757960×10^{-2}	2.602149×10^{-1}	
5	-1.118741×10^{-3}	1.614148×10^{-1}	
6	2.132163×10^{-2}	9.284823×10^{-2}	
7	-4.471172×10^{-2}	4.653053×10^{-2}	
8	-9.854229×10^{-1}	-1.897735×10^{-2}	1.573198×10^{0}

$56D$

Table 3.F.2. continued ...

m	$\theta_{m,1}$	$\theta_{m,2}$	$\theta_{m,3}$
0	1.203104×10^{0}	-1.507261×10^{0}	
1	2.441666×10^{0}	-2.057831×10^{0}	
2	-2.640687×10^{-1}	-2.441904×10^{0}	
3	-1.034006×10^{-1}	-2.683217×10^{0}	
4	-3.971784×10^{-2}	-2.837644×10^{0}	
5	-3.150485×10^{0}	-3.339892×10^{0}	
6	-3.131556×10^{0}	-3.018421×10^{0}	
7	2.628498×10^{-2}	6.996612×10^{-2}	
8	-4.843826×10^{-2}	3.419034×10^{-2}	
9	2.148987×10^{0}	-1.340285×10^{-2}	1.569093×10^{0}

$62D$

m	$\theta_{m,1}$	$\theta_{m,2}$	$\theta_{m,3}$
0	1.230945×10^{0}	-1.517193×10^{0}	
1	2.401905×10^{0}	-2.007318×10^{0}	
2	-2.972228×10^{-1}	-2.385337×10^{0}	
3	-1.225644×10^{-1}	-2.633640×10^{0}	
4	-5.173321×10^{-2}	3.463466×10^{-1}	
5	1.788989×10^{-2}	2.346525×10^{-1}	
6	1.530026×10^{-3}	1.539307×10^{-1}	
7	-1.557957×10^{-2}	9.494259×10^{-2}	
8	2.971593×10^{-2}	5.299712×10^{-2}	
9	-5.143106×10^{-2}	2.518837×10^{-2}	
10	-1.000439×10^{0}	-9.476049×10^{-3}	1.572013×10^{0}

$68D$

m	$\theta_{m,1}$	$\theta_{m,2}$	$\theta_{m,3}$
0	1.255609×10^{0}	-1.525138×10^{0}	
1	2.363995×10^{0}	-1.962631×10^{0}	
2	-3.306370×10^{-1}	-2.332034×10^{0}	
3	-1.424282×10^{-1}	-2.585746×10^{0}	
4	-6.401607×10^{-2}	-2.753835×10^{0}	
5	-3.168167×10^{0}	-3.412146×10^{0}	
6	-3.147378×10^{0}	-2.956692×10^{0}	
7	7.902081×10^{-3}	1.209643×10^{-1}	
8	-1.926609×10^{-2}	7.372203×10^{-2}	
9	3.236905×10^{-2}	4.033325×10^{-2}	
10	-5.191359×10^{-2}	1.862904×10^{-2}	
11	2.134980×10^{0}	-6.737058×10^{-3}	1.569908×10^{0}

$74D$

Table 3.F.3. Filter coefficients of the optimized analysis filters.
Here, $h_2(n) = (-1)^n h_0(n)$.

n	$h_0(n)$	$h_1(n)$
0	-4.374292×10^{-2}	4.634310×10^{-2}
1	0.	0.
2	2.187413×10^{-1}	-5.887902×10^{-2}
3	5.142650×10^{-1}	0.
4	6.439939×10^{-1}	-2.586593×10^{-1}
5	4.702579×10^{-1}	0.
6	1.285131×10^{-1}	6.567805×10^{-1}
7	-1.167911×10^{-1}	0.
8	-1.276070×10^{-1}	-6.521494×10^{-1}
9	-1.866174×10^{-2}	0.
10	5.207263×10^{-2}	2.661229×10^{-1}
11	1.853015×10^{-2}	0.
12	0.	0.
13	-7.561607×10^{-3}	0.

14A

n	$h_0(n)$	$h_1(n)$
0	1.508856×10^{-2}	1.146086×10^{-2}
1	0.	0.
2	-1.240142×10^{-1}	-4.235363×10^{-3}
3	-3.629856×10^{-1}	0.
4	-5.786821×10^{-1}	-8.859536×10^{-2}
5	-5.836909×10^{-1}	0.
6	-3.317034×10^{-1}	1.102295×10^{-1}
7	5.609474×10^{-3}	0.
8	1.887854×10^{-1}	1.538884×10^{-1}
9	1.413370×10^{-1}	0.
10	-8.854816×10^{-3}	-5.567716×10^{-1}
11	-8.487580×10^{-2}	0.
12	-5.173607×10^{-2}	6.769343×10^{-1}
13	1.523321×10^{-2}	0.
14	3.209455×10^{-2}	-4.199373×10^{-1}
15	8.536151×10^{-3}	0.
16	-8.226973×10^{-3}	1.076448×10^{-1}
17	-5.295414×10^{-3}	0.
18	0.	0.
19	1.357403×10^{-3}	0.

20A

Table 3.F.3. continued ...

n	$h_0(n)$	$h_1(n)$
0	-6.610215×10^{-3}	2.855522×10^{-3}
1	0.	0.
2	7.293751×10^{-2}	1.207897×10^{-3}
3	2.492439×10^{-1}	0.
4	4.731972×10^{-1}	-2.811234×10^{-2}
5	5.928850×10^{-1}	0.
6	4.799707×10^{-1}	1.711103×10^{-2}
7	1.730517×10^{-1}	0.
8	-1.242448×10^{-1}	8.899212×10^{-2}
9	-2.192919×10^{-1}	0.
10	-1.035946×10^{-1}	-1.587603×10^{-1}
11	5.847964×10^{-2}	0.
12	1.112246×10^{-1}	-3.098891×10^{-2}
13	4.453097×10^{-2}	0.
14	-3.649349×10^{-2}	4.247080×10^{-1}
15	-5.007246×10^{-2}	0.
16	-1.160400×10^{-2}	-6.622855×10^{-1}
17	2.024473×10^{-2}	0.
18	1.687641×10^{-2}	5.358590×10^{-1}
19	-9.017541×10^{-4}	0.
20	-7.500981×10^{-3}	-2.381708×10^{-1}
21	-2.622017×10^{-3}	0.
22	1.391935×10^{-3}	4.419665×10^{-2}
23	1.165396×10^{-3}	0.
24	0.	0.
25	-2.162591×10^{-4}	0.

26*A*

n	$h_0(n)$	$h_1(n)$
0	2.573300×10^{-3}	8.047708×10^{-4}
1	0.	0.
2	-3.924357×10^{-2}	1.290299×10^{-3}
3	-1.568026×10^{-1}	0.
4	-3.507838×10^{-1}	-8.817532×10^{-3}
5	-5.311317×10^{-1}	0.
6	-5.578907×10^{-1}	-1.974844×10^{-3}
7	-3.626494×10^{-1}	0.
8	-4.150979×10^{-2}	4.074192×10^{-2}
9	1.986892×10^{-1}	0.
10	2.151177×10^{-1}	-3.686652×10^{-2}
11	5.492987×10^{-2}	0.
12	-1.019617×10^{-1}	-7.703474×10^{-2}
13	-1.213350×10^{-1}	0.
14	-2.661536×10^{-2}	1.853781×10^{-1}
15	6.030054×10^{-2}	0.
16	6.170640×10^{-2}	-5.992912×10^{-2}
17	5.335049×10^{-3}	0.
18	-3.402822×10^{-2}	-3.066790×10^{-1}
19	-2.546774×10^{-2}	0.
20	3.410288×10^{-3}	6.108689×10^{-1}
21	1.582682×10^{-2}	0.
22	7.225177×10^{-3}	-5.954865×10^{-1}
23	-3.958486×10^{-3}	0.
24	-5.151197×10^{-3}	3.441615×10^{-1}
25	-6.590986×10^{-4}	0.
26	1.674461×10^{-3}	-1.118740×10^{-1}
27	7.986474×10^{-4}	0.
28	-2.251171×10^{-4}	1.504051×10^{-2}
29	-2.596104×10^{-4}	0.
30	0.	0.
31	3.490241×10^{-5}	0.

32*A*

Table 3.F.3. continued ...

n	$h_0(n)$	$h_1(n)$
0	-1.855681×10^{-3}	-1.955673×10^{-4}
1	0.	0.
2	3.115474×10^{-2}	-6.980589×10^{-4}
3	1.307698×10^{-1}	0.
4	3.084679×10^{-1}	-2.622994×10^{-4}
5	4.963823×10^{-1}	0.
6	5.639884×10^{-1}	2.490176×10^{-3}
7	4.191268×10^{-1}	0.
8	1.146772×10^{-1}	4.288086×10^{-3}
9	-1.619740×10^{-1}	0.
10	-2.375971×10^{-1}	-1.233833×10^{-2}
11	-1.059092×10^{-1}	0.
12	7.438688×10^{-2}	-1.259867×10^{-2}
13	1.374979×10^{-1}	0.
14	6.009871×10^{-2}	5.537584×10^{-2}
15	-4.707471×10^{-2}	0.
16	-7.611317×10^{-2}	-1.808911×10^{-2}
17	-2.442504×10^{-2}	0.
18	3.143969×10^{-2}	-1.244824×10^{-1}
19	3.635133×10^{-2}	0.
20	4.590481×10^{-3}	1.892941×10^{-1}
21	-1.811022×10^{-2}	0.
22	-1.309250×10^{-2}	2.115936×10^{-2}
23	2.481560×10^{-3}	0.
24	7.798018×10^{-3}	-4.059131×10^{-1}
25	2.382440×10^{-3}	0.
26	-2.587805×10^{-3}	6.343237×10^{-1}
27	-1.903071×10^{-3}	0.
28	5.829718×10^{-4}	-5.404007×10^{-1}
29	9.396435×10^{-4}	0.
30	-1.623744×10^{-4}	2.801204×10^{-1}
31	-4.568082×10^{-4}	0.
32	4.766664×10^{-5}	-8.223214×10^{-2}
33	2.071570×10^{-4}	0.
34	-5.791061×10^{-6}	9.990454×10^{-3}
35	-6.081297×10^{-5}	0.
36	0.	0.
37	7.388221×10^{-6}	0.

38A

n	$h_0(n)$	$h_1(n)$
0	-5.505547×10^{-2}	7.483747×10^{-2}
1	0.	0.
2	2.346066×10^{-1}	-5.502312×10^{-2}
3	5.190920×10^{-1}	0.
4	6.323345×10^{-1}	-2.827801×10^{-1}
5	4.645520×10^{-1}	0.
6	1.375228×10^{-1}	6.400065×10^{-1}
7	-1.118936×10^{-1}	0.
8	-1.384151×10^{-1}	-6.441590×10^{-1}
9	-3.154904×10^{-2}	0.
10	6.332796×10^{-2}	2.947170×10^{-1}
11	3.175373×10^{-2}	0.
12	0.	0.
13	-1.452804×10^{-2}	0.

14B

n	$h_0(n)$	$h_1(n)$
0	2.367805×10^{-2}	2.570762×10^{-2}
1	0.	0.
2	-1.477378×10^{-1}	1.147846×10^{-3}
3	-3.949987×10^{-1}	0.
4	-5.867340×10^{-1}	-1.153671×10^{-1}
5	-5.606071×10^{-1}	0.
6	-3.022072×10^{-1}	1.189883×10^{-1}
7	1.931235×10^{-2}	0.
8	1.883779×10^{-1}	1.459907×10^{-1}
9	1.415138×10^{-1}	0.
10	-1.158105×10^{-2}	-5.250885×10^{-1}
11	-9.254388×10^{-2}	0.
12	-6.465346×10^{-2}	6.635609×10^{-1}
13	1.584621×10^{-2}	0.
14	4.507339×10^{-2}	-4.626038×10^{-1}
15	1.771757×10^{-2}	0.
16	-1.395848×10^{-2}	1.432607×10^{-1}
17	-1.235187×10^{-2}	0.
18	0.	0.
19	3.825167×10^{-3}	0.

20B

Table 3.F.3. continued ...

n	$h_0(n)$	$h_1(n)$
0	-1.184029×10^{-2}	9.032410×10^{-3}
1	0.	0.
2	9.689282×10^{-2}	6.241750×10^{-3}
3	2.953830×10^{-1}	0.
4	5.088839×10^{-1}	-4.606146×10^{-2}
5	5.850045×10^{-1}	0.
6	4.307877×10^{-1}	2.090118×10^{-2}
7	1.194389×10^{-1}	0.
8	-1.476933×10^{-1}	1.019771×10^{-1}
9	-2.113317×10^{-1}	0.
10	-8.433602×10^{-2}	-1.737571×10^{-1}
11	7.117592×10^{-2}	0.
12	1.173803×10^{-1}	5.683934×10^{-4}
13	4.375403×10^{-2}	0.
14	-4.448229×10^{-2}	3.667789×10^{-1}
15	-6.140094×10^{-2}	0.
16	-1.593305×10^{-2}	-6.305451×10^{-1}
17	2.765989×10^{-2}	0.
18	2.769167×10^{-2}	5.722531×10^{-1}
19	7.902827×10^{-4}	0.
20	-1.468459×10^{-2}	-3.034597×10^{-1}
21	-7.639351×10^{-3}	0.
22	3.440293×10^{-3}	7.109424×10^{-2}
23	4.051065×10^{-3}	0.
24	0.	0.
25	-9.490798×10^{-4}	0.

n	$h_0(n)$	$h_1(n)$
0	6.236123×10^{-3}	3.221075×10^{-3}
1	0.	0.
2	-6.310720×10^{-2}	4.374439×10^{-3}
3	-2.158349×10^{-1}	0.
4	-4.214194×10^{-1}	-1.772368×10^{-2}
5	-5.615109×10^{-1}	0.
6	-5.128089×10^{-1}	-1.886201×10^{-3}
7	-2.639344×10^{-1}	0.
8	4.496744×10^{-2}	5.422797×10^{-2}
9	2.213111×10^{-1}	0.
10	1.782788×10^{-1}	-5.476527×10^{-2}
11	5.999040×10^{-3}	0.
12	-1.233676×10^{-1}	-6.131076×10^{-2}
13	-1.102726×10^{-1}	0.
14	-3.779811×10^{-3}	1.893439×10^{-1}
15	7.504508×10^{-2}	0.
16	6.294053×10^{-2}	-1.202808×10^{-1}
17	-3.816548×10^{-3}	0.
18	-4.543998×10^{-2}	-1.954483×10^{-1}
19	-3.093964×10^{-2}	0.
20	7.755171×10^{-3}	5.328076×10^{-1}
21	2.473195×10^{-2}	0.
22	1.181462×10^{-2}	-6.233141×10^{-1}
23	-7.378205×10^{-3}	0.
24	-1.110660×10^{-2}	4.399509×10^{-1}
25	-2.168956×10^{-3}	0.
26	4.675540×10^{-3}	-1.852059×10^{-1}
27	2.961965×10^{-3}	0.
28	-8.645123×10^{-4}	3.424477×10^{-2}
29	-1.246897×10^{-3}	0.
30	0.	0.
31	2.305526×10^{-4}	0.

Table 3.F.3. continued ...

n	$h_0(n)$	$h_1(n)$
0	-3.070163×10^{-3}	1.154833×10^{-3}
1	0.	0.
2	3.949265×10^{-2}	2.477408×10^{-3}
3	1.512907×10^{-1}	0.
4	3.318940×10^{-1}	-6.392643×10^{-3}
5	5.043774×10^{-1}	0.
6	5.478266×10^{-1}	-5.498151×10^{-3}
7	3.913990×10^{-1}	0.
8	9.660015×10^{-2}	2.567090×10^{-2}
9	-1.641054×10^{-1}	0.
10	-2.362609×10^{-1}	-1.117982×10^{-2}
11	-1.115188×10^{-1}	0.
12	7.004689×10^{-2}	-5.107734×10^{-2}
13	1.477064×10^{-1}	0.
14	7.937494×10^{-2}	8.235845×10^{-2}
15	-4.117609×10^{-2}	0.
16	-9.443453×10^{-2}	9.531343×10^{-3}
17	-4.787590×10^{-2}	0.
18	2.981133×10^{-2}	-1.696326×10^{-1}
19	5.843420×10^{-2}	0.
20	2.427615×10^{-2}	1.946717×10^{-1}
21	-2.224626×10^{-2}	0.
22	-3.334972×10^{-2}	4.029168×10^{-2}
23	-9.160667×10^{-3}	0.
24	1.533944×10^{-2}	-3.996391×10^{-1}
25	1.644052×10^{-2}	0.
26	1.339059×10^{-3}	6.083500×10^{-1}
27	-8.993753×10^{-3}	0.
28	-6.379141×10^{-3}	-5.370399×10^{-1}
29	1.370091×10^{-3}	0.
30	4.193960×10^{-3}	3.038849×10^{-1}
31	1.383956×10^{-3}	0.
32	-1.419148×10^{-3}	-1.028283×10^{-1}
33	-1.074699×10^{-3}	0.
34	2.076629×10^{-4}	1.504679×10^{-2}
35	3.636557×10^{-4}	0.
36	0.	0.
37	-5.321347×10^{-5}	0.

n	$h_0(n)$	$h_1(n)$
0	1.544776×10^{-3}	4.059522×10^{-4}
1	0.	0.
2	-2.489196×10^{-2}	1.200802×10^{-3}
3	-1.051206×10^{-1}	0.
4	-2.548108×10^{-1}	-2.096930×10^{-3}
5	-4.324794×10^{-1}	0.
6	-5.384691×10^{-1}	-4.014265×10^{-3}
7	-4.752295×10^{-1}	0.
8	-2.365695×10^{-1}	1.074685×10^{-2}
9	5.759273×10^{-2}	0.
10	2.340497×10^{-1}	1.647602×10^{-3}
11	2.006396×10^{-1}	0.
12	2.340183×10^{-2}	-3.030394×10^{-2}
13	-1.311868×10^{-1}	0.
14	-1.416011×10^{-1}	2.877490×10^{-2}
15	-2.868483×10^{-2}	0.
16	8.369217×10^{-2}	3.444300×10^{-2}
17	9.540775×10^{-2}	0.
18	1.815379×10^{-2}	-9.703998×10^{-2}
19	-5.710477×10^{-2}	0.
20	-6.090759×10^{-2}	4.641722×10^{-2}
21	-7.078549×10^{-3}	0.
22	3.905807×10^{-2}	1.193689×10^{-1}
23	3.567570×10^{-2}	0.
24	-3.877203×10^{-4}	-2.265914×10^{-1}
25	-2.527760×10^{-2}	0.
26	-1.837040×10^{-2}	9.487921×10^{-2}
27	3.766163×10^{-3}	0.
28	1.477948×10^{-2}	2.399724×10^{-1}
29	7.699258×10^{-3}	0.
30	-4.131468×10^{-3}	-5.360743×10^{-1}
31	-7.360789×10^{-3}	0.
32	-2.148407×10^{-3}	5.899450×10^{-1}
33	2.912423×10^{-3}	0.
34	2.878095×10^{-3}	-4.195041×10^{-1}
35	-1.378605×10^{-5}	0.
36	-1.477536×10^{-3}	1.967421×10^{-1}
37	-6.338804×10^{-4}	0.
38	4.133510×10^{-4}	-5.503998×10^{-2}
39	3.581741×10^{-4}	0.
40	-4.933691×10^{-5}	6.569483×10^{-3}
41	-1.002017×10^{-4}	0.
42	0.	0.
43	1.195991×10^{-5}	0.

Table 3.F.3. continued ...

n	$h_0(n)$	$h_1(n)$
0	-1.235074×10^{-3}	1.366830×10^{-4}
1	0.	0.
2	2.043547×10^{-2}	4.380463×10^{-4}
3	8.865715×10^{-2}	0.
4	2.224174×10^{-1}	-7.312674×10^{-4}
5	3.940905×10^{-1}	0.
6	5.190792×10^{-1}	-1.671554×10^{-3}
7	4.984779×10^{-1}	0.
8	3.001578×10^{-1}	4.201837×10^{-3}
9	1.015035×10^{-2}	0.
10	-2.081153×10^{-1}	1.462370×10^{-3}
11	-2.324123×10^{-1}	0.
12	-8.141850×10^{-2}	-1.365552×10^{-2}
13	9.923946×10^{-2}	0.
14	1.608772×10^{-1}	1.085318×10^{-2}
15	7.492463×10^{-2}	0.
16	-5.748947×10^{-2}	2.040215×10^{-2}
17	-1.114676×10^{-1}	0.
18	-5.448640×10^{-2}	-4.618188×10^{-2}
19	3.952235×10^{-2}	0.
20	7.656397×10^{-2}	1.028053×10^{-2}
21	3.450593×10^{-2}	0.
22	-2.979326×10^{-2}	7.620881×10^{-2}
23	-5.069790×10^{-2}	0.
24	-1.878789×10^{-2}	-1.058258×10^{-1}
25	2.256949×10^{-2}	0.
26	3.148667×10^{-2}	-7.219360×10^{-3}
27	8.087255×10^{-3}	0.
28	-1.619828×10^{-2}	1.839262×10^{-1}
29	-1.775470×10^{-2}	0.
30	-1.937565×10^{-3}	-2.197374×10^{-1}
31	1.055599×10^{-2}	0.
32	8.736305×10^{-3}	2.847504×10^{-3}
33	-7.760608×10^{-4}	0.
34	-6.045937×10^{-3}	3.428594×10^{-1}
35	-3.490633×10^{-3}	0.
36	1.391733×10^{-3}	-5.707176×10^{-1}
37	2.890813×10^{-3}	0.
38	9.418950×10^{-4}	5.496404×10^{-1}
39	-1.033009×10^{-3}	0.
40	-1.067479×10^{-3}	-3.560653×10^{-1}
41	-1.883665×10^{-5}	0.
42	5.065419×10^{-4}	1.549319×10^{-1}
43	2.153236×10^{-4}	0.
44	-1.329655×10^{-4}	-4.066910×10^{-2}
45	-1.123729×10^{-4}	0.
46	1.502953×10^{-5}	4.596962×10^{-3}
47	2.949751×10^{-5}	0.
48	0.	0.
49	-3.334200×10^{-6}	0.

Table 3.F.3. continued ...

n	$h_0(n)$	$h_1(n)$
0	3.836044×10^{-2}	4.634054×10^{-2}
1	0.	0.
2	-1.818879×10^{-1}	5.038201×10^{-3}
3	-4.364313×10^{-1}	0.
4	-5.953777×10^{-1}	-1.366232×10^{-1}
5	-5.286855×10^{-1}	0.
6	-2.601431×10^{-1}	1.311681×10^{-1}
7	3.929512×10^{-2}	0.
8	1.837179×10^{-1}	1.185905×10^{-1}
9	1.322228×10^{-1}	0.
10	-2.272461×10^{-2}	-4.761299×10^{-1}
11	-9.642468×10^{-2}	0.
12	-7.203273×10^{-2}	6.438296×10^{-1}
13	1.858284×10^{-2}	0.
14	5.780570×10^{-2}	-5.166682×10^{-1}
15	2.784974×10^{-2}	0.
16	-2.230074×10^{-2}	1.993244×10^{-1}
17	-2.234920×10^{-2}	0.
18	0.	0.
19	8.622050×10^{-3}	0.

$20C$

n	$h_0(n)$	$h_1(n)$
0	-2.323520×10^{-2}	2.205322×10^{-2}
1	0.	0.
2	1.351674×10^{-1}	1.251767×10^{-2}
3	3.597419×10^{-1}	0.
4	5.492692×10^{-1}	-6.779288×10^{-2}
5	5.631551×10^{-1}	0.
6	3.593212×10^{-1}	3.238472×10^{-2}
7	5.031801×10^{-2}	0.
8	-1.703317×10^{-1}	1.010546×10^{-1}
9	-1.896229×10^{-1}	0.
10	-4.810714×10^{-2}	-1.859037×10^{-1}
11	8.688497×10^{-2}	0.
12	1.160597×10^{-1}	4.993698×10^{-2}
13	3.132201×10^{-2}	0.
14	-5.634256×10^{-2}	2.776255×10^{-1}
15	-6.848486×10^{-2}	0.
16	-1.382624×10^{-2}	-5.744821×10^{-1}
17	3.676692×10^{-2}	0.
18	3.880777×10^{-2}	6.050447×10^{-1}
19	1.528846×10^{-3}	0.
20	-2.549762×10^{-2}	-3.975286×10^{-1}
21	-1.603896×10^{-2}	0.
22	7.916250×10^{-3}	1.234208×10^{-1}
23	1.053797×10^{-2}	0.
24	0.	0.
25	-3.271727×10^{-3}	0.

$26C$

Table 3.F.3. continued ...

n	$h_0(n)$	$h_1(n)$
0	1.496707×10^{-2}	1.065789×10^{-2}
1	0.	0.
2	-1.019083×10^{-1}	1.046969×10^{-2}
3	-2.950838×10^{-1}	0.
4	-4.952344×10^{-1}	-3.347241×10^{-2}
5	-5.693765×10^{-1}	0.
6	-4.350582×10^{-1}	2.909494×10^{-3}
7	-1.476068×10^{-1}	0.
8	1.217690×10^{-1}	6.576102×10^{-2}
9	2.183449×10^{-1}	0.
10	1.193376×10^{-1}	-7.817171×10^{-2}
11	-4.595871×10^{-2}	0.
12	-1.337371×10^{-1}	-3.106655×10^{-2}
13	-8.330151×10^{-2}	0.
14	2.673383×10^{-2}	1.754621×10^{-1}
15	8.557101×10^{-2}	0.
16	5.386738×10^{-2}	-1.717389×10^{-1}
17	-1.960877×10^{-2}	0.
18	-5.662641×10^{-2}	-7.140571×10^{-2}
19	-3.118906×10^{-2}	0.
20	1.707595×10^{-2}	4.126346×10^{-1}
21	3.520814×10^{-2}	0.
22	1.497259×10^{-2}	-6.104145×10^{-1}
23	-1.356144×10^{-2}	0.
24	-2.060380×10^{-2}	5.338650×10^{-1}
25	-4.571973×10^{-3}	0.
26	1.145034×10^{-2}	-2.966897×10^{-1}
27	8.596066×10^{-3}	0.
28	-2.978920×10^{-3}	7.718677×10^{-2}
29	-4.777172×10^{-3}	0.
30	0.	0.
31	1.242828×10^{-3}	0.

32C

n	$h_0(n)$	$h_1(n)$
0	9.811255×10^{-3}	5.173349×10^{-3}
1	0.	0.
2	-7.665345×10^{-2}	7.229966×10^{-3}
3	-2.398916×10^{-1}	0.
4	-4.379021×10^{-1}	-1.613531×10^{-2}
5	-5.551294×10^{-1}	0.
6	-4.885365×10^{-1}	-5.311421×10^{-3}
7	-2.428178×10^{-1}	0.
8	4.913679×10^{-2}	3.934525×10^{-2}
9	2.167272×10^{-1}	0.
10	1.799614×10^{-1}	-3.039397×10^{-2}
11	1.535456×10^{-2}	0.
12	-1.232965×10^{-1}	-4.082131×10^{-2}
13	-1.261825×10^{-1}	0.
14	-2.083822×10^{-2}	1.001542×10^{-1}
15	7.876995×10^{-2}	0.
16	8.765079×10^{-2}	-4.669071×10^{-2}
17	1.473493×10^{-2}	0.
18	-5.492308×10^{-2}	-1.114084×10^{-1}
19	-5.867611×10^{-2}	0.
20	-6.936266×10^{-3}	2.150507×10^{-1}
21	3.856518×10^{-2}	0.
22	3.758526×10^{-2}	-1.029573×10^{-1}
23	9.934368×10^{-4}	0.
24	-2.709086×10^{-2}	-2.087334×10^{-1}
25	-2.189069×10^{-2}	0.
26	3.157377×10^{-3}	5.109277×10^{-1}
27	1.746522×10^{-2}	0.
28	1.089962×10^{-2}	-5.995040×10^{-1}
29	-4.327598×10^{-3}	0.
30	-1.071275×10^{-2}	4.489590×10^{-1}
31	-3.807417×10^{-3}	0.
32	5.126905×10^{-3}	-2.148628×10^{-1}
33	4.402844×10^{-3}	0.
34	-1.137470×10^{-3}	4.767007×10^{-2}
35	-2.107113×10^{-3}	0.
36	0.	0.
37	4.674901×10^{-4}	0.

38C

Table 3.F.3. continued ...

n	$h_0(n)$	$h_1(n)$
0	6.299385×10^{-3}	2.505546×10^{-3}
1	0.	0.
2	-5.696874×10^{-2}	4.613379×10^{-3}
3	-1.922887×10^{-1}	0.
4	-3.794394×10^{-1}	-7.444698×10^{-3}
5	-5.253341×10^{-1}	0.
6	-5.208488×10^{-1}	-6.383882×10^{-3}
7	-3.297258×10^{-1}	0.
8	-3.947725×10^{-2}	2.218634×10^{-2}
9	1.852436×10^{-1}	0.
10	2.215227×10^{-1}	-8.900904×10^{-3}
11	8.606603×10^{-2}	0.
12	-8.567513×10^{-2}	-3.376203×10^{-2}
13	-1.499304×10^{-1}	0.
14	-7.541837×10^{-2}	5.293895×10^{-2}
15	4.789700×10^{-2}	0.
16	1.052218×10^{-1}	2.894889×10^{-4}
17	5.680261×10^{-2}	0.
18	-3.242919×10^{-2}	-8.950757×10^{-2}
19	-7.451465×10^{-2}	0.
20	-3.939318×10^{-2}	1.029088×10^{-1}
21	2.454778×10^{-2}	0.
22	5.262124×10^{-2}	2.016134×10^{-2}
23	2.496353×10^{-2}	0.
24	-1.978449×10^{-2}	-1.855908×10^{-1}
25	-3.579008×10^{-2}	0.
26	-1.396373×10^{-2}	2.064846×10^{-1}
27	1.558328×10^{-2}	0.
28	2.317795×10^{-2}	7.844110×10^{-3}
29	6.384434×10^{-3}	0.
30	-1.204231×10^{-2}	-3.411766×10^{-1}
31	-1.360393×10^{-2}	0.
32	-1.396813×10^{-3}	5.673558×10^{-1}
33	8.197373×10^{-3}	0.
34	6.980896×10^{-3}	-5.542478×10^{-1}
35	-8.441601×10^{-4}	0.
36	-5.432104×10^{-3}	3.610968×10^{-1}
37	-2.527882×10^{-3}	0.
38	2.257675×10^{-3}	-1.500780×10^{-1}
39	2.174613×10^{-3}	0.
40	-4.291482×10^{-4}	2.852745×10^{-2}
41	-9.038060×10^{-4}	0.
42	0.	0.
43	1.717992×10^{-4}	0.

Table 3.F.3. continued ...

n	$h_0(n)$	$h_1(n)$
0	3.966714×10^{-3}	1.205975×10^{-3}
1	0.	0.
2	-4.200907×10^{-2}	2.790093×10^{-3}
3	-1.523008×10^{-1}	0.
4	-3.230052×10^{-1}	-3.211687×10^{-3}
5	-4.846032×10^{-1}	0.
6	-5.324929×10^{-1}	-5.184268×10^{-3}
7	-4.016326×10^{-1}	0.
8	-1.342772×10^{-1}	1.176537×10^{-2}
9	1.277326×10^{-1}	0.
10	2.371385×10^{-1}	-9.563574×10^{-5}
11	1.534397×10^{-1}	0.
12	-2.678986×10^{-2}	-2.364567×10^{-2}
13	-1.478179×10^{-1}	0.
14	-1.240704×10^{-1}	2.513069×10^{-2}
15	-1.223780×10^{-3}	0.
16	9.985373×10^{-2}	1.557631×10^{-2}
17	9.421869×10^{-2}	0.
18	6.364721×10^{-3}	-6.048799×10^{-2}
19	-7.124665×10^{-2}	0.
20	-6.954339×10^{-2}	4.139880×10^{-2}
21	-4.516505×10^{-3}	0.
22	5.260148×10^{-2}	5.048943×10^{-2}
23	4.955054×10^{-2}	0.
24	9.568094×10^{-4}	-1.226066×10^{-1}
25	-3.890252×10^{-2}	0.
26	-3.379700×10^{-2}	6.655157×10^{-2}
27	2.113655×10^{-3}	0.
28	2.837785×10^{-2}	1.045339×10^{-1}
29	2.158828×10^{-2}	0.
30	-4.165612×10^{-3}	-2.302169×10^{-1}
31	-1.979060×10^{-2}	0.
32	-1.255785×10^{-2}	1.474225×10^{-1}
33	4.805692×10^{-3}	0.
34	1.310494×10^{-2}	1.402904×10^{-1}
35	6.329953×10^{-3}	0.
36	-4.691326×10^{-3}	-4.492393×10^{-1}
37	-7.779870×10^{-3}	0.
38	-2.299578×10^{-3}	5.813097×10^{-1}
39	3.573910×10^{-3}	0.
40	4.132846×10^{-3}	-4.871437×10^{-1}
41	2.507075×10^{-4}	0.
42	-2.676986×10^{-3}	2.793143×10^{-1}
43	-1.494886×10^{-3}	0.
44	9.735015×10^{-4}	-1.015743×10^{-1}
45	1.036135×10^{-3}	0.
46	-1.594858×10^{-4}	1.664060×10^{-2}
47	-3.767963×10^{-4}	0.
48	0.	0.
49	6.172939×10^{-5}	0.

Table 3.F.3. continued ...

n	$h_0(n)$	$h_1(n)$
0	2.543807×10^{-3}	5.776660×10^{-4}
1	0.	0.
2	-3.118806×10^{-2}	1.610769×10^{-3}
3	-1.204284×10^{-1}	0.
4	-2.723899×10^{-1}	-1.267537×10^{-3}
5	-4.387807×10^{-1}	0.
6	-5.262056×10^{-1}	-3.568539×10^{-3}
7	-4.534693×10^{-1}	0.
8	-2.237543×10^{-1}	5.855130×10^{-3}
9	5.345022×10^{-2}	0.
10	2.252414×10^{-1}	2.619256×10^{-3}
11	2.054070×10^{-1}	0.
12	4.180549×10^{-2}	-1.487865×10^{-2}
13	-1.200825×10^{-1}	0.
14	-1.553794×10^{-1}	1.017898×10^{-2}
15	-5.698214×10^{-2}	0.
16	7.189854×10^{-2}	1.706194×10^{-2}
17	1.159408×10^{-1}	0.
18	5.107901×10^{-2}	-3.646554×10^{-2}
19	-4.816175×10^{-2}	0.
20	-8.698478×10^{-2}	1.049357×10^{-2}
21	-4.009365×10^{-2}	0.
22	3.552927×10^{-2}	4.850350×10^{-2}
23	6.499536×10^{-2}	0.
24	2.888206×10^{-2}	-7.050226×10^{-2}
25	-2.777611×10^{-2}	0.
26	-4.789591×10^{-2}	4.084510×10^{-3}
27	-1.907818×10^{-2}	0.
28	2.228407×10^{-2}	1.019727×10^{-1}
29	3.425984×10^{-2}	0.
30	1.124890×10^{-2}	-1.243129×10^{-1}
31	-1.769298×10^{-2}	0.
32	-2.350616×10^{-2}	-1.122346×10^{-3}
33	-5.539725×10^{-3}	0.
34	1.368588×10^{-2}	1.816790×10^{-1}
35	1.515546×10^{-2}	0.
36	1.698867×10^{-3}	-2.313869×10^{-1}
37	-9.973167×10^{-3}	0.
38	-8.990222×10^{-3}	5.041226×10^{-2}
39	4.167714×10^{-4}	0.
40	6.867099×10^{-3}	2.693288×10^{-1}
41	4.678399×10^{-3}	0.
42	-1.438907×10^{-3}	-5.199865×10^{-1}
43	-4.160525×10^{-3}	0.
44	-1.932038×10^{-3}	5.599947×10^{-1}
45	1.433994×10^{-3}	0.
46	2.303490×10^{-3}	-4.122640×10^{-1}
47	4.285001×10^{-4}	0.
48	-1.286605×10^{-3}	2.107532×10^{-1}
49	-8.147421×10^{-4}	0.
50	4.146013×10^{-4}	-6.791403×10^{-2}
51	4.782894×10^{-4}	0.
52	-5.948637×10^{-5}	9.744202×10^{-3}
53	-1.541260×10^{-4}	0.
54	0.	0.
55	2.211377×10^{-5}	0.

Table 3.F.3. continued ...

n	$h_0(n)$	$h_1(n)$
0	1.782610×10^{-3}	2.701193×10^{-4}
1	0.	0.
2	-2.409508×10^{-2}	8.607479×10^{-4}
3	-9.759425×10^{-2}	0.
4	-2.322606×10^{-1}	-4.720270×10^{-4}
5	-3.959603×10^{-1}	0.
6	-5.085791×10^{-1}	-2.159139×10^{-3}
7	-4.833801×10^{-1}	0.
8	-2.954028×10^{-1}	2.752473×10^{-3}
9	-2.161128×10^{-2}	0.
10	1.933615×10^{-1}	2.566140×10^{-3}
11	2.346038×10^{-1}	0.
12	1.043332×10^{-1}	-8.600169×10^{-3}
13	-7.678734×10^{-2}	0.
14	-1.645964×10^{-1}	3.338100×10^{-3}
15	-1.049617×10^{-1}	0.
16	3.111534×10^{-2}	1.321948×10^{-2}
17	1.178270×10^{-1}	0.
18	8.878153×10^{-2}	-2.012258×10^{-2}
19	-1.352453×10^{-2}	0.
20	-8.731545×10^{-2}	-1.797338×10^{-3}
21	-7.064505×10^{-2}	0.
22	7.611627×10^{-3}	3.609643×10^{-2}
23	6.622262×10^{-2}	0.
24	5.410573×10^{-2}	-3.631568×10^{-2}
25	-6.359139×10^{-3}	0.
26	-5.074475×10^{-2}	-1.740929×10^{-2}
27	-3.986647×10^{-2}	0.
28	6.710472×10^{-3}	7.523050×10^{-2}
29	3.864681×10^{-2}	0.
30	2.809507×10^{-2}	-5.777776×10^{-2}
31	-7.229594×10^{-3}	0.
32	-2.889969×10^{-2}	-4.534963×10^{-2}
33	-1.867821×10^{-2}	0.
34	7.354105×10^{-3}	1.357151×10^{-1}
35	2.090382×10^{-2}	0.
36	1.149009×10^{-2}	-9.461139×10^{-2}
37	-6.887401×10^{-3}	0.
38	-1.445922×10^{-2}	-7.751392×10^{-2}
39	-6.311087×10^{-3}	0.
40	5.960035×10^{-3}	2.305402×10^{-1}
41	9.378593×10^{-3}	0.
42	2.851414×10^{-3}	-1.937907×10^{-1}
43	-4.694469×10^{-3}	0.
44	-5.615350×10^{-3}	-5.713453×10^{-2}
45	-7.825710×10^{-4}	0.
46	3.406220×10^{-3}	3.707863×10^{-1}
47	2.919159×10^{-3}	0.
48	-2.697563×10^{-4}	-5.513894×10^{-1}
49	-2.104672×10^{-3}	0.
50	-1.263183×10^{-3}	5.191033×10^{-1}
51	5.504622×10^{-4}	0.
52	1.205532×10^{-3}	-3.448900×10^{-1}
53	3.090760×10^{-4}	0.
54	-6.029725×10^{-4}	1.606378×10^{-1}
55	-4.050824×10^{-4}	0.
56	1.766374×10^{-4}	-4.705794×10^{-2}
57	2.112913×10^{-4}	0.
58	-2.295249×10^{-5}	6.114768×10^{-3}
59	-6.189663×10^{-5}	0.
60	0.	0.
61	8.042925×10^{-6}	0.

Table 3.F.3. continued ...

n	$h_0(n)$	$h_1(n)$
0	1.417172×10^{-3}	1.331174×10^{-4}
1	0.	0.
2	-1.998759×10^{-2}	4.609250×10^{-4}
3	-8.330648×10^{-2}	0.
4	-2.048973×10^{-1}	-1.780452×10^{-4}
5	-3.629320×10^{-1}	0.
6	-4.886132×10^{-1}	-1.235135×10^{-3}
7	-4.959165×10^{-1}	0.
8	-3.433221×10^{-1}	1.329161×10^{-3}
9	-8.236903×10^{-2}	0.
10	1.561186×10^{-1}	1.857653×10^{-3}
11	2.440319×10^{-1}	0.
12	1.499404×10^{-1}	-4.786816×10^{-3}
13	-3.309146×10^{-2}	0.
14	-1.576876×10^{-1}	8.051460×10^{-4}
15	-1.370671×10^{-1}	0.
16	-8.767345×10^{-3}	8.794743×10^{-3}
17	1.059650×10^{-1}	0.
18	1.126595×10^{-1}	-1.074281×10^{-2}
19	2.065759×10^{-2}	0.
20	-7.550662×10^{-2}	-4.647998×10^{-3}
21	-8.979898×10^{-2}	0.
22	-2.097443×10^{-2}	2.377087×10^{-2}
23	5.658483×10^{-2}	0.
24	7.045850×10^{-2}	-1.773973×10^{-2}
25	1.704566×10^{-2}	0.
26	-4.399671×10^{-2}	-1.952533×10^{-2}
27	-5.430370×10^{-2}	0.
28	-1.196613×10^{-2}	4.926193×10^{-2}
29	3.482115×10^{-2}	0.
30	4.091221×10^{-2}	-2.385196×10^{-2}
31	7.131880×10^{-3}	0.
32	-2.761718×10^{-2}	-4.754702×10^{-2}
33	-2.985696×10^{-2}	0.
34	-3.169884×10^{-3}	8.778026×10^{-2}
35	2.159364×10^{-2}	0.
36	2.092635×10^{-2}	-3.014111×10^{-2}
37	3.059514×10^{-4}	0.
38	-1.645837×10^{-2}	-8.984884×10^{-2}
39	-1.389954×10^{-2}	0.
40	1.489545×10^{-3}	1.464064×10^{-1}
41	1.205347×10^{-2}	0.
42	8.607927×10^{-3}	-4.961672×10^{-2}
43	-2.338701×10^{-3}	0.
44	-8.406013×10^{-3}	-1.407423×10^{-1}
45	-4.830777×10^{-3}	0.
46	2.510113×10^{-3}	2.482500×10^{-1}
47	5.466961×10^{-3}	0.
48	2.323686×10^{-3}	-1.391602×10^{-1}
49	-2.191626×10^{-3}	0.
50	-3.278751×10^{-3}	-1.482309×10^{-1}
51	-8.239769×10^{-4}	0.
52	1.689715×10^{-3}	4.353207×10^{-1}
53	1.708717×10^{-3}	0.
54	4.324498×10^{-5}	-5.551649×10^{-1}
55	-1.077928×10^{-3}	0.
56	-7.482078×10^{-4}	4.767859×10^{-1}
57	2.243794×10^{-4}	0.
58	6.294485×10^{-4}	-2.948638×10^{-1}
59	1.842300×10^{-4}	0.
60	-2.931986×10^{-4}	1.289033×10^{-1}
61	-2.023156×10^{-4}	0.
62	8.084743×10^{-5}	-3.554415×10^{-2}
63	9.800101×10^{-5}	0.
64	-9.914516×10^{-6}	4.358865×10^{-3}
65	-2.702308×10^{-5}	0.
66	0.	0.
67	3.313905×10^{-6}	0.

Table 3.F.3. continued ...

n	$h_0(n)$	$h_1(n)$
0	-3.254804×10^{-2}	3.338605×10^{-2}
1	0.	0.
2	1.600837×10^{-1}	1.592299×10^{-2}
3	3.957186×10^{-1}	0.
4	5.660253×10^{-1}	-8.160940×10^{-2}
5	5.443471×10^{-1}	0.
6	3.185697×10^{-1}	4.066663×10^{-2}
7	1.781965×10^{-2}	0.
8	-1.753885×10^{-1}	9.767990×10^{-2}
9	-1.739248×10^{-1}	0.
10	-2.763006×10^{-2}	-1.894375×10^{-1}
11	9.180560×10^{-2}	0.
12	1.127195×10^{-1}	7.272149×10^{-2}
13	2.304147×10^{-2}	0.
14	-6.226398×10^{-2}	2.286128×10^{-1}
15	-7.086185×10^{-2}	0.
16	-1.068256×10^{-2}	-5.353428×10^{-1}
17	4.192834×10^{-2}	0.
18	4.470758×10^{-2}	6.105232×10^{-1}
19	1.238758×10^{-3}	0.
20	-3.288928×10^{-2}	-4.491334×10^{-1}
21	-2.207715×10^{-2}	0.
22	1.187258×10^{-2}	1.621310×10^{-1}
23	1.624113×10^{-2}	0.
24	0.	0.
25	-5.862824×10^{-3}	0.

$26D$

n	$h_0(n)$	$h_1(n)$
0	2.330616×10^{-2}	1.929333×10^{-2}
1	0.	0.
2	-1.296655×10^{-1}	1.529149×10^{-2}
3	-3.431041×10^{-1}	0.
4	-5.293513×10^{-1}	-4.665364×10^{-2}
5	-5.592648×10^{-1}	0.
6	-3.826137×10^{-1}	8.164201×10^{-3}
7	-8.775196×10^{-2}	0.
8	1.493044×10^{-1}	7.110545×10^{-2}
9	2.037048×10^{-1}	0.
10	8.306502×10^{-2}	-9.135101×10^{-2}
11	-6.734190×10^{-2}	0.
12	-1.317950×10^{-1}	-1.267867×10^{-2}
13	-6.436079×10^{-2}	0.
14	4.184261×10^{-2}	1.605338×10^{-1}
15	8.718130×10^{-2}	0.
16	4.525413×10^{-2}	-1.881158×10^{-1}
17	-2.845388×10^{-2}	0.
18	-6.145496×10^{-2}	-1.210289×10^{-2}
19	-2.915006×10^{-2}	0.
20	2.379750×10^{-2}	3.368129×10^{-1}
21	4.124906×10^{-2}	0.
22	1.541643×10^{-2}	-5.801067×10^{-1}
23	-1.844041×10^{-2}	0.
24	-2.743360×10^{-2}	5.693383×10^{-1}
25	-6.015501×10^{-3}	0.
26	1.770009×10^{-2}	-3.673356×10^{-1}
27	1.414394×10^{-2}	0.
28	-5.543508×10^{-3}	1.150462×10^{-1}
29	-9.125631×10^{-3}	0.
30	0.	0.
31	2.858065×10^{-3}	0.

$32D$

Table 3.F.3. continued ...

n	$h_0(n)$	$h_1(n)$
0	1.710503×10^{-2}	1.128329×10^{-2}
1	0.	0.
2	-1.056212×10^{-1}	1.228700×10^{-2}
3	-2.968934×10^{-1}	0.
4	-4.898762×10^{-1}	-2.661195×10^{-2}
5	-5.606364×10^{-1}	0.
6	-4.335216×10^{-1}	-3.554443×10^{-3}
7	-1.584473×10^{-1}	0.
8	1.075840×10^{-1}	4.856712×10^{-2}
9	2.166807×10^{-1}	0.
10	1.337119×10^{-1}	-4.405512×10^{-2}
11	-2.930060×10^{-2}	0.
12	-1.344958×10^{-1}	-3.146088×10^{-2}
13	-1.014230×10^{-1}	0.
14	9.974991×10^{-3}	1.039878×10^{-1}
15	8.918163×10^{-2}	0.
16	7.510579×10^{-2}	-7.299761×10^{-2}
17	-4.472472×10^{-3}	0.
18	-6.439333×10^{-2}	-7.396083×10^{-2}
19	-5.338424×10^{-2}	0.
20	5.010270×10^{-3}	2.027600×10^{-1}
21	4.622935×10^{-2}	0.
22	3.694576×10^{-2}	-1.541976×10^{-1}
23	-5.645313×10^{-3}	0.
24	-3.442017×10^{-2}	-1.085522×10^{-1}
25	-2.398181×10^{-2}	0.
26	7.894572×10^{-3}	4.256008×10^{-1}
27	2.393909×10^{-2}	0.
28	1.341905×10^{-2}	-5.947476×10^{-1}
29	-7.533342×10^{-3}	0.
30	-1.686647×10^{-2}	5.158141×10^{-1}
31	-6.085264×10^{-3}	0.
32	9.688719×10^{-3}	-2.963025×10^{-1}
33	8.829895×10^{-3}	0.
34	-2.677891×10^{-3}	8.189586×10^{-2}
35	-5.072216×10^{-3}	0.
36	0.	0.
37	1.401923×10^{-3}	0.

n	$h_0(n)$	$h_1(n)$
0	1.261020×10^{-2}	6.625193×10^{-3}
1	0.	0.
2	-8.591368×10^{-2}	9.170467×10^{-3}
3	-2.557582×10^{-1}	0.
4	-4.487911×10^{-1}	-1.491768×10^{-2}
5	-5.514423×10^{-1}	0.
6	-4.725458×10^{-1}	-7.103011×10^{-3}
7	-2.270485×10^{-1}	0.
8	5.431422×10^{-2}	3.194056×10^{-2}
9	2.132308×10^{-1}	0.
10	1.764869×10^{-1}	-1.953395×10^{-2}
11	1.754467×10^{-2}	0.
12	-1.216671×10^{-1}	-3.194513×10^{-2}
13	-1.303090×10^{-1}	0.
14	-2.864957×10^{-2}	6.502143×10^{-2}
15	7.716525×10^{-2}	0.
16	9.715556×10^{-2}	-2.293474×10^{-2}
17	2.607536×10^{-2}	0.
18	-5.480759×10^{-2}	-7.315460×10^{-2}
19	-7.171896×10^{-2}	0.
20	-1.969926×10^{-2}	1.182260×10^{-1}
21	4.039794×10^{-2}	0.
22	5.322008×10^{-2}	-3.256798×10^{-2}
23	1.323446×10^{-2}	0.
24	-3.149834×10^{-2}	-1.355411×10^{-1}
25	-3.824637×10^{-2}	0.
26	-7.154143×10^{-3}	2.202878×10^{-1}
27	2.398981×10^{-2}	0.
28	2.677545×10^{-2}	-9.370255×10^{-2}
29	2.970308×10^{-3}	0.
30	-1.895717×10^{-2}	-2.081192×10^{-1}
31	-1.755811×10^{-2}	0.
32	1.065654×10^{-3}	4.929633×10^{-1}
33	1.358416×10^{-2}	0.
34	1.024677×10^{-2}	-5.860274×10^{-1}
35	-2.445935×10^{-3}	0.
36	-1.030838×10^{-2}	4.559516×10^{-1}
37	-4.900777×10^{-3}	0.
38	5.319561×10^{-3}	-2.352903×10^{-1}
39	5.397257×10^{-3}	0.
40	-1.307989×10^{-3}	5.785386×10^{-2}
41	-2.785213×10^{-3}	0.
42	0.	0.
43	6.848361×10^{-4}	0.

Table 3.F.3. continued ...

n	$h_0(n)$	$h_1(n)$
0	9.205880×10^{-3}	3.888800×10^{-3}
1	0.	0.
2	-6.954724×10^{-2}	6.567161×10^{-3}
3	-2.189227×10^{-1}	0.
4	-4.069202×10^{-1}	-8.100208×10^{-3}
5	-5.336959×10^{-1}	0.
6	-5.002897×10^{-1}	-7.316951×10^{-3}
7	-2.912585×10^{-1}	0.
8	-7.289636×10^{-3}	2.030155×10^{-2}
9	1.939953×10^{-1}	0.
10	2.086029×10^{-1}	-6.803233×10^{-3}
11	6.864207×10^{-2}	0.
12	-9.455647×10^{-2}	-2.680992×10^{-2}
13	-1.477013×10^{-1}	0.
14	-6.930413×10^{-2}	3.889404×10^{-2}
15	5.236148×10^{-2}	0.
16	1.083258×10^{-1}	-6.337534×10^{-5}
17	5.848978×10^{-2}	0.
18	-3.388692×10^{-2}	-5.932399×10^{-2}
19	-8.077090×10^{-2}	0.
20	-4.625590×10^{-2}	6.580814×10^{-2}
21	2.431336×10^{-2}	0.
22	6.158857×10^{-2}	1.258190×10^{-2}
23	3.478694×10^{-2}	0.
24	-1.945853×10^{-2}	-1.098493×10^{-1}
25	-4.657077×10^{-2}	0.
26	-2.496830×10^{-2}	1.105107×10^{-1}
27	1.603321×10^{-2}	0.
28	3.516694×10^{-2}	2.391199×10^{-2}
29	1.692908×10^{-2}	0.
30	-1.395028×10^{-2}	-1.883485×10^{-1}
31	-2.564312×10^{-2}	0.
32	-1.030530×10^{-2}	2.104884×10^{-1}
33	1.149579×10^{-2}	0.
34	1.826606×10^{-2}	-1.309089×10^{-2}
35	5.635486×10^{-3}	0.
36	-9.957820×10^{-3}	-3.033155×10^{-1}
37	-1.206796×10^{-2}	0.
38	-1.638763×10^{-3}	5.379248×10^{-1}
39	7.423377×10^{-3}	0.
40	7.342434×10^{-3}	-5.590610×10^{-1}
41	-2.011906×10^{-4}	0.
42	-6.235789×10^{-3}	3.938309×10^{-1}
43	-3.579115×10^{-3}	0.
44	2.905965×10^{-3}	-1.835307×10^{-1}
45	3.235657×10^{-3}	0.
46	-6.377363×10^{-4}	4.027722×10^{-2}
47	-1.507862×10^{-3}	0.
48	0.	0.
49	3.309118×10^{-4}	0.

Table 3.F.3. continued ...

n	$h_0(n)$	$h_1(n)$
0	6.639258×10^{-3}	2.277431×10^{-3}
1	0.	0.
2	-5.606188×10^{-2}	4.567203×10^{-3}
3	-1.862037×10^{-1}	0.
4	-3.653612×10^{-1}	-4.187482×10^{-3}
5	-5.091685×10^{-1}	0.
6	-5.169971×10^{-1}	-6.258163×10^{-3}
7	-3.486625×10^{-1}	0.
8	-7.370956×10^{-2}	1.244183×10^{-2}
9	1.603618×10^{-1}	0.
10	2.275839×10^{-1}	-5.494592×10^{-4}
11	1.191606×10^{-1}	0.
12	-5.555562×10^{-2}	-2.046873×10^{-2}
13	-1.512736×10^{-1}	0.
14	-1.069962×10^{-1}	2.185430×10^{-2}
15	1.752210×10^{-2}	0.
16	1.065784×10^{-1}	9.420731×10^{-3}
17	8.770913×10^{-2}	0.
18	-4.300480×10^{-3}	-4.383229×10^{-2}
19	-7.829678×10^{-2}	0.
20	-6.999103×10^{-2}	3.328915×10^{-2}
21	2.022623×10^{-4}	0.
22	5.988535×10^{-2}	2.810507×10^{-2}
23	5.461379×10^{-2}	0.
24	-3.999567×10^{-5}	-7.937210×10^{-2}
25	-4.645237×10^{-2}	0.
26	-4.190083×10^{-2}	4.905718×10^{-2}
27	1.099063×10^{-3}	0.
28	3.653059×10^{-2}	5.603905×10^{-2}
29	3.122989×10^{-2}	0.
30	-2.634446×10^{-3}	-1.334975×10^{-1}
31	-2.836578×10^{-2}	0.
32	-2.249628×10^{-2}	8.044048×10^{-2}
33	3.671195×10^{-3}	0.
34	2.192947×10^{-2}	8.796950×10^{-2}
35	1.546102×10^{-2}	0.
36	-4.629999×10^{-3}	-2.240763×10^{-1}
37	-1.626471×10^{-2}	0.
38	-9.820721×10^{-3}	1.736195×10^{-1}
39	4.626789×10^{-3}	0.
40	1.187019×10^{-2}	7.971353×10^{-2}
41	5.717694×10^{-3}	0.
42	-4.809680×10^{-3}	-3.871913×10^{-1}
43	-7.906151×10^{-3}	0.
44	-2.406672×10^{-3}	5.604402×10^{-1}
45	3.845800×10^{-3}	0.
46	5.042150×10^{-3}	-5.185899×10^{-1}
47	6.435286×10^{-4}	0.
48	-3.724547×10^{-3}	3.329675×10^{-1}
49	-2.461602×10^{-3}	0.
50	1.573779×10^{-3}	-1.406929×10^{-1}
51	1.903437×10^{-3}	0.
52	-3.091660×10^{-4}	2.763886×10^{-2}
53	-8.042830×10^{-4}	0.
54	0.	0.
55	1.579999×10^{-4}	0.

Table 3.F.3. continued ...

n	$h_0(n)$	$h_1(n)$
0	-4.786556×10^{-3}	1.330828×10^{-3}
1	0.	0.
2	4.521403×10^{-2}	3.098201×10^{-3}
3	1.578362×10^{-1}	0.
4	3.256672×10^{-1}	-2.014829×10^{-3}
5	4.799745×10^{-1}	0.
6	5.232099×10^{-1}	-4.854501×10^{-3}
7	3.968277×10^{-1}	0.
8	1.405778×10^{-1}	7.322157×10^{-3}
9	-1.152125×10^{-1}	0.
10	-2.320220×10^{-1}	2.097572×10^{-3}
11	-1.641120×10^{-1}	0.
12	8.715785×10^{-3}	-1.462856×10^{-2}
13	1.404794×10^{-1}	0.
14	1.369436×10^{-1}	1.122587×10^{-2}
15	2.290649×10^{-2}	0.
16	-9.179901×10^{-2}	1.199379×10^{-2}
17	-1.090713×10^{-1}	0.
18	-2.964910×10^{-2}	-3.023841×10^{-2}
19	6.411531×10^{-2}	0.
20	8.654856×10^{-2}	1.390610×10^{-2}
21	2.796687×10^{-2}	0.
22	-4.777489×10^{-2}	3.017673×10^{-2}
23	-6.846169×10^{-2}	0.
24	-2.333688×10^{-2}	-5.307471×10^{-2}
25	3.711759×10^{-2}	0.
26	5.407170×10^{-2}	1.487650×10^{-2}
27	1.800799×10^{-2}	0.
28	-2.985631×10^{-2}	5.858144×10^{-2}
29	-4.219003×10^{-2}	0.
30	-1.287483×10^{-2}	-8.608589×10^{-2}
31	2.426073×10^{-2}	0.
32	3.246185×10^{-2}	1.674484×10^{-2}
33	8.460521×10^{-3}	0.
34	-1.990387×10^{-2}	9.869897×10^{-2}
35	-2.433137×10^{-2}	0.
36	-4.745099×10^{-3}	-1.382565×10^{-1}
37	1.601510×10^{-2}	0.
38	1.768914×10^{-2}	3.199605×10^{-2}
39	2.059408×10^{-3}	0.
40	-1.283046×10^{-2}	1.495363×10^{-1}
41	-1.228030×10^{-2}	0.
42	4.975485×10^{-5}	-2.369895×10^{-1}
43	9.752146×10^{-3}	0.
44	8.006885×10^{-3}	1.138989×10^{-1}
45	-1.111343×10^{-3}	0.
46	-7.369022×10^{-3}	1.752272×10^{-1}
47	-4.782362×10^{-3}	0.
48	2.003430×10^{-3}	-4.538947×10^{-1}
49	4.965898×10^{-3}	0.
50	2.302653×10^{-3}	5.621883×10^{-1}
51	-1.854137×10^{-3}	0.
52	-3.347191×10^{-3}	-4.698678×10^{-1}
53	-8.255145×10^{-4}	0.
54	2.196518×10^{-3}	2.767396×10^{-1}
55	1.618368×10^{-3}	0.
56	-8.461222×10^{-4}	-1.066030×10^{-1}
57	-1.100081×10^{-3}	0.
58	1.497552×10^{-4}	1.886767×10^{-2}
59	4.237629×10^{-4}	0.
60	0.	0.
61	-7.500178×10^{-5}	0.

Table 3.F.3. continued ...

n	$h_0(n)$	$h_1(n)$
0	3.496933×10^{-3}	7.771098×10^{-4}
1	0.	0.
2	-3.662916×10^{-2}	2.058921×10^{-3}
3	-1.337574×10^{-1}	0.
4	-2.890154×10^{-1}	-8.634418×10^{-4}
5	-4.482555×10^{-1}	0.
6	-5.203508×10^{-1}	-3.535345×10^{-3}
7	-4.345816×10^{-1}	0.
8	-2.040397×10^{-1}	4.121965×10^{-3}
9	6.236620×10^{-2}	0.
10	2.223863×10^{-1}	2.845963×10^{-3}
11	1.997897×10^{-1}	0.
12	4.123006×10^{-2}	-9.925363×10^{-3}
13	-1.168854×10^{-1}	0.
14	-1.559426×10^{-1}	4.985715×10^{-3}
15	-6.395798×10^{-2}	0.
16	6.597838×10^{-2}	1.125134×10^{-2}
17	1.196379×10^{-1}	0.
18	6.316468×10^{-2}	-1.965069×10^{-2}
19	-4.021235×10^{-2}	0.
20	-9.317019×10^{-2}	3.201005×10^{-3}
21	-5.562521×10^{-2}	0.
22	2.698595×10^{-2}	2.640256×10^{-2}
23	7.353539×10^{-2}	0.
24	4.651589×10^{-2}	-3.299667×10^{-2}
25	-1.985810×10^{-2}	0.
26	-5.872392×10^{-2}	-2.730232×10^{-3}
27	-3.754092×10^{-2}	0.
28	1.597059×10^{-2}	5.004913×10^{-2}
29	4.697081×10^{-2}	0.
30	2.938535×10^{-2}	-5.080382×10^{-2}
31	-1.359803×10^{-2}	0.
32	-3.750261×10^{-2}	-1.318960×10^{-2}
33	-2.223693×10^{-2}	0.
34	1.204545×10^{-2}	8.417880×10^{-2}
35	2.957608×10^{-2}	0.
36	1.614705×10^{-2}	-7.665443×10^{-2}
37	-1.068743×10^{-2}	0.
38	-2.298870×10^{-2}	-2.555383×10^{-2}
39	-1.116345×10^{-2}	0.
40	9.514645×10^{-3}	1.322826×10^{-1}
41	1.738873×10^{-2}	0.
42	7.129705×10^{-3}	-1.224232×10^{-1}
43	-8.163198×10^{-3}	0.
44	-1.279052×10^{-2}	-2.754546×10^{-2}
45	-4.137321×10^{-3}	0.
46	6.955109×10^{-3}	1.997945×10^{-1}
47	8.959320×10^{-3}	0.
48	1.846890×10^{-3}	-2.256278×10^{-1}
49	-5.506991×10^{-3}	0.
50	-5.967595×10^{-3}	3.846769×10^{-2}
51	-4.697334×10^{-4}	0.
52	4.377235×10^{-3}	2.650000×10^{-1}
53	3.610797×10^{-3}	0.
54	-5.837621×10^{-4}	-5.007630×10^{-1}
55	-3.006267×10^{-3}	0.
56	-1.880081×10^{-3}	5.469935×10^{-1}
57	8.053667×10^{-4}	0.
58	2.162932×10^{-3}	-4.178828×10^{-1}
59	7.353431×10^{-4}	0.
60	-1.281812×10^{-3}	2.272688×10^{-1}
61	-1.027882×10^{-3}	0.
62	4.532093×10^{-4}	-8.035529×10^{-2}
63	6.266872×10^{-4}	0.
64	-7.294796×10^{-5}	1.293388×10^{-2}
65	-2.215774×10^{-4}	0.
66	0.	0.
67	3.566479×10^{-5}	0.

Table 3.F.3. continued ...

n	$h_0(n)$	$h_1(n)$
0	-2.581183×10^{-3}	4.548110×10^{-4}
1	0.	0.
2	2.969260×10^{-2}	1.353830×10^{-3}
3	1.130783×10^{-1}	0.
4	2.551648×10^{-1}	-2.785456×10^{-4}
5	4.149981×10^{-1}	0.
6	5.100794×10^{-1}	-2.472378×10^{-3}
7	4.626613×10^{-1}	0.
8	2.627922×10^{-1}	2.207872×10^{-3}
9	-4.259944×10^{-3}	0.
10	-1.999767×10^{-1}	2.764426×10^{-3}
11	-2.246918×10^{-1}	0.
12	-9.102816×10^{-2}	-6.441915×10^{-3}
13	8.260914×10^{-2}	0.
14	1.627533×10^{-1}	1.526340×10^{-3}
15	1.020345×10^{-1}	0.
16	-3.165150×10^{-2}	9.281018×10^{-3}
17	-1.183608×10^{-1}	0.
18	-9.260736×10^{-2}	-1.202934×10^{-2}
19	9.255600×10^{-3}	0.
20	8.886278×10^{-2}	-2.164103×10^{-3}
21	7.914832×10^{-2}	0.
22	-5.880622×10^{-5}	2.082942×10^{-2}
23	-6.874290×10^{-2}	0.
24	-6.600699×10^{-2}	-1.880579×10^{-2}
25	-3.044282×10^{-3}	0.
26	5.462179×10^{-2}	-1.061345×10^{-2}
27	5.414651×10^{-2}	0.
28	3.221338×10^{-3}	3.856089×10^{-2}
29	-4.411565×10^{-2}	0.
30	-4.380101×10^{-2}	-2.646122×10^{-2}
31	-2.154265×10^{-3}	0.
32	3.601641×10^{-2}	-2.511518×10^{-2}
33	3.481950×10^{-2}	0.
34	6.337907×10^{-4}	6.381555×10^{-2}
35	-2.941123×10^{-2}	0.
36	-2.712678×10^{-2}	-3.584292×10^{-2}
37	8.181299×10^{-4}	0.
38	2.393391×10^{-2}	-4.600449×10^{-2}
39	2.059380×10^{-2}	0.
40	-2.065429×10^{-3}	9.921186×10^{-2}
41	-1.919637×10^{-2}	0.
42	-1.513096×10^{-2}	-5.133619×10^{-2}
43	2.878379×10^{-3}	0.
44	1.516989×10^{-2}	-7.140463×10^{-2}
45	1.067923×10^{-2}	0.
46	-3.401973×10^{-3}	1.511454×10^{-1}
47	-1.163015×10^{-2}	0.
48	-7.109591×10^{-3}	-8.736825×10^{-2}
49	3.453675×10^{-3}	0.
50	8.697777×10^{-3}	-9.111237×10^{-2}
51	4.410023×10^{-3}	0.
52	-3.364556×10^{-3}	2.333874×10^{-1}
53	-6.157450×10^{-3}	0.
54	-2.362331×10^{-3}	-1.913745×10^{-1}
55	2.869827×10^{-3}	0.
56	4.189741×10^{-3}	-4.662057×10^{-2}
57	1.051619×10^{-3}	0.
58	-2.473019×10^{-3}	3.447914×10^{-1}
59	-2.575204×10^{-3}	0.
60	-7.648307×10^{-5}	-5.287201×10^{-1}
61	1.765990×10^{-3}	0.
62	1.420085×10^{-3}	5.189616×10^{-1}
63	-2.837535×10^{-4}	0.
64	-1.372120×10^{-3}	-3.653447×10^{-1}
65	-5.725996×10^{-4}	0.
66	7.419604×10^{-4}	1.843106×10^{-1}
67	6.387522×10^{-4}	0.
68	-2.419209×10^{-4}	-6.009564×10^{-2}
69	-3.537204×10^{-4}	0.
70	3.565693×10^{-5}	8.857549×10^{-3}
71	1.153328×10^{-4}	0.
72	0.	0.
73	-1.699900×10^{-5}	0.

CHAPTER IV
M-CHANNEL FIR PR LINEAR-PHASE QMF BANKS

It is proved in [31] that for a two-channel FIR QMF bank with lossless $\mathbf{E}(z)$, only trivial filters in the form of sums of delays exist. The reason [31] is that the lossless property put too many constraints on $\mathbf{E}(z)$. Instead of forcing $\mathbf{E}(z)$ to be lossless, let us derive a general condition for an FIR perfect-reconstruction system. Figures 1.2(b), 2.6 and 2.7 are redrawn as Figures 4.1(a), 4.1(b) and 4.1(c), respectively. It is clear from Fig. 4.1(c) that it is a perfect-reconstruction system if we choose [12] $\mathbf{R}(z) = \mathbf{E}^{-1}(z)$. If the analysis filters are FIR, the choice $\mathbf{R}(z) = \mathbf{E}^{-1}(z)$ gives rise to FIR synthesis filters as well, provided that $\det \mathbf{E}(z) = bz^{-r}$, where b and r are a nonzero constant and a nonnegative integer, respectively. In this chapter, the term "perfect reconstruction" is taken to be synonymous to the condition $\det \mathbf{E}(z) = bz^{-r}$ (even though this is not a necessary condition with IIR perfect-reconstruction systems).

The theory of perfect reconstruction when M is a power of 2 is well known [18], [19]. The design method in [18] is based on spectral factorization of an FIR half-band filter. Some methods of perfect reconstruction for an arbitrary number of channels have been reported recently [7, 20]. The method described in [7] constrains the polyphase transfer matrix $\mathbf{E}(z)$ to be FIR and lossless (i.e., $\mathbf{E}(e^{j\omega})$ to be unitary for all ω). The coefficents here are assumed to be real. Under this condition if the matrix $\mathbf{R}(z)$ is chosen as $\mathbf{R}(z) = \mathbf{E}^T(z^{-1})$, then the system of Fig. 4.1(a) is forced to be a PR system. In [11], a procedure for the design of two-channel perfect-reconstruction systems with linear-phase FIR filters is given, based on judicious factorization of a linear- phase FIR halfband filter. The number of

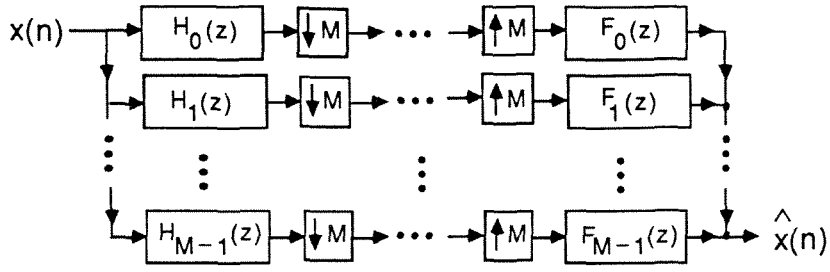

Fig. 4.1(a). The M-channel maximally decimated parallel QMF bank.

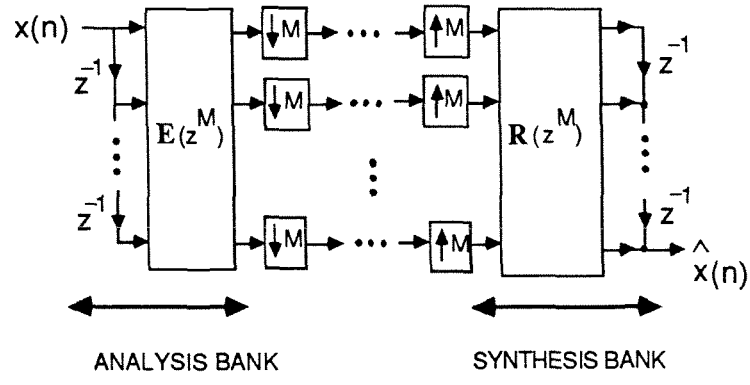

Fig. 4.1(b). Polyphase implementation of Fig. 4.1(a).

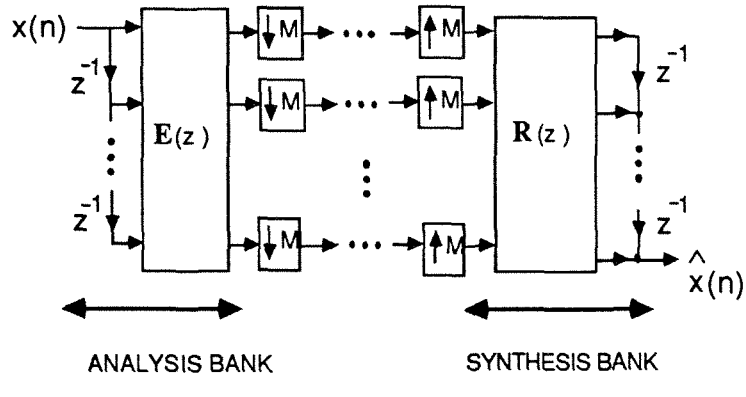

Fig. 4.1(c). An equivalent structure for Fig. 4.1(b).

possible spectral factors, hence, grows exponentially with respect to the degree of the filters; besides, the resulting filters are not guaranteed to be optimal.

Our goal in this chapter is to impose both the PR and the linear-phase properties on the analysis filters of the QMF bank in Fig. 4.1(a). First, in Section 4.1, we study the necessary form of $\mathbf{E}(z)$ such that $H_k(z)$, $0 \leq k \leq M-1$ are linear-phase FIR filters. Next, we concentrate on a special class (to be elaborated) of these linear-phase FIR QMF banks. Our restriction to this subclass is primarily motivated by analytic tractability. Having limited our study to a subclass of these PR structures, the conditions on the lengths and the symmetries of $H_k(z)$ are derived by imposing the perfect-reconstruction condition on the above $\mathbf{E}(z)$. We will also give the exact number of linear-phase perfect-reconstruction structures for this subclass. For the two-channel case, this class covers all nontrivial LP PR FIR QMF structures [30]. The lattice structures for the two-channel and three-channel PR LP FIR QMF banks are elaborately studied in Sections 4.2 and 4.3, respectively. Once this linear-phase perfect-reconstruction lattice structure for 3−channel QMF bank is obtained, the pairwise symmetry property [59] is incorporated on it to speed up the convergence time in the design process. Design examples and systems complexity are also included.

4.1. M-channel LP PR FIR QMF Banks.

Let $H_k(z)$, $0 \leq k \leq M-1$ be the M (causal) linear-phase analysis filters with center c_k. We define the degree of $H_k(z)$ as $N_k - 1 \triangleq 2c_k$. For a given M, we can uniquely write $N_k - 1$ as $m_k M + i_k$, where $0 \leq i_k \leq M-1$ and m_k are integers. This representation will be used subsequently. In terms of the polyphase components

$E_{kj}(z)$, the filter $H_k(z)$ is represented as [7, 17]

$$H_k(z) = \sum_{j=0}^{M-1} z^{-j} E_{kj}(z^M). \tag{4.1}$$

We shall define the center of $E_{kj}(z)$ as c_{kj}, where

$$2c_{kj} \triangleq \begin{cases} m_k, & j \le i_k; \\ m_k - 1, & j > i_k. \end{cases} \tag{4.2}$$

First, let us find the relations among the polyphase component $E_{kj}(z)$, which yields linear-phase analysis filters. Once these relations are known, we can further study the perfect-reconstruction aspect of these structures.

The impulse response of a linear-phase filter $H_k(z)$ could be either a symmetric or an antisymmetric sequence; i.e.,

$$\tilde{H}_k(z) = z^{N_k-1} J_k H_k(z), \tag{4.3}$$

where

$$J_k = \begin{cases} 1, & H_k(z) \text{ is symmetric;} \\ -1, & H_k(z) \text{ is anti-symmetric.} \end{cases} \tag{4.4}$$

Using (4.1) in (4.3) and noting that $N_k - 1 = m_k M + i_k$, we obtain

$$\sum_{j=0}^{M-1} z^j \tilde{E}_{kj}(z^M) = z^{(m_k M + i_k)} J_k \sum_{j=0}^{M-1} z^{-j} E_{kj}(z^M) \tag{4.5}$$

$$= z^{(m_k M + i_k)} J_k \sum_{j=0}^{i_k} z^{-j} E_{kj}(z^M) + z^{(m_k M + i_k)} J_k \sum_{j=i_k+1}^{M-1} z^{-j} E_{kj}(z^M)$$

$$= J_k \sum_{j=0}^{i_k} z^{(i_k - j)} \left[z^{m_k M} E_{kj}(z^M) \right] + J_k \sum_{j=i_k+1}^{M-1} z^{(M + i_k - j)} \left[z^{(m_k - 1)M} E_{kj}(z^M) \right].$$

Making changes of variables, the above equation becomes

$$\sum_{j=0}^{M-1} z^j \tilde{E}_{kj}(z^M) = J_k \sum_{j=0}^{i_k} z^j \left[z^{m_k M} E_{k,i_k - j}(z^M) \right] + J_k \sum_{j=i_k+1}^{M-1} z^j \left[z^{(m_k - 1)M} E_{k,M+i_k - j}(z^M) \right]. \tag{4.6}$$

Comparing like powers of both sides of (4.6), we have the following necessary form of $\mathbf{E}(z)$, which yields linear-phase analysis filters. Thus,

$$\tilde{E}_{kj}(z) = z^{m_k} J_k \times \begin{cases} E_{k,(i_k-j)}(z), & j \leq i_k; \\ z^{-1} E_{k,(M+i_k-j)}(z), & j > i_k. \end{cases} \tag{4.7}$$

The above relation has been known before in a slightly different notation [14]. Let us now concentrate on a subclass of systems that satisfies (4.7), namely, the class where all i_k are equal; i.e., $i_0 = i_1 = \ldots = i_{M-1} = I$. From now on, we consider only this class. The restriction of our discussion to this class is motivated primarily by the tractability of the possible combinations of PR systems belonging to this subclass.

Recalling that $N_k = m_k M + i_k + 1$, we see that for this particular subclass, the sum of the lengths of the analysis filters is a multiple of M. $\mathbf{E}(z)$ in (4.7) becomes

$$\tilde{E}_{kj}(z) = z^{m_k} J_k \times \begin{cases} E_{k,(I-j)}(z), & j \leq I; \\ z^{-1} E_{k,(M+I-j)}(z), & j > I. \end{cases} \tag{4.8}$$

The above form of $\mathbf{E}(z)$ yields a linear-phase QMF structure. It does not, however, guarantee perfect-reconstruction yet. To achieve this additional goal, namely, perfect reconstruction, let us study $\mathbf{E}(z)$ carefully. It can be verified that (4.8) is equivalent to

$$\tilde{\mathbf{E}}(z) = \Lambda_1(z) \mathbf{P} \mathbf{E}^T(z) \Lambda_2(z), \tag{4.9}$$

where $\Lambda_1(z)$ and $\Lambda_2(z)$ are diagonal matrices such that

$$(\Lambda_1)_{jj} = \begin{cases} 1, & j \leq I; \\ z^{-1}, & j > I, \end{cases} \quad \text{and} \quad (\Lambda_2)_{jj} = z^{m_j} J_j. \tag{4.10}$$

Here, $\mathbf{P}$ is a permutation matrix of the form

$$\mathbf{P} = \begin{pmatrix} \Gamma_{(I+1)} & \mathbf{0} \\ \mathbf{0} & \Gamma_{(M-1-I)} \end{pmatrix}, \tag{4.11}$$

where

$$\Gamma_I = \begin{pmatrix} 0 & & 1 \\ & \iddots & \\ 1 & & 0 \end{pmatrix}_{(I\times I)} . \tag{4.12}$$

For a PR system, $\det \mathbf{E}(z) = bz^{-r}$. Taking the determinant of both sides in (4.9),

$$\det \tilde{\mathbf{E}}(z) = \det \Lambda_1(z) \det \mathbf{P} \det \mathbf{E}^T(z) \det \Lambda_2(z) \tag{4.13}$$

or equivalently,

$$bz^r = bz^{-(M-1-I)} z^{-r} z^{\left(\sum_{k=0}^{M-1} m_k\right)} \left(\prod_{k=0}^{M-1} J_k\right) \det \mathbf{P}. \tag{4.14}$$

Comparing both sides of (4.14), we have the two following conditions:

$$2r = \left(\sum_{k=0}^{M-1} m_k\right) - (M-1-I), \tag{4.15a}$$

$$\left(\prod_{k=0}^{M-1} J_k\right) \det \mathbf{P} = 1. \tag{4.15b}$$

The first equation in (4.15) yields the same condition on the filter lengths as above. Namely, the sum of the lengths of the analysis filters is a multiple of M. From Eq. (4.15b) one can obtain the total number of possible combinations of analysis filters which yield LP PR systems.

We have shown in [30] that in the case of two-channel LP PR FIR QMF banks, there are only two structures in which all i_k are the same. For an arbitrary number of channels, partly because of the two choices that J_k can take (namely, J_k can be either 1 or -1), and partly because of the M choices that I can take (i.e., $0 \leq I \leq M-1$), the counting of combinations that yield LP PR FIR QMF banks is not simple. For instance, if $M = 3$, there are 3 possible combinations which the triplets J_0, J_1 and J_2 can take. These are the combinations in which either one or two or all three of the J_k are 1. (The case where none of the J_k is 1, i.e., all J_k are -1,

can not be a PR structure. In other words, the DC component of the signal $x(n)$ can not be reconstructed since all analysis filter $H_k(z)$ have zeros at $\omega = 0$!) Moreover, for each of the above triplets J_0, J_1 and J_2, there are 3 possibilities because I can be either 0 or 1 or 2. Thus, there are in total 3^2 structures that yield LP analysis filters in our subclass. In general, there are M^2 LP structures. Which one of these can be both LP and PR?

Let us turn our attention to (4.15b), which governs the number of combinations of analysis filters that yield LP PR FIR filters. Let

$$\begin{cases} \Delta_S = \text{Number of combinations of } J_k \text{ such that } \prod_{k=0}^{S-1} J_k = 1, \\ \Theta_S = \text{Number of combinations of } J_k \text{ such that } \prod_{k=0}^{S-1} J_k = -1, \\ R_1 = \text{Number of combinations of } I \text{ such that } \det \mathbf{P} = 1; \end{cases} \tag{4.16}$$

then the total number of combinations of analysis filters which are LP PR and are obeying (4.15b) (denoted as $Total$) is:

$$Total = \Delta_M R_1 + \Theta_M (M - R_1) = R_1(\Delta_M - \Theta_M) + M\Theta_M. \tag{4.17}$$

Let us calculate Δ_S, Θ_S and R_1 separately, as follows:

Calculating R_1:

From (4.11),

$$\det \mathbf{P} = \det \Gamma_{I+1} \det \Gamma_{M-1-I}, \tag{4.18}$$

where

$$\det \Gamma_k = \begin{cases} 1; & k = 4r, 4r+1, \\ -1; & k = 4r+2, 4r+3. \end{cases} \tag{4.19}$$

Here, r is a positive integer. By taking I in the range from 0 to $M-1$ and using

(4.19) in (4.18), one can verify that

$$R_1 = \begin{cases} M/2; & M \text{ is even}, \\ M; & M = 4r+1, \\ 0; & M = 4r+3, \end{cases} \tag{4.20}$$

where r is a positive integer.

Calculating Δ_S:

We are interested in the number of combinations of J_k for which $\prod_{k=0}^{S-1} J_k = 1$, where J_k can be either 1 or -1. As mentioned above, the case where all $J_k = -1$ is excluded since a PR system is not possible for this case.

Even S Since S is even and, furthermore, since J_k can be either 1 or -1, the number of J_k that takes the values -1 has to be even. In other words, there will be 0, or 2, ..., or S values of J_k that take the value -1. That gives us, in total, $(S/2+1)$ combinations. Excluding the case where all J_k are -1, we have a net total of $S/2$ combinations in which $\prod_{k=0}^{S-1} J_k = 1$.

Odd S: Similar to the above even case, the number of J_k that takes the value -1 in this case has to be even. Thus, there will be 0, or 2, ..., or $(S-1)$ values of J_k that take the value -1 and thus, $\Delta_S = (S+1)/2$. Combining both cases, Δ_S is:

$$\Delta_S = \begin{cases} S/2; & \text{even } S, \\ (S+1)/2; & \text{odd } S. \end{cases} \tag{4.21}$$

Calculating Θ_S:

Use the same counting argument as in the Δ_S case where the only difference is that the number of J_k taking the values -1 is odd. Thus,

$$\Theta_S = \begin{cases} S/2; & \text{even } S, \\ (S-1)/2; & \text{odd } S. \end{cases} \tag{4.22}$$

In summary, the total number of LP PR FIR QMF structures is

$$Total = R_1(\Delta_M - \Theta_M) + M\Theta_M, \tag{4.23}$$

where R_1, Δ_M and Θ_M are as in (4.20), (4.21) and (4.22). We have calculated *Total* for several M in Table 4.1. We observe that for $M = 2$, this result agrees with previous work [30]. For this particular subclass, let us summarize all results on the LP PR QMF bank in the following fact.

Fact : For an $M-$channel FIR QMF bank in which all i_k are the same, the total number of combinations of LP PR analysis filter banks is given in (4.23). The polyphase transfer matrix $\mathbf{E}(z)$ satisfies (4.8) or equivalently, (4.9). The lengths of the analysis filters $H_k(z)$, N_k satisfy the condition: $\sum_{k=0}^{M-1} N_k = M(2r + M)$, where r is some positive integer and $N_k - 1 = m_k M + i_k$.

Table 4.1
Number of combinations of LP PR systems for the case where all i_k are the same

M	2	3	4	5	6	7
Total	2	3	8	15	18	21

From the above discussions, it is clear that there are several possible combinations of analysis filters that yield LP PR FIR QMF banks. In order to develop a design procedure for such systems, we shall adopt the same strategy as in some of our previous work [7,19]. This strategy is to construct a lattice structure for the analysis bank such that the properties of interest are *structurally enforced.* In other words, regardless of the values of the multipliers in the structure, the FIR filter bank would satisfy the LP PR property. If we invent such a structure, we

can optimize the multiplers in the structure to obtain an analysis filter with good stopband attenuations, without sacrificing the LP PR property.

Now, because of the existence of several possible combinations of analysis filters giving rise to the LP PR property, it is not possible to find a single general lattice structure that covers all of these cases. Our main purpose in the next section is to demonstrate that it is indeed possible to obtain lattice structures if we restrict the filter bank to be a subclass of all the possible combinations. To be specific, if we set $I = M - 1$ in the above discussions, it turns out to be easy to obtain such lattice structures.

4.2. Two-channel LP PR FIR QMF Banks.

For a two-channel FIR QMF system, the QMF bank of Fig. 4.1(a) - 4.1(c) is simplified to Fig. 4.2(a) - 4.2(c). Writing the analysis filters $H_k(z)$ in terms of their polyphase components $E_{k,\ell}(z)$, we have

$$\begin{pmatrix} H_0(z) \\ H_1(z) \end{pmatrix} = \mathbf{E}(z^2) \begin{pmatrix} 1 \\ z^{-1} \end{pmatrix}. \tag{4.24}$$

Evidently from Fig, 4.2(c), we can obtain a perfect-reconstruction system if we choose $\mathbf{R}(z) = \mathbf{E}^{-1}(z)$. If the analysis filters are FIR, the choice $\mathbf{R}(z) = \mathbf{E}^{-1}(z)$ gives rise to FIR synthesis filters, provided that $\det \mathbf{E}(z) = bz^{-r}$, where b and r are a nonzero constant and a nonnegative integer, respectively. Our aim is to obtain a structure for the pair of transfer functions $[H_0(z), H_1(z)]$ with overall form as in Fig. 4.3. The structure should have the following features *regardless* of the multiplier values in the structure:

1. $H_0(z)$ and $H_1(z)$ are linear-phase FIR filters.

2. $\det \mathbf{E}(z) = bz^{-r}$.

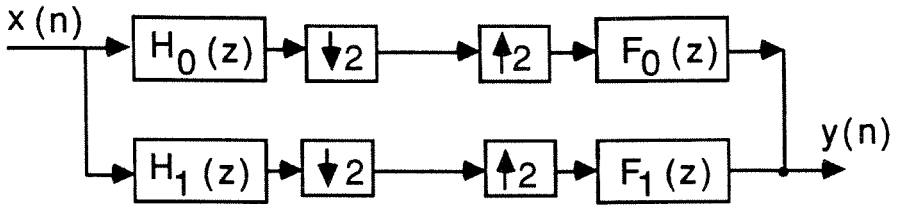

Fig. 4.2(a). The 2-channel QMF bank.

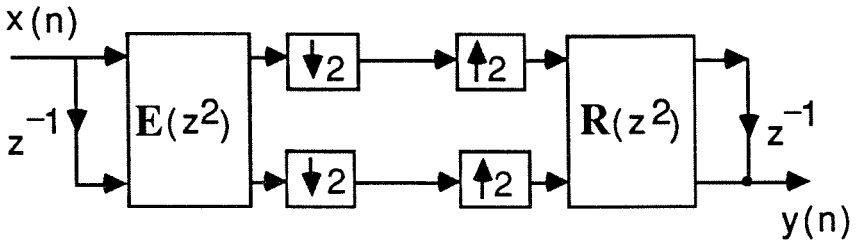

Fig. 4.2(b). An equivalent structure for Fig. 4.2(a).

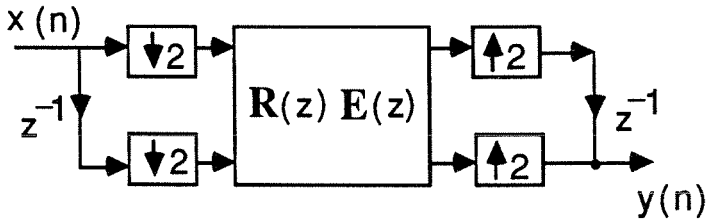

Fig. 4.2(c). A redrawing of Fig. 4.2(b).

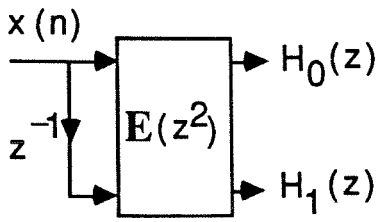

Fig. 4.3. Pertaining to the discussion of a perfect-reconstruction pair.

Such a structure will be called a linear-phase perfect-reconstruction structure, and such a pair $[H_0(z), H_1(z)]$ will be called a perfect-reconstruction pair. Most of the two-channel QMF designs satisfy the power-complementary property (i.e., $|H_0(e^{j\omega})|^2 + |H_1(e^{j\omega})|^2 = 1$) either approximately, as in [2], [26], or exactly as in perfect-reconstruction systems [6], [7], [18], [19]. This condition, however, is *not necessary* for perfect reconstruction [20], [30]. In fact, if we constrain $H_0(z)$ and $H_1(z)$ to be linear-phase filters, it will be necessary to give up the power-complementary property [31]. All the QMF analysis filter designs in this subsection (two-channel) have linear-phase and perfect-reconstruction property, accomplished by relaxing the power-complementary requirement.

As discussed in the above section, there are two PR FIR QMF structures that yield linear-phase analysis filters. We showed in [30] that these two choices are the only ones that yield nontrivial LP PR FIR analysis filters. These choices are:

1. $i_0 = i_1 = I = 1$. Here, the orders of $H_0(z)$ and $H_1(z)$ are odd since $N_k - 1 = 2m_k + 1$. Furthermore, from (4.11), $\mathbf{P} = \begin{pmatrix} 0 & 1 \\ 1 & 0 \end{pmatrix}$. Thus, $J_0 = J_1 = -1$ or in other words, the two analysis filters $H_0(z)$ and $H_1(z)$ have opposite symmetry. We will denote this case by "Type A."

2. $i_0 = i_1 = I = 0$. Opposite the above case, the orders of $H_k(z)$ are now even. Based on (4.15b) and the fact that $I = 0$, we have $\mathbf{P} = \begin{pmatrix} 1 & 0 \\ 0 & 1 \end{pmatrix}$ and therefore $J_0 J_1 = 1$. Thus, the two analysis filters are both symmetric. (The case where $J_0 = J_1 = -1$ is of no interest to us since perfect reconstruction is not possible.) We denote this case by "Type B."

Furthermore, the lengths of $H_0(z)$ and $H_1(z)$ satisfy $N_0 + N_1 = 4r$, where r is a

positive integer. We will now elaborate on the structures and implementations of Type A and Type B in Sections 4.2.1 and 4.2.2, respectively. Accompanying the design in each subsection is the comparison between the new proposed structures and the corresponding conventional ones. Examples are given to verify the theory.

Let us now discuss the properties of the synthesis filters of a two-channel FIR PR system. From Fig. 4.2(c), with $\mathbf{R}(z) = \mathbf{E}^{-1}(z)$, we have

$$\begin{bmatrix} F_0(z) \\ F_1(z) \end{bmatrix} = [\mathbf{E}^{-1}(z^2)]^T \begin{bmatrix} z^{-1} \\ 1 \end{bmatrix}.$$

Since $\det \mathbf{E}(z) = bz^{-r}$, the above equation becomes

$$\begin{bmatrix} F_0(z) \\ F_1(z) \end{bmatrix} = \frac{1}{bz^{-2r}} \begin{bmatrix} 0 & -1 \\ 1 & 0 \end{bmatrix} \mathbf{E}(z^2) \begin{bmatrix} 1 \\ -z^{-1} \end{bmatrix}. \tag{4.25}$$

Simplifying the above expression, we have

$$\begin{bmatrix} F_0(z) \\ F_1(z) \end{bmatrix} = \frac{z^{2r}}{b} \begin{bmatrix} -H_1(-z) \\ H_0(-z) \end{bmatrix}. \tag{4.26}$$

Note that the above relation (4.26) between the synthesis and analysis filters holds regardless of the phase responses of $H_k(z)$. Moreover, if the analysis filters have linear phase, then so do the synthesis filters. The noncausal factor z^{2r} can be dropped in practice.

4.2.1. *Analysis filters and lattice structures for Type A systems.*

Recall that the word "Type A" implies that $[H_0(z), H_1(z)]$ is a linear-phase FIR SAOO pair, and that $\det \mathbf{E}(z)$ is a delay. Our aim here is to obtain FIR lattice structures for the pair $[H_0(z), H_1(z)]$ such that it is guaranteed to be Type A. We shall first propose a structure, and then prove that (almost) any Type A pair can be realized by the structure, so that the structure is a general tool for optimal design of such pairs of filters. (The parenthetical adverb "almost" is elaborated towards

the end of this section.) The basic ingredient of the proof will be to show that such a pair can be systematically synthesized in the proposed structural form. In the following discussions, the synthesis procedures are primarily *tools* for such proofs.

Without loss of generality, we assume that $H_0(z)$ and $H_1(z)$ are symmetric and antisymmetric, respectively. Their lengths, N_0 and N_1, are both even. We start with a structure closely related to the well-known linear prediction lattice [21], [23] shown in Fig. 4.4 (for the moment let us ignore the last section $\begin{bmatrix} 1 & 1 \\ 1 & -1 \end{bmatrix}$). Traditionally, in the linear prediction lattice, the coefficients k_m, which are real-valued, are constrained to be $k_m^2 < 1$. This constraint is a necessary and sufficient condition for the FIR transfer function $T_N(z)$ to have minimum-phase (i.e., all N zeros strictly are inside the unit circle). The FIR function $U_N(z)$ is automatically constrained by the structure to be such that $U_N(z) = z^{-N}T_N(z^{-1}) = \hat{T}_N(z)$. Thus, $[T_N(z), U_N(z)]$ is an MIP (which stands for mirror-image pair), and $U_N(z)$ is a maximum-phase FIR filter.

If we permit k_m to be arbitrary real numbers (i.e., not constrained to be $k_m^2 < 1$), then $U_N(z)$ and $T_N(z)$ are still related as $U_N(z) = \hat{T}_N(z)$, but $U_N(z)$ can now have arbitrary phase response. Caution should, however, be exercised concerning the possibility of $k_m^2 = 1$, which leads to "singularities" as elaborated a few paragraphs later. We shall now exploit the fundamental features of this structure (unconstrained k_m, with $k_m^2 \neq 1$) to obtain Type A pairs eventually.

Given the pair $[H_0(z), H_1(z)]$, the idea is to generate the MIP $[T_N(z), U_N(z)]$, which can be synthesized in the form of a lattice. If $H_0(z)$ and $H_1(z)$ have the same lengths, $(N_0 = N_1)$ the MIP can be generated as

$$\begin{bmatrix} T_N(z) \\ U_N(z) \end{bmatrix} = \frac{1}{2}\begin{bmatrix} 1 & 1 \\ 1 & -1 \end{bmatrix}\begin{bmatrix} H_0(z) \\ H_1(z) \end{bmatrix}. \tag{4.27}$$

If, on the other hand, we have $N_0 < N_1$, the centers of symmetries of $H_0(z)$ and $H_1(z)$ should first be aligned. The MIP is then generated as

$$\begin{bmatrix} T_N(z) \\ U_N(z) \end{bmatrix} = \frac{1}{2} \begin{bmatrix} 1 & 1 \\ 1 & -1 \end{bmatrix} \begin{bmatrix} z^{-(\frac{N_1-N_0}{2})} H_0(z) \\ H_1(z) \end{bmatrix}. \tag{4.28}$$

The inverse relation is evidently

$$\begin{bmatrix} z^{-(\frac{N_1-N_0}{2})} H_0(z) \\ H_1(z) \end{bmatrix} = \begin{bmatrix} 1 & 1 \\ 1 & -1 \end{bmatrix} \begin{bmatrix} T_N(z) \\ U_N(z) \end{bmatrix},$$

which is represented in Fig. 4.4. The purpose of the delay $z^{-(N_1-N_0)/2}$ is to align the centers of symmetry of both $H_0(z)$ and $H_1(z)$. For arbitrary choices of $H_0(z)$ and $H_1(z)$, the filters $T_N(z)$ and $U_N(z)$ obtained from (4.28) no longer have minimum phase and maximum phase. However, by permitting unconstrained real values for k_m, one can still realize the pair $[T_N(z), U_N(z)]$ by using the structure of Fig. 4.4.

To comprehend the nature of the synthesis problem at hand, we shall for a moment relax the perfect-reconstruction constraint. Thus, let $[T_N(z), U_N(z)]$ be any MIP of order N. The procedure to synthesize a lattice of the form in Fig. 4.4 can be understood by referring to Fig. 4.5(a), which shows the m^{th} section of Fig. 4.4. Since the polynomials $T_m(z)$ and $U_m(z)$ are given as

$$\begin{bmatrix} T_m(z) \\ U_m(z) \end{bmatrix} = \begin{bmatrix} 1 & k_m \\ k_m & 1 \end{bmatrix} \begin{bmatrix} T_{m-1}(z) \\ z^{-1} U_{m-1}(z) \end{bmatrix}, \tag{4.29}$$

we can invert the relation to obtain

$$\begin{bmatrix} T_{m-1}(z) \\ z^{-1} U_{m-1}(z) \end{bmatrix} = \frac{1}{1-k_m^2} \begin{bmatrix} 1 & -k_m \\ -k_m & 1 \end{bmatrix} \begin{bmatrix} T_m(z) \\ U_m(z) \end{bmatrix}, \tag{4.30}$$

provided that $k_m^2 \neq 1$. Thus, given the MIP $[T_N(z), U_N(z)]$, we can iteratively compute the lower-order pairs $[T_k(z), U_k(z)]$, $k = N-1, N-2, \ldots$ by repeated application of (4.30), resulting in the structure of Fig. 4.4. The quantity k_m, which results in a reduced-order pair $[T_{m-1}(z), U_{m-1}(z)]$, is given by $k_m = t_{m,m}/t_{m,0}$, where

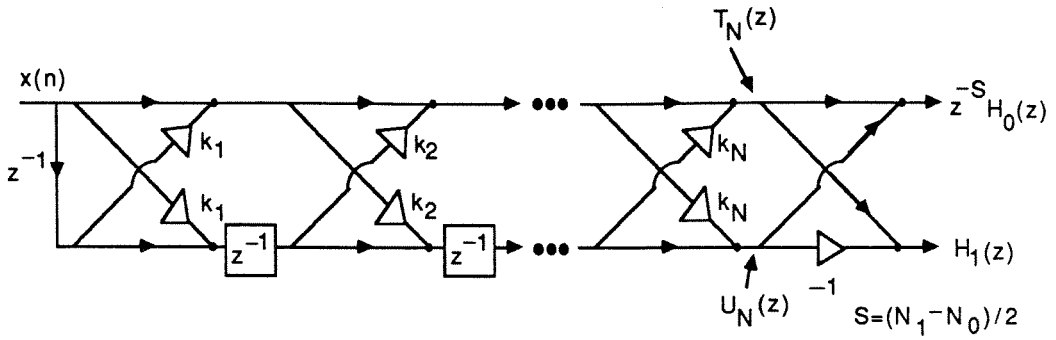

Fig. 4.4. The 2x2 LPC lattice structure and its resulting SA LP pair $[H_0(z), H_1(z)]$.

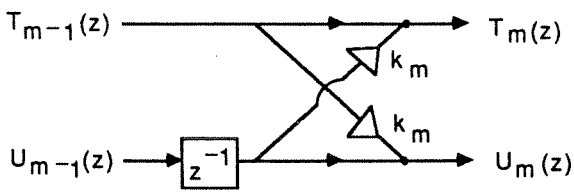

Fig. 4.5(a). Type I building block.

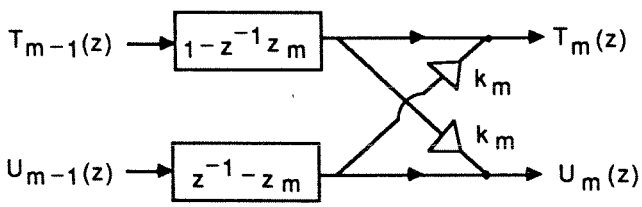

Fig. 4.5(b). Type II building block for the SAOO or SAEE LP FIR lattice structure.

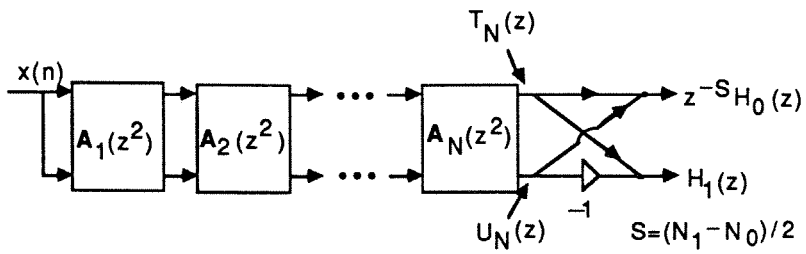

Fig. 4.5(c). The SAOO or SAEE LP FIR lattice structure.

$t_{m,i}$ is the i^{th} coefficient of the impulse response of $T_m(z)$; i.e., $T_m(z) = \sum_{i=0}^{m} t_{m,i} z^{-i}$. It can be verified that $[T_{m-1}(z), U_{m-1}(z)]$ is an MIP (assuming, of course, that $[T_m(z), U_m(z)]$ is an MIP). This procedure is the familiar "downward recursion" in Levinson's algorithm [21], [23], [24] with the exception that k_m is now arbitrary (rather than constrained to be $k_m^2 < 1$ as in Levinson's algorithm).

Now, the above procedure works for any MIP $[T_N(z), U_N(z)]$, provided that $k_m^2 \neq 1$ at any stage. If $k_m^2 = 1$ for some m, the 2×2 matrices in (4.29), (4.30) are singular. The meaning of this *singularity situation* is discussed further in Appendix 4.A. In what follows, we shall outline a method to overcome singularity situations.

The iteration in (4.29) is not the only means of constructing a lower-order MIP $[T_{m-1}(z),\ U_{m-1}(z)]$ from an MIP $[T_m(z),\ U_m(z)]$. A more general procedure would be to define

$$T_{m-1}(z) = \frac{1}{1-k_m^2}\left(\frac{1}{1-z^{-1}z_m}\right)[T_m(z) - k_m U_m(z)] \tag{4.31a}$$

and

$$U_{m-1}(z) = \frac{1}{1-k_m^2}\left(\frac{1}{z^{-1}-z_m}\right)[-k_m T_m(z) + U_m(z)], \tag{4.31b}$$

which works as follows: z_m is an arbitrary real number. The parameter k_m is chosen to be

$$k_m = \frac{T_m(z_m)}{U_m(z_m)}, \tag{4.32}$$

so that $T_m(z) - k_m U_m(z)$ has a zero at $z = z_m$, canceling the denominator $1 - z^{-1}z_m$ in (4.31a). Since $[T_m(z), U_m(z)]$ is MIP, the factor $(z^{-1} - z_m)$ is canceled off in (4.31b) by the same choice of k_m. Furthermore, since the pair $[1 - z^{-1}z_m, z^{-1} - z_m]$ is MIP, the pair $[T_{m-1}(z), U_{m-1}(z)]$ is guaranteed to be a reduced-order FIR MIP!

The purpose of the number z_m is to avoid the possibility of k_m^2's being unity.

Since $T_m(z) \pm U_m(z)$ is a finite-degree polynomial, it has only m zeros so that there is guaranteed to exist z_m such that $T_m(z_m) + U_m(z_m) \neq 0$, $T_m(z_m) - U_m(z_m) \neq 0$, and $U_m(z_m) \neq 0$. Except for this restriction, z_m is entirely arbitrary. In order to find a z_m that works, it is only necessary to try out at most $3m$ values, say, $z_m = k$, $k = 0, 1, \ldots, 3m-1$. In Appendix 4.B it is shown that such a z_m is guaranteed to exist as long as there is no common factor between $T_N(z)$ and $U_N(z)$. (It is also shown in Appendix 4.C that such a common factor cannot exist if $[H_0(z), H_1(z)]$ is a PR pair). Fig. 4.5(b) shows the structural interpretation of the new order-reduction scheme. The resulting structure for arbitrary MIP $[T_N(z), U_N(z)]$ is as in Fig. 4.5(c) with building blocks $\mathbf{A}_m(z)$ as in Fig. 4.5(b). It is clear that any arbitrary MIP $[T_N(z), U_N(z)]$ can be represented in this form and that for arbitrary k_m, z_m ($k_m^2 \neq 1$), the structure gives rise to only MIP $[T_N(z), U_N(z)]$. Notice that the traditional structure of Fig. 4.4 is obtained as a special case with $z_m = 0$. Readers familiar with the relation between the linear-prediction IIR lattice and FIR lattice structure [21] will recognize that the relation between Fig. 4.5(b) and the IIR allpass structures in [24, page 483] is similar. For convenience of discussion, the building blocks in Fig. 4.5(a) and 4.5(b) will respectively be called Types I and II. These are equivalent when $z_m = 0$.

The structures for $[H_0(z), H_1(z)]$ proposed in Figs. 4.4, 4.5 and 4.6 are not in the form of Fig. 4.3, and this gap should now be bridged. First consider Fig. 4.3. It is clear that we can represent $[H_0(z), H_1(z)]$ as

$$\begin{bmatrix} H_0(z) \\ H_1(z) \end{bmatrix} = \mathbf{G}(z) \begin{bmatrix} 1 \\ z^{-1} \end{bmatrix}, \tag{4.33}$$

where $\mathbf{G}(z)$ is a 2×2 FIR transfer matrix with $\det \mathbf{G}(z) =$ delay. However, since this is not in the form (4.24) (i.e., $\mathbf{G}(z)$ is not equal to $\mathbf{E}(z^2)$), we cannot conclude that $\det \mathbf{E}(z) =$ delay. Thus, it is *not true* that all $[H_0(z), H_1(z)]$ pairs represented

by Fig. 4.4 lead to FIR perfect reconstruction analysis banks. If we impose the stipulation that $k_m = 0$ for even m in Fig. 4.4, then $\mathbf{G}(z) = \mathbf{E}(z^2)$, and $\det \mathbf{E}(z)$ is indeed a delay. What is *more* important, however, is the following stronger result:

Lemma 4.1: Let $[H_0(z), H_1(z)]$ be a Type A pair such that we can synthesize it in the form of Fig. 4.4, such that $k_m \neq \pm 1$ for any m. Then the even-numbered coefficients k_{2m} automatically turn out to be zero, if $\det \mathbf{E}(z)$ is a delay.

Proof: The proof is inductive. Suppose that we are given an m^{th} order MIP $[T_m(z), U_m(z)]$, which at the same time is a PR pair; i.e.,

$$\begin{bmatrix} T_m(z) \\ U_m(z) \end{bmatrix} = \mathbf{E}_m(z^2) \begin{bmatrix} 1 \\ z^{-1} \end{bmatrix}, \quad \text{with} \quad \det \mathbf{E}_m(z) = cz^{-r}. \tag{4.34a}$$

The coefficient of the z^0 power in $\det \mathbf{E}_m(z)$ is $(t_{m,0}t_{m,m-1} - t_{m,1}t_{m,m})$, which should be 0. This condition together with $k_m = t_{m,m}/t_{m,0}$ yields

$$k_m = \frac{t_{m,m}}{t_{m,0}} = \frac{t_{m,m-1}}{t_{m,1}}. \tag{4.34b}$$

Substituting (4.34b) in (4.30), we obtain $t_{m-1,m-1} = u_{m-1,0} = 0$. Thus, an order reduction by two is automatically enforced, so that

$$\begin{bmatrix} T_{m-2}(z) \\ z^{-2}U_{m-2}(z) \end{bmatrix} = \frac{1}{(1-k_m^2)} \begin{bmatrix} 1 & -k_m \\ -k_m & 1 \end{bmatrix} \begin{bmatrix} T_m(z) \\ U_m(z) \end{bmatrix}. \tag{4.35}$$

By combining (4.35) and (4.34a) we also see that $[T_{m-2}(z), U_{m-2}(z)]$ is an MIP PR pair. So if we start with an MIP PR pair $[T_N(z), U_N(z)]$ and repeat the above order reduction process, we see that $k_m = 0$ for even m and Fig. 4.7 reduces to a PR structure as shown in Fig. 4.8. QED

Since we restrict z_m to be zero in Lemma 4.1, it therefore does not cover all Type A pairs of filters. The pairs of filters which the structure of Fig. 4.8 excludes are essentially the ones which, during the synthesis process, yield internal transfer

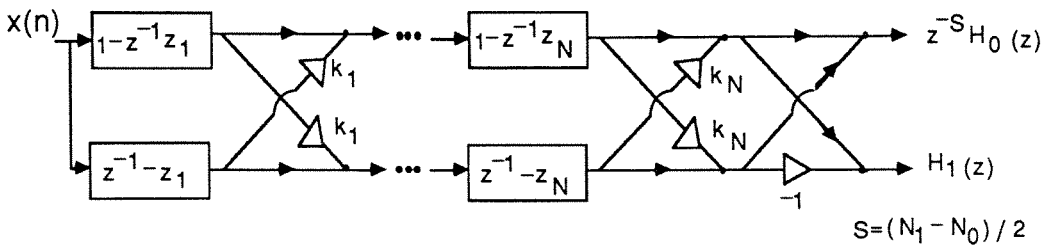

Fig. 4.6. The SAOO or SAEE LP FIR lattice structure.

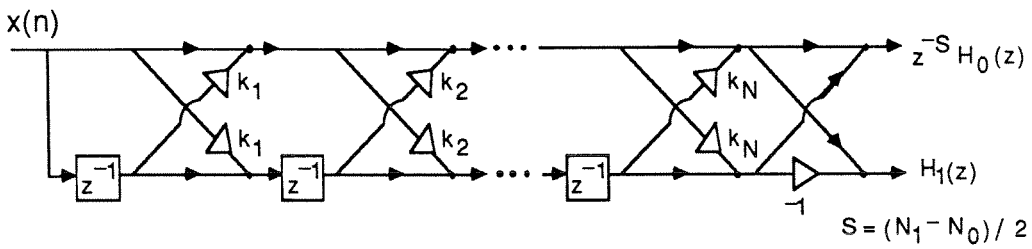

Fig. 4.7. A redrawing of Fig. 4.6 with $z_{m=0}$.

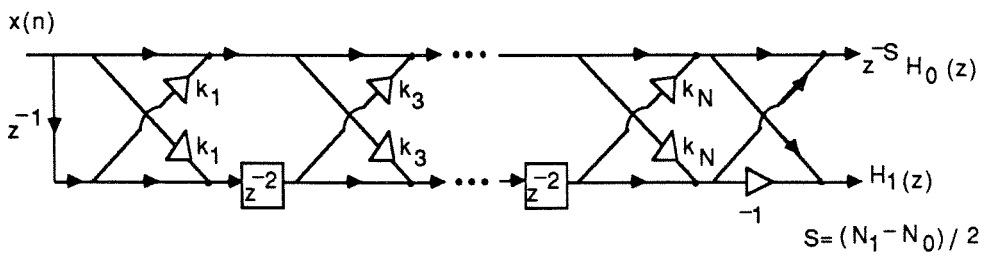

Fig. 4.8. The lattice structure for Type A system. N is odd.

function pairs (the $[T_m(z), U_m(z)]$ pairs) such that $t_{m,0} = \pm t_{m,m}$, forcing $k_m = \pm 1$. Suppose that the optimal filter happens to be one of these excluded filters. Then in practice, we can still always get as close to it as possible by using the structure of Fig. 4.8. Thus, these excluded filters are not expected to result in serious loss of generality.

A result similar to Lemma 4.1 does not hold for the structure with the generalized building blocks shown in Fig. 4.6. Even if such a result were true, the quantity $\mathbf{E}^{-1}(z)$ that arises in the synthesis bank would contain the inverses of these building blocks. These inverse building blocks would contain the two factors $1/(1 - z^{-1}z_m)$ and $1/(z^{-1} - z_m)$ at least one of which is necessarily unstable (i.e., synthesis filters are IIR and unstable) for any choice of z_m. This observation excludes the consideration of Fig. 4.6 for the rest of this section.

Example 4.1: In the optimization procedure, we additionally use two scale factors β_1 and β_2 at the end of the structure in Fig. 4.8. The objective function to be minimized is

$$\Phi = \int_0^{\omega_p} \left[1 - |H_0(e^{j\omega})|\right]^2 d\omega + \int_{\omega_S}^{\pi} \left[H_0(e^{j\omega})\right]^2 d\omega + \int_{\omega_S}^{\pi} \left[1 - |H_1(e^{j\omega})|\right]^2 d\omega + \int_0^{\omega_p} \left[H_1(e^{j\omega})\right]^2 d\omega. \tag{4.36}$$

A mathematical optimization subroutine [10] is used to search for an optimal solution. In order to initialize the lattice coefficients, we use the tabulated linear-phase filters designed earlier by Johnston [32], [2, page 401]. For our example, the filter 64D was used for $H_0(z)$, and $H_1(z)$ was taken to be $H_0(-z)$. With this "initial pair", the lattice of Fig. 4.4 was synthesized. Since the filters obtained from [2, page 401] give only an approximation to a PR pair, the even-numbered coefficients k_{2m} do not turn out to be zero. These were forced to be zero during initialization,

and the odd-numbered coefficients reoptimized, using [10]. The frequency responses of these reoptimized filters are shown in Fig. 4.9(a). The number of lattice sections in the example is equal to 32 and the transition bandwidth is $\Delta f = 0.086$. Notice that these filters form an exact PR pair and retain the PR property in spite of quantization of the coefficients k_m to any desired level. The synthesis filters $F_0(z)$ and $F_1(z)$ can be obtained by using (4.26). Table 4.2 displays the lattice coefficients k_{2m+1}, and the impulse responses of both analysis filters. Table 4.2 displays only the first half of the coefficients of $H_0(z)$ and $H_1(z)$, since the impulse responses are symmetric and antisymmetric, respectively.

It is interesting to compare the above perfect-reconstruction design with Johnston's 64D filter in [2, page 401] (to be referred to as the 64D filter in the following discussion). Both designs have linear phase and filter lengths equal to 64. The PR pair has a minimum stopband attenuation of about 42 dB and a reconstruction error equal to zero. On the other hand, the 64D filter has a better minimum stopband attenuation of about 65 dB, but a nonzero reconstruction error (defined in [2]) of about 0.002 dB. Both designs have about the same transition bandwidth, viz., $\Delta f = 0.086$. The tradeoff is therefore very clear. For comparison, the frequency responses of the 64D-analysis filters are shown in Fig. 4.9(b), and the impulse response coefficients in Table 4.3. Notice that the significantly large coefficients in the 64D filter agree closely with those in the PR pair. The 64D filters satisfy the relation $H_1(z) = H_0(-z)$, whereas the PR pair does not. It can, in fact, be shown that with $H_1(z) = H_0(-z)$, it is impossible to force $\det \mathbf{E}(z)$ to be an exact delay unless $H_0(z)$ is a trivial function (See Appendix 4.D). Notice, finally, that some of the trailing coefficients in the PR pair (Table 4.2) are very small (compared to the ones in Table 4.3). These can be replaced with "zero" without significant effect on

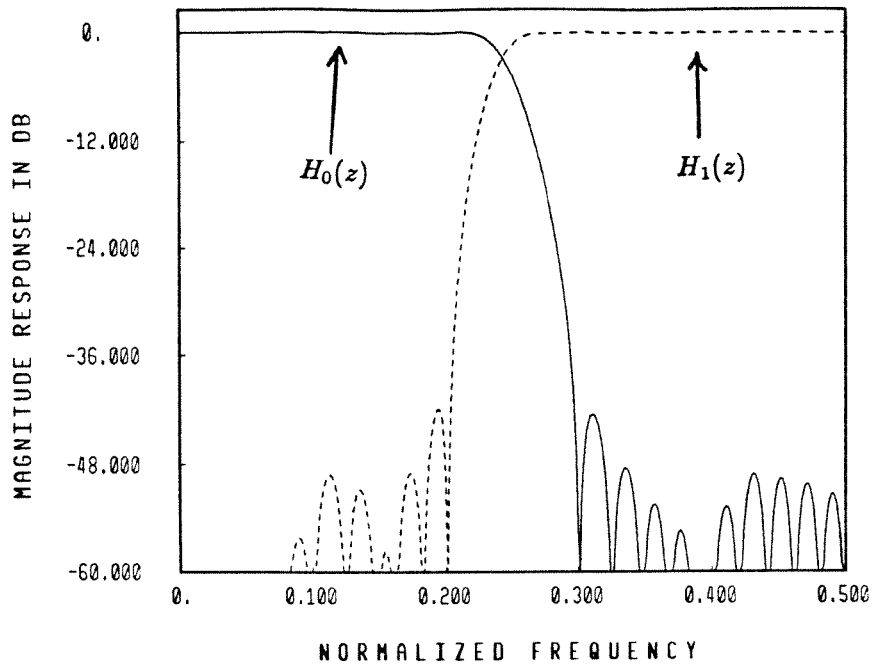

Fig. 4.9a. Ex. 4.1. Magnitude response plots for the optimized analysis filters. Each filter has length =64.

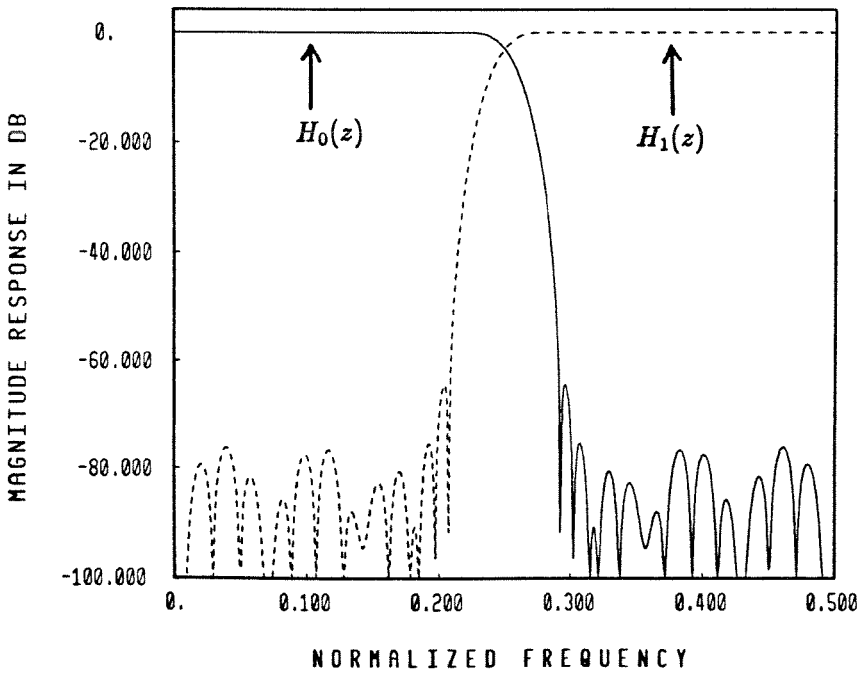

Fig. 4.9b. Ex. 4.1. Magnitude response plots for the $64D$ analysis filters. Each filter has length =64.

Table 4.2
Lattice coefficients and impulse responses of the optimized analysis filters in Ex. 4.1. (SAOO) $\beta_1 = 9.3367072622762 \times 10^{-10}$, $\beta_2 = 8.6458769493813 \times 10^{-10}$.

m	Lattice Coeff. k_{2m+1}	Filter Coefficients $h_{0,m}$	Filter Coefficients $h_{1,m}$
0	−0.16748024178056	$-2.8047649315578 \times 10^{-8}$	$2.7701557075405 \times 10^{-8}$
1	−0.98630142049519	$4.6974270887493 \times 10^{-9}$	$-4.6394634766867 \times 10^{-9}$
2	46.797422738757	$-9.0320483808830 \times 10^{-6}$	$8.8828615641826 \times 10^{-6}$
3	1.0155415002447	$1.5395771337727 \times 10^{-6}$	$-1.5142595131503 \times 10^{-6}$
4	−0.98123943672420	$-3.8484265421346 \times 10^{-4}$	$3.6797322378863 \times 10^{-4}$
5	71.799272118326	$7.3072834050915 \times 10^{-5}$	$-7.0105005042002 \times 10^{-5}$
6	0.99604836163496	$-5.4844133513744 \times 10^{-4}$	$3.3979745779936 \times 10^{-5}$
7	73.293136853215	$4.4822758623806 \times 10^{-4}$	$-3.4610132423983 \times 10^{-4}$
8	−0.32992582104225	$-3.1420371203276 \times 10^{-4}$	$-2.9314605847016 \times 10^{-6}$
9	−0.58756852009572	$6.0057015567620 \times 10^{-5}$	$4.6300165292477 \times 10^{-4}$
10	0.68608642287498	$9.0093326906975 \times 10^{-4}$	$-9.6019269511046 \times 10^{-4}$
11	−6.8758613928422	$1.6949632352623 \times 10^{-4}$	$-5.3867082067374 \times 10^{-4}$
12	−1.0899663381059	$-1.7113555648237 \times 10^{-3}$	$2.6665204377661 \times 10^{-3}$
13	0.70138304837561	$-8.8586614964934 \times 10^{-4}$	$1.3763566255439 \times 10^{-3}$
14	1.9359402130086	$2.1821453210951 \times 10^{-3}$	$-3.9203746653654 \times 10^{-3}$
15	32.412571811713	$1.8133626090971 \times 10^{-3}$	$-3.2204697559136 \times 10^{-3}$
16	−2.2762581355052	$-2.5292916536995 \times 10^{-3}$	$5.2062396452593 \times 10^{-3}$
17	−1.0546765432115	$-4.1596794940782 \times 10^{-3}$	$6.1298978924939 \times 10^{-3}$
18	−14.637818055814	$3.5887675000538 \times 10^{-3}$	$-6.2739942846780 \times 10^{-3}$
19	0.91309339992145	$7.6713479773340 \times 10^{-3}$	$-1.0972495757049 \times 10^{-2}$
20	0.20497603236147	$-5.7266129912836 \times 10^{-3}$	$6.2975034654359 \times 10^{-3}$
21	−8.7549576287234	$-1.2745794143760 \times 10^{-2}$	$1.8004225149880 \times 10^{-2}$
22	−34.634777587712	$9.5185739377873 \times 10^{-3}$	$-4.2379770697116 \times 10^{-3}$
23	0.84932894911060	$2.0342217498768 \times 10^{-2}$	$-2.7168914395689 \times 10^{-2}$
24	−2.7082137206053	$-1.6072095730447 \times 10^{-2}$	$-1.0169910794786 \times 10^{-3}$
25	−1.0358588647791	$-3.1588256584766 \times 10^{-2}$	$3.9969783616942 \times 10^{-2}$
26	11.636158464610	$2.7807655367843 \times 10^{-2}$	$1.2025400363970 \times 10^{-2}$
27	1.2034512561861	$5.0150998969974 \times 10^{-2}$	$-6.0718905144588 \times 10^{-2}$
28	−0.20699149394524	$-5.2720604380285 \times 10^{-2}$	$-3.6911412178463 \times 10^{-2}$
29	−0.19132416529613	$-9.3506916444599 \times 10^{-2}$	$1.0590613371084 \times 10^{-1}$
30	0.68112439023728	$1.4064635171445 \times 10^{-1}$	$1.2541814981813 \times 10^{-1}$
31	−31.040193536859	$4.5677057793319 \times 10^{-1}$	$-4.7085951885497 \times 10^{-1}$

Table 4.3
Impulse responses of the Johnston's 64D filters in Ex. 4.1.

m	Coefficients $h_{0,m}$	Coefficients $h_{1,m}$
0	3.596189×10^{-5}	3.596189×10^{-5}
1	-1.123515×10^{-4}	1.123515×10^{-4}
2	-1.104587×10^{-4}	-1.104587×10^{-4}
3	2.790277×10^{-4}	-2.790277×10^{-4}
4	2.298438×10^{-4}	$2.298438 \times 10-4$
5	-5.953563×10^{-4}	5.953563×10^{-4}
6	-3.823631×10^{-4}	-3.823631×10^{-4}
7	1.138260×10^{-3}	-1.138260×10^{-3}
8	5.308539×10^{-4}	5.308539×10^{-4}
9	-1.986177×10^{-3}	1.986177×10^{-3}
10	-6.243724×10^{-4}	-6.243724×10^{-4}
11	3.235877×10^{-3}	-3.235877×10^{-3}
12	5.743159×10^{-4}	5.743159×10^{-4}
13	-4.948147×10^{-3}	4.948147×10^{-3}
14	-2.583767×10^{-4}	-2.583767×10^{-4}
15	7.367171×10^{-3}	-7.367171×10^{-3}
16	-4.857935×10^{-4}	-4.857935×10^{-4}
17	-1.050689×10^{-2}	1.050689×10^{-2}
18	1.894714×10^{-3}	1.894714×10^{-3}
19	1.459396×10^{-2}	-1.459396×10^{-2}
20	-4.313674×10^{-3}	-4.313674×10^{-3}
21	-1.994365×10^{-2}	1.994365×10^{-2}
22	8.287560×10^{-3}	8.287560×10^{-3}
23	2.716055×10^{-2}	-2.716055×10^{-2}
24	-1.485397×10^{-2}	-1.485397×10^{-2}
25	-3.764973×10^{-2}	3.764973×10^{-2}
26	2.644700×10^{-2}	2.644700×10^{-2}
27	5.543245×10^{-2}	-5.543245×10^{-2}
28	-5.095487×10^{-2}	-5.095487×10^{-2}
29	-9.779096×10^{-2}	9.779096×10^{-2}
30	1.382363×10^{-1}	1.382363×10^{-1}
31	4.600981×10^{-1}	-4.600981×10^{-1}

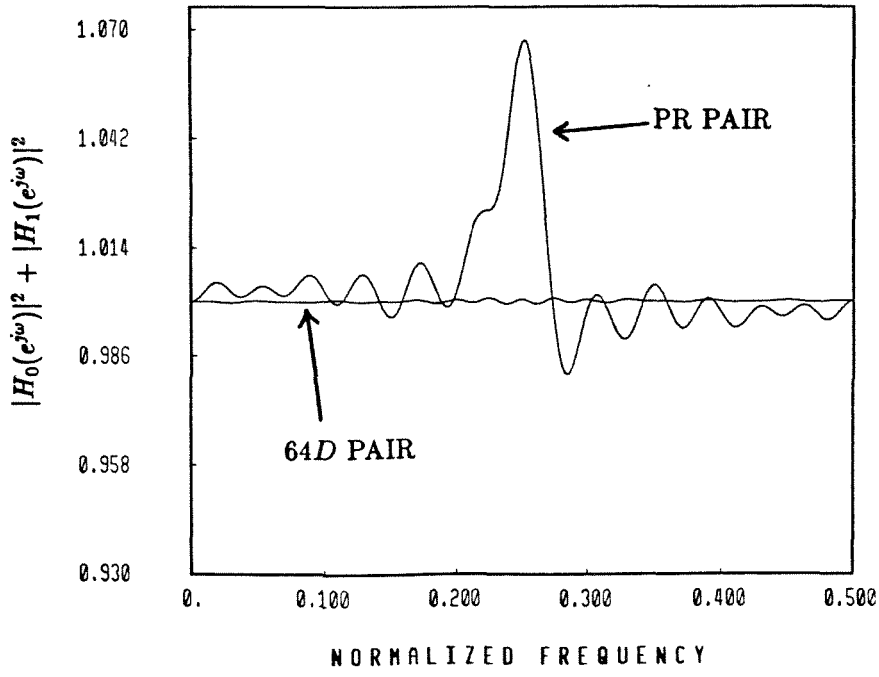

Fig. 4.9c. Ex. 4.1. The plots of $|H_0(e^{j\omega})|^2 + |H_1(e^{j\omega})|^2$ for the $64D$ pair of filters and the new PR pair of filters.

the PR property.

A second major difference between the above PR design and the 64D filter is that the 64D pair $[H_0(z), H_1(z)]$ is approximately power-complementary; i.e., $|H_0(e^{j\omega})|^2 + |H_1(e^{j\omega})|^2 \simeq 1$ (see Fig. 4.9(c)). In fact, the design procedure in [32] is such that $\int_0^\pi \left[1 - |H_0(e^{j\omega})|^2 - |H_1(e^{j\omega})|^2\right]^2 d\omega$ is minimized. On the other hand, the PR pair does *not* satisfy the power-complementary property (see Fig. 4.9(c)). In fact, the main basis of the PR designs introduced in this paper is the fact that PR property can be accomplished exactly for linear-phase filters, by giving up power-complementarity of the pair $[H_0(z), H_1(z)]$ as well as the relation $H_1(z) = H_0(-z)$, which are two restrictions forced in most of the earlier designs [26], [32-34]. After relaxing these two restrictions, we can obtain good PR pairs which in addition have linear phase.

4.2.1.a *Implementation Complexity:*

A further interesting point of comparison between the 64D design and our PR design is the number of multiplication and addition operations per unit time (abbreviated MPU and APU, respectively) [4] required to implement the analysis bank. A direct form implementation of the 64D filter pair $[H_0(z), H_1(z)]$ would appear to require $2 \times 64 = 128$ MPU. However, there are three simplifying factors involved, viz., (a) the relation $H_1(z) = H_0(-z)$; (b) the symmetry relation $h_0(n) = h_0(N' - 1 - n)$, where N' is the length of $H_0(z)$ and (c) the decimation by a factor of 2. Only two of these three factors can be simultaneously exploited, because N' is even (see [26] for details). As a result, we require $128/4 = 32$ MPU to implement the 64D pair using a direct form polyphase structure. The number of APUs required is 32.

[4] A unit of time is defined to be the sampling period of the input sequence $x(n)$ in Fig. 4.1(a).

Now consider the PR pair of length 64 designed above (Table 4.2 and Fig. 4.9(a)), implemented in lattice form of Fig. 4.8. There are 32 lattice sections in the structure. Each lattice section can be implemented efficiently using only one multiplication and three addition operations (see [27] and [28]). Second, both the decimators can be moved to the left of all the building blocks in Fig. 4.8 (which are functions of z^2) by replacing z^{-2} with z^{-1} in these building blocks (see [2] or use the identity (a) in Fig. 11 of [29]). With such rearrangement, each lattice building block operates at the lower rate, and so the total number of MPUs is equal to $(32+2)/2 = 17$. The number of APUs required can be similarly verified to be 49. In conclusion, for the same filter length, the PR pair requires only 17 MPU and 49 APU, whereas the 64D pair requires 32 MPU and 32 APU.

The significant features of the above comparison are summarized in Table 4.4. As a final observation, suppose we consider Johnston's 32D pair in [2]. This filter has the same number of MPU and nearly the same attenuation as the PR pair under discussion, and in addition has a reconstruction error = 0.025 dB [2]. In other words, the 32D pair and the above PR pair have nearly the same cost (assuming that the multiplication time significantly dominates addition time) and the same performance, except for the reconstruction error. The only price paid for perfect reconstruction appears to be the overall group delay of the QMF bank, which is 63 for the PR pair, and 31 for the $32D$ pair.

The structure in Fig. 4.8 can be partly generalized for the case where M is an even integer. We discuss this briefly in Appendix 4.E.

Table 4.4
Comparison between Johnston's 64D filters and the new PR filters.

Feature	Johnston's 64D Pair of Filters	The new PR Pair of Filters
Phase Response	Linear	Linear
Filter Length	64	64
Stopband Attenuation	65 dB	42.5 dB
Reconstruction Error	0.002dB	No error
Number of MPU for Analysis Bank Implementation	32	17
Number of APU for Analysis Bank Implementation	32	49
Power Complementarity	Approximately holds	Does not hold
Relation between Analysis Filters	$H_1(z) = H_0(-z)$	Not explicit. Implicitly such that $\det \mathbf{E}(z) =$ delay
Overall Group Delay of QMF bank	63	63

4.2.2. *Analysis filters and lattice structures for Type B systems.*

Recall that for a Type B pair, the FIR filters $H_0(z)$ and $H_1(z)$ have even orders and symmetric impulse responses, and the determinant of $\mathbf{E}(z)$ is a delay. Let $[H_0(z), H_1(z)]$ be a Type B pair with orders N_0-1 and N_1-1, respectively. Without loss of generality, assume that $N_1 \geq N_0$. As we have shown from Section 4.1; i.e., (4.15), the lengths of these filters satisfy the condition

$$N_0 + N_1 = 4r_1, \qquad r_1 = \text{nonnegative integer}, \tag{4.37}$$

which we call the "length condition." Based on the fact that both N_0 and N_1 are odd, it can be shown that the only choice for N_0 and N_1, which satisfies (4.37), is:

$$N_1 = N_0 + 4L + 2, \qquad L = \text{nonnegative integer.} \tag{4.38}$$

In other words, the lengths of any Type B pair of filters have to obey both (4.37) and (4.38), simultaneously.

We would like to find a structure that covers all Type B pairs of filters $[H_0(z), H_1(z)]$. We accomplish this by showing that every such pair can be synthesized as a cascaded lattice. The building blocks of the lattice will be such that the Type B property propagates down the structure. Consider Fig. 4.10(a) where the pair $[P_r(z), Q_m(z)]$ is a Type B pair with orders $r = (m - 4\ell - 2)$ and m, respectively, with even m. Let $P_r(z) = \sum_{j=0}^{m-4\ell-2} p_{r,j} z^{-j}$ and $Q_m(z) = \sum_{j=0}^{m} q_{m,j} z^{-j}$. We shall assume that

$$p_{r,0} = q_{m,0} \neq 0, \tag{4.39}$$

which will be justified soon. Since m is even, the order of $[P_r(z), Q_m(z)]$ satisfies the length condition.

For convenience, let us express the pair $[P_r(z), Q_m(z)]$ in polyphase form; i.e.,

$$\begin{bmatrix} P_r(z) \\ Q_m(z) \end{bmatrix} = \begin{bmatrix} P_{r,0}(z^2) & P_{r,1}(z^2) \\ Q_{m,0}(z^2) & Q_{m,1}(z^2) \end{bmatrix} \begin{bmatrix} 1 \\ z^{-1} \end{bmatrix} = \mathbf{E}_m(z^2) \begin{bmatrix} 1 \\ z^{-1} \end{bmatrix}. \tag{4.40}$$

The elements of $\mathbf{E}_m(z)$ have orders given by

$$Order[\mathbf{E}_m(z)] = \begin{bmatrix} \frac{m}{2} - 2\ell - 1 & \frac{m}{2} - 2\ell - 2 \\ \frac{m}{2} & \frac{m}{2} - 1 \end{bmatrix}. \tag{4.41}$$

The determinant $P_{r,0}(z)Q_{m,1}(z) - P_{r,1}(z)Q_{m,0}(z)$ is a linear-phase polynomial (because $P_r(z)$ and $Q_m(z)$ are linear-phase polynomials of even order). Since this determinant is *also* equal to a delay, the following equation holds:

$$P_{r,0}(z)Q_{m,1}(z) - P_{r,1}(z)Q_{m,0}(z) = z^{-(\frac{m}{2} - \ell - 1)}. \tag{4.42}$$

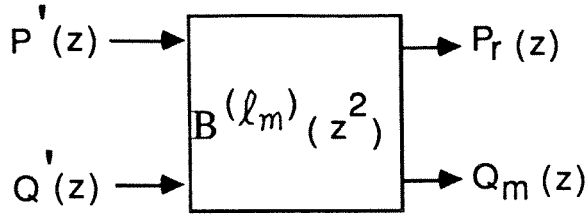

Fig. 4.10(a). Pertaining to the downward recursion of Type B system.

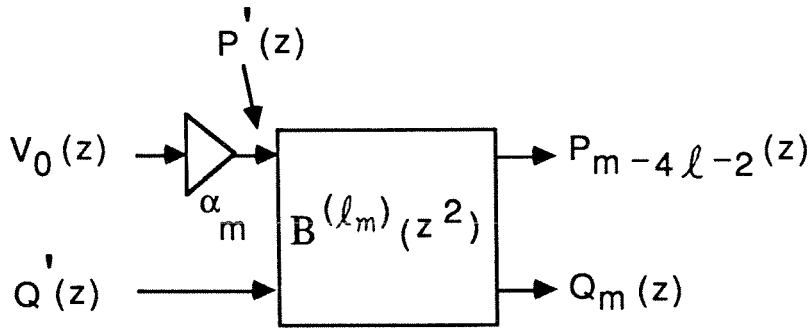

Fig. 4.10(b). The building block for Type B system where $p'_0 \neq 0$ and $q'_0 \neq 0$.

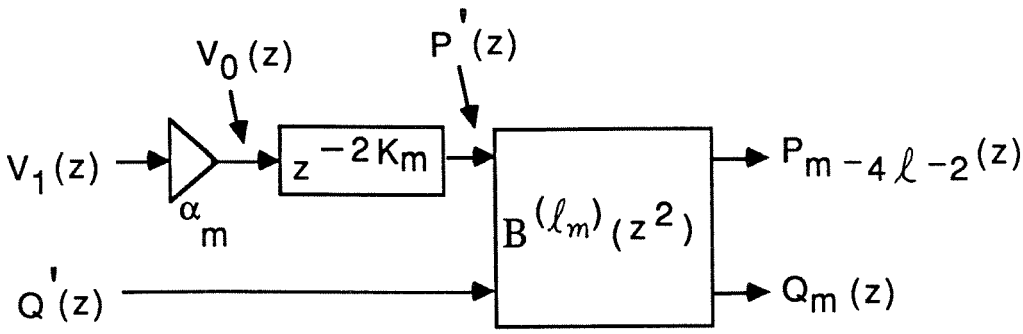

Fig. 4.10(c). The building block for Type B system.

Our aim is to use (4.42) to extract the building block $\mathbf{B}^{(\ell_m)}(z^2)$ in Fig. 4.10(a) such that the *remainder* pair $[P'(z), Q'(z)]$ is also a Type B pair with orders $(m-4\ell-4)$ and $(m-4\ell-2)$, respectively. Since both pairs $[P_r(z), Q_m(z)]$ and $[P'(z), Q'(z)]$ are PR pairs, the building block should be a function of z^2, which justifies the notation $\mathbf{B}^{(\ell_m)}(z^2)$. Furthermore, the determinant of $\mathbf{B}^{(\ell_m)}(z^2)$ is required to be a delay, in view of the PR property.

Denoting the elements of $\mathbf{B}^{(\ell_m)}(z)$ by $B_{i,j}^{(\ell_m)}(z)$, Fig. 4.10(a) yields

$$\begin{bmatrix} P_r(z) \\ Q_m(z) \end{bmatrix} = \begin{bmatrix} B_{0,0}^{(\ell_m)}(z^2) & B_{0,1}^{(\ell_m)}(z^2) \\ B_{1,0}^{(\ell_m)}(z^2) & B_{1,1}^{(\ell_m)}(z^2) \end{bmatrix} \begin{bmatrix} P'(z) \\ Q'(z) \end{bmatrix} \tag{4.43}$$

$$= \begin{bmatrix} B_{0,0}^{(\ell_m)}(z^2)P'(z) + B_{0,1}^{(\ell_m)}(z^2)Q'(z) \\ B_{1,0}^{(\ell_m)}(z^2)P'(z) + B_{1,1}^{(\ell_m)}(z^2)Q'(z) \end{bmatrix}. \tag{4.44}$$

The orders of the components in (4.43) are related as

$$\begin{bmatrix} m-4\ell-2 \\ m \end{bmatrix} = \begin{bmatrix} Order[B_{0,0}^{(\ell_m)}(z^2)] & Order[B_{0,1}^{(\ell_m)}(z^2)] \\ Order[B_{1,0}^{(\ell_m)}(z^2)] & Order[B_{1,1}^{(\ell_m)}(z^2)] \end{bmatrix} \begin{bmatrix} m-4\ell-4 \\ m-4\ell-2 \end{bmatrix}. \tag{4.45}$$

Both pairs $[P_r(z), Q_m(z)]$ and $[P'(z), Q'(z)]$ are symmetric polynomials; therefore, it can be shown that $B_{i,j}^{(\ell_m)}(z^2)$ also have to be symmetric polynomials. Moreover, from the first equation of (4.44), in order to yield a symmetric polynomial in the left-hand side, $B_{0,0}^{(\ell_m)}(z^2)P'(z)$ and $B_{0,1}^{(\ell_m)}(z^2)Q'(z)$ have to have the same orders so that the centers of symmetry align. Thus, from (4.45), $Order[B_{0,0}^{(\ell_m)}(z^2)] = 2$ and $Order[B_{0,1}^{(\ell_m)}(z^2)] = 0$. Similarly, by considering the second equation of (4.44), $Order[B_{1,0}^{(\ell_m)}(z^2)] = (4\ell+4)$ and $Order[B_{1,1}^{(\ell_m)}(z^2)] = (4\ell+2)$. In summary, to obtain a symmetric pair $[P'(z), Q'(z)]$ with orders $(m-4\ell-4)$ and $(m-4\ell-2)$ from a symmetric pair $[P_r(z), Q_m(z)]$ with orders $(m-4\ell-2)$ and m, all the elements of the building block $\mathbf{B}^{(\ell_m)}(z^2)$ are symmetric polynomials and moreover, the orders of the elements can be summarized as

$$Order[\mathbf{B}^{(\ell_m)}(z^2)] = \begin{bmatrix} 2 & 0 \\ 4\ell+4 & 4\ell+2 \end{bmatrix}. \tag{4.46}$$

We now propose a particular form for $\mathbf{B}^{(\ell_m)}(z^2)$ and through the "downward recursion" on the pair $[P_r(z), Q_m(z)]$ show that this particular form of $\mathbf{B}^{(\ell_m)}(z^2)$ is indeed sufficient to cover all Type B pairs. The proposed form is

$$\mathbf{B}^{(\ell_m)}(z) = \begin{bmatrix} 1+z^{-1} & 1 \\ T(z) & U(z) \end{bmatrix}, \tag{4.47}$$

where $T(z)$ and $U(z)$ are symmetric polynomials of orders $(2\ell+2)$ and $(2\ell+1)$, respectively; i.e., $T(z) = \sum_{j=0}^{2\ell+2} t_j z^{-j}$ and $U(z) = \sum_{j=0}^{2\ell+1} u_j z^{-j}$. We assume that $t_0 = u_0 = 1$ (see justification later). From (4.47), the condition "$\det \mathbf{B}^{(\ell_m)}(z) =$ a delay" is equivalent to

$$(1+z^{-1})U(z) - T(z) = cz^{-(\ell+1)}. \tag{4.48}$$

Equating the like powers of z in (4.48), we obtain

$$\begin{cases} t_0 = u_0, \\ t_k = u_{k-1} + u_k, & 1 \le k \le \ell. \\ c = 2u_\ell - t_{\ell+1} \neq 0. \end{cases} \tag{4.49}$$

Thus, any choices of u_k and t_k that satisfy (4.49) guarantee that $\det \mathbf{B}^{(\ell_m)}(z) = cz^{-(\ell+1)}$. In the synthesis procedure, we show how to find $u_k, 1 \le k \le \ell$ such that the orders of $[P'(z), Q'(z)]$ are $(m-4\ell-4)$ and $(m-4\ell-2)$. Then $\det \mathbf{B}^{(\ell_m)}(z)$ is forced to be a delay by choosing t_k as in (4.49), and the synthesis procedure is completed. Noticing from (4.49) that $t_{\ell+1}$ is arbitrary, we assume that it is chosen such that $c \neq 0$. From Fig. 4.10(a) we then have

$$\begin{bmatrix} P'(z) \\ Q'(z) \end{bmatrix} = \frac{z^{2(\ell+1)}}{c} \begin{bmatrix} U(z^2) & -1 \\ -T(z^2) & 1+z^{-2} \end{bmatrix} \begin{bmatrix} P_r(z) \\ Q_m(z) \end{bmatrix}. \tag{4.50}$$

Since we are interested in obtaining causal filters $P'(z), Q'(z)$, we should choose $U(z)$ such that

$$U(z^2)P_r(z) - Q_m(z) = z^{-2(\ell+1)}\alpha_0(z) \tag{4.51}$$

and

$$-T(z^2)P_r(z) + (1+z^{-2})Q_m(z) = z^{-2(\ell+1)}\alpha_1(z) \tag{4.52}$$

for some causal FIR $\alpha_0(z), \alpha_1(z)$. Now, forcing the condition (4.51) automatically guarantees (4.52) because (4.51) implies

$$(1+z^{-2})U(z^2)P_r(z) - (1+z^{-2})Q_m(z) = z^{-2(\ell+1)}(1+z^{-2})\alpha_0(z),$$

which, in view of (4.48), simplifies to the form (4.52). It therefore remains only to satisfy (4.51). For convenience, write $P_r(z)$ and $Q_m(z)$ in the polyphase forms $P_r(z) = P_{r,0}(z^2) + z^{-1}P_{r,1}(z^2)$ and $Q_m(z) = Q_{m,0}(z^2) + z^{-1}Q_{m,1}(z^2)$, respectively. Then (4.51) breaks into two equations:

$$U(z)P_{r,0}(z) - Q_{m,0}(z) = z^{-(\ell+1)}\beta_0(z) \tag{4.53}$$

$$U(z)P_{r,1}(z) - Q_{m,1}(z) = z^{-(\ell+1)}\beta_1(z) \tag{4.54}$$

for some causal FIR $\beta_0(z), \beta_1(z)$. We now show that (4.53) implies (4.54) automatically, because of the constraint (4.42). For this, note that $m - 4\ell - 2$ is the degree of $P_r(z)$ so that $\frac{m}{2} - 2\ell - 1 > 0$, which implies $\frac{m}{2} - \ell - 1 \geq \ell + 1$. As a result, (4.42) implies in particular

$$P_{r,0}(z)Q_{m,1}(z) - P_{r,1}(z)Q_{m,0}(z) = z^{-(\ell+1)}\delta_0(z) \tag{4.55}$$

for some causal FIR $\delta_0(z)$. Multiplying both sides of (4.53) by $P_{r,1}(z)$ and substituting (4.55) results in

$$U(z)P_{r,0}(z)P_{r,1}(z) - P_{r,0}(z)Q_{m,1}(z) = z^{-(\ell+1)}\delta_1(z) \tag{4.56}$$

for some causal FIR $\delta_1(z)$. Since $p_{r,0} \neq 0$ by assumption, (4.56) implies (4.54), proving that (4.53) implies (4.54).

Summarizing, we can ensure that we obtain a causal reduced-degree a Type B pair $[P'(z), Q'(z)]$ in Fig. 4.10(a) simply by satisfying (4.53)! The condition (4.53) can be satisfied by choosing the coefficients $u_n, 1 \leq n \leq \ell$ of $U(z)$ such

that $U(z)P_{r,0}(z) = Q_{m,0}(z) + z^{-(\ell+1)}\beta_0(z)$. This can be written as a triangular set of equations

$$\begin{bmatrix} p_{r,0} & 0 & \cdots & 0 \\ p_{r,2} & p_{r,0} & \cdots & 0 \\ \vdots & \vdots & \ddots & \vdots \\ p_{r,2\ell} & p_{r,2\ell-2} & \cdots & p_{r,0} \end{bmatrix} \begin{bmatrix} 1 \\ u_1 \\ \vdots \\ u_\ell \end{bmatrix} = \begin{bmatrix} q_{m,0} \\ q_{m,2} \\ \vdots \\ q_{m,2\ell} \end{bmatrix}. \tag{4.57}$$

The first equation above is automatically satisfied because of (4.39). The remaining equations can be satisfied by solving for a unique set $u_1, \ldots u_\ell$ because $p_{r,0} \neq 0$ in (4.57).

In summary, we first find $U(z)$ satisfying (4.57) and then find $T(z)$ using (4.49). Consequently, $\mathbf{B}^{(\ell_m)}(z)$ is determined. To be able to apply the same synthesis procedure on the Type B pair $[P'(z), Q'(z)]$, its coefficients have to satisfy a condition analogous to (4.39). Denoting the coefficients of $P'(z)$ and $Q'(z)$ by p'_j and q'_j, this condition is satisfied by a scale factor α_m if $p'_0 \neq 0$ and $q'_0 \neq 0$. The complete building block for the case where $p'_0 \neq 0$ and $q'_0 \neq 0$ is shown in Fig. 4.10(b). Clearly, (4.39) cannot be satisfied by just a scale factor if $p'_0 = 0$ or $q'_0 = 0$. We now elaborate on the remedy for this case (i.e., the case where $p'_0 = 0$ or $q'_0 = 0$).

The remedy is to choose the extra freedom $t_{\ell+1}$ such that $q'_0 \neq 0$. With $q'_0 \neq 0$, we show now that if $p'_0 = 0$, then we can always pull out a delay of the specific form z^{-2K_m} (as demonstrated in Fig. 4.10(c)) such that the first coefficient of $V_0(z)$ is nonzero. (Having done so, the pair $[V_1(z), Q'(z)]$ is a causal Type B pair. We can therefore repeat the above order reduction process.) For this, represent the pair $P'(z)$ and $Q'(z)$ in polyphase form:

$$\begin{bmatrix} P'(z) \\ Q'(z) \end{bmatrix} = \begin{bmatrix} P'_0(z^2) & P'_1(z^2) \\ Q'_0(z^2) & Q'_1(z^2) \end{bmatrix} \begin{bmatrix} 1 \\ z^{-1} \end{bmatrix} = \mathbf{E}'(z^2) \begin{bmatrix} 1 \\ z^{-1} \end{bmatrix}. \tag{4.58a}$$

We know that the determinant of $\mathbf{E}'(z)$ is a delay, by our above construction of the

pair $[P'(z), Q'(z)]$. Thus,

$$P'_0(z)Q'_1(z) - P'_1(z)Q'_0(z) = z^{-(\frac{m}{2}-2\ell-2)}. \tag{4.58b}$$

If, for some reason, we have $p'_0 = 0$, then $P'_0(z)Q'_1(z)$ has the form $z^{-1}\alpha(z)$, where $\alpha(z)$ is some causal FIR system. Because of (4.58b) this implies that $P'_1(z)Q'_0(z)$ has this form as well. Since $q'_0 \neq 0$, this necessarily implies $p'_1 = 0$. In other words, $p'_0 = 0$ implies $p'_1 = 0$ as well. More generally, it is easily verified based on this type of argument that if $p'_n = 0$ for $0 \leq n \leq K$ with $p'_{K+1} \neq 0$, then K is odd. This means we can factorize $P'(z)$ as $P'(z) = z^{-2K_m}V_0(z)$.

With this, Fig. 4.10(a) becomes Fig. 4.10(c), where the pair $[V_0(z), Q'(z)]$ now satisfies $v_{0,0} \neq 0, q'_0 \neq 0$. We now insert a scale factor α_m as shown in Fig. 4.10(c) such that the pair $[V_1(z), Q'(z)]$ in Fig. 4.10(c) is a Type B pair with orders $(m-4\ell-4-4K_m)$ and $(m-4\ell-2)$, respectively. Moreover, it satisfies $v_{1,0} = q'_0 \neq 0$, which is analogous to (4.39). Consequently, the order reduction process can now be repeated to obtain a Type B structure as shown in Fig. 4.11, where $\mathbf{A}_j(z^2)$ is shown in Fig. 4.10(c). Note that Fig. 4.10(b) is the same as Fig. 4.10(c) when $K_m = 0$.

The only remaining question to be answered is whether or not we can choose $t_{\ell+1}$ such that $q'_0 \neq 0$ (and $c \neq 0$). The answer is in the affirmative. From (4.50),

$$q'_0 = q_{m,2\ell+2} + q_{m,2\ell+4} - \sum_{j=0}^{\ell} t_j p_{r,2\ell+2-2j} - t_{\ell+1}p_{r,0}. \tag{4.59}$$

It is clear from the above equation and the assumption $p_{r,0} \neq 0$ that we have to choose $t_{\ell+1}$ such that

$$t_{\ell+1} \neq \frac{1}{p_{r,0}}\left[q_{m,2\ell+2} + q_{m,2\ell+4} - \sum_{j=0}^{\ell} t_j p_{r,2\ell+2-2j}\right]. \tag{4.60}$$

We summarize the synthesis procedure as follows:

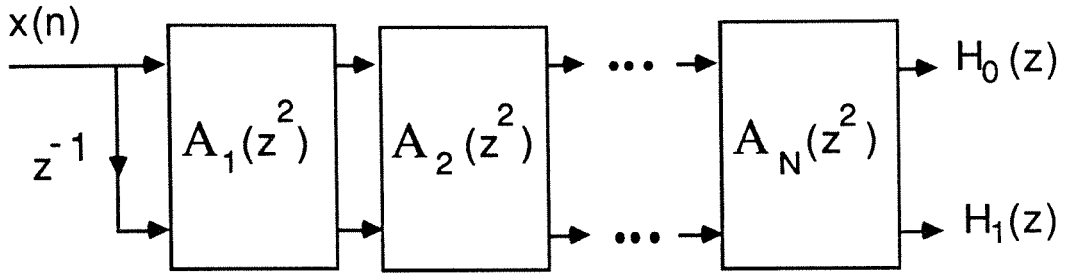

Fig. 4.11. The lattice structure for Type B system.

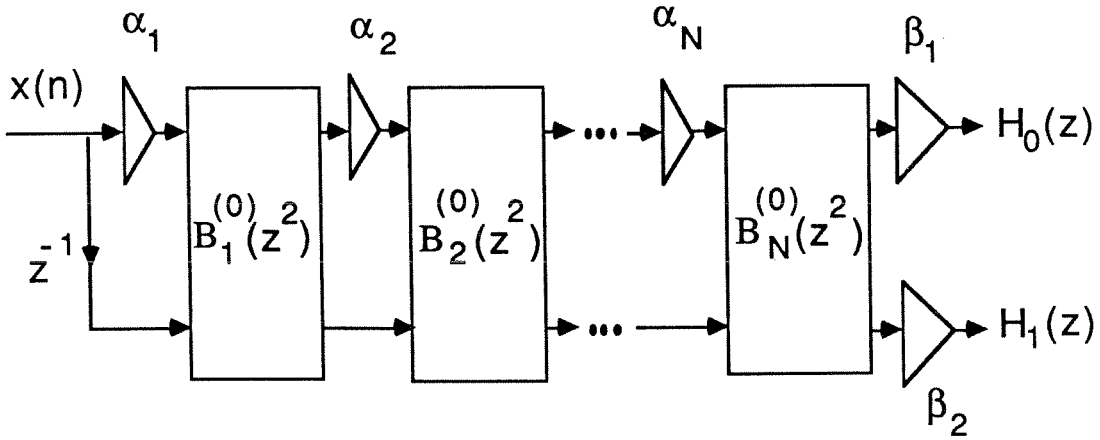

Fig. 4.12. The lattice structure for Type B system used in the optimization procedure. Here $\ell_m=0$ and $K_m=0$.

Given a Type B pair $[P_r(z), Q_m(z)]$ of order $(m - 4\ell - 2)$ and m (where m is even) which satisfies (4.39), do the following:

- Compute $u_n, 0 \leq n \leq \ell$ using (4.57) and t_n using (4.49). Choose the coefficient $t_{\ell+1}$ such that $q'_0 \neq 0$. This determines $\mathbf{B}^{(\ell_m)}(z)$.
- If $p'_0 \neq 0$, then scale the pair $[P'(z), Q'(z)]$ to satisfy $p'_0 = q'_0$. The complete building block is shown in Fig. 4.10(b).
- If $p'_0 = 0$, then pull out the delay z^{-2K_m}, with appropriate K_m. Then scale the pair $[V_0(z), Q'(z)]$ to obtain $[V_1(z), Q'(z)]$, which satisfies $v_{1,0} = q'_0$. The resulting block is shown in Fig. 4.10(c).

Since Fig. 4.10(b) is a special case ($K_m = 0$) of Fig. 4.10(c), therefore the most general building block $\mathbf{A}_j(z)$ of the overall Type B structure (in Fig. 4.11) is as in Fig. 4.10(c).

Example 4.2: The building blocks in Fig. 4.11 have the two added freedoms, namely, ℓ_m and K_m. To simplify the optimization process, we choose $\ell_m = K_m = 0$ for all blocks $\mathbf{A}_j(z)$ in Fig. 4.11. The resulting structure to be used in the optimization procedure is shown in Fig. 4.12, where

$$B_m^{(0)}(z) = \begin{bmatrix} 1 + z^{-1} & 1 \\ 1 + a_m z^{-1} + z^{-2} & 1 + z^{-1} \end{bmatrix}. \tag{4.61}$$

Even though the structure has $2N$ parameters α_m, a_m, $1 \leq m \leq N$, there are only N degrees of freedom. This is evident from the derivation of the structure above. Thus the parameters a_m are precisely the free parameters $t_{\ell+1}$ used in (4.49), and can be chosen arbitrarily. In the design example we fixed the parameters a_m to be equal to 64 and optimized α_m. The choice $a_m = 64$ is, however, entirely arbitrary

and not based on any engineering judgement. At this point in time, we do not have any indication that a particular set of a_m should be preferred to another.

We have $N = 11$, and the transition bandwidth $\Delta f = 0.1$ in the example. The orders of $H_0(z)$ and $H_1(z)$ are thus 22 and 24, respectively. We minimize the objective function described in (4.36) using [10]. The magnitude responses of the optimized analysis filters are shown in Fig. 4.13(a). The lattice coefficients α_m and the impulse responses of both filters are summarized in Table 4.5. The complexity of this structure can be readily computed by noting that there is only one multiplier per building block in Fig. 4.12, namely, α_m ($a_m = 64$ can be realized by shifting). Moreover, each building block can be implemented with 5 addition operations. Thus, with a factor of 2 saving in the decimation ratio, the complexity of the analysis bank is $(N+2)/2 = (11+2)/2 = 6.5$ MPU and $5N/2 = 27.5$ APU.

The fact that we can obtain a linear-phase PR pair, with even orders for the filters and with both filters symmetric, is not entirely surprising. Indeed, procedures for design of QMF banks with linear-phase even-order filters have been presented in [26], which are *approximately* PR. The results we have presented above, however, have exact PR property. It should be noticed that Johnston's filters [2,32] were designed for even-length case, and therefore are not suitable for comparison with the Type B PR system reported in this paper.

4.2.2.a. *Comparison of Type A and Type B systems.*

To compare the two types of PR systems reported in this paper, we design a Type A pair with the same number of sections and transition band as the Type B pair in example 4.2, i.e., $N = 11$ and $\Delta f = 0.1$. The frequency response of this

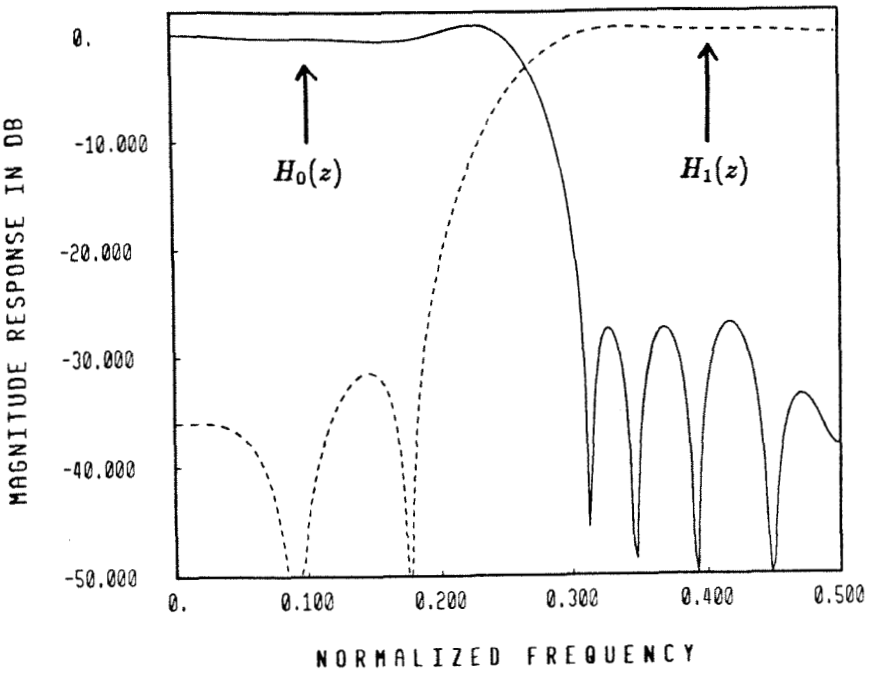

Fig. 4.13a. Ex. 4.2. Magnitude response plots for the optimized analysis filters (Type B). The filter lengths are 23 and 25,respectively.

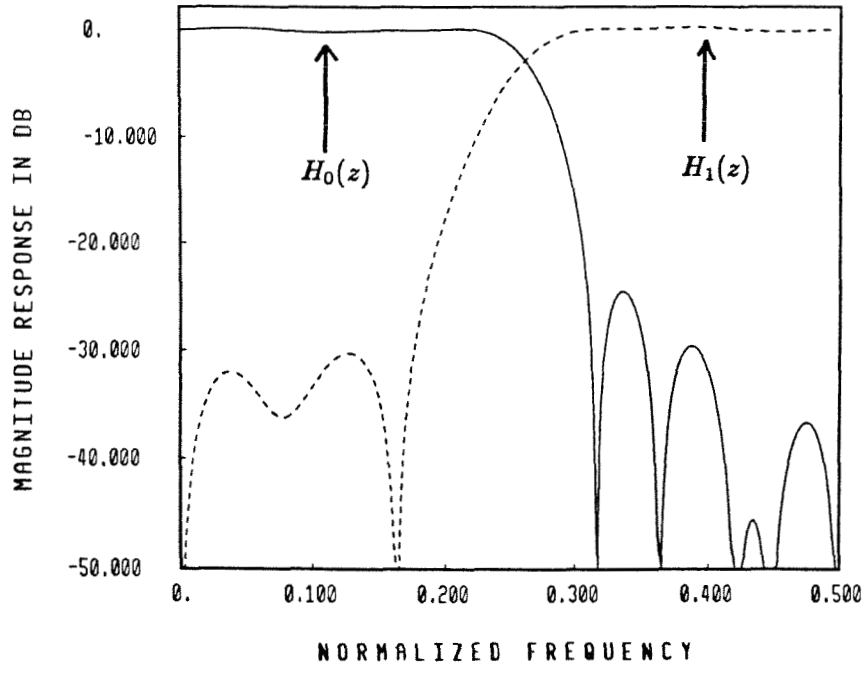

Fig. 4.13b. Ex. 4.2. Magnitude response plots for the optimized analysis filters (Type A). The filter lengths are 22 each.

Type A pair is shown in Fig. 4.13(b). The lengths of the Type A analysis filters are 22. The passband and stopband errors of $H_0(z)$ and $H_1(z)$ for both PR systems are summarized in Table 4.6. The number of MPUs and APUs required for both types are also included in the table. From the table it is evident that both systems have nearly identical filtering performance, and require the same number of MPUs. Type B systems, however, require a larger number of APUs.

Table 4.5
Lattice coefficients and impulse responses of the optimized analysis filters in Ex. 4.2. (SSEE) $\beta_1 = 7.81221 \times 10^{-15}$, $\beta_2 = 1.37742 \times 10^{-18}$.

m	Lattice Coeff. α_{2m+1}	Filter Coefficients $h_{0,m}$	Filter Coefficients $h_{1,m}$
0	−0.37779962858106	$5.9250950404227 \times 10^{-3}$	$1.0446957436687 \times 10^{-6}$
1	28.980740681587	$-1.5683167986894 \times 10^{-2}$	$-2.7652111453693 \times 10^{-6}$
2	−47.817981025871	$4.5594028972112 \times 10^{-3}$	$8.2562648947712 \times 10^{-6}$
3	−26.815036810932	$3.6047559927372 \times 10^{-2}$	$-1.3369902864879 \times 10^{-5}$
4	−1012355.8728888	$-2.2314449066179 \times 10^{-2}$	$-3.7402147190058 \times 10^{-3}$
5	−1.0003784977510	$-4.2444851133377 \times 10^{-2}$	$9.9426163128459 \times 10^{-4}$
6	0.00041704202379460	$4.0981175348012 \times 10^{-2}$	$5.2822531950793 \times 10^{-4}$
7	−164.81675604153	$6.3735691673040 \times 10^{-2}$	$-3.1883222956165 \times 10^{-2}$
8	−7501.9622674952	$-8.7080719666949 \times 10^{-2}$	$-1.1276359972347 \times 10^{-3}$
9	−1.1059836252728	$-6.4640370944037 \times 10^{-2}$	$9.5100122977005 \times 10^{-2}$
10	0.10978902673135	$3.1314592005381 \times 10^{-1}$	$-9.5195769252465 \times 10^{-4}$
11		$5.6912350680866 \times 10^{-1}$	$-3.1042174432319 \times 10^{-1}$
12			$5.0039707172893 \times 10^{-1}$

Table 4.6
Comparison between Type A and Type B PR systems for the design example. Here δ_1 and δ_2 denote the peak-ripple sizes in passband and stopband, respectively. Both types require 6.5 MPUs for the analysis bank. The Type A system requires 17.5 APU, where the Type B system requires 27.5 APUs.

	Type A		Type B	
	$H_0(z)$	$H_1(z)$	$H_0(z)$	$H_1(z)$
Filter length	22	22	23	25
δ_1	2.46×10^{-2}	2.60×10^{-2}	3.27×10^{-2}	3.49×10^{-2}
δ_2	5.92×10^{-2}	3.07×10^{-2}	4.49×10^{-2}	2.67×10^{-2}

The purpose of the next section is to demonstrate that three-channel LP PR FIR QMF banks that yield filters with good attenuation are indeed possible. As indicated in Table 4.1, there are three possible LP PR structures for $M = 3$; let us concentrate on the structure where $I = M - 1 = 2$. Even with this restriction, we shall find in Sec. 4.3 that the analysis filters have very good attenuation characteristics. However, the theoretical development is fairly complicated. We have therefore attempted to make the presentation as complete as possible in order to enable the reader to appreciate the complexity of deriving such a QMF bank. Once such a structure is constructed theoretically, its implementation is, however, not nearly as complicated! This is demonstrated at the end of the next section by a design example, and an explicit complexity count.

4.3. An LP PR FIR QMF Lattice Structure for 3–channel QMF Bank.

From Table 4.1, there are three possibilities here. For one of them, it is easy to see how to decompose $\mathbf{E}(z)$, which satisfies the property $\det \mathbf{E}(z) = bz^{-r}$ under the linear-phase constraint. We shall address only this case, as the other two appeared to be not easily tractable. Here, we discuss the case where $I = M - 1 = 2$ and $H_k(z)$ have the same degrees. Recalling the form for $\mathbf{E}(z)$ in (4.8), which yields LP analysis filters, and simplifying it for this particular case, we have

$$\tilde{E}_{kj}(z) = z^{m_k} J_k E_{k,(2-j)}(z); \quad 0 \le k \le 2. \tag{4.62}$$

From (4.11), $\mathbf{P} = \begin{pmatrix} 0 & 0 & 1 \\ 0 & 1 & 0 \\ 1 & 0 & 0 \end{pmatrix}$ and thus from (4.15b), $\prod_{k=0}^{2} J_k = -1$. Consequently, two analysis filters are symmetric, whereas the remaining one is antisymmetric. Recall that $H_0(z)$ and $H_2(z)$ are lowpass and highpass filters, respectively. $H_0(z)$ thus, cannot be antisymmetric since antisymmetric LP filters have a zero at $\omega = 0$.

Likewise, odd-order symmetric LP filters have a zero at $\omega = \pi$ and therefore, $H_2(z)$ should not be symmetric. Of course, even-order symmetric $H_2(z)$ would also work; however, it would limit our design only to filters of even length. Consequently, the first two filters, $H_0(z)$ and $H_1(z)$ are symmetric, while $H_2(z)$ is antisymmetric. In other words, $J_0 = J_1 = 1$ and $J_2 = -1$. Writing $\mathbf{E}(z)$ from (4.62) results explicitly in

$$\mathbf{E}(z) = \begin{pmatrix} E_{00}(z) & E_{01}(z) & \hat{E}_{00}(z) \\ E_{10}(z) & E_{11}(z) & \hat{E}_{10}(z) \\ E_{20}(z) & E_{21}(z) & -\hat{E}_{20}(z) \end{pmatrix}, \tag{4.63}$$

where $E_{01}(z)$ and $E_{11}(z)$ are symmetric polynomials, whereas $E_{21}(z)$ is an antisymmetric polynomial. The above $\mathbf{E}(z)$ guarantees that the corresponding analysis filters are linear-phase. To impose the PR condition, namely, $\det \mathbf{E}(z) = bz^{-r}$, we decompose $\mathbf{E}(z)$ into lower-order building blocks as follows:

$$\mathbf{E}(z) = \mathbf{E}'(z)\mathbf{A}(z). \tag{4.64}$$

The strategy here is to find $\mathbf{A}(z)$ such that $\mathbf{E}'(z)$ has the same form as $\mathbf{E}(z)$. If we continue to decompose $\mathbf{E}'(z)$ by repeatedly applying (4.64), we will be able to obtain a cascade of building blocks in the form of $\mathbf{E}(z) = \mathbf{B}(z) \prod_{i=0}^{L-1} \mathbf{A}_{L-1-i}(z)$. For clarification, the subscript on $\mathbf{A}$ is added. Here, $\mathbf{B}$ is the first-order block, which has the same form as in (4.63). This decomposition is not a general way to decompose $\mathbf{E}(z)$. In other words, the resulting structure obtained from this decomposition procedure is not guaranteed to cover all triplets of LP PR analysis filters in which $\prod_{k=0}^{2} J_k = -1$ and $I = 2$.

Let the elements of $\mathbf{E}'(z)$ and $\mathbf{A}(z)$ be $E'_{k\ell}(z)$ and $A_{k\ell}(z)$. Then (4.64) yields: (assuming that the orders of $E'_{k\ell}(z)$ are the same and so are the degrees of $A_{k\ell}(z)$)

$$\begin{pmatrix} E_{00}(z) & E_{01}(z) & \hat{E}_{00}(z) \\ E_{10}(z) & E_{11}(z) & \hat{E}_{10}(z) \\ E_{20}(z) & E_{21}(z) & -\hat{E}_{20}(z) \end{pmatrix} = \begin{pmatrix} E'_{00}(z) & E'_{01}(z) & \hat{E}'_{00}(z) \\ E'_{10}(z) & E'_{11}(z) & \hat{E}'_{10}(z) \\ E'_{20}(z) & E'_{21}(z) & -\hat{E}'_{20}(z) \end{pmatrix} \mathbf{A}(z). \tag{4.65}$$

Similarly to $\mathbf{E}(z)$, $E'_{01}(z)$ and $E'_{11}(z)$ are symmetric polynomials, whereas $E'_{21}(z)$ is antisymmetric. We would like to find the conditions on $A_{k\ell}(z)$ such that both $\mathbf{E}(z)$ and $\mathbf{E}'(z)$ have the form as in (4.63). From (4.65), these conditions reflect into the following equations:

$$\begin{cases} E'_{00}(z)(A_{02}(z)-\hat{A}_{20}(z))+E'_{01}(z)(A_{12}(z)-\hat{A}_{10}(z))=\hat{E}'_{00}(z)(\hat{A}_{00}(z)-A_{22}(z)), \\ E'_{10}(z)(A_{02}(z)-\hat{A}_{20}(z))+E'_{11}(z)(A_{12}(z)-\hat{A}_{10}(z))=\hat{E}'_{10}(z)(\hat{A}_{00}(z)-A_{22}(z)), \\ E'_{20}(z)(A_{02}(z)-\hat{A}_{20}(z))+E'_{21}(z)(A_{12}(z)-\hat{A}_{10}(z))=-\hat{E}'_{20}(z)(\hat{A}_{00}(z)-A_{22}(z)), \\ E'_{00}(z)(A_{01}(z)-\hat{A}_{21}(z))+E'_{01}(z)(A_{11}(z)-\hat{A}_{11}(z))=\hat{E}'_{00}(z)(\hat{A}_{01}(z)-A_{21}(z)), \\ E'_{10}(z)(A_{01}(z)-\hat{A}_{21}(z))+E'_{11}(z)(A_{11}(z)-\hat{A}_{11}(z))=\hat{E}'_{10}(z)(\hat{A}_{01}(z)-A_{21}(z)), \\ E'_{20}(z)(A_{01}(z)-\hat{A}_{21}(z))+E'_{21}(z)(A_{11}(z)-\hat{A}_{11}(z))=-\hat{E}'_{20}(z)(\hat{A}_{01}(z)-A_{21}(z)). \end{cases} \tag{4.66}$$

We wish to choose $A_{ij}(z)$ such that the above equations hold for any $\mathbf{E}'(z)$ of the form as in (4.63). In particular, let $E'_{01}(z)=1$ and $E'_{00}(z)=0$. From the first and the fourth equations in (4.66), we have $A_{12}(z)=\hat{A}_{10}(z)$, $A_{11}(z)=\hat{A}_{11}(z)$. Using these relations, Eq. (4.66) is reduced to

$$\begin{cases} E'_{00}(z)(A_{02}(z)-\hat{A}_{20}(z))=\hat{E}'_{00}(z)(\hat{A}_{00}(z)-A_{22}(z)), \\ E'_{10}(z)(A_{02}(z)-\hat{A}_{20}(z))=\hat{E}'_{10}(z)(\hat{A}_{00}(z)-A_{22}(z)), \\ E'_{20}(z)(A_{02}(z)-\hat{A}_{20}(z))=-\hat{E}'_{20}(z)(\hat{A}_{00}(z)-A_{22}(z)), \\ E'_{00}(z)(A_{01}(z)-\hat{A}_{21}(z))=\hat{E}'_{00}(z)(\hat{A}_{01}(z)-A_{21}(z)), \\ E'_{10}(z)(A_{01}(z)-\hat{A}_{21}(z))=\hat{E}'_{10}(z)(\hat{A}_{01}(z)-A_{21}(z)), \\ E'_{20}(z)(A_{01}(z)-\hat{A}_{21}(z))=-\hat{E}'_{20}(z)(\hat{A}_{01}(z)-A_{21}(z)). \end{cases}$$

To find the corresponding relations of the remaining $A_{ij}(z)$, let $E'_{00}(z)=E'_{20}(z)=1$. This choice of $\mathbf{E}'(z)$ will yield $A_{20}(z)=\hat{A}_{02}(z)$, $A_{22}(z)=\hat{A}_{00}(z)$ and $A_{21}(z)=\hat{A}_{01}(z)$. In summary, $A_{ij}(z)$ has to satisfy the following conditions if (4.66) holds for all choice of $\mathbf{E}'(z)$ of the form as in (4.63).

$$\begin{cases} A_{20}(z)=\hat{A}_{02}(z), & A_{12}(z)=\hat{A}_{10}(z), & A_{22}(z)=\hat{A}_{00}(z), \\ A_{21}(z)=\hat{A}_{01}(z), & A_{11}(z)=\hat{A}_{11}(z). \end{cases} \tag{4.67}$$

$\mathbf{A}(z)$ then takes the form

$$\mathbf{A}(z)=\begin{pmatrix} A_{00}(z) & A_{01}(z) & \hat{A}_{20}(z) \\ A_{10}(z) & A_{11}(z) & \hat{A}_{10}(z) \\ A_{20}(z) & \hat{A}_{01}(z) & \hat{A}_{00}(z) \end{pmatrix}, \tag{4.68}$$

where $A_{11}(z)$ is symmetric. Continuing the decomposition process and putting subscript on $\mathbf{A}(z)$, we see that $\mathbf{E}(z)$ is realized as a cascade of lower order building blocks, i.e.,

$$\mathbf{E}(z) = \mathbf{B}(z) \prod_{i=0}^{L-1} \mathbf{A}_{L-1-i}(z) \tag{4.69}$$

where L is the number of $\mathbf{A}_i(z)$ blocks in the structure. The analysis bank in Fig. 4.1(b) thus becomes Fig. 4.14 where $\mathbf{A}_i(z)$ is as in (4.68) and $\mathbf{B}(z)$ has the same form as in (4.63). We now can impose the PR condition $\det \mathbf{E}(z) = z^{-r}$ on each building block so that the overall structure is a PR system.

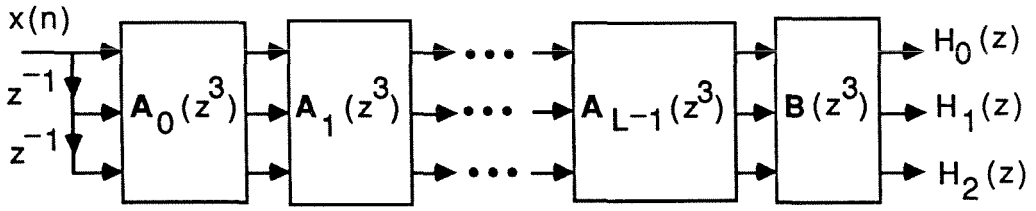

Fig. 4.14. Decomposition of $\mathbf{E}(z^3)$ into a cascade of building blocks.

The simplest $\mathbf{B}(z)$ which satisfies simultaneously (4.63) and $\det \mathbf{B}(z) = z^{-r}$ is

$$\mathbf{B} = \begin{pmatrix} 1 & 0 & 1 \\ 0 & 1 & 0 \\ 1 & 0 & -1 \end{pmatrix}. \tag{4.70}$$

Since the above choice for $\mathbf{B}(z)$ is a constant matrix, $\mathbf{A}_i(z)$ must be a function of z. Consider the following form for $\mathbf{A}_i(z)$:

$$\mathbf{A}_i(z) = \mathbf{U}_i \Lambda(z) \mathbf{V}_i \tag{4.71}$$

where $\mathbf{U}_i$ and $\mathbf{V}_i$ are nonsingular matrices and

$$\Lambda(z) = \begin{pmatrix} 1 & 0 & 0 \\ 0 & z^{-1} & 0 \\ 0 & 0 & z^{-2} \end{pmatrix}. \tag{4.72}$$

Clearly, $\det \Lambda(z) = z^{-3}$. To satisfy the form in (4.68) for $\mathbf{A}(z)$, $\mathbf{U}_i$ and $\mathbf{V}_i$ have to take special forms. From (4.68),

$$\mathbf{A}_i(z) = \Gamma_3 \hat{\mathbf{A}}_i(z) \Gamma_3, \tag{4.73}$$

where Γ_3 is defined in (4.12). Substituting (4.71) into (4.73), $\mathbf{U}_i$ and $\mathbf{V}_i$ satisfy

$$\begin{cases} \mathbf{U}_i = \Gamma_3 \mathbf{U}_i \Gamma_3, \\ \mathbf{V}_i = \Gamma_3 \mathbf{V}_i \Gamma_3. \end{cases} \tag{4.74}$$

In other words, both $\mathbf{U}_i$ and $\mathbf{V}_i$ have the form

$$\mathbf{U}_i = \mathbf{V}_i = \begin{pmatrix} 1 & a_i & b_i \\ c_i & d_i & c_i \\ b_i & a_i & 1 \end{pmatrix}. \tag{4.75}$$

With the above $\mathbf{A}_i(z)$ and $\mathbf{B}$, $\mathbf{E}(z)$ becomes

$$\mathbf{E}(z) = \mathbf{B}\mathbf{U}_{L-1}\Lambda(z)\mathbf{V}_{L-1}\mathbf{U}_{L-2}\Lambda(z)\mathbf{V}_{L-2}\ldots\mathbf{U}_0\Lambda(z)\mathbf{V}_0. \tag{4.76}$$

Observing from (4.75), $\mathbf{V}_i\mathbf{U}_j$ satisfies $\mathbf{V}_i\mathbf{U}_j = \Gamma_3\mathbf{V}_i\mathbf{U}_j\Gamma_3$ and has the same form as $\mathbf{U}_i$ in addition to being a nonsingular matrix. Therefore, we can use the general symbol $\mathbf{W}_i$ for $\mathbf{U}_i$, $\mathbf{V}_i$ and $\mathbf{V}_i\mathbf{U}_j$. The polyphase transfer matrix $\mathbf{E}(z)$ in (4.76) is equivalent to

$$\mathbf{E}(z) = \mathbf{B}\mathbf{W}_{L-1}\Lambda(z)\mathbf{W}_{L-2}\Lambda(z)\ldots\mathbf{W}_1\Lambda(z)\mathbf{W}_0, \tag{4.77}$$

where

$$\mathbf{W}_i = \begin{pmatrix} 1 & a_i & b_i \\ c_i & d_i & c_i \\ b_i & a_i & 1 \end{pmatrix}. \tag{4.78}$$

Fig. 4.14 thus becomes Fig. 4.15, where $\mathbf{B}$, $\Lambda(z)$ and $\mathbf{W}_i$ are as in (4.70), (4.72) and (4.78). Assuming that $d_i \neq 0$, the above $\mathbf{W}_i$ can be factorized as

$$\mathbf{W}_i = \begin{pmatrix} 1 & 0 & 0 \\ 0 & d_i & 0 \\ 0 & 0 & 1 \end{pmatrix} \begin{pmatrix} 1 & a_i & b_i \\ c_i/d_i & 1 & c_i/d_i \\ b_i & a_i & 1 \end{pmatrix}.$$

Furthermore, we notice that the mulitplier d_i can be propagated through the entire analysis bank and can be grouped into the multipler β_2 at the end of Fig. 4.15. By propagating d_i through the analysis bank, the multipliers a_i, b_i, and c_i in $\mathbf{W}_i$ are changed. The building block $\mathbf{W}_i$ in Fig. 4.15 thus takes the following form

$$\mathbf{W}_i = \begin{pmatrix} 1 & a_i & b_i \\ c_i & 1 & c_i \\ b_i & a_i & 1 \end{pmatrix}, \tag{4.79}$$

where the set of lattice coefficients a_i, b_i, c_i is different from the one in (4.78). In summary, Fig. 4.15 is the analysis bank of a LP PR FIR QMF structure, which yields $H_k(z)$ of the same degrees. Moreover, $H_0(z)$ and $H_1(z)$ are symmetric, whereas $H_2(z)$ is antisymmetric. The degree of $H_k(z), 0 \leq k \leq 2$ is $6L-4$, where L is the number of $\mathbf{W}_i(z)$ blocks in the analysis bank.

Without loss of generality, let us assume that $H_0(z)$, $H_1(z)$ and $H_2(z)$ are lowpass, bandpass and highpass filters, respectively. To design $H_k(z)$, we define an objective function that represents both the stopband and passband errors as follows:

$$\Phi_1 = \sum_{k=0}^{2} \int_{k^{th} stopband} |H_k(e^{j\omega}|^2 d\omega + \sum_{k=0}^{2} \int_{k^{th} passband} |z^{(N_k-1)/2} - H_k(e^{j\omega})|^2 d\omega.$$

The optimization of the parameters of $\mathbf{W}_i$ (so as to minimize Φ_1) can be done by employing standard gradient algorithms [10]. This usually consumes time since the objective function Φ_1 is a nonlinear function of many parameters. Suppose that $H_k(z)$ has pairwise-symmetry property [59]; i.e.,

$$H_2(z) = H_0(-z), \quad H_1(z) = \alpha_1(z^2)$$

for some $\alpha_1(z)$. It is shown in [59] that the structure presented in Fig. 9 of [59] yields filters that satisfy the pairwise symmetry condition for odd M. For $M = 3$, Fig. 9 of [59] simplifies to Fig. 4.16, where

$$\mathbf{E}_1(z) = \mathbf{W}_{L-1}\Lambda(z)\mathbf{W}_{L-2}\ldots\Lambda(z)\mathbf{W}_0. \tag{4.80}$$

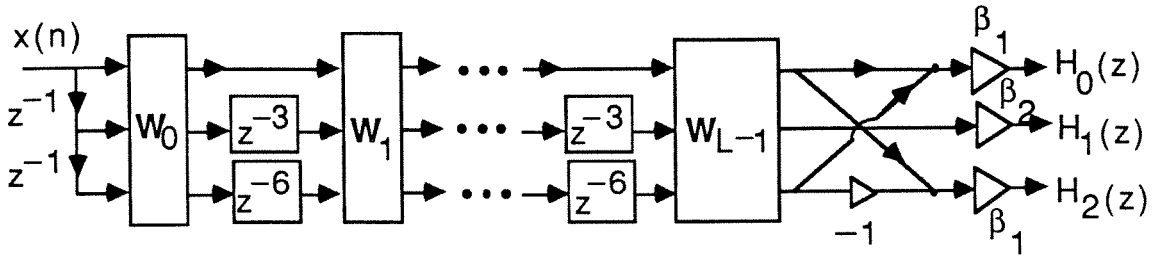

Fig. 4.15. The LP PR analysis bank.

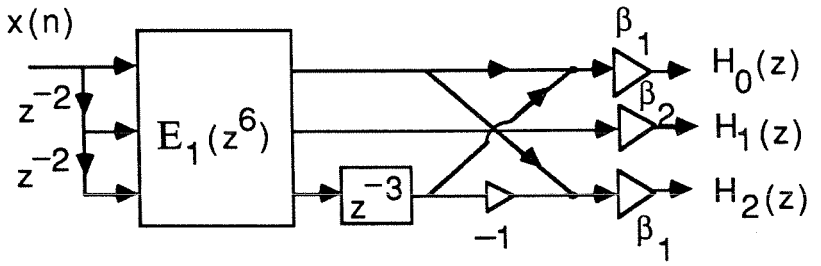

Fig. 4.16. The LP PR pairwise-symmetric analysis bank.

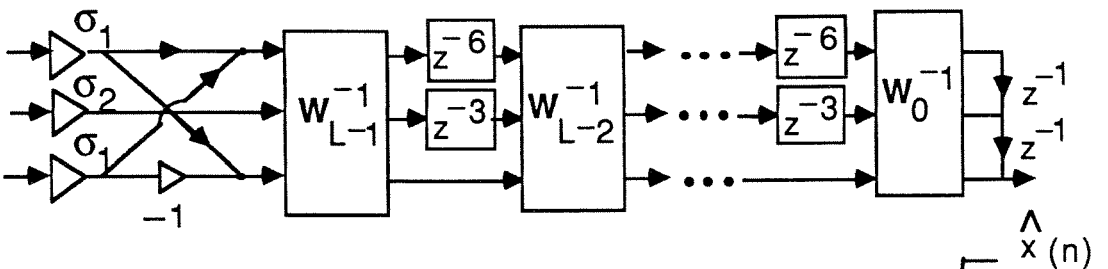

Fig. 4.17. The synthesis bank of Fig. 4.15. Here $\sigma_1 = 1/(\beta_1\sqrt{2})$ and $\sigma_2 = 1/(\beta_2)$.

In other words, the structure in Fig. 4.16 is an analysis bank of a LP PR FIR QMF structure. Furthermore, $H_k(z)$ satisfies the pairwise-symmetric property described above. Since $\mathbf{E}_1(z)$ is a function of z^6 instead of z^3 as in Fig. 4.15, for a given order of the analysis filter, the structure in Fig. 4.16 has approximately half the number of variables compared to those in structure in Fig. 4.15. Consequently, the convergence of the optimization using pairwise symmetric structure will be much faster than the one in Fig. 4.15.

With the above pairwise symmetry property enforced in the structure, it is now sufficient to optimize

$$\Phi_2 = \int_{\frac{\pi}{3}+\epsilon}^{\pi} |H_0(e^{j\omega})|^2 d\omega + \int_0^{\frac{\pi}{3}-\epsilon} |z^{(N_0-1)/2} - H_0(e^{j\omega})|^2 d\omega$$

$$+ \int_0^{\frac{\pi}{3}-\epsilon} |H_1(e^{j\omega})|^2 d\omega + \int_{\frac{\pi}{3}+\epsilon}^{\frac{\pi}{2}} |z^{(N_1-1)/2} - H_1(e^{j\omega})|^2 d\omega, \tag{4.81}$$

where ϵ depends on the desired stopband edges. Therefore, if we can impose the pairwise-symmetry condition on the structure of Fig. 4.15, then we would save approximately half of the computation time in terms of the stopband and passband errors computations in the objective function. Thus, together with the saving in the number of variables to be optimized, we would expect a faster convergence time for the pairwise symmetric LP PR structure in Fig. 4.16.

4.3.1. *Comments on the synthesis filters $F_k(z)$*:

The synthesis filters $F_k(z)$ of the PR structure are obtained as

$$F_k(z) = \sum_{\ell=0}^{2} z^{-(2-\ell)} R_{\ell k}(z^3), \tag{4.82}$$

where $\mathbf{R}(z) = \mathbf{E}^{-1}(z)$. By computing $\mathbf{E}^{-1}(z)$ explicitly, we will show that $F_k(z)$ are also linear-phase filters of the same symmetries as that of $H_k(z)$. Calculating

$\mathbf{R}(z)$ from (4.63), we observe that $R_{\ell k}(z)$ satisfies the condition

$$\tilde{R}_{\ell k}(z) = z^{m_k} J_k R_{(2-\ell),k}(z), \tag{4.83}$$

which has the same form as in (4.62) (except for the transposition). Thus, $F_k(z)$ is also linear phase of the same symmetries as $H_k(z)$. By inverting the analysis bank in Fig. 4.15 and 4.16, we will conclude below that $F_k(z)$ has the same degree as $H_k(z)$.

In general, $F_k(z)$ has a higher degree compared to $H_k(z)$ because of the inversion process of $\mathbf{E}(z)$. Hence, if we implement the analysis bank as in (4.77), then

$$\mathbf{R}(z) = \mathbf{W}_0^{-1}\Lambda^{-1}(z)\mathbf{W}_1^{-1}\ldots\Lambda^{-1}(z)\mathbf{W}_{L-1}^{-1}\mathbf{B}^{-1}.$$

By noting that $\Lambda^{-1}(z) = z^{-2}\Gamma_3\Lambda(z)\Gamma_3$, the corresponding synthesis bank of Fig. 4.15 is drawn in Fig. 4.17. It is clear from Fig. 4.17 that in this particular instance, $F_k(z)$ actually has the same degree as $H_k(z)$. Further conclusion can be drawn for the synthesis filters corresponding to the analysis bank in Fig. 4.16; namely, the synthesis filters also satisfy the pairwise symmetric property. In other words, $F_2(z) = -F_0(-z)$ and $F_1(z) = z^{-3}\alpha_2(z^2)$ for some function $\alpha_2(z)$. In short, if we implement the analysis filters as in Fig. 4.15 or 4.16, then the synthesis filters are also linear phase with the same corresponding symmetries as $H_k(z)$ and their degrees are the same as that of $H_k(z)$.

4.3.2. Comments on the LP PR pairwise symmetry analysis bank of Fig. 4.16

Fig. 4.16 is an LP PR analysis bank that yields pairwise symmetric analysis filters. We obtain this structure by using $\mathbf{E}_1(z)$ in (4.80) with z replaced by z^2. The degrees of $H_0(z), H_1(z)$ and $H_2(z)$ are thus $(12L-5), (12L-8)$ and $(12L-5)$, respectively. In addition to the pairwise-symmetric property, namely, $h_2(n) =$

$(-1)^n h_0(n)$ and $h_1(n) = 0$ for even n, the coefficients of $H_k(z)$ also satisfy:

$$\begin{cases} h_0(1) = h_0(12L-6) = h_2(1) = h_2(12L-6) = 0, \\ h_1(n) = 0, & n \text{ odd.} \end{cases}$$

Using the above fact to compute the degrees of $E_{kj}(z)$, we have

$$deg[\mathbf{E}(z)] = \begin{pmatrix} 4L-3 & 4L-2 & 4L-3 \\ 4L-4 & 4L-3 & 4L-4 \\ 4L-3 & 4L-2 & 4L-3 \end{pmatrix}. \tag{4.84}$$

From the above lengths of $H_k(z)$, $I = 1$ instead of $I = 2$ as in the structure of Fig. 4.15. Moreover, the lengths of $H_k(z)$ are not the same. This, however, is not surprising since we have taken a LP PR structure in which $I = 2$ and N_k are the same and have transformed it into a structure in which $I = 1$ and N_k are not the same, by imposing the pairwise-symmetric property.

Example 4.3: Using the structure in Fig. 4.16 and taking the number of $\mathbf{W}_i$ blocks to be $L = 5$, we design $H_k(z)$ for $\epsilon = 0.1\pi$. The degrees of the analysis filters are $55, 52$ and 55, respectively. The 15 variables in the lattice structure and the 2 additional multipliers at the output were optimized using the IMSL subroutine [10] on a computer to minimize (4.81). The resulting frequency response magnitudes are shown in Fig. 4.18(a). The lattice coefficients and impulse responses of $H_k(z)$ are given in Tables 4.7 and 4.8, respectively. Table 4.8 only displays half the number of coefficients of $H_k(z)$, since they are linear phase filters. The pairwise symmetry property is apparent in Table 4.8. The frequency response magnitudes of the synthesis filters associated with the analysis filters in Example 4.3 are shown in Fig. 4.18(b). We display only half the number of coefficients of $F_k(z)$ in Table 4.9 since $F_k(z)$ are linear-phase filters.

In most of the earlier designs of PR systems [7, 19, 59], the LBR condition was enforced on the structure, and consequently, the analysis filters satisfied the power-

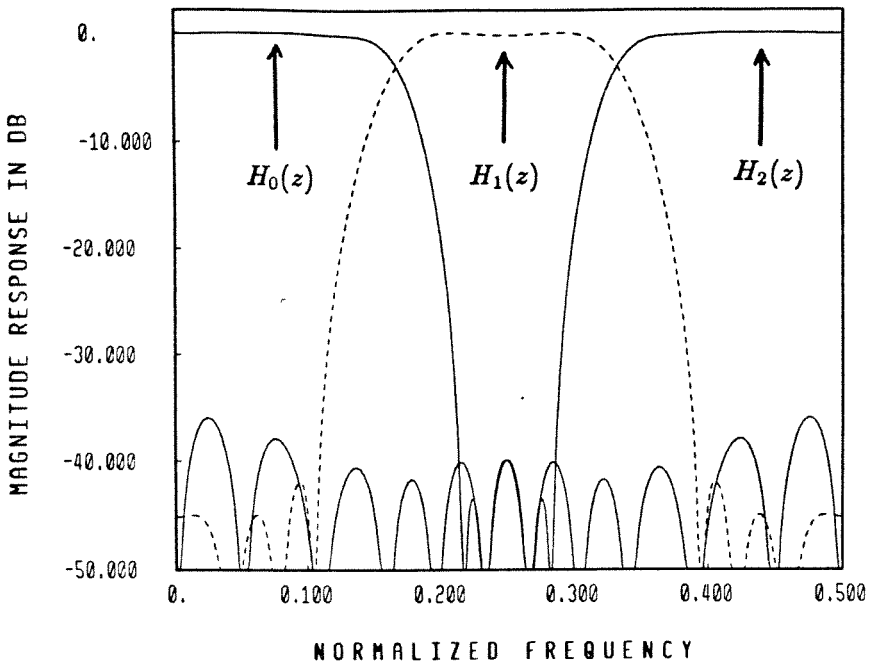

Fig. 4.18a. Ex. 4.3. Magnitude response plots for the corresponding analysis filters.

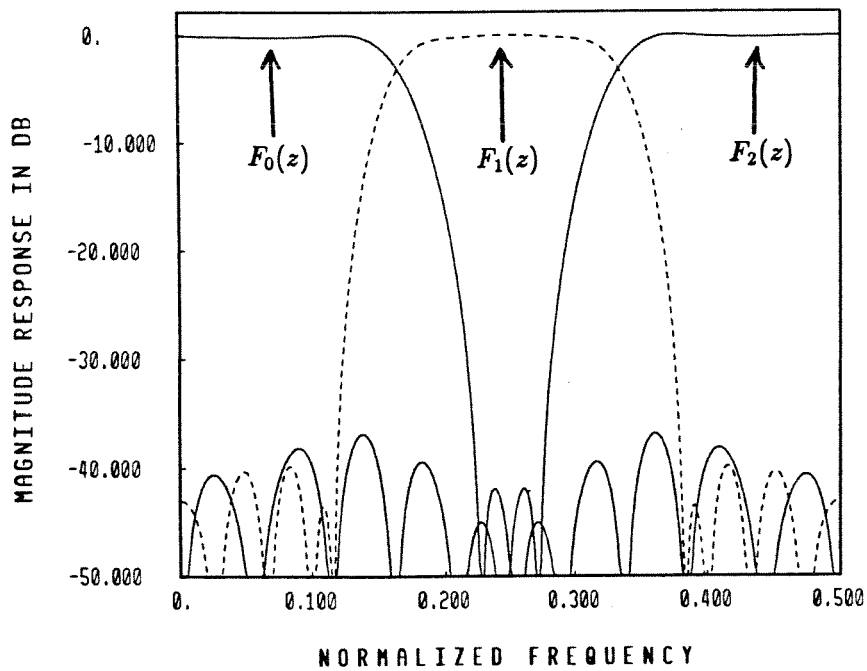

Fig. 4.18b. Ex. 4.3. Magnitude response plots for the corresponding synthesis filters.

Table 4.7
Lattice coefficients of the optimized analysis bank in Ex. 4.3.
$\beta_1 = -4.1034794220864 \times 10^{-9}$ and $\beta_2 = 1.5707941418142 \times 10^{-1}$.

m	Lattice Coefficients a_m	Lattice Coefficients b_m	Lattice Coefficients c_m
0	$-2.3282102148565 \times 10^{3}$	$-5.5293447341746 \times 10^{3}$	$6.1485544476533 \times 10^{-1}$
1	$5.4771339365037 \times 10^{4}$	$-1.7872270513189 \times 10^{2}$	$-1.9882974847877 \times 10^{-5}$
2	$-1.3351781493993 \times 10^{6}$	$1.3096283152688 \times 10^{0}$	$-7.4289672830093 \times 10^{-7}$
3	$-8.6710986482818 \times 10^{6}$	$4.3087219824673 \times 10^{1}$	$-2.1443436695392 \times 10^{-8}$
4	$-3.7906401528742 \times 10^{8}$	$-6.8094743277621 \times 10^{0}$	$-6.3599130248406 \times 10^{-8}$

Table 4.8
Impulse responses of the optimized analysis filters in Ex. 4.3. Here $N_0 - 1 = 55$ and $N_1 - 1 = 52$. Furthermore, $h_0(m) = h_0(N_0 - 1 - m)$, $h_1(m) = h_1(N_1 - 1 - m)$ and $h_2(m) = (-1)^m h_0(m)$.

m	Filter Coefficients $h_0(m)$	Filter Coefficients $h_1(m)$	Filter Coefficients $h_2(m)$
0	$-4.1034799150810 \times 10^{-9}$	$-9.9901150220313 \times 10^{-9}$	$-4.1034799150810 \times 10^{-9}$
1	0.	0.	0.
2	$9.5537638547501 \times 10^{-6}$	$2.3259087841885 \times 10^{-5}$	$9.5537638547501 \times 10^{-6}$
3	$2.7942540296973 \times 10^{-8}$	0.	$-2.7942540296973 \times 10^{-8}$
4	$2.2689555060244 \times 10^{-5}$	$5.5238789890867 \times 10^{-5}$	$2.2689555060244 \times 10^{-5}$
5	$-6.5056107748452 \times 10^{-5}$	0.	$6.5056107748452 \times 10^{-5}$
6	$-1.3835938232415 \times 10^{-4}$	$-3.3676459377498 \times 10^{-4}$	$-1.3835938232415 \times 10^{-4}$
7	$-1.5450393805053 \times 10^{-4}$	0.	$1.5450393805053 \times 10^{-4}$
8	$1.6807358248882 \times 10^{-4}$	$2.2796523469311 \times 10^{-4}$	$1.6807358248882 \times 10^{-4}$
9	$9.4189414966001 \times 10^{-4}$	0.	$-9.4189414966001 \times 10^{-4}$
10	$7.9474660355847 \times 10^{-4}$	$1.5044677383506 \times 10^{-3}$	$7.9474660355847 \times 10^{-4}$
11	$-5.3803123943823 \times 10^{-4}$	0.	$5.3803123943823 \times 10^{-4}$
12	$-2.7006977979884 \times 10^{-3}$	$-3.9523449509934 \times 10^{-3}$	$-2.7006977979884 \times 10^{-3}$
13	$-3.9715006886561 \times 10^{-3}$	0.	$3.9715006886561 \times 10^{-3}$
14	$2.3956889217717 \times 10^{-3}$	$6.8329546163215 \times 10^{-3}$	$2.3956889217717 \times 10^{-3}$
15	$9.6102366520721 \times 10^{-3}$	0.	$-9.6102366520721 \times 10^{-3}$
16	$5.8659326584867 \times 10^{-3}$	$9.1535965074864 \times 10^{-3}$	$5.8659326584867 \times 10^{-3}$
17	$-1.2145874803718 \times 10^{-2}$	0.	$1.2145874803718 \times 10^{-2}$
18	$-1.5561448572774 \times 10^{-2}$	$-4.7294831413144 \times 10^{-2}$	$-1.5561448572774 \times 10^{-2}$
19	$-4.9352298948535 \times 10^{-3}$	0.	$4.9352298948535 \times 10^{-3}$
20	$2.4192899584657 \times 10^{-2}$	$3.4028581273034 \times 10^{-2}$	$2.4192899584657 \times 10^{-2}$
21	$2.8655843071586 \times 10^{-2}$	0.	$-2.8655843071586 \times 10^{-2}$
22	$-6.8884118701520 \times 10^{-3}$	$9.4252950512146 \times 10^{-2}$	$-6.8884118701520 \times 10^{-3}$
23	$-5.7672278487990 \times 10^{-2}$	0.	$5.7672278487990 \times 10^{-2}$
24	$-5.6803993889263 \times 10^{-2}$	$-2.8879891452761 \times 10^{-1}$	$-5.6803993889263 \times 10^{-2}$
25	$4.3175380598407 \times 10^{-2}$	0.	$-4.3175380598407 \times 10^{-2}$
26	$2.0762730202796 \times 10^{-1}$	$3.8301848634403 \times 10^{-1}$	$2.0762730202796 \times 10^{-1}$
27	$3.3497547410063 \times 10^{-1}$		$-3.3497547410063 \times 10^{-1}$

Table 4.9
Impulse responses of the synthesis filters in Ex. 4.3. Here $N_0' - 1 = = 55$ and $N_1' - 1 = 58$. Furthermore, $f_0(m) = f_0(N_0' - 1 - m)$, $f_1(m) = f_1(N_1' - 1 - m)$ and $f_2(m) = (-1)^{(m+1)} f_0(m)$.

m	Filter Coefficients $f_0(m)$	Filter Coefficients $f_1(m)$	Filter Coefficients $f_2(m)$
0	$-5.0856051950609 \times 10^{-7}$	0.	$5.0856051950609 \times 10^{-7}$
1	0.	0.	0.
2	$1.2071726295669 \times 10^{-6}$	0.	$-1.2071726295669 \times 10^{-6}$
3	$6.8043026031286 \times 10^{-7}$	$-3.4038856600144 \times 10^{-6}$	$6.8043026031286 \times 10^{-7}$
4	$-1.4547832873095 \times 10^{-6}$	0.	$1.4547832873095 \times 10^{-6}$
5	$-1.6151406864545 \times 10^{-6}$	$8.0798202875348 \times 10^{-6}$	$-1.6151406864545 \times 10^{-6}$
6	$-1.0954083283872 \times 10^{-4}$	0.	$1.0954083283872 \times 10^{-4}$
7	$1.9464322001326 \times 10^{-6}$	$-9.7371222896162 \times 10^{-6}$	$1.9464322001326 \times 10^{-6}$
8	$2.6002386734911 \times 10^{-4}$	0.	$-2.6002386734911 \times 10^{-4}$
9	$1.3510398808581 \times 10^{-4}$	$-7.2376456380997 \times 10^{-4}$	$1.3510398808581 \times 10^{-4}$
10	$-2.9880316517939 \times 10^{-4}$	0.	$2.9880316517939 \times 10^{-4}$
11	$-3.2070536761859 \times 10^{-4}$	$1.7180453614011 \times 10^{-3}$	$-3.2070536761859 \times 10^{-4}$
12	$-1.1666078385066 \times 10^{-3}$	0.	$1.1666078385066 \times 10^{-3}$
13	$3.6701223936154 \times 10^{-4}$	$-1.9730196839034 \times 10^{-3}$	$3.6701223936154 \times 10^{-4}$
14	$2.5801957392175 \times 10^{-3}$	0.	$-2.5801957392175 \times 10^{-3}$
15	$2.8033633714558 \times 10^{-3}$	$-8.4270347872648 \times 10^{-3}$	$2.8033633714558 \times 10^{-3}$
16	$1.6293136197350 \times 10^{-3}$	0.	$-1.6293136197350 \times 10^{-3}$
17	$-6.4013608859602 \times 10^{-3}$	$1.8738254668239 \times 10^{-2}$	$-6.4013608859602 \times 10^{-3}$
18	$-1.4974601249272 \times 10^{-2}$	0.	$1.4974601249272 \times 10^{-2}$
19	$1.7020623944998 \times 10^{-3}$	$8.8661384068888 \times 10^{-3}$	$1.7020623944998 \times 10^{-3}$
20	$2.2605984154776 \times 10^{-2}$	0.	$-2.2605984154776 \times 10^{-2}$
21	$2.9538667731008 \times 10^{-2}$	$-4.8496302353281 \times 10^{-2}$	$2.9538667731008 \times 10^{-2}$
22	$-4.7736225613466 \times 10^{-3}$	0.	$4.7736225613466 \times 10^{-3}$
23	$-5.7106872050697 \times 10^{-2}$	$3.2040864597603 \times 10^{-2}$	$-5.7106872050697 \times 10^{-2}$
24	$-5.8850606121214 \times 10^{-2}$	0.	$5.8850606121214 \times 10^{-2}$
25	$3.9318475835318 \times 10^{-2}$	$9.9810904531240 \times 10^{-2}$	$3.9318475835318 \times 10^{-2}$
26	$2.0744767026860 \times 10^{-1}$	0.	$-2.0744767026860 \times 10^{-1}$
27	$3.3879421236868 \times 10^{-1}$	$-2.8455714941648 \times 10^{-1}$	$3.3879421236868 \times 10^{-1}$
28		0.	
29		$3.7311674030318 \times 10^{-1}$	

complementary property; i.e., $\sum_{k=0}^{M-1} |H_k(e^{j\omega})|^2 = 1$. However, the LBR condition is not necessary for PR systems, and as demonstrated in Fig. 4.18(c) for our design example, $\sum_{k=0}^{2} |H_k(e^{j\omega})|^2 \neq 1$ (solid line) and $\sum_{k=0}^{2} |F_k(e^{j\omega})|^2 \neq 1$ (broken line). In other words, the filters $H_k(z)$ are not power-complementary triplets.

Implementation of this system on a fixed-point machine might require a very large number of bits because of the large dynamic range spanned by the coefficients in Tables 4.7 and 4.8. However, a single precision floating point implementation was found to be very satisfactory in this case. In order to demonstrate the perfect-reconstruction property of the QMF bank characterized by the impulse responses in Tables 4.8 and 4.9 and by the lattice coefficients in Table 4.7, the complete systems of Fig. 4.1(a) (direct-form) and of Fig. 4.16 (lattice-form) were simulated in Fortran on a VAX 11/750 machine, using both single and double precisions. Table 4.10 shows an arbitrary input $x(n)$ and the reconstructed signal $\hat{x}(n)$. It is clear that the system has perfect-reconstruction property except for round-off errors. From the double-precision implementation, the lattice structure seems to be numerically much more robust than the direct form.

Note that single precision corresponds to 24 bits of mantissa and 8 bits of exponent, identical to the arithmetic operations in the AT& T DSP 32 signal processor. The conclusion is that the perfect-reconstruction system can be implemented on such a commercial DSP chip easily, and the fact that the filter coefficients span a large dynamic range is immaterial in such implementations.

Table 4.10
An arbitrary input sequence $x(n)$ and the reconstructed signal $\hat{x}(n)$ for the design example. Here $\hat{x}(n+N-1)$ is shown in order to align the samples.

n	$x(n)$	$\hat{x}(n+N-1)$ Direct Form Single precision	$\hat{x}(n+N-1)$ Direct Form Double precision	$\hat{x}(n+N-1)$ Lattice Structure Single precision	$\hat{x}(n+N-1)$ Lattice Structure Double precision
0	1.00000	1.00000	1.0000012161693	1.00000	1.0000000000000
1	2.00000	2.00000	1.9999999838918	2.00000	2.0000000000000
2	3.00000	3.00000	3.0000013029297	3.00000	3.0000000000000
3	4.00000	4.00000	4.0000016419205	4.00000	4.0000000000000
4	5.00000	5.00000	5.0000003711781	5.00000	5.0000000000000
5	6.00000	6.00000	6.0000033301603	6.00000	6.0000000000000
6	7.00000	7.00000	7.0000020906728	7.00000	7.0000000000000
7	8.00000	8.00000	8.0000011335777	7.99999	8.0000000000000
8	9.00000	9.00000	9.0000045952801	9.00000	9.0000000000000
9	10.00000	10.00000	10.000000041374	10.00000	10.0000000000000
10	11.00000	11.00000	11.000001869694	11.00000	11.0000000000000

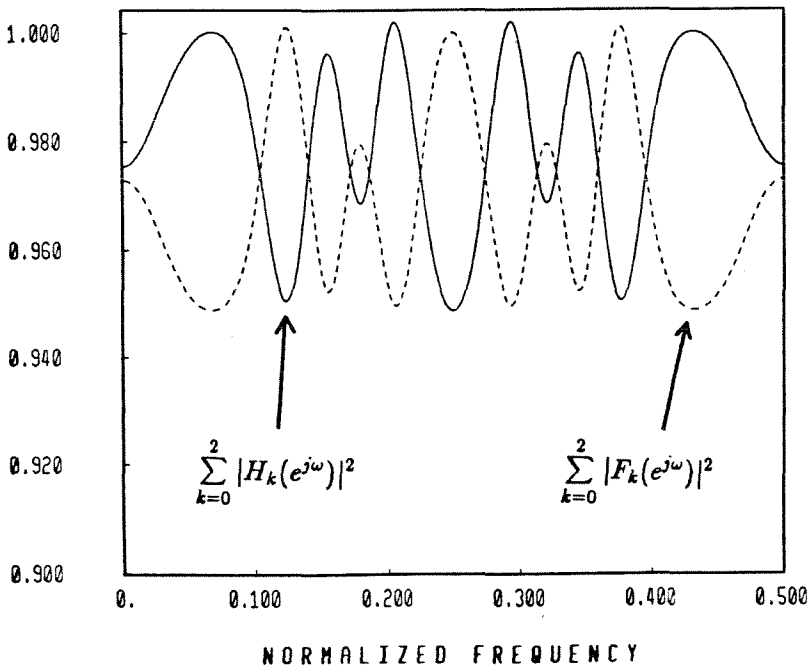

Fig. 4.18c. Ex. 4.3. The plots of $\sum_{k=0}^{2} |H_k(e^{j\omega})|^2$ (solid line) and $\sum_{k=0}^{2} |F_k(e^{j\omega})|^2$ (broken line).

4.3.3. *Implementation of the PR system:*

From (4.79),

$$\mathbf{W}_i^{-1} = \frac{1}{\Delta_i} \begin{pmatrix} 1 - a_i c_i & a_i(b_i - 1) & a_i c_i - b_i \\ c_i(b_i - 1) & 1 - b_i^2 & c_i(b_i - 1) \\ a_i c_i - b_i & a_i(b_i - 1) & 1 - a_i c_i \end{pmatrix},$$

where $\Delta_i = (1 - b_i)(1 + b_i - 2a_i c_i)$. Let us use b bits to implement each multiplier in $\mathbf{W}_i$. It appears at first that we would require infinite precision to implement each multiplier in $\mathbf{W}_i^{-1}$ since it involves a division by Δ_i. These terms Δ_i, however, can be grouped with the multipliers β_i at the end of the structure. Each multiplier in the above $\mathbf{W}_i^{-1}$ thus requires only $2b$ bits to implement. Therefore, to preserve the PR property of the system, we need b and $2b$ bits to implement each multiplier in the analysis and synthesis banks, respectively.

Suppose that exact PR is not required under coefficient quantization; then we can efficiently realize the QMF bank as follows:

4.3.4. *Implementation of $H_k(z)$ and $F_k(z)$:*

At first sight, $\mathbf{W}_i$ in (4.79) requires 6 multipliers to implement. The total number of multipliers required to implement the analysis bank in Fig. 4.15 is therefore $(6L + 3)$. However, $\mathbf{W}_i$ can be factorized as:

$$\mathbf{W}_i = \begin{pmatrix} 1 & 0 & 0 \\ 0 & c_i & 0 \\ 0 & 0 & 1 \end{pmatrix} \begin{pmatrix} 1 & 1 & b_i \\ 1 & \frac{1}{a_i c_i} & 1 \\ b_i & 1 & 1 \end{pmatrix} \begin{pmatrix} 1 & 0 & 0 \\ 0 & a_i & 0 \\ 0 & 0 & 1 \end{pmatrix}. \tag{4.85}$$

Defining $\mathbf{W}_i'$ to be

$$\mathbf{W}_i' = \begin{pmatrix} 1 & 1 & b_i \\ 1 & \frac{1}{a_i c_i} & 1 \\ b_i & 1 & 1 \end{pmatrix}, \tag{4.86}$$

$\mathbf{W}_i \mathbf{W}_{i+1}$ is implemented as follows: the two multipliers a_i and c_{i+1} can be combined, so Fig. 4.15 is equivalent to Fig. 4.19. In general, the total number of

multipliers needed to implement the analysis bank (Fig. 4.19) is only $(4L+3)$. The corresponding synthesis bank of Fig. 4.19 is shown in Fig. 4.20, where $(\mathbf{W}_i')^{-1}$ is

$$(\mathbf{W}_i')^{-1} = \frac{1}{\Delta_i'} \begin{pmatrix} \frac{1}{a_i c_i} - 1 & b_i - 1 & 1 - \frac{b_i}{a_i c_i} \\ b_i - 1 & 1 - b_i^2 & b_i - 1 \\ 1 - \frac{b_i}{a_i c_i} & b_i - 1 & \frac{1}{a_i c_i} - 1 \end{pmatrix}, \tag{4.87}$$

where $\Delta_i' = (1-b_i)(\frac{1+b_i}{a_i c_i} - 2)$. Thus, $(\mathbf{W}_i')^{-1}$ appears to require 9 multipliers to implement and the overall synthesis bank of Fig. 4.20 requires in total $(10L+3)$ multipliers to implement. But $(\mathbf{W}_i')^{-1}$ can be realized as

$$(\mathbf{W}_i')^{-1} = \frac{1}{\Delta_i'} \begin{pmatrix} 1 & 0 & 0 \\ 0 & b_i - 1 & 0 \\ 0 & 0 & 1 \end{pmatrix} \mathbf{W}_i'' \begin{pmatrix} 1 & 0 & 0 \\ 0 & b_i - 1 & 0 \\ 0 & 0 & 1 \end{pmatrix}, \tag{4.88}$$

where

$$\mathbf{W}_i'' = \begin{pmatrix} \frac{1}{a_i c_i} - 1 & 1 & 1 - \frac{b_i}{a_i c_i} \\ 1 & \frac{1+b_i}{1-b_i} & 1 \\ 1 - \frac{b_i}{a_i c_i} & 1 & \frac{1}{a_i c_i} - 1 \end{pmatrix}. \tag{4.89}$$

Using the same grouping argument as in the implementation of $H_k(z)$, Fig. 4.20 is equivalent to Fig. 4.21, where

$$\gamma_1 = \frac{1}{\sqrt{2}\beta_1} \prod_{\ell=0}^{L-1} \Delta_\ell; \quad \gamma_2 = \frac{b_{L-1}}{c_{L-1}\beta_2} \prod_{\ell=0}^{L-1} \Delta_\ell, \tag{4.90}$$

and

$$\eta_i = \begin{cases} \frac{b_i - 1}{a_i}; & i = 0, \\ \frac{(b_i - 1)(b_{i-1} - 1)}{a_i c_{i-1}}; & \text{otherwise.} \end{cases} \tag{4.91}$$

The number of multipliers in this implementation is $(6L+3)$. Note that all multipliers in both analysis and synthesis banks of Fig. 4.19 and 4.21 are quantized to b bits and consequently, the PR property is lost.

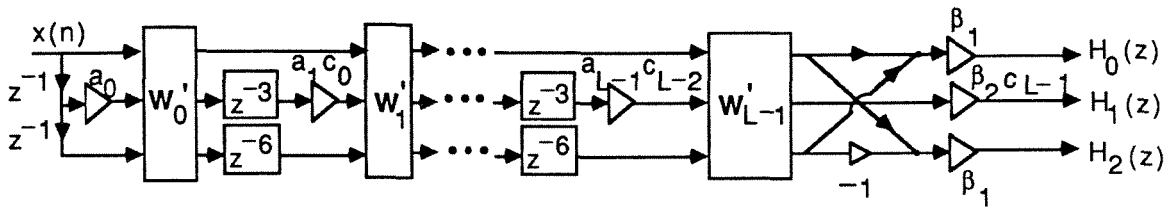

Fig. 4.19. Implementation of the analysis bank of the approximate PR system.

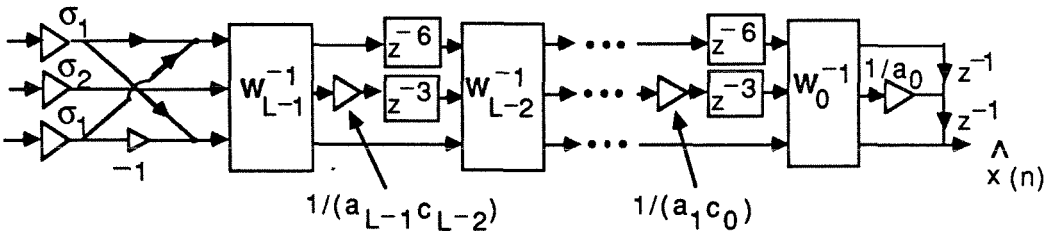

Fig. 4.20. The synthesis bank of Fig. 4.19. Here $\sigma_1 = 1/(\beta_1\sqrt{2})$ and $\sigma_2 = 1/(\beta_2 c_{L-1})$.

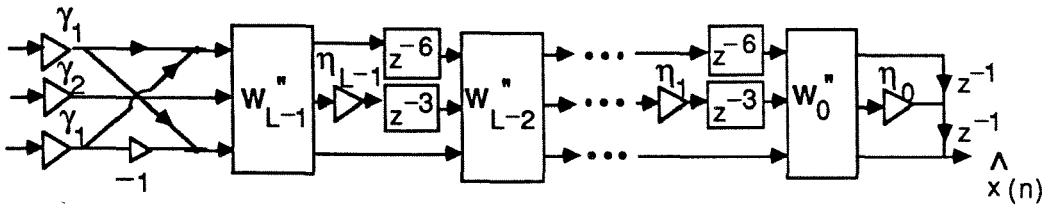

Fig. 4.21. Implementation of the analysis bank of the approximate PR system.

4.3.5. *Implementation complexity:*

To demonstrate the advantage of the lattice structure implementation in Fig. 4.16 over the direct-form implementation in Fig. 4.1(a), let us compare the number of multiplication and addition operations per unit time (abbreviated as MPU and APU, respectively)[5].

4.3.5.a. *Direct-form implementation:*

A direct-form implementation of the filter triplet $[H_0(z), H_1(z), H_2(z)]$ would appear to require $\sum_{k=0}^{2} N_k$ MPU and $\sum_{k=0}^{2} N_k - 1$ APU. Writing them in terms of L and noting that $N_0 - 1 = N_2 - 1 = 12L - 5$ and $N_1 - 1 = 12L - 8$, it requires $\sum_{k=0}^{2} N_k = (36L - 15)$ MPU and $\sum_{k=0}^{2} N_k - 1 = (36L - 18)$ APU. However, there are three simplifying factors involved, viz., (a) the pairwise-symmetry condition, (b) the linear-phase property and (c) the decimation by a factor of 3. As elaborated next, all of the above factors can be exploited to some extent.

Suppose that we implement the analysis bank of the PR system in Fig. 4.1(a) by taking advantage of only (a) and (b); then the linear phase condition yields a factor of 2 savings in MPU. In addition, the MPU and APU can be further cut down by a factor of 2 since $H_2(z) = H_0(-z)$. Moreover, in the implementation of $H_1(z)$, which is a function of z^2, a factor of 4 savings in MPU and a factor of 2 savings in APU are obtained. In summary, the total MPU and APU required to realize the structure in Fig. 4.1(a) in direct form without utilizing the decimation factor are $(12L - 4)/2 + (12L - 8)/4 + 1 = (9L - 3) = 42$ MPU and $(12L - 3) + (6L - 4) = (18L - 7) = 83$ APU, respectively.

[5] A unit of time is defined to be the sampling period of the input sequence $x(n)$ in Fig. 4.1(a).

On the other hand, let us first decimate by a factor of 3 as in Fig. 4.1(c) and implement the system at a lower rate. In doing so, we would need to realize the polyphase components $E_{kj}(z)$ directly. Since $I = 1$ in this system, $\mathbf{E}(z)$ in (4.8) becomes:

$$\begin{cases} \tilde{E}_{k0}(z) = z^{m_k} J_k E_{k1}(z), \\ \tilde{E}_{k2}(z) = z^{m_k} J_k E_{k2}(z), \end{cases} \qquad 0 \le k \le 2, \tag{4.92}$$

where the degree of $E_{kj}(z)$ is given in (4.84). Furthermore, because of the pairwise-symmetric condition, $E_{kj}(z)$ obeys

$$\begin{cases} E_{20}(z) = E_{00}(-z), E_{21}(z) = -E_{01}(-z), E_{22}(z) = E_{02}(-z), \\ E_{10}(z) = \varsigma_0(z^2), E_{11}(z) = z^{-1}\varsigma_1(z^2), E_{12}(z) = \varsigma_2(z^2), \end{cases} \tag{4.93}$$

where $\varsigma_i(z)$ are appropriate FIR functions. Combining (4.92) and (4.93), $\mathbf{E}(z)$ is:

$$\mathbf{E}(z) = \begin{pmatrix} E_{00}(z) & \hat{E}_{00}(z) & E_{02}(z) \\ E_{10}(z) & E_{11}(z) & E_{12}(z) \\ E_{00}(-z) & -\hat{E}_{00}(-z) & E_{02}(-z) \end{pmatrix}. \tag{4.94}$$

Because of the special form of $E_{kj}(z)$ in (4.93), let us consider the implementation complexity of $E_{kj}(z)$ for $k = 0, 2$ and for $k = 1$ seperately.

• $\underline{k = 0, 2}$

We would expect a factor of 4 in savings from the special relation of $E_{k0}(z)$ and $E_{k1}(z)$ for $k = 0, 2$ in (4.94). However, the minus sign in front of $\hat{E}_{00}(-z)$ in the last row denies us a factor of 2 in savings. In other words, we can not fully utilize the above relation. The saving is thus only a factor of 2 and consequently, the complexity is $2(4L-3) = (8L-6) = 34$ MPU and $4(4L-4)+2 = (16L-14) = 66$ APU. From (4.84) and (4.93), $E_{k2}(z)$ are odd degree linear-phase functions, and therefore their complexity is $(2L-1) = 9$ MPU and $2(4L-3) = (8L-6) = 34$ APU.

• $\underline{k = 1}$

Taking advantage of the special form of $E_{1j}(z)$ in (4.93), the numbers of MPU and APU required to realize $E_{10}(z)$ and $E_{11}(z)$ is $(2L-1) = 9$ MPU and $2(2L-2)+1 = (4L-3) = 17$ APU. The remaining component $E_{12}(z)$ is an even degree linear phase function as well as a function of z^2, therefore its complexity is $L = 5$ MPU and $(2L-2) = 8$ APU. With the additional factor of 3 due to decimation, the total complexity of the analysis bank implemented in polyphase direct form is thus $(13L-8)/3 = 19$ MPU and $(30L-22)/3 \approx 43$ APU.

Lattice structure implementation:

At each stage of the lattice structure in Fig. 4.16, the new sequences are computed at a lower rate as: (Fig. 4.22)

$$\begin{pmatrix} v_0(n) \\ v_1(n) \\ v_2(n) \end{pmatrix} = \begin{pmatrix} 1 & a_i & b_i \\ c_i & 1 & c_i \\ b_i & a_i & 1 \end{pmatrix} \begin{pmatrix} u_0(n) \\ u_1(n-2) \\ u_2(n-4) \end{pmatrix} \tag{4.95}$$

The above operation requires 4 multiplications and 6 additions. Together with the multipliers β_1, β_2 and the 2-point DFT at the output of the lattice structure, the total complexity here is $(4L+3)$ MPU and $(6L+2)$ APU. Due to the decimation factor of 3, the complexity of the analysis bank implementation using lattice structure is $(4L+3)/3 \approx 8$ MPU and $(6L+2)/3 \approx 11$ APU.

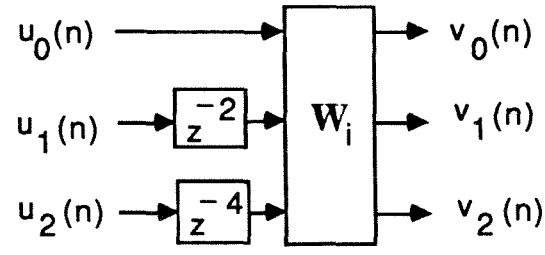

Fig. 4.22. One stage of the implementation of the analysis bank in Fig. 4.16.

Comparing the complexity of both implementations, i.e., direct form and lattice structure, we observe that lattice structure is a very efficient implementation. It should be noticed, however, that the lattice structure is not minimal in terms of number of delays because this number exceeds the filter degrees.

4.3.6. Comments on the generality of the LP PR structures

The above structures in Fig. 4.15 (and Fig. 4.16) for the three-channel LP PR QMF filter bank are by no means general. That is, they do not cover all possible three-channel LP PR QMF banks. There are two reasons for its nongenerality. First of all, these are special cases where $I = 2$ for the structure of Fig. 4.15 and $I = 1$ for the structure in Fig. 4.16. Secondly, even for these special classes, the above decomposition in (4.64) with the choices of $\mathbf{A}_i(z)$ in (4.73) and $\mathbf{B}(z)$ in (4.70) does not cover all LP PR FIR analysis banks satisfying the above constraints on filter lengths. However, the importance of these structures and the corresponding decomposition technique should not be overlooked, because we are able to design filters with high attenuations that have not been done before. In other words, the design filters in Ex. 4.3 are the first of their kind which can incorporate both linear phase and perfect reconstruction for three-channel QMF banks. Moreover, its complexity is low because of its pairwise-symmetry property. Furthermore, immediate generalization of the above structures in Figs. 4.15 and 4.16 is possible by using the same form with the appropriate dimensions. We will elaborate on this issue below.

4.3.7. Generalization of the structure of LP PR FIR QMF banks for odd M

The LP PR structure for Fig. 4.15 can be generalized to cover QMF banks that have more channels than 3. Since M is odd, we represent it as $M = 2L' + 1$.

Let $H_k(z)$ be the analysis filters of order $N_k - 1$, $0 \leq k \leq M-1$. Furthermore, assume the first $(L'+1)$ filters to be symmetric and the remaining L' filters to be antisymmetric. $\mathbf{B}$ and $\Lambda(z)$ in (4.70) and (4.72), respectively, can be generalized to be

$$\mathbf{B} = \begin{pmatrix} 1 & 0 & \dots & 0 & 0 & 0 & \dots & 0 & 1 \\ 0 & 1 & \dots & 0 & 0 & 0 & \dots & 1 & 0 \\ \vdots & \vdots & \ddots & \vdots & \vdots & \vdots & \iddots & \vdots & \vdots \\ 0 & 0 & \dots & 1 & 0 & 1 & \dots & 0 & 0 \\ 0 & 0 & \dots & 0 & 1 & 0 & \dots & 0 & 0 \\ 0 & 0 & \dots & 1 & 0 & -1 & \dots & 0 & 0 \\ \vdots & \vdots & \iddots & \vdots & \vdots & \vdots & \ddots & \vdots & \vdots \\ 0 & 1 & \dots & 0 & 0 & 0 & \dots & -1 & 0 \\ 1 & 0 & \dots & 0 & 0 & 0 & \dots & 0 & -1 \end{pmatrix}, \quad \Lambda(z) = \begin{pmatrix} \mathbf{I}_{L'} & \mathbf{0} & \mathbf{0} \\ \mathbf{0} & z^{-1} & \mathbf{0} \\ \mathbf{0} & \mathbf{0} & z^{-2}\mathbf{I}_{L'} \end{pmatrix}. \tag{4.96}$$

The matrix $\mathbf{A}_i(z)$ satisfies the condition (4.73); namely, $\mathbf{A}_i(z) = \Gamma_3 \hat{\mathbf{A}}_i(z) \Gamma_3$. Carrying through the same argument as in Section 3, $\mathbf{W}_i$ thus takes the form

$$\mathbf{W}_i = \begin{pmatrix} \mathbf{W}_{00} & \mathbf{W}_{01} & \mathbf{W}_{02} \\ \mathbf{W}_{10} & 1 & \mathbf{W}_{10}\Gamma_3 \\ \Lambda_{L'}\mathbf{W}_{02}\Gamma_{L'} & \Gamma_{L'}\mathbf{W}_{01} & \Gamma_{L'}\mathbf{W}_{00}\Gamma_{L'} \end{pmatrix}, \tag{4.97}$$

where $\Gamma_{L'}$ is defined as in (4.12), and $\mathbf{W}_{00}$, $\mathbf{W}_{02}$, $\mathbf{W}_{01}$, and $\mathbf{W}_{10}$ have dimensions $(L' \times L')$, $(L' \times L')$, $(L' \times 1)$, and $(1 \times L')$, respectively. The generalized structure is shown in Fig. 4.23, where $\mathbf{W}_i$ and $\mathbf{B}$ are as in (4.97) and (4.96), respectively.

On the other hand, the pairwise-symmetric LP PR FIR QMF analysis bank in Fig. 4.16 can be appropriately generalized. Let us first consider the pairwise-symmetric structure in Fig. 9 of [59]. Redrawing it using the above $\mathbf{B}$ in (4.96) yields Fig. 4.24. Here $\mathbf{E}_1(z)$ is as in (4.80), where $\Lambda(z)$ and $\mathbf{W}_i$ are as in (4.96) and (4.97), respectively. The matrix $\hat{\mathbf{B}}$ in Fig. 4.24 is an orthogonal matrix of unit norm [59]. In summary, Fig. 4.24 is the analysis bank of the LP PR FIR QMF structure, which yields pairwise-symmetric analysis filters.

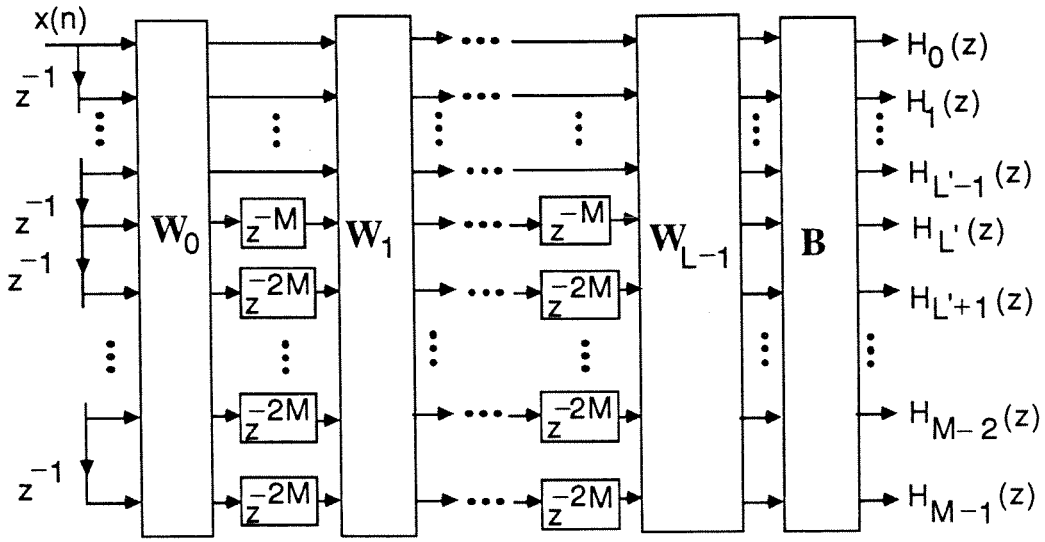

Fig. 4.23. The lattice structure for M-channel LP PR QMF analysis bank.

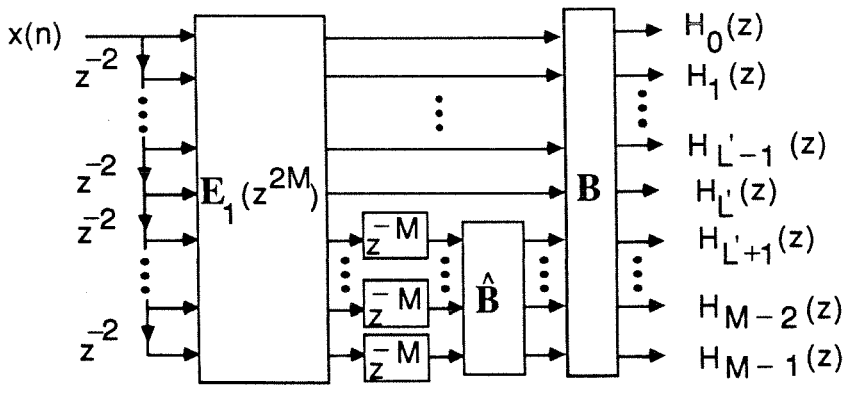

Fig. 4.24. The lattice structure for M-channel pairwise-symmetric LP PR QMF analysis bank.

4.3.8. *Price paid for perfect reconstruction*

It is often assumed that perfect-reconstruction QMF banks are much more expensive than approximate-reconstruction systems with comparable stopband attenuations for $H_k(z)$'s. This impression, however is not necessarily true. In fact, perfect-reconstruction systems implemented with lattice structures [19, 30, 59] often have computational complexity comparable to the well-known approximate reconstruction systems.

To demonstrate this point, notice that in example 4.3, the computational complexity of the PR lattice is only 8 MPU and 11 APU. Suppose now that we design a linear-phase equiripple FIR filter $G_0(z)$ with precisely the same passband and stopband ripples, and the same transition band as $H_0(z)$. Such a filter has order 19. Similarly, if we design a linear-phase equiripple filter $G_1(z)$ comparable to $H_1(z)$, its order is 20. Finally, define $G_2(z) = G_0(-z)$ so that we have a linear phase triplet $[G_0(z), G_1(z), G_2(z)]$ with exactly identical properties as the perfect reconstruction triplet $[H_0(z), H_1(z), H_2(z)]$. Using the above complexity calculation in the polyphase direct-form implementation, the pair of filters $G_0(z)$ and $G_2(z)$ can be realized using 13 MPU and 28 APU. Taking advantage of the special form of $G_1(z)$, namely, linear phase and function of z^2, its complexity is 6 MPU and 10 APU, respectively. In total, this triplet can be implemented with $19/3 \approx 7$ MPU and $38/3 \approx 13$ APU.

In summary, the perfect reconstruction triplet $[H_0(z), H_1(z), H_2(z)]$ (implemented as a lattice) requires 8 MPU and 11 APU, whereas the comparable nonperfect-reconstruction triplet $[G_0(z), G_1(z), G_2(z)]$ requires 7 MPU and 13 APU. (The non-PR triplet, of course, can be implemented only in direct form.) The PR sys-

tem thus has competitive complexity, which appears to be counter-intuitive! The fact of the matter is that the PR property permits the use of a computationally efficient lattice structure, which does not exist for arbitrary (non PR) triplets.

The principal price we actually pay for perfect reconstruction lies in the group delay created by the analysis/synthesis system. In the PR case, this is 55 samples, whereas for a non-PR triplet, this is only 20.

Appendix 4.A. Singularity issues

Given the MIP $[T_N(z), U_N(z)]$, consider the synthesis procedure of the lattice of Fig. 4.4 again. The synthesis procedure is to compute recursively lower-order MIP according to the relation

$$\begin{bmatrix} T'_{m-1}(z) \\ z^{-1}U'_{m-1}(z) \end{bmatrix} = \begin{bmatrix} 1 & -k_m \\ -k_m & 1 \end{bmatrix} \begin{bmatrix} T'_m(z) \\ U'_m(z) \end{bmatrix}, \tag{4.A1}$$

with $T'_N(z) = T_N(z)$ and $U'_N(z) = U_N(z)$. The coefficient k_m is computed as

$$k_m = \frac{t'_{m,m}}{t'_{m,0}}. \tag{4.A2}$$

The unprimed polynomials in (4.30) are essentially scaled versions of the primed ones in (4.A1). The inverse of the relation (4.A1) is

$$\begin{bmatrix} T'_m(z) \\ U'_m(z) \end{bmatrix} = \frac{1}{1-k_m^2} \begin{bmatrix} 1 & k_m \\ k_m & 1 \end{bmatrix} \begin{bmatrix} T'_{m-1}(z) \\ z^{-1}U'_{m-1}(z) \end{bmatrix}, \tag{4.A3}$$

which results in the lattice structure of Fig. 4.4 (except for the scale factor $1-k_m^2$), upon repeated application of the above recursion.

Assume now that at some stage, $k_m^2 = 1$. This means that the recursion (4.A1) would give $T'_{m-1}(z) = \pm z^{-1}U'_{m-1}(z)$. However, the inverse relation (4.A3) is now meaningless (and so is the scaled inverse relation (4.29)), because the 2×2 matrix in (4.A1) is singular. This means that we cannot get back $[T_m(z), U_m(z)]$ by starting from $[T_{m-1}(z), U_{m-1}(z)]$; i.e., there simply does not exist a lattice of the form of Fig. 4.4 in this case. (Notice that under this situation, an attempt to use (4.29) would lead to the conclusion $T_m(z) = \pm U_m(z)$, which of course is not necessary for "$k_m^2 = 1$" to happen.)

Next, conversely, suppose we have the lattice of Fig. 4.4 already synthesized for some MIP $[T_N(z), U_N(z)]$, and we replace k_m with unity for some m. This means

from (4.29) (which *now* holds!) that $T_m(z) = U_m(z)$, which in turn means that $T_N(z)$ and $U_N(z)$ share the common factor $T_m(z)$. An attempt to synthesize *this* $[T_N(z), U_N(z)]$, using (4.A1), will once again bring about the situation $k_m^2 = 1$, but the synthesis procedure *cannot* be carried out beyond this point.

Appendix 4.B. Existence of z_m

As explained in Sec. 4.2.1, a singularity situation can be avoided by using the modified recursion (4.31a), (4.31b) with k_m, as in (4.32). We can find a z_m such that $k_m^2 \neq 1$ (and $k_m^2 < \infty$), as long as none of the three polynomials

$$P_1(z) = T_m(z) - U_m(z) \tag{4.A4}$$

$$P_2(z) = T_m(z) + U_m(z) \tag{4.A5}$$

$$P_3(z) = U_m(z) \tag{4.A6}$$

is identically zero. If $[H_0(z), H_1(z)]$ is such that one of these polynomials is identically zero for some m, what does this signify?

Assume that we start with $m = N$ and carry out (4.31) until we arrive at the situation when one of the three polynomials $P_1(z)$, $P_2(z)$ and $P_3(z)$ is zero. If $P_1(z) \equiv 0$ or $P_2(z) \equiv 0$, this means $T_m(z) = \pm U_m(z)$, which in turn means (See Fig. 4.25) that $T_m(z)$ is a common factor between $H_0(z)$ and $H_1(z)$. If, on the other hand, $U_m(z) = 0$, this means $T_m(z) = 0$ as well, since $T_m(z) = \hat{U}_m(z)$, and this implies that $H_0(z) = H_1(z) \equiv 0$.

In conclusion, if $H_0(z)$ and $H_1(z)$ are not identically zero, and do not share a common factor, then there will exist a z_m such that $k_m^2 \neq 1$ for every m.

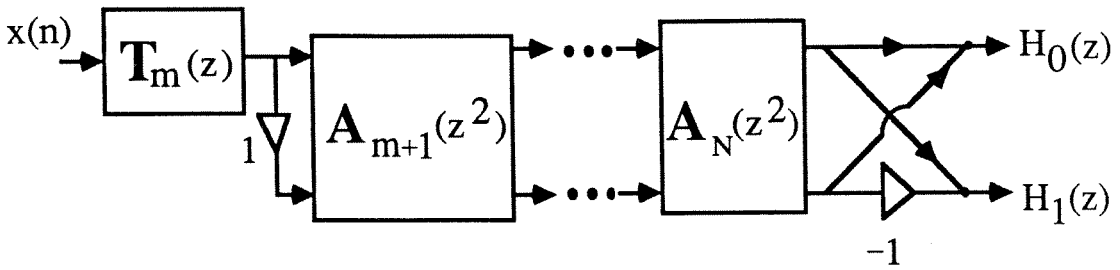

Fig. 4.25. Pertaining to Appendix 4.B.

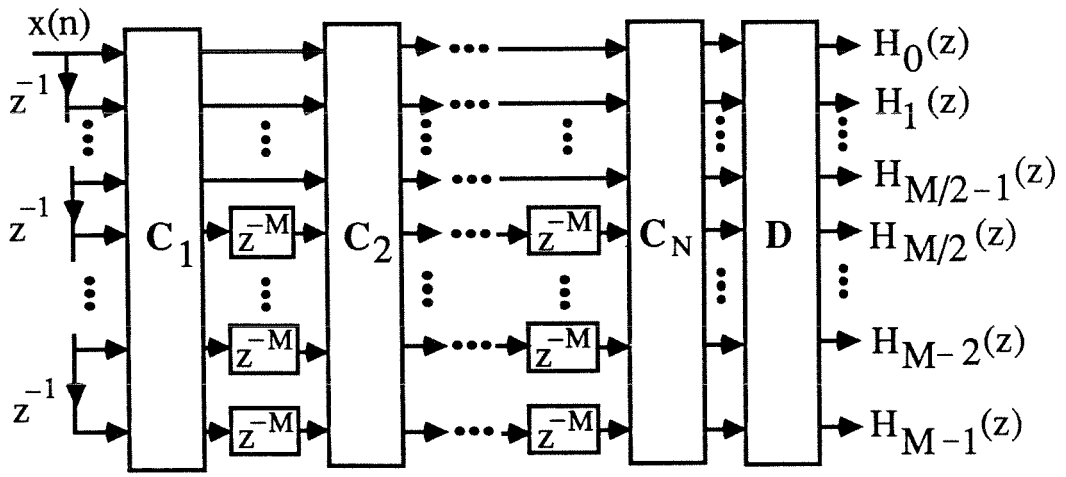

Fig. 4.26. The lattice structure for the M-channel SAOO LP QMF bank. (Even M).

Appendix 4.C. Existence of common factors

Consider the QMF bank of Fig. 4.2(a), where the four filters are FIR. If $H_0(z)$ and $H_1(z)$ have a common zero on the unit circle of the form $(1 - z^{-1}e^{j\omega_0})$, then an input $x(n) = e^{j\omega_0 n}$ cannot be "perfectly reconstructed." In fact, if $H_0(z)$ and $H_1(z)$ share any common factor $(1 - z^{-1}\alpha)$, then an exponential input $x(n) = \alpha^n$ would produce an identically zero output $\hat{x}(n)$, violating the PR property. Without loss of generality, we can therefore assume that $H_0(z)$ and $H_1(z)$ do not have any common factors.

Appendix 4.D.

Let the FIR filters $H_0(z)$ and $H_1(z)$ be related as $H_1(z) = H_0(-z)$. Then the polyphase-component matrix $\mathbf{E}(z)$ has the form

$$\mathbf{E}(z) = \begin{bmatrix} E_{00}(z) & E_{01}(z) \\ E_{00}(z) & -E_{01}(z) \end{bmatrix},$$

so that $\det \mathbf{E}(z) = -2E_{00}(z)E_{01}(z)$. If this has to be a delay, then we must have $E_{00}(z) = c_0 z^{-n_0}$ and $E_{01}(z) = c_1 z^{-n_1}$ for some integers n_0, $n_1 \geq 0$. This means $H_0(z) = c_0 z^{-2n_0} + c_1 z^{-(2n_1+1)}$, which is a very restricted class of transfer functions indeed. In order to obtain a good PR pair, it is therefore essential to remove the restriction $H_1(z) = H_0(-z)$.

Appendix 4.E. M-Channel Generalizations (Even M, SAOO)

Let $H_k(z)$ be the analysis filters of odd order $N_k - 1$, $0 \leq k \leq M - 1$. Furthermore, we assume that the first $M/2$ filters are symmetric and the last $M/2$ ones are antisymmetric. Consider $H_k(z)$ and $H_{M-1-k}(z)$ for $0 \leq k \leq M/2 - 1$. Since they have odd orders and opposite symmetries, they constitute an SAOO pair, which we discussed in Section 4.2.1 above. Thus, one obvious extension from the two-channel SAOO case to the M-channel case (even M, SAOO) is that we consider $M/2$ SAOO

pairs in such a way that they do *not* interact with each other. In other words, each SAOO pair $[H_k(z), H_{M-1-k}(z)]$, $0 \leq k \leq M/2-1$ is realized as in Fig. 4.8, with z^{-2} replaced by z^{-M}. These pairs can then be appropriately combined. The overall PR structure is shown in Fig. 4.26, where the building blocks are

$$\mathbf{C}_i = \begin{bmatrix} \mathbf{I} & \Theta \\ \mathbf{P}_0\Theta\mathbf{P}_0 & \mathbf{I} \end{bmatrix}, \quad \mathbf{D} = \begin{bmatrix} 1 & 0 & \dots & 0 & 0 & \dots & 0 & 1 \\ 0 & 1 & \dots & 0 & 0 & \dots & 1 & 0 \\ \vdots & \vdots & \ddots & \vdots & \vdots & \iddots & \vdots & \vdots \\ 0 & 0 & \dots & 1 & 1 & \dots & 0 & 0 \\ 0 & 0 & \dots & 1 & -1 & \dots & 0 & 0 \\ \vdots & \vdots & \iddots & \vdots & \vdots & \ddots & \vdots & \vdots \\ 0 & 1 & \dots & 0 & 0 & \dots & -1 & 0 \\ 1 & 0 & \dots & 0 & 0 & \dots & 0 & -1 \end{bmatrix},$$

where

$$\Theta = \begin{bmatrix} \mathbf{0} & \dots & \alpha_0 \\ \vdots & \iddots & \vdots \\ \alpha_{M/2-1} & \dots & \mathbf{0} \end{bmatrix}, \quad \mathbf{P}_0 = \begin{bmatrix} \mathbf{0} & \dots & 1 \\ \vdots & \iddots & \vdots \\ 1 & \dots & \mathbf{0} \end{bmatrix}.$$

This structure (Fig. 4.26) yields PR odd-order linear-phase filters with opposite symmetry. We, however, do not have the most general structure for this purpose, at this time. This is currently under study.

APPENDIX A - Eigenfilters

A.1. Introduction

It is well known that most linear-phase, finite-impulse-response filter (FIR) design problems can be satisfactorily handled by using the McClellan-Parks (MP) algorithm [62] for weighted equiripple filters. These filters have the advantage of providing the designer with the most optimal design in the sense of smallest filter length for a given set of specifications. In contrast, a number of authors have also considered the *least-squares* approach for FIR filter design [63]-[66]. As outlined in [2],[33],[66], there are some advantages under certain situations, where these methods have to be preferred over the Remez exchange techniques.[6] Most least-squares techniques advanced so far are based on solving a set of linear, simultaneous equations by matrix inversion.

Consider a typical lowpass design problem: We wish to approximate a "desired response" $D(\omega)$ with a Type 1 linear-phase FIR filter transfer function $H(z)$

$$H(z) = \sum_{n=0}^{N-1} h_n \, z^{-n}. \qquad (A.1)$$

(A Type 1 filter has $h_n = h_{N-1-n}$ and moreover, the order $N-1$ is even [22]). The desired response is

$$D(w) = \begin{cases} 1 & 0 \le \omega \le \omega_p \\ 0 & \omega_S \le \omega \le \pi \\ \text{don't care} & \omega_p < \omega < \omega_S \end{cases}, \qquad (A.2)$$

whereas the amplitude response of $H(z)$ is [22]

$$H_0(e^{j\omega}) = \sum_{n=0}^{N-1} h_n \, e^{-j(n-M)\omega} = \sum_{n=0}^{M} b_n \cos n\omega, \qquad (A.3)$$

[6] "Remez exchange algorithm" and the "MP approach" are used synonymously in this appendix.

where $M = (N-1)/2$ and

$$b_n = \begin{cases} 2\, h_{\frac{N-1}{2}-n}, & n \neq 0 \\ h_{\frac{N-1}{2}}, & n = 0 \end{cases} . \qquad (A.4)$$

The least-squares (LS) approach [63] to this problem is to formulate an objective function

$$E_{LS} = \int_R \left[D(w) - H_0(e^{j\omega}) \right]^2 \frac{d\omega}{\pi}, \qquad (A.5)$$

where R is the region $0 \leq \omega \leq \pi$, but excludes the transition band. The parameters b_n are found by minimizing E_{LS}. The actual computation of b_n can be performed [63] by solving simultaneously a set of linear equations (or by matrix inversion):

$$\mathbf{b} = \mathbf{A}^{-1}\, \mathbf{c}, \qquad (A.6)$$

where $\mathbf{b} = (b_0\, b_1\, \ldots\, b_M)^t$; $\mathbf{c}$ and $\mathbf{A}$ are quantities depending upon ω_p and ω_S. By incorporating a weighting function into the integrand of Equation (A.5), one can attain a tradeoff between passband and stopband accuracies.

Several interesting design examples can be found in [63]. Figure A.1 shows a typical magnitude response $|H_0(e^{j\omega})|$ of such a least-squares FIR filter. A particular special case of the above approach gives rise to the prolate-spheroidal wave sequence as the solution [63]. This corresponds to minimizing

$$E_{LS} = \int_{\omega_S}^{\pi} \left[D(w) - H_0(e^{j\omega}) \right]^2 \frac{d\omega}{\pi} \qquad (A.7)$$

under a suitable constraint (such as $\sum {h_n}^2 = 1$). The resulting amplitude response is typically as shown in Figure A.2. The prolate-spheroidal solution vector $\mathbf{h} = [h_0, h_1, \ldots, h_{N-1}]^t$ (and hence $\mathbf{b}$) can be found as the eigenvector of a real symmetric positive definite matrix [63] (which happens to be Toeplitz). For reasonably large N, this solution $\mathbf{h}$ can be approximated to a very high degree of accuracy by closed-form expressions based on the zeroth-order Bessel function $I_0(x)$. Such closed form

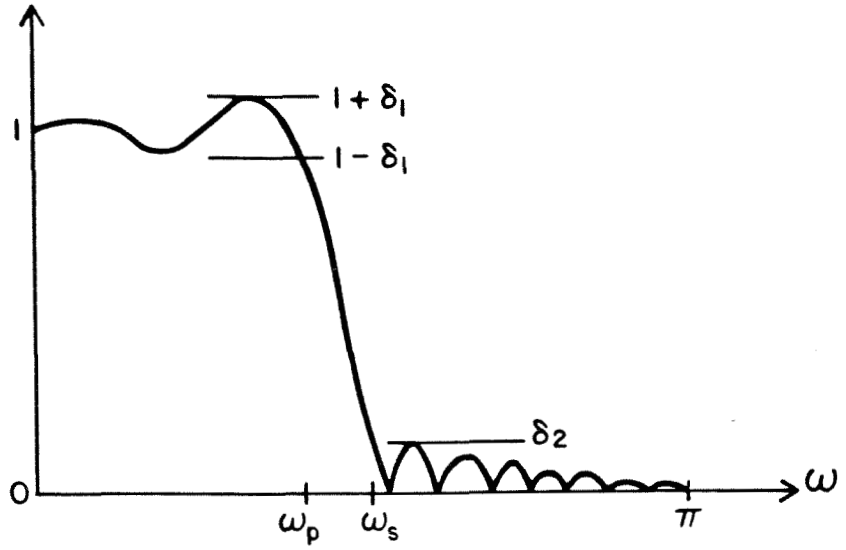

Fig. A.1 Typical magnitude response of a least-squares FIR filter.

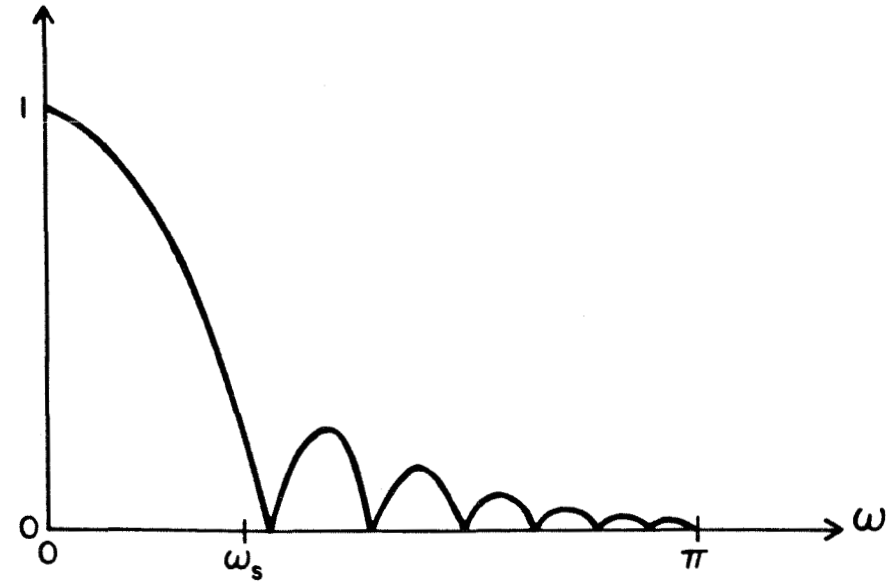

Fig. A.2 Typical magnitude response of a Kaiser window.

expressions have been introduced and used by Kaiser [76] for the design of "Kaiser window." Since the Kaiser window is a closed form approximation for the above eigenvectors, the latter need not be computed by elaborate eigensystem subroutines.

Notice that the least-squares filter response shown in Figure A.2 is itself not a "good" lowpass response; in order to obtain an acceptable lowpass response (based on the LS approach), the passband region $0 \leq \omega \leq \omega_p$ must be included in the objective function E_{LS} of Equation (A.5). Fig. A.2 represents a specific instance of the LS problem, where the solution-vector is an eigenvector of an appropriate real symmetric positive-definite matrix. On the other hand, Fig. A.1 represents another instance of the LS problem, where the solution corresponds to an acceptably good lowpass response, but cannot be obtained as the eigenvector of an appropriate matrix. The question that arises in this context is, can we formulate an appropriate objective function E such that the filter coefficients can be obtained from an eigenvector of an appropriate matrix, and at the same time give rise to a lowpass response as in Fig. A.1 ? In other words, can we obtain a linear-algebraic generalization of the prolate-sequences (or, the Kaiser window) so that the resulting vector itself has a response as in Fig. A.1 ?

The purpose of this appendix is to address this question. The answer turns out to be in the affirmative, and we discuss the solution and several applications of this result. Such FIR filters whose coefficients are the components of eigenvectors will be termed "eigenfilters." The idea of using an eigenvector in order to find the coefficients of a FIR filter has been used earlier in other contexts [74]. The well-known technique of Pisarenko [75] for harmonic retrieval is such an example. Even though eigenvectors have been used in the past for filtering applications (for example, see [33]), we believe that the present formulation is novel in the sense that

it takes care of the passband accuracy directly. Section A.2 formulates the new quadratic objective function and includes design examples of such lowpass filters. Eigenfilters are used in Section A.3 to design a spectral factor of an m^{th}-band filter. This spectral factorization procedure has a direct application in the initialization of perfect-reconstruction structure in which its polyphase matrices are lossless. In the last section, we make comments on the computational aspects involved in finding the appropriate eigenvector.

A.2. Linear-Phase FIR Lowpass Eigenfilters

Let $H(z)$ be an FIR transfer function as in (A.1). We wish to obtain a lowpass frequency response as in Fig. A.1, by minimizing an error measure of the form

$$E = \mathbf{v}^t \, \mathbf{P} \, \mathbf{v}, \tag{A.8}$$

where $\mathbf{P}$ is a real, symmetric and positive definite matrix, depending upon the design requirement, and $\mathbf{v}$ is a real vector related to h_n in some simple manner (to be elaborated). We assume an implicit constraint $\mathbf{v}^t \, \mathbf{v} = 1$ to avoid trivial solutions. We wish the error measure E to reflect both the passband deviation and the stopband deviation from the ideal values of (A.2). Once such a measure is formed, the solution vector $\mathbf{v}$ is simply the eigenvector of $\mathbf{P}$ corresponding to its minimum eigenvalue in view of the well-known Rayleigh's principle [77]. We impose the additional condition that the resulting transfer function $H(z)$ should have linear phase, i.e.,

$$h_n = h_{N-1-n}, \tag{A.9}$$

where the order $N-1$ could be either even (Type 1) or odd (Type 2) [22]. We do not consider antisymmetric impulse-response sequences in this section because they cannot be used in lowpass designs [22].

With $H(z)$ satisfying (A.9), its frequency response takes the form

$$H(e^{j\omega}) = e^{-j\frac{N-1}{2}\omega}\, H_0(e^{j\omega}), \tag{A.10}$$

where $H_0(e^{j\omega})$ is real-valued, given by [22]

$$H_0(e^{j\omega}) = \begin{cases} \sum_{n=0}^{M} b_n \cos n\omega, & N-1 \text{ even}; \\ \sum_{n=0}^{M-1} b_n \cos\,(n+\frac{1}{2})\omega, & N-1 \text{ odd}. \end{cases} \tag{A.11}$$

The quantity M in (A.11) is defined as $M = (N-1)/2$ for even $N-1$, and $M = N/2$ for odd $N-1$. Defining

$$\mathbf{b} = \begin{cases} [b_0\, b_1\, \ldots\, b_{M-1}\, b_M]^t, & N-1 \text{ even}; \\ [b_0\, b_1\, \ldots\, b_{M-2}\, b_{M-1}]^t, & N-1 \text{ odd} \end{cases} \tag{A.12a}$$

and

$$\mathbf{c}(\omega) = \begin{cases} [1\ \cos\omega\ \cos 2\omega\ \ldots\ \cos M\omega]^t, & N-1 \text{ even}; \\ [\cos\frac{\omega}{2}\ \cos\frac{3\omega}{2}\ \ldots\ \cos\,(M-\frac{1}{2})\omega]^t, & N-1 \text{ odd}, \end{cases} \tag{A.12b}$$

we can write (A.11) as

$$H_0(e^{j\omega}) = \mathbf{b}^t\, \mathbf{c}(\omega). \tag{A.13}$$

For notational simplicity, $\mathbf{c}(\omega)$ will often be denoted as $\mathbf{c}$. For even $N-1$, the quantities b_n are as in (A.4). For odd $N-1$, $b_n = 2h_{M-1-n}$.

With the "desired response" as in (A.2), the "stopband error" can now be defined as

$$E_S = \frac{1}{\pi}\int_{\omega_S}^{\pi} \left[D(w) - H_0(e^{j\omega})\right]^2 d\omega = \frac{1}{\pi}\int_{\omega_S}^{\pi} \mathbf{b}^t\, \mathbf{c}\, \mathbf{c}^t\, \mathbf{b}\, d\omega = \mathbf{b}^t\, \mathbf{P}_S \mathbf{b}, \tag{A.14}$$

where $\mathbf{P}_S$ is given by

$$\mathbf{P}_S = \frac{1}{\pi}\int_{\omega_S}^{\pi} \mathbf{c}\, \mathbf{c}^t d\omega \tag{A.15}$$

and is a real, symmetric and positive definite matrix (unless $\omega_S = \pi$, which is a case of no interest).

If the passband error measure E_p is also defined according to the integral of (A.5), the total error measure cannot be written in the form (A.8). Accordingly, let us define E_p differently. First, notice that the zero-frequency response is given by

$$H_0(e^{j0}) \;=\; \mathbf{1}^t\mathbf{b}, \tag{A.16}$$

where the vector $\mathbf{1}$ is defined as

$$\mathbf{1} \;=\; [1\,1\,\ldots\,1]^t. \tag{A.17}$$

The quantity $e_p(w) = (\mathbf{1}-\mathbf{c})^t\mathbf{b}$ therefore represents the deviation of the response $H_0(e^{j\omega})$ from the zero-frequency response.[7] Accordingly, a positive-valued (quadratic) error measure for the passband can be taken as

$$E_p = \frac{1}{\pi}\int_0^{\omega_p} {e_p}^2(w)d\omega \;=\; \frac{1}{\pi}\int_0^{\omega_p} \mathbf{b}^t(\mathbf{1}-\mathbf{c})\,(\mathbf{1}-\mathbf{c})^t\mathbf{b}d\omega, \tag{A.18}$$

which can be written in the form

$$E_p \;=\; \mathbf{b}^t\mathbf{P}_p\mathbf{b}, \tag{A.19}$$

where $\mathbf{P}_p$ is given by

$$\mathbf{P}_p = \frac{1}{\pi}\int_0^{w_p} (\mathbf{1}-\mathbf{c})\,(\mathbf{1}-\mathbf{c})^t d\omega \tag{A.20}$$

and is a real, symmetric, positive definite matrix (unless $\omega_p = 0$). Thus, the total measure to be minimized is

$$E \;=\; \mathbf{b}^t\mathbf{P}\;\mathbf{b}, \tag{A.21}$$

where

$$\mathbf{P} \;=\; (1-\alpha)\;\mathbf{P}_p + \alpha\;\mathbf{P}_S \tag{A.22}$$

[7] The only motivation for taking zero frequency as a reference for passband error formulation is that it brings the vector $\mathbf{b}$ into the reference, and this enables us to write E_p as a quadratic in $\mathbf{b}$. This in turn leads to the eigen-formulation.

The quantity α, which is in the range $0 \leq \alpha \leq 1$, controls the relative accuracies of approximation in the pass and stopbands. Notice that the elements of $\mathbf{P}$ are given by

$$\mathbf{P}(n,m) = \frac{(1-\alpha)}{\pi}\int_0^{w_p}(1-\cos n\omega)(1-\cos m\omega)d\omega \qquad N \text{ is odd} \quad (23a)$$

$$+\frac{\alpha}{\pi}\int_{w_S}^{\pi}(\cos n\omega \cos m\omega)d\omega$$

$$\mathbf{P}(n,m) = \frac{(1-\alpha)}{\pi}\int_0^{w_p}(1-\cos(n+\frac{1}{2})\omega)(1-\cos(m+\frac{1}{2})\omega)d\omega, \qquad N \text{ even} \quad (A.23b)$$

$$+\frac{\alpha}{\pi}\int_{w_S}^{\pi}[\cos(n+\frac{1}{2})\omega][\cos(m+\frac{1}{2})\omega]d\omega.$$

In summary, we have been able to formulate the linear-phase lowpass FIR design problem in the form of an eigenproblem. Given the band edges ω_p and ω_S, and the parameter α, the matrix $\mathbf{P}$ can be computed. It is easy to obtain closed-form expressions for the integrals in (A.23) and hence, the elements $\mathbf{P}(n,m)$ are easily computed, once α, ω_p and ω_S are known. It then remains only to compute the eigenvector of a real, symmetric and positive definite matrix, corresponding to the smallest eigenvalue. The resulting filter is guaranteed to have linear phase because the vector $\mathbf{b}$ rather than the vector $\mathbf{h}$ is directly involved in the optimization problem. The eigenvector $\mathbf{b}$ can be used to obtain the filter coefficients h_n in (A.1). We now proceed with design examples to demonstrate the procedures.

Example A.1: A lowpass filter with $N-1 = 28$, $\omega_p = 0.3\pi$, $\omega_S = 0.4\pi$ and $\alpha = 0.1$ was designed using the above approach. The resulting frequency response is shown in Fig. A.3, which also includes the plot for the case of $\alpha = 0.5$. The effect of α is clearly seen from the figure.

Comments on the choice of α: It is clear from (A.22) that a larger value of α leads

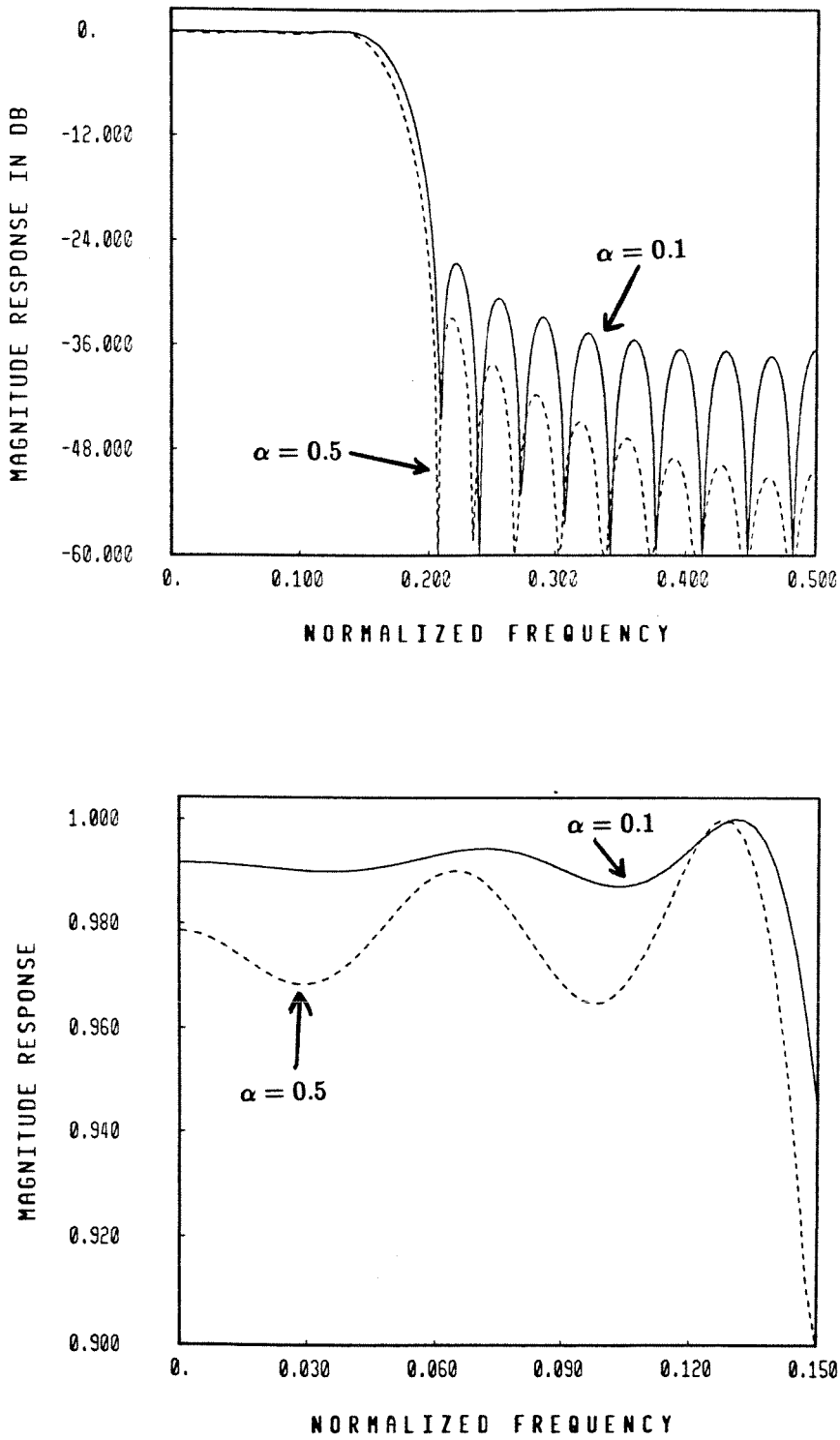

Fig. A.3 Ex. A.1 (a) Magnitude response plot of FIR eigenfilter.

(b) Passband details for the FIR eigenfilter.

to better stopband attenuation at the cost of increased passband ripple. Given the set of specifications ω_p, ω_S, passband tolerance δ_1 and stopband tolerance δ_2, it is necessary to estimate $N-1$ and α in order to design the eigenfilter. An approximate estimate for $N-1$ can be obtained based on the relations in [78]. Even though the estimates in [78] hold only for equiripple designs, the required order for an eigenfilter is only slightly larger. The choice of α governs the ratio δ_1/δ_2. At this point in time, we do not have a procedure for estimating α, starting from a desired δ_1/δ_2 ratio. Further study of the behavior of eigenfilters is necessary in order to fill this gap.

Example A.2: The design of highpass and bandpass eigenfilters can be accomplished with equal ease. For example, a Type 1 bandpass filter can be designed by defining the objective function E as $E = \alpha E_1 + \beta E_2 + (1-\alpha-\beta)E_3$, where $\alpha, \beta > 0$ and $1-\alpha-\beta > 0$. E_1 and E_2 represent the stopband errors:

$$E_1 = \frac{1}{\pi}\mathbf{b}^t \int_0^{\omega_1} \mathbf{c}\mathbf{c}^{\mathbf{t}} dw\, \mathbf{b}, \qquad E_2 = \frac{1}{\pi}\mathbf{b}^t \int_{\omega_4}^{\pi} \mathbf{c}\mathbf{c}^{\mathbf{t}} dw\, \mathbf{b},$$

and E_3 is the quadratic measure of passband error defined as

$$E_3 = \frac{1}{\pi}\mathbf{b}^t \int_{\omega_2}^{\omega_3} (\mathbf{a}-\mathbf{c})(\mathbf{a}-\mathbf{c})^t dw\, \mathbf{b}.$$

Here $\mathbf{a}$ is a constant vector of the form

$$\mathbf{a} = [1 \;\; \cos\omega_0 \;\; \cos 2\omega_0 \;\; \ldots],$$

and $\omega_1, \omega_2, \omega_3$, and ω_4 are the band edges as shown in Fig. A.4a. The quantity ω_0 is taken as $\omega_0 = (\omega_2 + \omega_3)/2$. Figure A.4b shows the response for a design example where the order is $N-1 = 50$, and the band edges are $\omega_1 = 0.3\pi$, $\omega_2 = 0.35\pi$, $\omega_3 = 0.7\pi$ and $\omega_4 = 0.8\pi$.

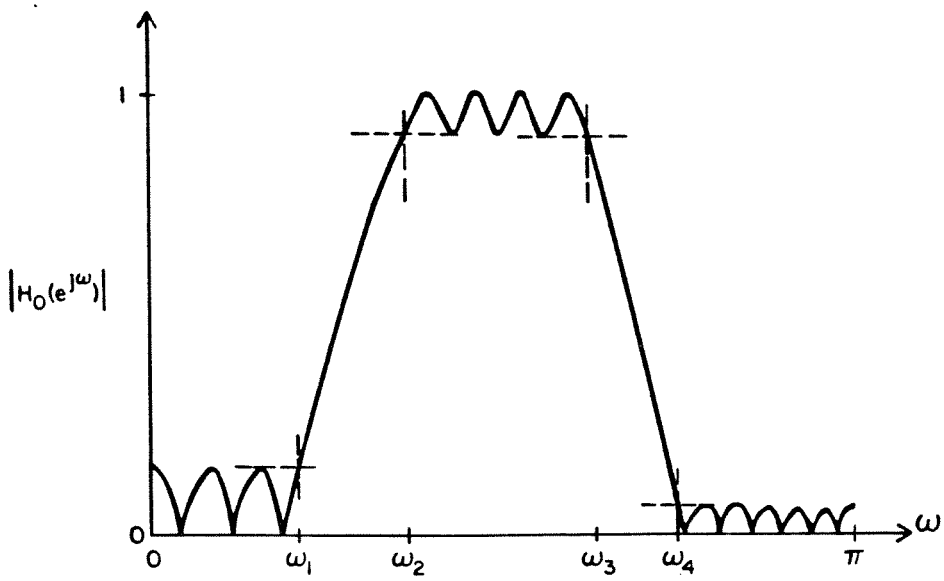

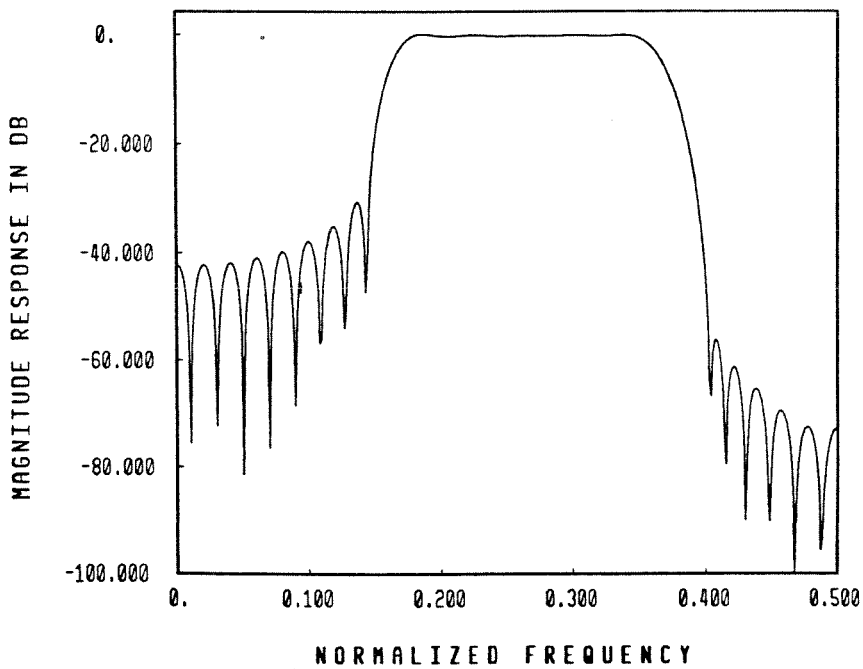

Fig. A.4 Ex. A.2 (a) Typical magnitude response of a bandpass FIR filter.

(b) Magnitude response plot of a bandpass FIR eigenfilter.

A.3. Spectral Factors of m^{th}-band FIR filters

Let $G(z)$ be an even-order linear-phase FIR m^{th}-band filter with order $\ell-1$ and real coefficients $g(n)$. To avoid the case where $g(0) = g(\ell-1) = 0$, we assume that $\ell-1$ is not an integer multiple of $2m$. Since $G(z)$ is a linear-phase filter, its zeros on the unit circle occur in conjugate pairs, whereas its zeros on the real axis occur in reciprocal pairs and its zeros neither on the unit circle nor on the real axis occur in reciprocal conjugate quadruples. To be able to have a spectral factor, $G(e^{j\omega})$ has to be a nonnegative valued function. Consequently, its zeros on the unit circle have to be double zeros. In other words, if z_0 is a zero of $G(z)$ on the unit circle, then both z_0 and z_0^* are double zeros. On the other hand, if z_0 is a zero neither on the unit circle nor on the real axis, then z_0^*, z_0^{-1} and $(z_0^{-1})^*$ are also zeros of $G(z)$. Similarly, z_0 and z_0^{-1} is a pair of zeros on the real axis. Let's group the zeros on the unit circle into $G_1^2(z)$ and the zeros not on the unit circle into $G_0(z)$. We then have $G(z) = G_0(z)G_1^2(z)$, so that the spectral factor $\hat{G}(z)$ is $\hat{G}_0(z)G_1(z)$, where $\hat{G}_0(z)$ is the spectral factor of $G_0(z)$. The problem statement is thus as follows: Find $\hat{G}(z)$ such that

1. $G(z) = \hat{G}(z)\hat{G}(z^{-1})$ is an m^{th}-band filter and
2. $E = \int_{\omega_S}^{\pi} |\hat{G}(e^{j\omega})|^2 d\omega$ is minimized.

Minimizing E in step 2 above is the same as minimizing

$$E = \int_{\omega_S}^{\pi} |G(e^{j\omega})| d\omega = \int_{\omega_S}^{\pi} |G_0(e^{j\omega})||G_1(e^{j\omega})|^2 d\omega. \qquad (A.24)$$

We now discuss an iterative procedure to design the m^{th}-band filter $G(z)$ and its spectral factor $\hat{G}(z)$. The iterative procedure works as follows:

1. Initialize $G_0(e^{j\omega})$ to be unity. Find $G_1(e^{j\omega})$ such that $\int_{\omega_S}^{\pi} |G_1(e^{j\omega})|^2 d\omega$ is minimized, using the eigenfilter method.

2. Fix $G_1(z)$ and readjust $G_0(z)$ by solving a set of linear equations, so that $G(z) = G_0(z)G_1^2(z)$ has m^{th}-band property [67].

3. By fixing $G_0(z)$ to be the solution obtained in step 2, find $G_1(z)$ using the WE approach such that

$$E = \int_{\omega_S}^{\pi} |G_0(e^{j\omega})||G_1(e^{j\omega})|^2 d\omega \text{ is minimized.}$$

4. If the resulting $G_0(z)G_1^2(z)$ is not satisfacting, go to step 2.

Very few repetitions of these steps result in excellent design. Trivial solutions to the minimization steps can be avoided by constraining the total energy of $G_1(z)$ to be unity. Even though the passband error of $G(z)$ does not enter the error function in (A.24), the passband of $G(z)$ comes out to be good because of the m^{th}-band property of $G(z)$. The order of $G_0(z)$ is typically much smaller than that of $G(z)$, and moreover it has no zeros on the unit circle, so it is a simple matter to find a spectral factor $\hat{G}_0(z)$ of $G_0(z)$ and obtain $\hat{G}(z) = \hat{G}_0(z)G_1(z)$. The readjustment of $G_0(z)$ in step 2 is elaborated here, using m^{th}-band property.

Let $2\ell_0$, ℓ_1 and $\ell - 1$ be the orders of $G_0(z)$, $G_1(z)$ and $G(z)$. Thus, $G(z)$ and $\hat{G}(z)$ have orders $2(\ell_0+\ell_1)$ and $(\ell_0+\ell_1)$, respectively. Denote the filter coefficients of $G_0(z)$, $G_1(z)$, $G_1'(z)(\triangleq G_1^2(z))$ and $G(z)$ by $g_0(n)$, $g_1(n)$, $g_1'(n)$ and $g(n)$, respectively. As mentioned earlier, $\ell_0+\ell_1 \neq km$ for any positive integer k. Since $G(z)$ is required to be an m^{th}-band filter, every m^{th} coefficient from the mid-point has to be zero;

i.e.,

$$\begin{cases} g\left(\dfrac{\ell-1}{2}-km\right)=g(\ell_0+\ell_1-km)=0, & k>0; \\ g(\ell_0+\ell_1)=\dfrac{1}{m}. \end{cases} \tag{A.25}$$

The number of known coefficients in $G(z)$ is therefore

$$L=\left\lfloor\frac{\ell}{m}\right\rfloor=\left\lfloor\frac{2(\ell_0+\ell_1)+1}{m}\right\rfloor. \tag{A.26}$$

In terms of filter coefficients, $G(z)=G_0(z)G_1^2(z)=G_0(z)$. $G_1'(z)$ is equivalent to

$$g(n)=\sum_{k=0}^{2\ell_0} g_0(k)g_1'(n-k). \tag{A.27}$$

For a given filter $G_1'(z)$, there are $(2\ell_0+1)$ unknown coefficients of $G_0(z)$ and L fixed values of $g(n)$. Consequently, if $L=2\ell_0+1$, then we can uniquely solve for $g_0(n)$ in terms of $g_1'(n)$ such that (A.25) holds. In other words, $g_0(n)$ is uniquely determined in

$$\begin{pmatrix} \ddots & \vdots & \vdots & \vdots & \iddots \\ \cdots & g_1'(\ell_1-m+1) & g_1'(\ell_1-m) & g_1'(\ell_1-m-1) & \cdots \\ \cdots & g_1'(\ell_1+1) & g_1'(\ell_1) & g_1'(\ell_1-1) & \cdots \\ \cdots & g_1'(\ell_1+m+1) & g_1'(\ell_1+m) & g_1'(\ell_1+m-1) & \cdots \\ \iddots & \vdots & \vdots & \vdots & \ddots \end{pmatrix}$$

$$\cdot\begin{pmatrix} \vdots \\ g_0(\ell_0-1) \\ g_0(\ell_0) \\ g_0(\ell_0+1) \\ \vdots \end{pmatrix}=\begin{pmatrix} \vdots \\ g(\ell_1-m+\ell_0) \\ g(\ell_1+\ell_0) \\ g(\ell_1+m+\ell_0) \\ \vdots \end{pmatrix}=\begin{pmatrix} \vdots \\ 0 \\ \dfrac{1}{m} \\ 0 \\ \vdots \end{pmatrix}. \tag{A.28}$$

Using (A.26) in $L=2l_0+1$, we have

$$\left\lfloor\frac{2(\ell_0+\ell_1)+1}{m}\right\rfloor=2\ell_0+1. \tag{A.29}$$

Equivalently,

$$2\ell_0+1\le\frac{2(\ell_0+\ell_1)+1}{m}<2\ell_0+2 \tag{A.30}$$

or

$$2\ell_0(m-1)+(m-1)\le 2\ell_1<2\ell_0(m-1)+(2m-1). \tag{A.31}$$

As long as the order of $G_1'(z)$ (which is $2\ell_1$) satisfies (A.31), we can always solve Equation (A.28) for $g_0(n)$. (A.28) can be further simplified by observing that $g(n)$, $g_0(n)$ and $g_1'(n)$ are symmetric sequences. Thus, only the first $\frac{L+1}{2}$ equations are sufficient to describe (A.28); i.e.,

$$\begin{pmatrix} g_1'(\ell_1 - m\ell' + \ell_0) & \dots & g_1'(\ell_1 - m\ell') \\ +g_1'(\ell_1 - m\ell' - \ell_0) & & \\ \vdots & \ddots & \vdots \\ 2g_1'(\ell_1 + \ell_0) & \dots & g_1'(\ell_1) \end{pmatrix} \cdot \begin{pmatrix} g_0(0) \\ \vdots \\ g_0(\ell_0) \end{pmatrix} =$$

$$\begin{pmatrix} g(\ell_1 - m\ell' + \ell_0) \\ \vdots \\ g(\ell_1 + \ell_0) \end{pmatrix} = \begin{pmatrix} 0 \\ \vdots \\ \frac{1}{m} \end{pmatrix}, \quad (A.32)$$

where $\ell' = \frac{\ell - 1}{2}$. (A.32) can be compactly rewritten as

$$\mathbf{A}\mathbf{g}_0 = \mathbf{d}, \quad (A.33)$$

where $\mathbf{g}_0 = [g_0(0) \ \dots \ g_0(\ell_0)]^T$, $\mathbf{d} = [0 \ \dots \ 0 \ \frac{1}{m}]^T$, and $\mathbf{A}$ is as in (A.32). $\mathbf{A}, \mathbf{g}_0$ and $\mathbf{d}$ have dimensions $(\ell_0+1)\times(\ell_0+1)$, $(\ell_0+1)\times 1$ and $(\ell_0+1)\times 1$, respectively. By noting that all elements in $\mathbf{d}$ are zero except the last one, $\mathbf{g}_0$ can be obtained by

$$g_0(n) = \left(\frac{(-1)^{\ell_0+n+1}}{m}\right)\left(\frac{\triangle_{(\ell_0+1),n}}{\triangle}\right), \quad (A.34)$$

where $\triangle_{i,j}$ and $\triangle$ are the cofactor of the (i,j) element and the determinant of $\mathbf{A}$, respectively.

In summary, given ℓ_0, ω_p, ω_S and m, we pick ℓ_1 using (A.31). Having fixed the orders of $G_0(z)$ and $G_1(z)$, we design the m^{th}-band filter by iterative procedure described above. The spectral factor $\hat{G}(z)$ of $G(z)$ is thus $\hat{G}_0(z)G_1(z)$, where $\hat{G}_0(z)$ is the spectral factor of $G_0(z)$.

Example A.3: We design a 3^{rd} band linear phase FIR filter of length 62, with cutoff frequencies at $.2\bar{3}\pi$ and $.4\bar{3}\pi$. Here, $\ell_0 = 10$ and $\ell_1 = 21$. Fig. A.5 shows the magnitude responses of $G(z)$ and $\hat{G}(z)$. $\hat{G}(z)$ has order 31 and has the largest possible number of zeros on the unit circle (under the constraint that $\hat{G}(z)\hat{G}(z^{-1})$ is an m-th band filter.)

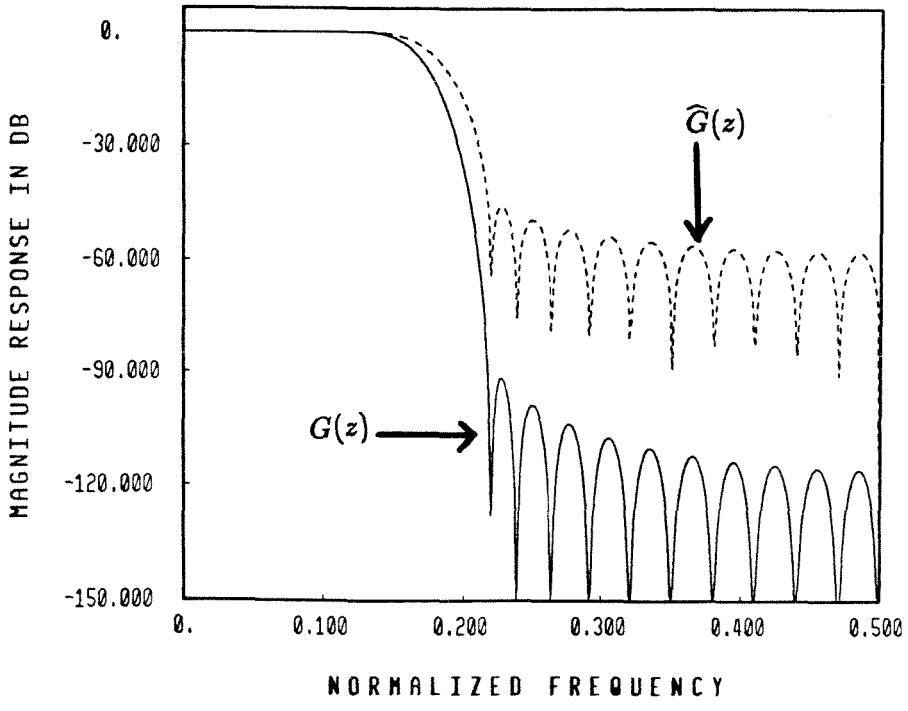

Fig. A.5 Ex. A.3 Magnitude responses of $G(z)$ and its spectral factor $\hat{G}(z)$.

A.4. Eigenvector computation and related issues

A major fraction of the design-time for our method is spent in the computation of the eigenvector. Since we are interested only in one eigenvector (corresponding to an extremal eigenvalue), this computation can be done efficiently (without invoking general methods such as the QR technique [87]). It is well known [83],[84] that to compute the dominant eigenvalue and its corresponding eigenvector, the iterative power method is simple and fast if the ratio $\left|\frac{\lambda_N}{\lambda_{N-1}}\right|$ is large, where λ_k are the eigenvalues of $\mathbf{P}$ with

$$|\lambda_N| \geq |\lambda_{N-1}| \geq \ldots \geq |\lambda_2| \geq |\lambda_1|.$$

At the $k+1^{th}$ iteration of the power method, a vector $\mathbf{x}_{k+1}$ is computed from the previous iterate $\mathbf{x}_k$ as

$$\mathbf{y}_{k+1} = \mathbf{P}\mathbf{x}_k \qquad (A.35a)$$

$$\mathbf{x}_{k+1} = \mathbf{y}_{k+1}/\|\mathbf{y}_{k+1}\|, \qquad (A.35b)$$

where $\|\mathbf{v}\|$ denotes the L_2 norm of vector $\mathbf{v}$. The difference between $\mathbf{x}_k$ and $\mathbf{x}_{k+1}$, defined by $\|\mathbf{x}_{k+1} - \mathbf{x}_k\|$, is compared to a prescribed small constant ϵ, and if

$$\|\mathbf{x}_{k+1} - \mathbf{x}_k\| \leq \epsilon, \qquad (A.36)$$

then $\mathbf{x}_{k+1}$ is a good approximation of the eigenvector corresponding to the maximum eigenvalue. A typical value for ϵ is about 1.0×10^{-6}.

We, however, wish to compute the *minimum* eigenvalue and its corresponding eigenvector. In other words, at each iteration we would like to compute

$$\mathbf{x}_{k+1} = \mathbf{P}^{-1}\mathbf{x}_k. \qquad (A.37)$$

Given $\mathbf{x}_k$, we would like to find $\mathbf{x}_{k+1}$ without inverting $\mathbf{P}^{-1}$. Rewrite (A.37) as

$$\mathbf{x}_k = \mathbf{P}\mathbf{x}_{k+1}. \qquad (A.38)$$

It is well known [83],[84] that a real, symmetric and positive definite matrix $\mathbf{P}$ can be decomposed into

$$\mathbf{P} = \mathbf{L}\mathbf{L}^t, \tag{A.39}$$

where $\mathbf{L}$ is a real lower triangle matrix. Eq. (A.38) then becomes

$$\mathbf{x}_k = \mathbf{L}\mathbf{L}^t\mathbf{x}_{k+1}. \tag{A.40}$$

Let

$$\mathbf{v}_{k+1} = \mathbf{L}^t\mathbf{x}_{k+1}, \tag{A.41}$$

then

$$\mathbf{x}_k = \mathbf{L}\mathbf{v}_{k+1}. \tag{A.42}$$

We can find $\mathbf{v}_{k+1}$ in Eq. (A.42), given $\mathbf{x}_k$ and $\mathbf{L}$, by recursively solving a set of linear equations. Let l_{ij} be the element in the i^{th} row and j^{th} column of $\mathbf{L}$; then we can show that

$$v_{k+1}(n) = \frac{1}{l_{nn}}\left\{x_k(n) - \sum_{j=0}^{n-1} l_{nj}v_{k+1}(j)\right\} \tag{A.43}$$

Since $\mathbf{P}$ is positive definite, l_{nn} in (A.43) are evidently nonzero. Using (A.43), we first solve for $v_{k+1}(0)$ and recursively solve for all $v_{k+1}(n)$ for $1 \leq n \leq N-1$, where N is the dimension of $\mathbf{L}$. (In (A.43), $x_k(n)$ denotes the n^{th} element of vector $\mathbf{x}_k$.) It takes $\frac{N(N-1)}{2}$ multiplications, N divisions and $\frac{N(N-1)}{2}$ additions to compute $\mathbf{v}_{k+1}$. Similarly, we can find $\mathbf{x}_{k+1}$ in (A.41) given $\mathbf{v}_{k+1}$ and $\mathbf{L}$. The total time required per iteration is thus

$$\left[(t_a + t_m)\frac{N(N-1)}{2} + Nt_d\right] \times 2 = (t_a + t_m)N(N-1) + 2Nt_d,$$

where t_a, t_m, t_d are, respectively, the required computer times for addition, multiplication and division.

Note that the speed of convergence depends on the ratio $\frac{\lambda_2}{\lambda_1}$ since we are dealing with $\mathbf{P}^{-1}$ rather than $\mathbf{P}$. Instead of proceeding as in (A.41), (A.42) one could invert $\mathbf{P}$ beforehand, store it as $\mathbf{Q}$ and then perform the iteration

$$\mathbf{y}_{k+1} = \mathbf{Q}\mathbf{x}_k \qquad (A.44a)$$

$$\mathbf{x}_{k+1} = \mathbf{y}_{k+1}/\|\mathbf{y}_{k+1}\|. \qquad (A.44b)$$

The operation (A.44a) requires N^2 multiplications and $N(N-1)$ additions and the time required for this is

$$t_a N(N-1) + t_m N^2,$$

which is nearly the same as the time required for performing (A.41), (A.42). However, there is an overhead cost associated with the computation of $\mathbf{Q}$.

Example A.4: Table A.1 indicates a comparison of design time for half-band filters, using the eigenfilter approach and the Remez exchange approach, for various tolerances. The ratio $\frac{\lambda_2}{\lambda_1}$ and the number of iterations required for eigenvector computation are also given. We observe that $\frac{\lambda_2}{\lambda_1}$ is large and hence the number of iterations for eigenvector computation is impressively small for all the entries in Table A.1. Our experience based on a large number of design examples has convinced us that the ratio λ_2/λ_1 is large in all practical cases. Accordingly, the eigenvector computation never creates any numerical or stability problems, and is invariably fast. Single precision arithmetic is found to be sufficient in all design examples.

There exist some recent methods for computing eigenvectors (corresponding to extremal eigenvalues) based on gradient techniques [88]. These could prove to be even faster than the iterative power method, but we have not studied this possibility in the context of our paper.

Table A.1

Comparison of the eigenfilter and the Remez exchange approaches in half-band filter designs.

	EIGENFILTER					REMEZ EXCHANGE		
ω_p	$N-1$	δ_1	$\frac{\lambda_2}{\lambda_1}$	Number of iterations	CPU time (sec.)	$N-1$	δ_1	CPU time (sec.)
$.4\pi$	14	0.054	62	4	0.3	10	0.0485	0.4
$.42\pi$	18	0.0403	152	4	0.4	14	0.0402	0.5
$.425\pi$	22	0.0317	309	3	0.5	18	0.0265	0.6
$.435\pi$	26	0.0245	614	3	0.7	22	0.0233	0.7
$.435\pi$	30	0.0188	1090	3	0.8	26	0.0146	0.8
$.44\pi$	34	0.0142	1887	3	1.0	30	0.0120	0.9
$.445\pi$	42	0.00812	4588	3	1.4	38	0.0072	1.5
$.445\pi$	46	0.00604	6634	3	1.5	42	0.0049	1.4
$.47\pi$	58	0.0166	2230	3	2.6	54	0.017	1.8
$.47\pi$	62	0.0146	2810	3	2.6	58	0.0137	2.5
$.47\pi$	66	0.0124	350	3	2.9	62	0.011	2.2
$.47\pi$	74	0.00964	5176	3	3.6	66	0.009	2.6
$.47\pi$	78	0.00842	6150	3	3.9	70	0.0073	2.8
$.4725\pi$	90	0.00607	13117	3	5.1	78	0.00672	3.7
$.4725\pi$	98	0.00447	19562	3	5.9	90	0.00376	4.1
$.475\pi$	130	0.00135	91752	3	10.0	122	0.0014	6.8
$.49\pi$	202	0.00106	21069	3	24.5	162	0.00104	12.4

N-1 is the required order for peak passband ripple δ_1 and width $2(\pi/2 - \omega_p)$.

APPENDIX B - Design of half-band FIR filters

Linear phase FIR half-band filters have found several applications in the past [6],[91]. For instance, in the design of sharp cutoff FIR filters, a multistage design based on half-band filters is very efficient [2]. The efficiency of half-band filters derives from the fact that about 50% of the filter coefficients are zero, thus, cutting down the implementation cost. Half-band filters have also been used in multirate filter-bank applications, either directly or indirectly [5],[6].

Let $H(z)$ denote the transfer function of a (linear-phase, FIR) half-band filter of order $N-1$:

$$H(z) = \sum_{n=0}^{N-1} h(n) z^{-n}, \quad h(n) \text{ real.} \tag{B.1}$$

These filters are restricted to be of Type 1 (i.e., $N-1$ is even and $h(n) = h(N-1-n)$ [22]). The frequency response is thus of the form $H(e^{j\omega}) = e^{-j\omega\frac{N-1}{2}} H_0(e^{j\omega})$ where $H_0(e^{j\omega})$ represents the real-valued amplitude response. A typical plot of $H_0(e^{j\omega})$ is shown in Fig. B.1, assuming an equiripple type of design. There is a symmetry with respect to the half-band frequency $\frac{\pi}{2}$; i.e., the band edges are related as

$$\omega_p + \omega_S = \pi, \tag{B.2a}$$

and the ripples are related as

$$\delta_1 = \delta_2 = \delta. \tag{B.2b}$$

In view of this symmetry, the impulse response $h(n)$ satisfies

$$h(n) = \begin{cases} 0, & n - \dfrac{N-1}{2} = \text{even and nonzero;} \\ \dfrac{1}{2}, & n = \dfrac{N-1}{2}. \end{cases} \tag{B.3}$$

The simplest way to design equiripple half-band filters is to invoke the widely used McClellan-Parks algorithm [92] with the specifications satisfying (B.2a) and (B.2b).

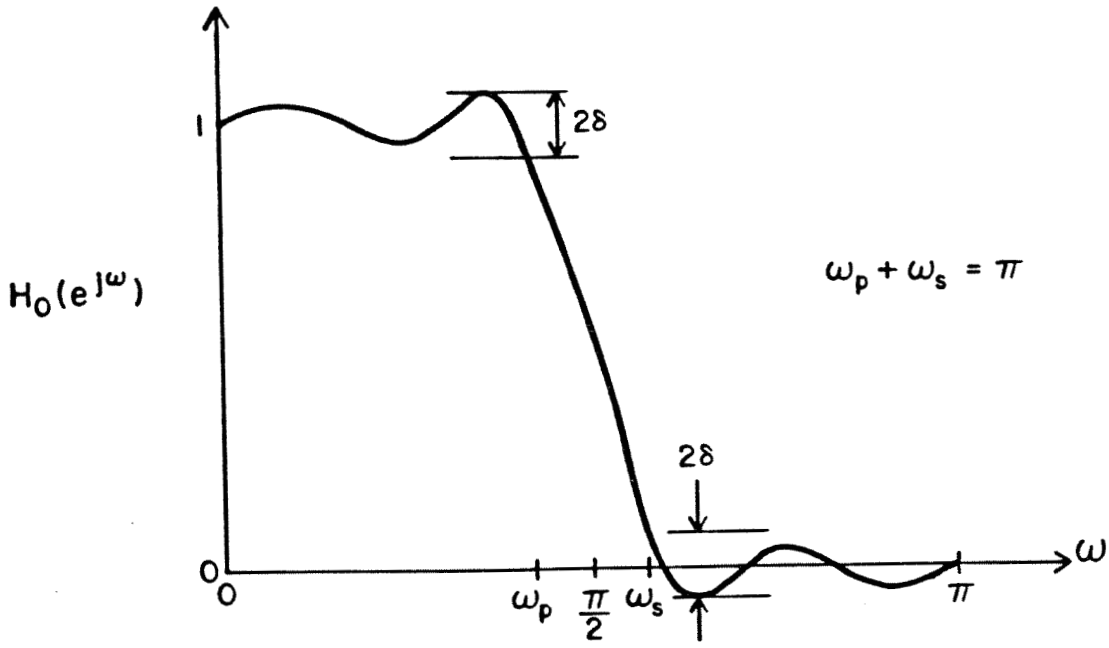

Fig. B.1 Typical amplitude response of a half-band FIR filter.

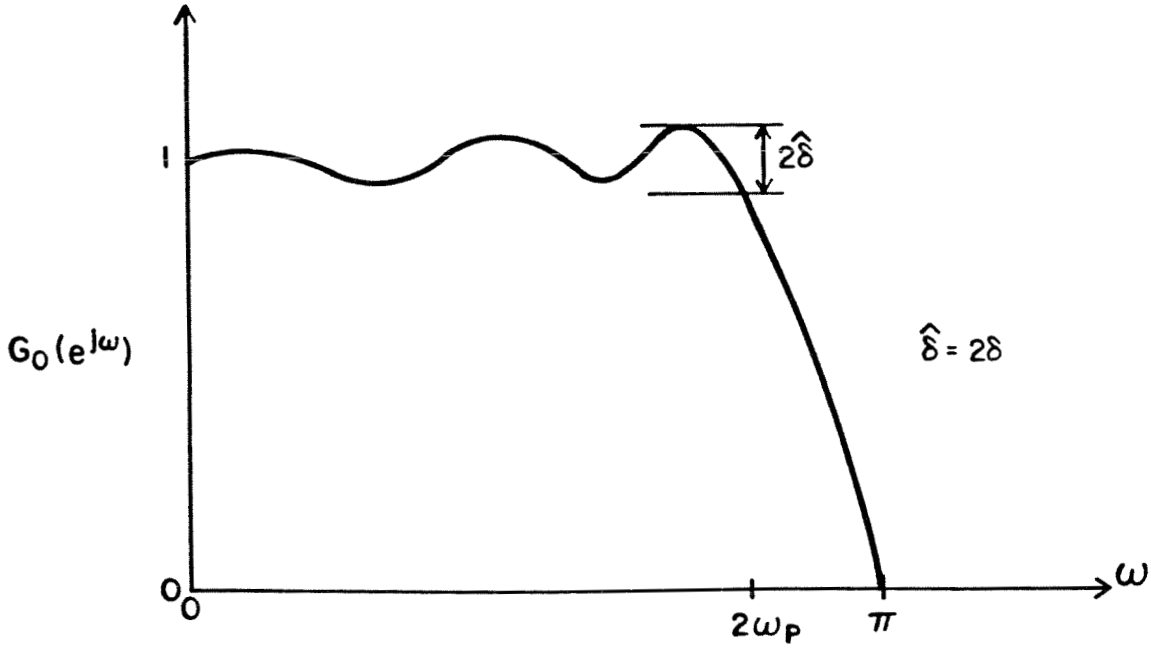

Fig. B.2 Amplitude response of $G(z)$.

(If equiripple nature is not a requirement, then window designs are the fastest [2]). The resulting filter satisfies (B.3) with reasonable accuracy. The only disadvantage with this procedure is that those coefficients which are supposed to satisfy (B.3) are treated as unknowns in the optimization, and accordingly the design time is longer than necessary.

In this appendix, we describe a method (the "half-band trick") for considerably reducing the design time by exploiting the partial knowledge (B.3) about the impulse-response coefficients. The technique also leads to a structural interpretation of half-band filters, which enables us to implement these filters in such a way that, if the structure has low passband sensitivity, then it ***automatically*** has low stopband sensitivity as well. (This is significant in view of the fact that low passband and low stopband sensitivities are often conflicting requirements [93]).

B.1. The "half-band" design trick.

First notice that in view of (B.3), we can always assume $(N-1)/2$ to be odd. (Indeed, if $(N-1)/2$ were even, then (B.3) would imply $h(0) = h(N-1) = 0$; by redefining $h(1)$ to be $h(0)$ we can cut down the order to $N-3$). Given the specifications ω_p, ω_S, and δ, let us first design a one-band prototype linear-phase filter $G(z)$ of order $(N-1)/2$ with specifications as shown in Fig. B.2. $G(z)$ has a zero at $\omega = \pi$, since $(N-1)/2$ is odd [22]. Its passband extends from 0 to $2\omega_p$ and the transition band is from $2\omega_p$ to π. If we now define

$$H(z) = \frac{G(z^2) + z^{-\frac{N-1}{2}}}{2}, \qquad (B.4)$$

then $H(z)$ is a half-band filter, with specifications as in Fig. B.1. The conditions (B.2a), (B.2b) and (B.3) are satisfied *exactly*. The impulse response of $H(z)$ is

evidently related to that of $G(z)$ by

$$h(n) = \begin{cases} \frac{1}{2}g(\frac{n}{2}), & \text{n even} \\ 0, & \text{n odd} \neq \frac{N-1}{2} \\ \frac{1}{2}, & \text{n} = \frac{N-1}{2}. \end{cases} \qquad (B.5)$$

$G(z)$ can be designed with the help of the McClellan-Parks program. This design time is considerably lower than the time required to design $H(z)$ directly, since the order of $G(z)$ is only $(N-1)/2$. Moreover, for large $N-1$, the design accuracy is better.

Example B.1: A half-band linear-phase FIR filter of order $N-1 = 34$, and $\omega_p = 0.45\pi$ is designed using the above method. The magnitude responses of $G(e^{j\omega})$ and $H(e^{j\omega})$ are shown in Fig. B.3. To demonstrate the saving in design time of the above method, we compare the design time of this method with the conventional method for several half-band filters with various specifications. Table B.1 summarizes the results. For higher orders, the savings is quite significant (about a factor of 7 for $N-1 = 82$).

Table B.1

Comparison of the improved and direct methods in half-band filter designs.

$N-1$	Δf	δ_1	IMPROVED METHOD CPU Time (sec.)	DIRECT METHOD CPU Time (sec.)
18	.1	1.135×10^{-2}	0.6	1.9
30	.1	1.350×10^{-3}	1.0	4.3
42	.1	1.715×10^{-4}	1.4	6.4
50	.05	3.550×10^{-3}	1.8	9.4
62	.05	1.255×10^{-3}	2.4	14.9
82	.05	2.275×10^{-4}	3.8	25.2

$N-1$ is the required order for peak passband ripple δ_1 and transition width Δf .

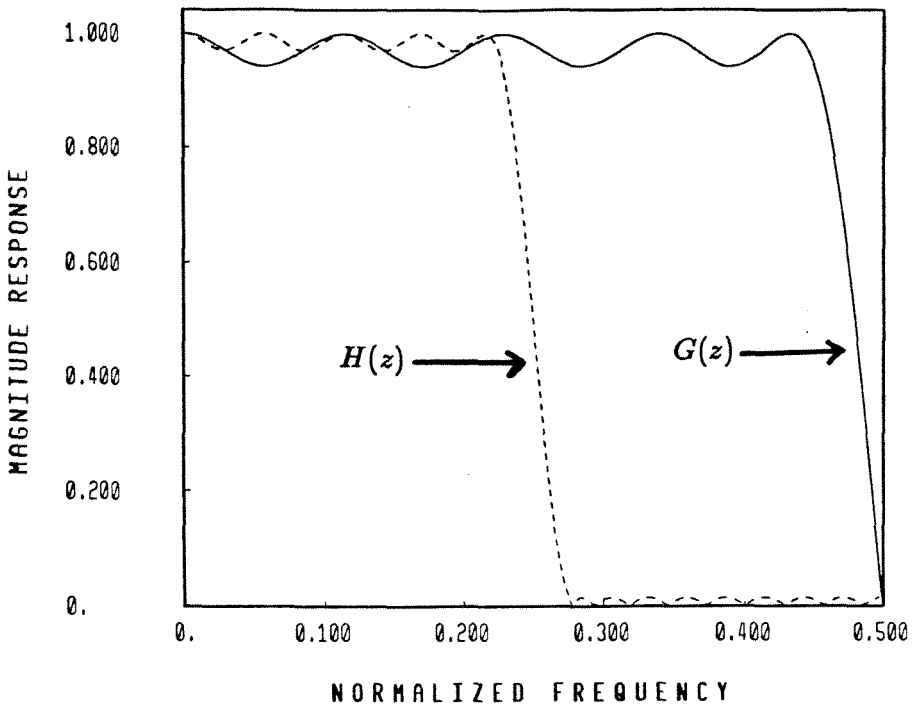

Fig. B.3 Ex. B.1 Magnitude response plots of $G(z)$ and the half-band filter.

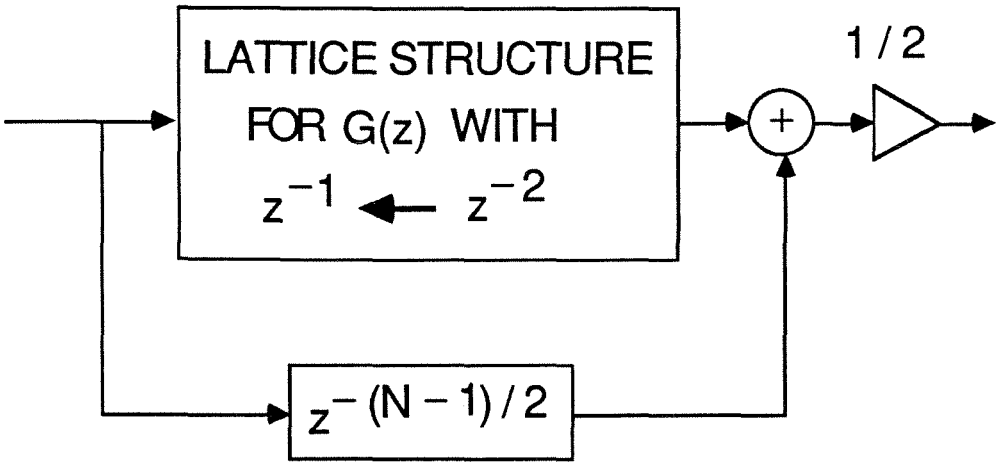

Fig. B.4 Structure for half-band filter.

B.1.a. *Discussion on the low-sensitivity structure for half-band filters.*

It is well known [8],[93] that a digital filter structure having low passband sensitivity does not necessarily have low stopband sensitivity, and vice versa. The coefficient-sensitivity problem in FIR structures have been analyzed in the past [63],[54],[94]. Based on the notion of structural passivity, certain lattice structures are proposed in [54] that can be used to synthesize low-sensitivity structures for any arbitrary FIR transfer function.

The lattice structures in [54] satisfy two crucial properties: First, they provide very low passband sensitivity. Second, if the transfer function has linear phase, this linearity is maintained even when the lattice coefficients are quantized. Now assume that we first implement the one-band filter $G(z)$, using such a structure. Then $G(z)$ has low passband sensitivity. When the lattice coefficients are quantized, the magnitude response of the transfer function $G_q(z)$ remains very close to $G(z)$. Since $G_q(z)$ retains linear phase and has odd order $(N-1)/2$, it continues to have the zero at $\omega = \pi$ in spite of quantization. Suppose we realize $H(z)$ from this structure for $G(z)$, exactly as suggested by (B.4) (see Fig. B.4). Then the stopband response of $H(z)$ is exactly an image of its passband response, even if the coefficients of the lattice are quantized! Thus, $H_q(z)$ (the response of the quantized lattice) continues to remain a half-band filter and has low passband as well as stopband sensitivities.

REFERENCES

[1] D. Esteban and C. Galand, "Application of quadrature mirror filters to split-band voice coding schemes," Proceedings of the IEEE International Conf. ASSP, Hartford, Connecticut, pp. 191-195, May 1977.

[2] R. E. Crochiere and L. R. Rabiner, *Multirate Digital Signal Processing*, Prentice Hall: Englewood Cliffs, NJ, 1983.

[3] T. P. Barnwell III, "Subband coder design incorporating recursive quadrature filters and optimum ADPCM coders, " *IEEE Trans. on Acoustics, Speech and Signal Processing*, Vol. ASSP-30, 751-765, Oct. 1982.

[4] R. V. Cox, D. E. Boch, K. B. Bauer, J. D. Johnston and J. H. Snyder, "The analog voice privacy system," IEEE International Conference on ASSP, pp. 341-344, April 1986.

[5] M. J. T. Smith and T. P. Barnwell III, "A procedure for designing exact reconstruction filter banks for tree structured subband coders," IEEE International Conf. on Acoustics, Speech and Signal Processing, pp. 27.1.1-27.1.4, San Diego, California, March 1984.

[6] F. Mintzer, "Filters for distortion-free two-band multirate filter banks," *IEEE Trans. on Acoustics, Speech and Signal Processing*, vol. ASSP-33, 626-630, June 1985.

[7] P. P. Vaidyanathan, "Theory and design of M-channel maximally-decimated quadrature mirror filters with arbitrary M, having perfect reconstruction property," *IEEE Trans. on Acoustics, Speech and Signal Processing*, vol. ASSP-35, 476-492, April 1987.

[8] P. P. Vaidyanathan and S. K. Mitra, "Low passband sensitivity digital filters: A generalized viewpoint and synthesis procedures," *Proceedings of the IEEE*, 404-423, April 1984.

[9] F. D. Murnaghan, *The Unitary and Rotation Groups*, Spartan Books: Washington, D.C., 1962.

[10] The IMSL Library: A set of Fortran subroutines for mathematics and statistics.

[11] M. Vetterli, "Filter banks allowing for perfect reconstruction," in *Signal Processing*, vol. 10, no. 3, 219-244, April 1986.

[12] M. J. Smith and T. P. Barnwell III, "A unifying framework for analysis/ synthesis systems based on maximally decimated filter banks," Proc. IEEE International Conf. ASSP, Tampa, Florida, pp. 521-524, March 1985.

[13] T. H. Ramstad, "Analysis/synthesis filter banks with critical sampling," International Conference on Digital Signal Processing, Florence, September 1984.

[14] K. Swaminathan and P. P. Vaidyanathan, "Theory and design of Uniform DFT, Parallel, Quadrature Mirror Filter Banks," *IEEE Trans. on Circuit and Systems*, vol. CAS-33, 1170-1191, Dec. 1986.

[15] P.P. Vaidyanathan, Z. Doganata and T. Nguyen, "More results on the perfect reconstruction problem in M-band parallel QMF banks," Proc. of the IEEE Int. Symp. on Circuits and Systems, Philadelphia, May 1987.

[16] V. Belevitch, *Classical Network Synthesis*, Holden-Day: San Francisco, California, 1968.

[17] M. G. Bellanger, G. Bonnerot, and M. Coudreuse, "Digital filtering by polyphase networks: application to sample-rate alternation and filter banks," *IEEE Trans. on Acoustics, Speech and Signal Processing*, Vol. ASSP-24, 109-114, April 1976.

[18] M. J. T. Smith and T. P. Barnwell III, "Exact reconstruction techniques for tree structured subband coders," *IEEE Trans. on ASSP*, 434-441, June 1986.

[19] P. P. Vaidyanathan and P. Q. Hoang, "Lattice structures for optimal design and robust implementation of two-channel perfect-reconstruction QMF banks," *IEEE Trans. on ASSP*, 81-94, Jan. 1988.

[20] M. Vetterli, "A theory of multirate filter banks," *IEEE Trans. on ASSP*, 356-372, March 1987.

[21] J. D. Markel and A. H. Gray, Jr., *Linear Prediction of Speech*, Springer-Verlag: New York, 1976.

[22] L. R. Rabiner and B. Gold, *Theory and application of digital signal processing*, Prentice-Hall: Englewoods Cliffs, NJ: 1975.

[23] J. Makhoul, "Stable and efficient lattice methods for linear prediction," *IEEE Trans. on Acoustics, Speech and Signal Processing*, vol. ASSP-25, 423-428, Oct. 1977.

[24] P. P. Vaidyanathan and S. K. Mitra, "A unified structural interpretation of some well-known stability-test procedures for linear systems," *Proc. of the IEEE*, vol. 75, No. 4, 478-497, April 1987.

[25] P. P. Vaidyanathan and S. K. Mitra, "Discrete version of Richards' theorem and application to cascaded lattice realization of digital filter transfer matrices

and functions," *IEEE Trans. on Circuits and Systems*, vol. CAS-33, 26-34, Jan. 1986.

[26] C.R. Galand and H.J. Nussbaumer, "New quadrature mirror filter structures," *IEEE Trans. on Acoustics, Speech and Signal Processing*, vol. ASSP-32, No. 3, 522-531, June 1984.

[27] J. Makhoul, "A class of all-zero lattice digital filters: Properties and applications," *IEEE Trans. on Acoustics, Speech and Signal Processing*, vol. ASSP-26, 304-314, Aug. 1978.

[28] Z. Doganata and P.P. Vaidyanathan, "On one-multiplier implementations of FIR lattice structures," *IEEE Trans. on Circuit and Systems*, vol. CAS-34, No. 12, 1608-1609, Dec. 1987.

[29] P.P. Vaidyanathan, "Quadrature mirror filter banks, M-band extensions and perfect-reconstruction techniques," *IEEE ASSP Magazine*, Vol. 4, No. 3, 4-20, July 1987.

[30] T.Q. Nguyen and P.P. Vaidyanathan, "Two-channel perfect-reconstruction FIR QMF structures which yield linear-phase analysis and synthesis filters," *IEEE Trans. on Acoust., Speech and Signal Processing*, May 1989, to appear.

[31] P.P. Vaidyanathan, "On power-complementary FIR filters," *IEEE Trans. on CAS*, Vol. CAS-32, No. 12, 1308-1310, Dec. 1985.

[32] J.D. Johnston, "A filter family designed for use in quadrature mirror filter banks," Proc. of Int. Conf. Acoustics, Speech and Signal Processing, pp. 291-294, April 1980.

[33] V.K. Jain and R.E. Crochiere, "Quadrature mirror filter design in the time domain," *IEEE Trans. on Acoustics, Speech and Signal Processing*, 353-361, April 1984.

[34] P. P. Vaidyanathan, "Multirate digital filters, filter banks, polyphase networks, and applications: a tutorial," Caltech report, Sept. 1988.

[35] M. Vetterli and D. LeGall, "Analysis and design of perfect reconstruction filter banks satisfying symmetry constraints," Proc. of the 22^{nd} Conf. on Information Sciences and Systems, pp. 670-675, Princeton, March 1988.

[36] P. P. Vaidyanathan, T. Q. Nguyen, Z. Doganata and T. Saramaki, "Improved technique for design of perfect-reconstruction FIR QMF banks with lossless polyphase matrices," *IEEE Trans. on Acoustic, Speech and Signal Processing*, to appear.

[37] Z. Doganata, P. P. Vaidyanathan, and T. Q. Nguyen, "General Synthesis procedures for FIR lossless transfer matrices for perfect-reconstruction multirate filter bank applications," *IEEE Trans. on Acoustics, Speech and Signal Processing*, Vol. ASSP-36, 1561-1574, Oct. 1988.

[38] P. P. Vaidyanathan, "A tutorial on multirate digital filter banks," Proc. of the IEEE Int. Symp. on Circuits and Systems, Espoo, Finland, June 1988.

[39] T. Q. Nguyen, T. Saramaki and P. P. Vaidyanathan, "Eigenfilters for the design of special transfer functions with applications in multirate signal processing," Proc. IEEE Int. Conf. ASSP., pp. 1467-1470, New York, April 1988.

[40] J. H. McClellan and T. W. Parks, "A unified approach to the design of optimum FIR linear phase digital filters," *IEEE Trans. on Circuit Theory*, Vol.

20, 697-701, Nov. 1973.

[41] G. A. Mian and A. P. Nainer, "A fast procedure to design equiripple minimum-phase FIR filters," *IEEE Trans. on Circuits and Systems*, Vol. 29, 327-331, May 1982.

[42] P. P. Vaidyanathan, "Design and implementation of digital FIR filters," in *Handbook on Digital Signal Processing*, pp. 55-172, Editor D. F. Elliot, Academic Press Inc.: San Diego, 1987.

[43] P. P. Vaidyanathan and T. Q. Nguyen, "Eigenfilters: a new approach to least squares FIR filter design and applications including Nyquist filters," *IEEE Trans. on Circuits and Systems*, Vol. 34, 11-23, Jan. 1987.

[44] B. D. O. Anderson and S. Vongpanitlerd, *Network analysis and Synthesis*, Prentice Hall Inc.: Englewood Cliffs, 1973.

[45] A. Croisier, D. Esteban, and C. Galand, "Perfect channel splitting by use of interpolation/decimation/tree decomposition techniques," presented at the Int. Conf. on Information Science and Systems, Patras, Greece, 1976.

[46] H. J. Nussbaumer, "Pseudo QMF filter bank," IBM Tech. Disc. Bulletin, Vol. 24, No. 6, pp. 3081-3087, Nov. 1981.

[47] P. L. Chu, "Quadrature mirror filter design for an arbitrary number of equal bandwidth channels," *IEEE Trans. on ASSP*, Vol. ASSP-33, 203-218, Feb. 1985.

[48] J. H. Rothweiler, "Polyphase quadrature filters - A new subband coding technique," Proc. of the IEEE Int. Conf. on ASSP, Boston, MA, pp. 1280-1283, March 1983.

[49] L. Hitz and B. D. O. Anderson, "Discrete positive-real functions and their application to system stability," *Proc. Inst. Elect. Eng.*, 153-155, Jan. 1969.

[50] P. P. Vaidyanathan, "The discrete-time bounded-real lemma," *IEEE Trans. on Circuits and Systems*, Vol. CAS-32, 918-924, Sept. 1985.

[51] J. Franklin, *Matrix Theory*, Prentice Hall Inc.: Englewood Cliffs, New Jersey, 1968.

[52] P. P. Vaidyanathan, "Passive cascaded-lattice structures for low-sentivity FIR filter design, with applications to filter banks," *IEEE Trans. on Circuits and Systems*, Vol. CAS-33, 1045-1064, Nov. 1986.

[53] Michael R. Portnoff, "Time-frequency representation of digital signals and systems based on short-time Fourier analysis," *IEEE Trans. on ASSP*, Vol. ASSP-28, No. 1, 55-69, Feb. 1980.

[54] P. P. Vaidyanathan, "New cascaded lattice structures for FIR filters having extremely low coefficient sensitivity," IEEE Int. Conf. ASSP, pp. 497-500, Tokyo, Japan, April 1986.

[55] P. P. Vaidyanathan, "Passive cascaded lattice structures for low sensitivity FIR filter design, with applications to filter banks," *IEEE Trans. on Circuits and Systems*, Vol. CAS-33, 1045-1064, Nov. 1986.

[56] A. Fettweis, "Pseudopassivity, sensitivity, and stability of wave digital filters," *IEEE Trans. on Circuit Theory*, Vol. 19, 668-673, Nov. 1972.

[57] T. Kailath, *Linear Systems*, Prentice Hall Inc.: Englewood Cliffs, N. J., 1980.

[58] P. E. Gill, W. Murray, and M. H. Wright, *Practical Optimization*, Academic Press: London, 1981.

[59] T. Q. Nguyen and P. P. Vaidyanathan, "Maximally decimated perfect reconstruction FIR filter banks with pairwise mirror-image analysis (and synthesis) frequency responses," *IEEE Trans. on Acoustics, Speech and Signal Processing*, Vol. 36, 693-706, May 88.

[60] R. E. Blahut, *Fast algorithms for digital signal processing*, Addison-Wesley: Reading, MA, 1985.

[61] C. R. Galand and H. J. Nussbaumer, "Quadrature mirror filters with perfect-reconstruction and reduced computational complexity," Proc. IEEE Int. COnf. ASSP, pp. 525-528, Tampa, FL., April 1985.

[62] J. H. McClellan and T. Parks, "A unified approach to the design of optimum FIR linear-phase digital filters," *IEEE Trans. on Circuit Theory*, Vol. CT-20, 697-701, Nov. 1973.

[63] D. W. Tufts and J. T. Francis, "Designing digital lowpass filters: Comparison of some methods and criteria," *IEEE Trans. on Audio and Electroacoustics*, Vol. AU-18, 487-494, Dec. 1970.

[64] W. C. Kellogg, "Time domain design of nonrecursive least mean-square digital filters," *IEEE Trans. on Audio and Electroacoustics*, Vol. AU-20, 155-158, June 1972.

[65] D. C. Farden and L. L. Scharf, "Statistical design of nonrecursive digital filters," *IEEE Trans. on Acoustics, Speech and Signal Processing*, Vol. ASSP-22, 188-196, June 1974.

[66] Y. C. Lim and S. R. Parker, "Discrete coefficient FIR digital filter design based upon an LMS criteria," *IEEE Trans. on Circuits and Systems*, Vol. CAS-30, 723-739, Oct 1983.

[67] F. Mintzer, "On half-band, third-band and N^{th} band FIR filters and their design," *IEEE Trans. on Acoustics, Speech and Signal Processing*, Vol. ASSP-30, 734-738, Oct. 1982.

[68] J. K. Liang, R. J. P. Defigueiredo and F. C. Lu, "Design of optimal Nyquist, partial response, N^{th} band, and nonuniform tap spacing FIR digital filters using linear programming techniques," *IEEE Trans. on Circuits and Systems*, Vol. CAS-32, 386-392, April 1985.

[69] A. Antoniou, *Digital Filters: analysis and design*, McGraw-Hill, Inc., 1979.

[70] D. W. Burlage, R. C. Houts and G. L. Vaughn, "Time-domain design of frequency-sampling digital filters for pulse shaping using linear programming techniques," *IEEE Trans. on Acoustics, Speech and Signal Processing*, Vol. ASSP- 22, 180-185, June 1974.

[71] K. Feher, M. El-Torky, and R. DeCristofaro, "Optimum pulse shaping application of binary transversal filters used in satellite communication," *Radio Electronics Engr.*, Vol. 47, no. 6, 249-256, June 1977.

[72] K. Feher and R. Decristofaro, "Transversal filter design and application in satellite communication," *IEEE Trans. Commun.*, Vol. COM-24, 1262-1268, Nov. 1976.

[73] K. Nakayama and T. Mizukami, "A new IIR Nyquist filter with zero intersymbol interference and its frequency response approximation," *IEEE Trans. Circuits and Systems*, Vol. CAS-29, 23-34, Jan. 1982.

[74] J. Makhoul, "On the eigenvectors of symmetric Toeplitz matrices," *IEEE Trans. on Acoustics, Speech and Signal Processing*, Vol. ASSP-29, 868-872, Aug. 1981.

[75] S.M. Kay and S.L. Marple, Jr., "Spectrum Analysis- A modern perspective," *Proc. of the IEEE*, Vol. 69, 1380-1419, Nov. 1981.

[76] J.F. Kaiser, "Nonrecursive digital filter design using the I_0-sinh window function," Proc. IEEE Intl. Symp. on Circuits and Systems, pp. 20-23, April 1974.

[77] B. Nobel and J.W. Daniel, *Applied linear algebra*, Prentice Hall Inc.: Englewood Cliffs, N.J., 1977.

[78] L.R. Rabiner, "Approximate design relationships for lowpass FIR filters," *IEEE Trans. Audio and Electroacoustics*, Vol. AU-21, 456-460, Oct. 1973.

[79] O. Herrmann, "On the approximation problem in nonrecursive digital filter design," *IEEE Trans. Circuit Theory*, Vol. CT-18, 411-413, May 1971.

[80] J.F. Kaiser, "Design subroutine (MXFLAT) for symmetric FIR lowpass digital filters, with maximally-flat pass and stopbands," in *Programs for Digital Signal Processing*, IEEE Press, 1979.

[81] P.P. Vaidyanathan, "Optimal design of linear-phase FIR digital filters with very flat passbands and equiripple stopbands," *IEEE Trans. on Circuits and Systems*, Vol. CAS-32, 904-917, Sept. 1985.

[82] J.F. Kaiser and K. Steiglitz, "Design of FIR filters with flatness constraints," in IEEE Int. Conf. Acoustics, Speech, and Signal Processing, Boston, MA, pp. 197-199, Apr. 1983.

[83] P. P. Vaidyanathan, P. A. Regalia and S. K. Mitra, "Design of doubly-complementary IIR digital filters using single complex allpass filter, with multirate applications," IEEE Circuits and Systems, 378-389, April 1987.

[84] G.W. Stewart, *Introduction to Matrix Computation*, Academic Press Inc.: New York, N.Y., 1973.

[85] C. Charalambous, "Acceleration of the least pth algorithm for minimax optimization with engineering applications," *Mathematical Programming*, vol. 17, 270-297, 1979.

[86] C. Charalambous and A. Antoniou, "Equalization of recursive digital filters," IEE. Proc. Part G, vol. 127, pp. 219-225, 1980.

[87] J. H. Wilkinson, *The Algebraic Eigenvalue Problem*, Oxford University Press: London, 1965.

[88] Y. H. Hu and P. K. Chou, "Effective adaptive Pisarenko Spectrum estimate", Proc. of the IEEE Int. Conf. on Acoustics, Speech and Signal Processing, pp. 577-580, Tokyo, Japan, 1986.

[89] P. P. Vaidyanathan and T. Q. Nguyen, "A 'trick' for the design of FIR half-band filters," *IEEE Trans. Circuits and Systems*, vol. CAS-34, 297-300, March 1987.

[90] M. Renfors and T. Saramaki, "Recursive N-th band digital filters," (parts I and II), *IEEE Trans. on CAS*, 24-51, Jan. 1987.

[91] M. G. Bellanger, J. L. Daguet, and G. P. Lepagnol, "Interpolation, extrapolation and reduction of computation speed in digital filters," *IEEE Trans. on Acoustics, Speech and Signal Processing*, Vol. ASSP-22, 231-235, Aug. 1974.

[92] J. H. McClellan, T. W. Parks, and L. R. Rabiner, "A computer program for designing optimum FIR linear phase digital filters," *IEEE Trans. on Audio and Electroacoustics*, Vol. AU-21, 506-526, Dec. 1973.

[93] O. Herrmann and W. Schuessler, "On the accuracy problem in the design of nonrecursive digital filters," *Arch. Electronik Ubertragungstechnik*, Vol. 24, 525-526, 1970.

[94] D. S. K. Chan and L. R. Rabiner, "Analysis of quantization errors in the direct form for finite impulse response digital filters," *IEEE Trans. on Audio and Electroacoustics*, Vol. AU-21, 354-366, Aug. 1973.

[95] A. V. Oppenheim and R. W. Shafer, *Digital signal processing*, Prentice Hall, Inc.: Englewood Cliffs, N. J., 1975.

[96] A. V. Oppenheim, A. S. Wilsky and I. T. Young, *Signals and Systems*, Prentice Hall, Inc.: Englewood Cliffs, N. J., 1983.

[97] P. P. Vaidyanathan and Z. Doganata, "The role of lossless systems in modern digital signal processing: A tutorial," *IEEE Trans. on Education*, to appear.

[98] L. R. Rabiner and R. W. Schafer, *Digital processing of speech signals*, Prentice Hall, Inc.: Englewoods Cliffs, N. J., 1978.